DOKUZ EYLÜL UNIVERSITY
GRADUATE SCHOOL OF NATURAL AND APPLIED SCIENCES

A MODELING STUDY FOR LOAD TRANSFER MECHANISMS OF SLOPE STABILIZING PILES

by
Mehmet Rifat KAHYAOĞLU

January, 2010
İZMİR

A MODELING STUDY FOR LOAD TRANSFER MECHANISMS OF SLOPE STABILIZING PILES

A Thesis Submitted to the

Graduate School of Natural and Applied Sciences of Dokuz Eylül University

In Partial Fulfillment of the Requirements for the Degree of Doctor of Philosophy

in Civil Engineering, Geotechnics Program

by

Mehmet Rifat KAHYAOĞLU

January, 2010

İZMİR

Ph.D. THESIS EXAMINATION RESULT FORM

We have read the thesis entitled **"A MODELING STUDY FOR LOAD TRANSFER MECHANISMS OF SLOPE STABILIZING PILES"** completed by **MEHMET RİFAT KAHYAOĞLU** under supervision of **PROF. DR. ARİF ŞENGÜN KAYALAR** and we certify that in our opinion it is fully adequate, in scope and in quality, as a thesis for the degree of Doctor of Philosophy.

Prof. Dr. Arif Şengün KAYALAR

Supervisor

Prof. Dr. Necdet TÜRK	Assoc. Prof. Dr. Gürkan ÖZDEN
Thesis Committee Member	Thesis Committee Member
Prof. Dr. S. Feyza ÇİNİCİOĞLU	Assoc. Prof. Dr. Selçuk TOPRAK
Examining Committee Member	Examining Committee Member

Prof. Dr. Cahit HELVACI
Director
Graduate School of Natural and Applied Sciences

ACKNOWLEDGMENTS

The author is grateful to the chairman of the dissertation committee and supervisor Prof. Dr. Arif Ş. Kayalar for his technical guidance, constant support, and encouragement during the course of this study. The author is very fortunate and honored that he could have learned from his advisor on a daily basis how to be a better person in every aspect. Knowledge imparted from him will benefit the author's whole life. Special thanks are due to Assoc. Prof. Dr. Gürkan Özden who served as a co-adviser in this research. This study would not have been possible without his significant contribution, and the author is truly indebted to him. Anything good in this dissertation is achieved through his kindness, while anything bad should be blamed on the author as a personal shortcoming. Sincere appreciation is extended to Prof. Dr. Necdet Türk for carefully reviewing the manuscript of this dissertation. The quality of this thesis was improved substantially from his constructive comments. Thanks are also extended to the remaining members of the supervising committee, Prof. Dr. Feyza Çinicioğlu and Assoc. Prof. Dr. Selçuk Toprak, for their guidance and interest in serving on this committee.

Much thanks and appreciation is due to Dr. Okan Önal who gave invaluable help, needed advice, and training to the author during the experimental portion and writing stage of this research. Acknowledgement is due to Gökhan İmançlı for his hand in the experimental work. The author benefited a lot from the discussions and arguments with him. The author wishes to thank close friends, especially Musa Borca, Serkan Özen, İbrahim Alper Yalçın, Ender Başarı, Fatih Işık, Dr. Yeliz Yükselen Aksoy and Dr. Ali Hakan Ören for their camaraderie and assistance. The author really appreciates TÜBİTAK Scientist Training Group for financially supporting me. The author wishes to express in some way his deep thanks to his parents who have instilled in him a sense of motivation and perseverance without which it would have been difficult to finish this study. Finally, the author is very grateful to his wife, Sinem Kahyaoğlu, for sharing in all of the emotions and hardships of the last four years, and for smoothing over the rough times with her understanding, humor, concern, and constant love.

Mehmet Rifat KAHYAOĞLU

A MODELING STUDY FOR LOAD TRANSFER MECHANISMS OF SLOPE STABILIZING PILES

ABSTRACT

A slice from an infinitely long row of piles in an inclined sand bed was simulated with an experimental test setup. The experimental setup consisted of a box in which model tests are performed, a pluviation system to prepare homogeneous and uniform loose sand bed, aluminum model piles, load and deformation measurement and data acquisition systems. The test box, having the biggest dimensions amongst the published boxes, enables tests on both flexible and rigid piles in one and two rows with fixed pile tip. The movement of the soil was controlled by an automatically operated support to facilitate the soil slid under its own weight, whereas the sliding soil was forced to make uniform or triangular displacement in the previous researches. The effects of spacing, stiffness, and head fixity of piles and inclination of slope on the moment and lateral soil pressure distributions acting on slope stabilizing piles were investigated with a series of model tests. The behavior of soil around piles, the effect of soil-pile displacements on the load transfer from soil to piles and the group behavior of piles were examined.

Surficial soil displacements were also monitored and relative displacements between the soil particles were determined by recording time-lapse images throughout the test in order to observe the trace of soil arching mechanism on the soil surface.

Real slope stabilizing piles constructed as double row were back analyzed. In the light of back analyses, the loads acting on pile rows, considering the loads calculated by theories based on plastic deformation were found out and the importance of pile socket length and third dimension effects were determined.

Keywords: Slope stabilizing piles, model tests, load transfer mechanism, soil-pile displacement behavior

ŞEV STABİLİTESİ KAZIKLARINDA YÜK TRANSFER MEKANİZMASI İÇİN MODEL ÇALIŞMA

ÖZ

Eğimli gevşek kum zemin içerisindeki sonsuz sayıdaki kazıkların bir dilimi, deney düzeneği ile simüle edilmiştir. Deney düzeneği; içerisinde model deneylerin gerçekleştirildiği test kutusu, uniform ve homojen gevşek kum zemin oluşturulmasını sağlayan yağmurlama sistemi, alüminyum model kazıklar, yük ve deformasyon ölçüm sistemleri ile veri toplama sisteminden oluşmaktadır. Dünyadaki en büyük boyutlara sahip olma özelliğini taşıyan test kutusu, ankastre kazık ucuna sahip tek ve iki sıra rijit ve esnek model kazık testlerine olanak sağlayabilmektedir. Zeminin dışarıdan bir kuvvetle yatay harekete zorlandığı önceki çalışmaların aksine, zeminin kayma yüzeyini temsilen eğimli bir yüzey üzerinden aşağı doğru hareketi deplasman ve hız kontrollü bir düzenekle sağlanmış, zemin sadece kendi ağırlığının etkisiyle kaydırılmıştır. Kazık mesafesinin, kazık rijitliğinin, kazık başı mesnetlenme koşulunun ve şev açısının şev stabilitesi kazıklarındaki moment ve zemin basıncı dağılımlarına etkileri çok sayıda model test ile araştırılmıştır. Kazık civarındaki zemin davranışı, zemin-kazık deplasman ilişkisinin zeminden kazığa yük aktarma mekanizmasına etkisi ve kazıklardaki grup etkisi incelenmiştir.

Ayrıca zemin yüzey deplasmanları da görüntülenmiştir. Zemin yüzeyinde kemerlenme mekanizmasını görüntüleyebilmek amacıyla yüzey zemin daneleri arasındaki göreli deplasman değerleri testler boyunca belli zaman aralıklarında fotoğraflar alınarak belirlenmiştir. Son olarak, şev stabilitesi amacıyla inşaa edilmiş olan iki sıra kazıklı sistemin geri analizleri yapılmıştır. Geri analizler ışığında, kazık sıralarına etki eden yüklere plastik deformasyona dayalı teoriler kullanılarak karar verilmiş, kazık davranışı üzerinde kazık soket boyu ve üçüncü boyut etkileri belirlenmiştir.

Anahtar sözcükler: Şev stabilitesi kazıkları, model deneyler, yük aktarma mekanizması, zemin-kazık deplasman davranışı

CONTENTS

Pages

CHAPTER ONE
INTRODUCTION

1. 1 General

The piles may be broadly classified as active or passive piles depending on how the lateral load is transmitted to the piles. Active piles are subjected to a horizontal load at the head and transmit this load to the soil along their lengths. On the other hand, passive piles, also referred as stabilizing piles, are loaded by lateral movement of surrounding soil, therefore in this case, soil movement is the cause and pile deflection is the effect.

The stabilization of slopes by installing a row of a large diameter cast in place reinforced concrete piles has come into widespread use as an effective means against excessive slope movement in recent years (Fukumoto, 1972; Fukuoka, 1977; Sommer, 1977; Viggiani, 1981; Ito and Matsui, 1977; Nethero, 1982; Gudehus and Schwarz, 1985; Carruba et al., 1989; Reese et al., 1992; Rollins and Rollins, 1992; Hong and Han, 1996; Poulos, 1995; Zeng and Liang, 2002; Christopher et al., 2007). Stabilizing effect is provided by the passive resistance of the pile below the slip surface and load transfer from the sliding mass to the underlying stationary soil or rock formation through the piles due to soil arching mechanism (Chen et al., 1997; Chen and Martin, 2002; Liang and Zeng, 2002; Kahyaoğlu et al., 2009).

Once the movement occurs within the slope above the sliding surface, soil is forced to squeeze between the piles and shear stresses are developed by the relative displacement of the two masses in the transition zone between the moving and stationary masses. The shearing resistance tends to keep the yielding mass on its original position by reducing the pressure on the yielding part and increasing the pressure on the adjoining stationary part (Bosscher and Gray, 1986; Adachi et al., 1989; Pan et al., 2000; Cai and Ugai, 2003; Zhao et al., 2008). This transferring process of forces is called soil arching which normally depends on soil properties,

spacing between piles, and relative movement between the soil and the pile (Chelapati, 1964; Ladanyi and Hoyaux, 1969; Evans, 1983; Iglesia, 1991).

Although many extensive theoretical and empirical approaches and modifications of these approaches are developed for the estimation of slope stabilizing pile response (Poulos, 1973; Ito and Matsui, 1975; Baguelin et al., 1976; Viggiani, 1981; Winter et al., 1983), a widely accepted general rules have not been developed for practical use due to complexity of the problem, inherent variability of soil properties and variety of affecting factors such as penetration depth to the stable soil, pile rigidity, relative strengths of sliding and stable soils, pile spacing, and the fixity condition at the pile top. The experimental data are also needed in order to assess the validity of the modified and existing theories describing slope stabilizing pile response and load transfer mechanism.

An experimental test setup has been established in order to simulate a slice from an infinitely long row of piles in an inclined sand bed. The effects of the pile spacing, pile stiffness, pile head fixity and slope inclination on the moment and lateral soil pressure distributions acting on slope stabilizing piles were investigated in a series of model tests. The behavior of soil around piles, the effect of soil-pile displacements on the load transfer from soil to piles and the group behavior of piles were examined.

1.2 Objective and Scope of Research

Load redistribution and its transfer to the piles due to the relative movement between the piles and the sliding soil is a fairly complex soil-structure interaction problem. This interaction is a function of soil type, pile spacing, pile bending stiffness, and length of the pile in the sliding soil. The analysis of a slope reinforced with piles requires that the forces acting on the stabilizing piles or the lateral force reactions to the sliding mass to be known. In order to achieve the first goal of this dissertation which is the evaluation of the load transfer mechanism of passive pile groups in purely cohesionless soils, three dimensional finite element analyses have been performed. The effects of relative pile/soil displacement, soil properties, and

pile spacing on soil arching and the load displacement behavior of piles are investigated by a series of numerical simulations. Firstly, three-dimensional finite element analyses have been carried out to determine lateral load distributions along single piles and group of free head piles that vary with pile spacing, pile arrangement and relative movement between the pile and soil. The main purpose is to consider the effect of pile spacing and pile arrangement on the load transfer mechanism and the group behavior of a pile in a row of piles.

Secondly, a series of model tests on flexible and rigid piles in one and two rows are carried out in a specially designed and manufactured box filled with sand. Soil movement is generated by its own weight on contrary to the previous experimental studies, where the sliding soil is forced to make uniform horizontal or triangular displacement. The behavior of soil around piles, the effect of soil-pile displacements on the load transfer from soil to piles are examined. The soil surface displacements were also monitored and evaluated via digital image analysis techniques in order to observe the soil arching mechanism on the soil surface for pile groups with different pile head condition. The objective of the work presented in this thesis is to provide experimental data to investigate the moment and pressure distributions acting on passive piles in a row and two rows in slope stabilization applications. The bending moment and pressure distribution are interpreted from the deformation of instrumented piles. This includes a better understanding of the load transfer process from soil to piles and the group behavior of piles with the effects of pile spacing, pile rigidity, pile head fixity, slope inclination and relative movement of pile rows.

Lastly, double-rows of passive piles constructed for the stabilization of a landslide were back analyzed by means of two different three dimensional finite element models. One of the models targeted structural analysis of the double row system with an emphasis on the influence of relative movement of the front and rear pile rows on load share between the front and rear pile rows. The second one was a full three dimensional model including piles and the surrounding soil. Measured displacements of piled retaining system were also compared with the back calculated displacements. In the light of back analyses, the loads acting on pile rows,

considering the loads calculated by theories based on plastic deformation are determined and the importance of pile socket length and third dimension effects are decided.

1.3 Organization of Dissertation

The dissertation consists of eight chapters. Chapter 1 (this chapter) outlines a general introduction and the objective and scope of this study and the organization of the dissertation.

A review of pertinent literature is presented in Chapter 2. This begins with general description of laterally loaded piles, followed by a summary of active and passive piles and current design methods for predicting limit soil pressure.

The investigation of single pile and group of free-head piles subjected to lateral soil movements via 3D finite element analysis are presented in Chapter 3. The effects of pile spacing, pile-soil interface roughness, relative displacement between the pile and soil and the variation of angle of internal friction on the lateral response of a pile in a row in cohesionless soil are presented in this chapter. The mobilization mechanism of resistance and the load transfer mechanism around passive pile groups are discussed from the standpoint of the arching effect.

The dimensional details of an experimental setup are presented in Chapter 4. Mean particle size of soil, the dimensions of testing box allowing flexible pile tests are determined considering scaling effects. Ultimate lateral soil pressures that would act on the model piles were estimated in order to consider the mode of failure. Also the prototype piles representing the characteristics of model piles are determined considering the scaling principals.

A description of the experimental apparatus is presented in Chapter 5. The apparatus consists of a model container, soil, a pluviation system, model piles, and an instrumentation system to measure moment, pressure, head displacements, and

loading of the piles. Chapter 5 also contains a summary of laboratory test procedures starting from the construction of the test setup to the evaluation of the measured data.

The testing program is described and experimental results are presented in Chapter 6. The description explains how the tests are divided among three groups to varying pile spacing, box inclination, and row numbers. Results for each test containing pile and box displacement, moment, and pressure distribution along pile length, and pile loads are also presented.

The determination of surficial soil displacements using digital image analysis techniques is presented in Chapter 7. Relative displacements between the soil particles were determined by recording time-lapse images throughout the tests containing free and fixed head rigid piles.

Analysis of a case study where double-rows of passive piles were used to stabilize a sliding soil mass is also presented in Chapter 8 with an emphasis on the influence of relative movement of the front and rear pile rows on load share between the front and rear pile rows. Field inclinometer readings were back analyzed and compared with computed pile displacements using two different 3D finite element analyses.

Finally, a summary of this thesis, and conclusions based on the results of this work are presented in Chapter 9.

CHAPTER TWO
LITERATURE REVIEW OF LATERALLY LOADED PILES

Lateral loads have at least the same importance as axial compressive loads on piles and therefore they must be carefully taken into consideration during design. The sources causing lateral loads include earthquakes, waves, wind, earth pressures and other external sources. These forces are typically more challenging to design because of their variability. The causes resulting in lateral loading of piles are extremely variable and all of them may not be analyzed by using a single technique (Hsiung and Chen, 1997).

The analysis of laterally loaded piles is considerably more complex than methods used to determine the capacity of axially loaded piles, which often may be solved by force equilibrium. Laterally loaded piles require a complete understanding of soil-structure interaction and should satisfy geotechnical and structural design criteria. A pile must also be evaluated to confirm its structural integrity. The behavior of laterally loaded piles involves a three dimensional, non-linear, soil-structure interaction. This response depends upon a combination of soil and structural properties (Bransby and Springman, 1999).

When laterally loaded piles are analyzed, the relationship between the length and flexibility of pile relative to the surrounding soil is important. Short piles behave as if they are more rigid causing the soil to reach its ultimate capacity prior to yielding of the pile. Alternatively, longer piles provide flexible responses that tend to deform when subjected to sufficiently large loads (Cai and Ugai, 2003).

The widespread acceptance of procedures of analyzing laterally loaded piles has increased significantly over the past several decades. Unfortunately, these methods do not apply to all loading scenarios where calculations incorporate changes occurring within both the pile and the surrounding soil.

Laterally loaded piles are described by a number of characteristics depending upon the geometry and material of the pile, soil properties and the source and duration of the lateral loading. Lateral loading of a pile may be due to ‘active’ loading where external loads are applied at the pile head or due to ‘passive’ loading where lateral movement of the soil induces bending stresses in the pile (Pan et al. 2002). In the following sections, active and passive piles are explained in more details, respectively.

2.1 Active Piles

Active piles are explained here in detail although they are not the main aim of this thesis, because analytical models proposed for active piles have been used to obtain a theoretical solution for passive piles.

The magnitude of the soil reaction to a laterally deforming pile is a function of the pile deflection, which depends on the pile rigidity and loading conditions. Thus solving the behavior of a pile under lateral loading involves solution of a complex soil-structure-interaction problem.

Lateral loads and moments on a vertical pile are resisted by the flexural stiffness of the pile and mobilization of resistance in the surrounding soil as the pile deflects. Figure 2.1 shows the mechanism where the ultimate soil resistance is mobilized to resist a combination of lateral force (P) and moment (M) applied at the top of a free-head pile.

The ultimate lateral resistance (Q_u) and the corresponding ultimate moment (M_u) can be related to the ultimate soil resistance (p_u). The soil resistance against the lateral movement of the pile can be considered in two components; the frontal normal reaction (Q) and the side friction reaction (F) (Briaud and Smith, 1983; Smith, 1987) as shown in Figure 2.2. Lateral capacity of flexible (long) piles is primarily dependent on the yield moment of the pile whereas the lateral capacity of short rigid piles is mostly dependent on the soil resistance.

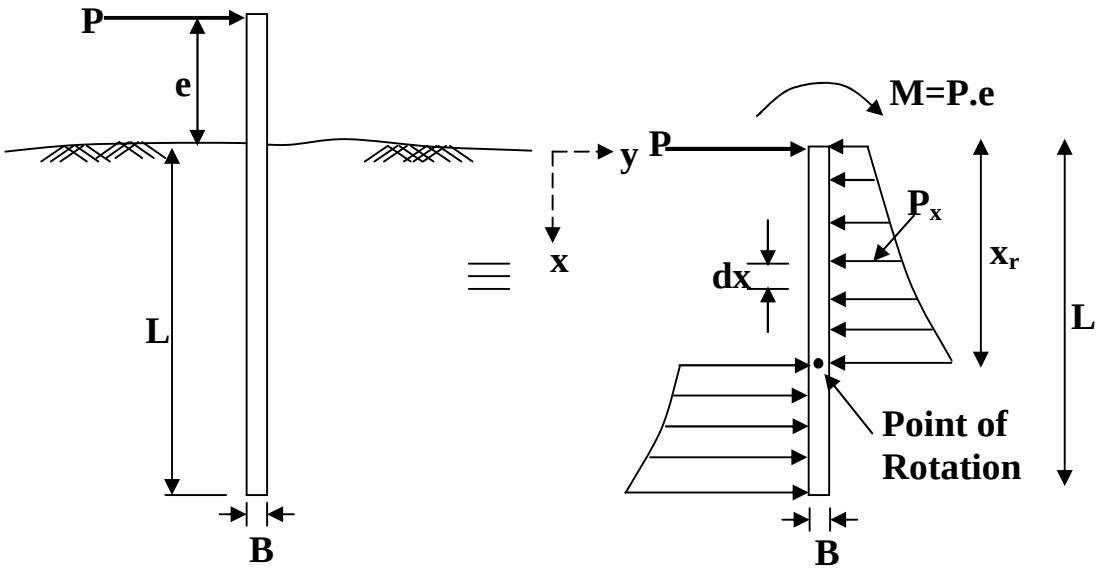

Figure 2.1 Mobilization of lateral resistance for a free head laterally loaded rigid pile (Briaud and Smith, 1983).

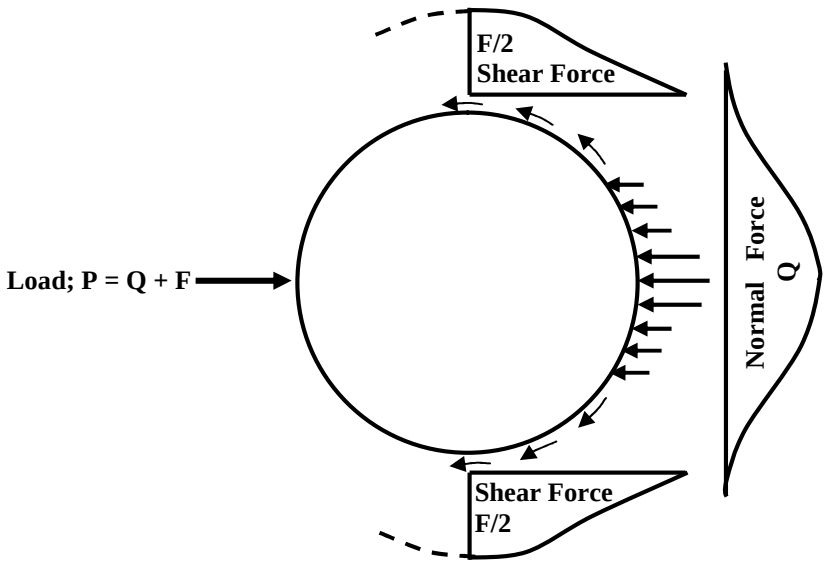

Figure 2.2 Distribution of front earth pressure and side shear around pile subjected to lateral load (Smith, 1987).

Laterally loaded piles should satisfy geotechnical and structural design criteria. In general, the geotechnical design criteria dictate pile dimensions (i.e. diameter and length) and pile type. The maximum moment in a free-head pile with a horizontal load at the top depends on the relative pile-soil stiffness factor and loading

conditions. It occurs typically at a depth of 0.1-0.4 times the length of the pile below the surface (Hsiung and Chen, 1997). The maximum deflection, on the other hand, usually takes place at the top of the pile. In current design practice where performance based design has become a crucial task in earthquake prone areas, geotechnical engineers are expected to predict accurately both maximum deflection and moment in the design stage (Hsiung, 2003).

Methods for calculating lateral resistance of vertical piles can be broadly divided into two categories: (a) Methods for calculating ultimate lateral resistance, and (b) Methods for calculating acceptable deflection at working lateral load. The latter approaches are usually preferred over the ultimate lateral resistance based methods since soil-structure interaction analyses of pile supported structures require evaluation of deformation levels (Moayed et al., 2008).

Many researchers (e.g. Brinch Hansen, 1961; Matlock and Reese, 1961; Broms, 1964; Spillers and Stoll, 1964; Davisson, 1970; Poulos, 1971; Petrasovits and Award, 1972; Banerjee and Davis, 1978; Kuhlemeyerr, 1979; Randolph, 1981; Meyerhof et al., 1981; Georgiadis and Butterfield, 1970; Vallabhan and Alikhanlou, 1982; Verrujit and Kooijman, 1989; Sun, 1994; Murthy and Subba Rao, 1995) have investigated the laterally loaded pile behavior and ultimate lateral resistance to piles. They assume some form of lateral soil pressure distribution along the length of the pile. A few investigators have measured actual soil pressure distribution along the length of rigid piles using pressure transducers (Adams and Radhakrishna, 1973; Chari and Meyerhof, 1983; Joo, 1985; Meyerhof and Sastry, 1985), and it was found that the actual soil pressure distributions were somewhat different from the assumptions made in their analysis. These methods use varying techniques towards the solution of this problem and can be broadly classified into five categories. In most of these categories the pile is modeled as an elastic beam.

Early research on laterally loaded piles was done by Brinch Hansen (1961) and Broms (1964). The Brinch Hansen’s Method is based on earth pressure theory for soils with both cohesion and friction. It is applicable for only short piles in layered

soils. It consists of determining the center of rotation by taking moment caused by all forces about the point of load application and equating it to zero. The Broms' method is based primarily on the use of limiting values of soil resistance and solution of the static equilibrium of the pile. In this approach the soil reaction is related to pile deformation at working loads by means of horizontal subgrade modulus (k_h). Although it offers ready-to-use design charts for free and fixed head piles, the Broms method is only applicable to fully homogenous cohesive and cohesionless soils.

The second category uses Winkler approach. The soil reaction force on any point on the beam is directly proportional to the displacement of the beam at that point, for modeling the soil behavior. The pile, in most cases, is modeled as an elastic beam and the soil is modeled as a set of nonlinear springs. The method can be applied to represent soil varying in any manner with depth and under static or cyclic loading conditions. The method can also handle nonlinear soil response reasonably well and has been found to predict response that compares favorably with field behavior in the design level up to large deflection range. However, unlike the elastic continuum method, soil interactions are not taken into account because it is assumed that the displacements at a point are not influenced by stresses and forces at other points within the soil (Doherty et al, 2005; Hartmann and Jahn, 2001).

The third category adopts an elastic continuum approach, which is theoretically sounder; Poulos (1971) proposed a linear analysis methodology based on the theory of elasticity where Mindlin's governing equations (1936) are integrated using a finite difference method. The soil in this case is assumed as an elastic, homogeneous, isotropic mass having constant elastic parameters E and ν with depth. Also the pile is considered to be a thin vertical strip having width or diameter (B), length (L), and constant flexibility (E_pI_p). The most significant simplification in the Poulos' approach is that soil and pile are assumed to be fully compatible and the horizontal shear stresses developed between the soil and the sides of the pile are not taken into account. The lateral behavior of a pile is influenced by the length-to-diameter ratio, L/B, stiffness of the pile and relative stiffness of the pile/soil material.

The fourth category is the finite element solution technique. The finite element method (FEM), which is more versatile than the finite difference method, has been widely used as the most efficient mean for evaluating soil-pile interaction (Wang, 1997; Almeida and Paiva, 2000). One of the primary advantages of the finite element method is that it can be easily extended to a stratified soil medium by taking material nonlinearity and slippage along the soil-pile interface into account. The pile-soil system can be analyzed three dimensionally. Although this is the case, 3D modeling of the pile and the surrounding soil requires intensive study during modeling stage resulting in high analyses costs which usually are not justified for majority of the projects. The complexity of the laterally loaded pile problem, however, not only arises due to the need for expensive analysis procedures but also due to the variability of soil properties and alterations of these properties as a result of pile manufacturing methods. Therefore, probabilistic approaches for reliability analyses are frequently recalled for laterally loaded piles in order to address inherent uncertainties.

In the next section, these categories are explained in more details.

2.1.1 Subgrade Reaction Approach

The subgrade reaction approach provides the simplest solution for the pile-soil problem under lateral loading and the origin of the method can be attributed to Winkler (1867). The method has been adopted and subsequently modified over the years for analyzing piles subjected to external load (Terzaghi, 1955; Matlock and Reese, 1960; Brinch Hansen, 1961; Broms, 1964; Reese, 1985). It has also been used in a limited way to analyze piles subjected to lateral ground movements (e.g., Fukuoka, 1977; Yoshida and Hamada, 1991; Reese et al., 1992; Meyersohn et al., 1992). The popularity of this particular method is due to conceptual simplicity and the ease with which nonlinear soil behavior can be introduced in the solution procedure. In this approach the pile is treated as an elastic laterally loaded beam. The soil is idealized as a series of independent springs with constant stiffness, where the lateral load at one point does not affect the lateral load at other points along the depth

of the pile. The spring forces are assumed to be proportional to the relative displacement between pile and soil.

The spring stiffness, or modulus of subgrade reaction, is defined as the ratio of the soil reaction per unit length of the pile as described in the following equation (Eq. 2.1):

$$p = K_h y \tag{2.1}$$

where p, is the soil resistance per unit length of the pile, K_h is the modulus of subgrade reaction, and y is the lateral deflection of the pile.

The behavior of the pile is assumed to follow the differential equation of a beam (Eq. 2.2):

$$E_p I_p \frac{d^4 y}{dz^4} + K_h y = 0 \tag{2.2}$$

where, z is the length along pile, and E_pI_p is the flexural stiffness of pile. Numerical and analytical solutions are readily available from the equation (Heteny, 1946).

When the pile is subjected to lateral soil movements, the loading arises from soil displacements, δ, and equation can be rewritten as

$$E_p I_p \frac{d^4 y}{dz^4} + k_h y = k_h \, d(z) \tag{2.3}$$

Ideally, the displacements, bending moments, and stress-strain of the pile can be obtained from the solution of above equation. The difficulties occur when assigning appropriate values to soil modulus, k_h. In fact, k_h is neither a constant, nor a unique property of the soil. It depends on several factors such as pile size, pile flexibility, and confining pressure (Terzaghi, 1955). Moreover, it exhibits considerable nonlinearity with displacement, y.

The soil reaction often varies with depth making necessary an expression to describe this change. There are several such approaches used to describe the variations in the modulus of subgrade reaction. The below equation (Eq. 2.4) uses an exponential relationship based on the modulus of subgrade reaction at the tip of the pile (Palmer and Thompson, 1948).

$$k_h = k_L \left(\frac{x}{L} \right)^n \tag{2.4}$$

where, k_L is modulus of subgrade reaction at the tip of pile, L is the length of pile, n is empirical constant (greater than or equal to zero) and x is the depth within soil.

In the above equation a value of n approaching 0.0 is typically used for clays providing a near constant modulus with depth. For sandy soils a value of n near 1.0 is preferred, allowing the modulus to increase linearly with depth. The below equation (Eq. 2.5) is an alternative which can describe linearly increasing modulus of subgrade reaction.

$$k_h = n_h \, x \tag{2.5}$$

where, n_h is coefficient of subgrade reaction.

2.1.2 *p-y Method*

The p-y method is an evolution from the subgrade reaction method. It shares similarities with the previous approach but contains one significant improvement. It allows the soil to provide a non-linear reaction.

A p-y curve represents the lateral soil reaction, load per unit length of shaft, p, for a given lateral, y, at a given depth on the pile shaft. The method was developed from the subgrade reaction, in which a pile is idealized as an elastic, transversely loaded beam supported by a series of unconnected linearly elastic springs representing the soil (i.e., Winkler’s soil model). Since the relationship between soil reaction and

lateral displacement for soils is nonlinear, the p-y method has been, hence, developed to overcome the shortcoming of the subgrade reaction method by the introduction of the nonlinear soil springs. Several methods to obtain p-y curves have been presented in the literature (McClelland and Focht, 1958; Matlock, 1970; Reese et al., 1974, Reese and Welch, 1975; Reese and Desai, 1997; Stevens and Audibert, 1979; Geogiadis and Butterfield, 1982; O'Neill and Gazioğlu, 1984; Murchison and O'Neill, 1984; Dunnavant and O'Neill, 1985). These methods rely on the results of several empirical measurements. Some researchers, (Gabr and Borden, 1990; Ruesta and Townsend 1997, Robertson et al. (1984, 1985, 1987)) have attempted to enhance p-y curve evaluation based on in-situ tests such as cone penetration, pressuremeter and dilatometer. However, such attempts have focused on soil part of soil pile interaction behaviors. Robertson et al. (1985) developed a method that used the results of a pushed in pressuremeter to evaluate p-y curves of a driven displacement pile.

At any location along the pile the reaction may be described by a unique distributed load versus displacement characteristics, known as a load transfer function (Reese, 1977). The use of load transfer functions provides flexibility and allows the response to vary in a nonlinear manner (Reese, 1977). His method offers a straightforward approach for describing the complex soil-structure interactions occurring when a vertical pile is laterally loaded.

The development of a set of p-y curves can introduce a solution to the differential equation, and provide a solution for the pile deflection, pile rotation, bending moment, shear and soil reaction for any load capable of being sustained by the pile.

The application of p-y analyses requires use of computer programs. A pile is divided into n intervals, with a node at the end of each interval. Soil is modeled as a series of nonlinear springs located at each node, the flexural stiffness of each interval is defined by the appropriate E_pI_p, and the load deformation properties of each spring are defined by a p-y curve.

Attempts towards deriving p-y curves using three dimensional finite element models have been provided by Brown et al. (1988 and 1989). A simple elastic-plastic material model is used to model undrained static loading case in clay soils. P-y curves are developed from the bending stresses in the pile, where nodal stresses along the pile are used to obtain bending. The results from the 3D finite element model were compared with the ones produced by the finite difference method using COM624 (1993), and the American Petroleum Institute (API) RP-2A (1979) design curves for soft clay. One commonly used set of curves has been given for loose, medium dense and dense cohesionless granular materials is based on finite element analyses by Clough and Duncan (1971).

One limitation associated with using a soil spring model is that the springs behave independently of time and do not account for dynamic loading conditions.

2.1.3 Continuum-based Method

In a continuum-based method such as the boundary element method or the finite element method, the continuity of the soil domain is inherent in formulations.

In a linear boundary element formulation, Mindlin's solution for a force at a point on semi-infinite solid (Mindlin, 1936) was used to analyze behavior of piles subjected to lateral loading, in which the soil was considered as a isotropic elastic continuum with modulus (E_s) and Poisson's ratio (ν) by many researchers (Douglas and Davis, 1964; Spillers and Stoll, 1964; Poulos, 1971a and 1971b; Banerjee and Davies, 1978). All these analyses are similar in principle; the differences arise largely in details in the assumptions regarding the pile action. For example, Douglas and Davis (1964) presented solutions for the displacement and rotation of a thin, rigid vertical plate subjected to a lateral load and bending moment in an elastic half space. Poulos (1971a) presented solutions for flexible vertical strips. The Poulos' analyses are described below.

The pile is assumed to be a thin rectangular vertical strip of width D, length L, and constant flexural rigidity E_pI_p where E_p is the elastic modulus of the pile and I_p is the moment of inertia of the pile section. The beam equation (Eq. 2.6)

$$E_p I_p \frac{d^4 y}{dz^4} = -p_h D \tag{2.6}$$

where y is the pile deflection at a point; z is the depth in soil; p_h is the horizontal soil pressure between soil and pile at the point.

The soil is assumed to be an ideal homogeneous, isotropic, semi-infinite elastic material, with a Young's modulus E_s and Poisson's ratio υ, which are unaffected by the presence of the pile. It is also assumed that the soil at the back of the pile near the surface adheres to the pile.

To simplify the analysis, possible horizontal shear stresses developed between the soil and the sides are neglected. Each element is assumed to be acted on by a uniform horizontal stress p_h, which is assumed to be constant across the width of the pile.

In purely elastic conditions within the soil, horizontal displacements of the soil and the pile are equal along the pile shaft. In this analysis, the soil and pile displacements at the element centers are assumed equal.

Solutions of the method, as mentioned above, are applicable only to the cases where the lateral forces are low and soil movements are within the elastic range. In order to account for nonlinear soil behavior, Poulos (1979) extended the elastic solutions to incorporate the local yielding of soil. Budhu and Davies (1987) also developed a method to incorporate soil yielding in analyzing laterally loaded piles. Both the methods of Poulos (1979) and Budhu and Davies (1987) use similar algorithm (i.e. the boundary element technique) and consider the bearing failure in the compressive soil zone for calculating the soil yielding stress. The main difference between the two methods is that Budhu and Davies (1987) takes into account the interface slip at the limiting shear stress and gapping in the tensile soil zone. An

account is then taken of the continuous nature of soil; parametric study using this method enhances the understanding of behavior of laterally loaded piles. However, the solutions are usually restrictive to homogeneous soils or soils with linear increasing modulus. In addition, although soil yielding has been incorporated using an elastic-perfectly plastic model, this would be of limited validity as a nonlinear analysis because the soil begins to behave nonlinearly well before the ultimate pressure is reached (Cerioni and Mingardi, 1996; Vitharana, 1997).

In this method, the soil is represented as a homogeneous, linear, and isotropic elastic material. The assumed soil properties are very different from these assumptions in reality. The major drawback of this method is the incapability of handling the nonlinear behavior of the soil. The soil modulus is not a constant but varies significantly with applied strain. The modulus is also dependent on confining pressure and increases with the measuring confining pressure at depth. Actual soil-pile interaction becomes more complicated by yielding of the soil and gap formation between the pile and the soil. The theory fails in accounting for some soil characteristics such as, pre-consolidation, and pile-soil separation.

To model nonlinearity and soil yielding, Poulos and Davis (1980) incorporated soil yield pressures and variations of elastic modulus in the solution procedure. In the modified procedure, an ultimate pressure, p_{hu}, is predefined. If the calculated pressure goes beyond the ultimate pressure, the pressure is readjusted to p_{hu} and the calculation is iterated until the yield condition is satisfied. The variation of modulus is incorporated by using a vector of modulus E_s, representing soil modulus at different depths, in place of a single value of E_s. These two modifications introduce nonlinearity and inhomogeneity for which Mindlin's solution is no longer valid. Poulos and Davis (1980) suggested that the modified method should be used in caution. The piles are assumed to be flat plates so that their incorporation in the model will be compatible with Mindlin's solution. In reality, piles have finite dimensions and the effects of their presence on the elastic solutions are not well-defined. Poulos and Davis (1980) have tested their method against some documented case histories (Heyman and Boersma, 1961; Leussink and Wenz, 1969). The

comparison produced mixed results, but the general trend was consistent with the measured values of pile stresses for the first two cases. Poulos and Davis (1980) suggested that this method can be extended for the analysis of pile groups with the expression about the influence of the pile group on the value of yield pressure, p_{hu}. Another issue that needs to be considered in pile group analysis is the effect of pile group on free-field soil displacement.

2.1.4 Finite Element Method

The finite element method (FEM) is considered to be the most powerful tool in modeling soil-structure interaction involving non-linear material behavior (Esqueda, 2004; Esqueda and Botello, 2005).

Versatility of the method allows modeling different pile and soil geometries, capability of using different boundary, and combined loading conditions. Discretization of the model into small entities allows finding solutions at each element and node in the mesh, feasibility for modeling different types of soil models and various material behaviors of piles. The ability to account for the continuity of soil behavior is the advantage of the method.

Several researchers have used the FEM to model the soil-pile interaction. Desai and Appel (1976) presented a finite element procedure that can allow nonlinear interaction effects, and simultaneous application of axial and lateral loads. The pile is modeled as a one-dimensional beam element and the interaction between the pile and the soil is simulated by a series of independent springs. The variations of the generalized displacements and internal forces are described by means of energy functional incorporating the joint structure concept. Thompson (1977) developed a two dimensional finite element model to produce p-y curves for laterally loaded piles. The soil was modeled as an elastic-hyperbolic material. Desai and Kuppusamy (1980) introduced a one dimensional finite element model, in which the soil and the pile were simulated as nonlinear springs and a beam column element, respectively. The Ramberg-Osgood model was used to define the soil behavior. Faruque and Desai

(1982) implemented both numerical and geometric non-linearity in their three-dimensional finite element model. The Drucker-Prager plasticity theory was developed to model the non-linear behavior of the soil. The researchers declared that the effect of geometric non-linearity can be crucial in the analysis of pile-soil interaction.

Among other factors, the success of a finite element analysis depends on the use of proper constitutive laws and proper choice of elements that can model the actual physical behavior. For example, proper interface elements are needed to model slip and possible gap formation between piles and the surrounding soil. To properly model soil-structure interaction between piles moving soil, it is necessary to have a three-dimensional representation. This involves large computational effort (Estorff and Firuziaan, 2000; Klar and Frydman, 2002; Maheshwari et al., 2004).

Greimann et al. (1987) conducted a three-dimensional finite element analysis to study pile stresses and pile-soil interaction in integral abutment bridges. The model accounted for both geometric and material non-linearities. Non-linear springs were used to represent the soil, and a modified Ramberg-Osgood cyclic model was used to obtain the tangent stiffness of the nonlinear spring elements. Koojman (1989) presented a quasi three-dimensional finite element model. The rational behind his model is that for laterally loaded piles, the effect of the vertical displacements is insignificant. Therefore, it is plausible to divide the soil into a number of interacting horizontal layers. For these layers an elastoplastic finite element discretization is used. The contact algorithm in this model was based on defining an interface element, which characterized the tangential and normal behavior of pile and soil contact. This simulated slip, and rebounding of the pile and the soil. Biinagte et al. (1991) developed a three-dimensional finite element analysis of soil-structure interaction. The model utilized an elastic-perfectly plastic theory implementing the Tresca and the Mohr-Coulomb failure criteria. The paper introduced recommendations for the design of piles and design values for thermal expansion coefficients. Kumar (1992) investigated the behavior of laterally loaded single piles and pile group using a three-dimensional non-linear finite element modeling.

The most sophisticated finite element models are capable of three-dimensional predictions using continuous, dynamic, nonlinear soil elements. One challenge is that these methods are often too complicated and time consuming for most design purposes. The current application of this method applied to dynamic loading conditions remains largely limited to academic research and for only the most sophisticated design projects. Nevertheless, this requires validation using results from well controlled tests.

2.2 Passive Piles

Typical examples of passive piles are; the piles adjacent to deep basement excavations and tunnels, slope stabilizing piles, and piles supporting bridge abutments adjacent to approach embankments.

Actually, pile used against the slope movement is one example of the typical passive piles. Recently, there has been an increasing interest in the use of piles for slope stabilization purpose. An increased popularity of using piles to stabilize an unstable slope in highway applications could be attributed to several factors: (1) various construction techniques are available for installing piles in almost any type of soil and rock conditions; (2) lateral load test can be performed to verify the lateral load-resistance capacity of the piles; (3) the use of piles avoids the need to address the right-of-way issues that may be needed for other types of slope stabilization methods; (4) the piles sometimes offer a reliable and economical solution compared to other slope stabilization methods; and (5) the piles are typically structurally capable of resisting long-term environmental effects. Since the displacement of the soil mass above the potentially sliding surface is expected to be more significant than that beneath the sliding surface, significant shear force and bending moment will develop in the drilled shaft at the location close to the potential sliding surface. This mechanism works in a way similar to a cantilever beam with the earth pressure on the drilled shaft as load and the part of the drilled shaft socked in rock as the fixed end. It is in this way the earth pressure developed due to a potential sliding soil mass is transferred to the soil beneath the potential sliding surface. Therefore, excessive

soil movement can be prevented, and thus a slope is stabilized through the reinforcement mechanism.

It is well known that problems arose from passive piles are more difficult than those from active ones, because the lateral force acting on the passive piles due to the movement of the slope is related to the interaction between the piles and the surrounding soils and hereby is unknown in advance. Ideally, the stabilization mechanisms of piles should be investigated using three dimensional, nonlinear theories accounting for the interaction effects. Such an approach is at present quite unfeasible due to uncertainties involved in the description of nonlinear behavior of the surrounding soil and the complexity of the geometry of the slope and the reinforcing system.

Arresting an unstable slope using a single row of piles requires the soil engineers to determine the following important key points: (1) piles diameter; (2) spacing between the piles to ensure development of soil arching; (3) the necessary socket length of the piles in the non-yielding strata (e.g., rock) so that the piles act as a cantilever against the moving soil; (4) location of the piles within the slope body so that the global factor of safety of the stabilized slope is optimized for the most economical configuration of the piles; (5) the forces transferred to the piles due to sliding mass.

There have been numerous documentations in the literature regarding the successful utilization of piles to stabilize slopes (e.g., Fukumoto, 1972 and 1973; Esu and D'Elia, 1974; Fukuoka, 1977; Sommer, 1977; Viggiani, 1981; Ito and Matsui, 1975 and 1977; Ito et al., 1979, 1981 and 1982; Nethero, 1982; Morgenstern, 1982; Gudehus and Schwarz, 1985; Carruba et al., 1989; Reese et al., 1992; Rollins and Rollins, 1992; Hong and Han, 1996; Poulos, 1995 and 1999; Zeng and Liang, 2002; Christopher et al., 2007). However, the available methods dealing with slope stabilizing piles do not provide enough information on how to stabilize landslides using piles especially because of the many idealized assumptions made by several investigators trying to overcome the complexity and difficulties encountered. In

addition, these idealized assumptions sometimes have led to over designing the slope stabilizing piles with respect to geotechnical and structural aspects, which in turn, would increase the cost associated with the construction process of the landslide repair. So, for these reasons, there is a compelling need to (a) develop a step-by-step design methodology that allows the engineers perform a complete design for landslides stabilization using piles; (b) perform real-time field instrumentation and monitoring to understand better the behavior of the piles and the overall stability of the slope/pile system; and (c) combine the theoretical and the actual findings to ensure an economical and safe design.

Reduction in shear strength of the soil and increase in shear stress are the basic causes of slope failure. Installing a row of piles, socketed enough into a stable soil and spaced properly apart so that soil can not flow around the shafts, would reduce the shear stresses; this in turn, would lead to satisfactory stabilization of slope. Once the excessive movement occurs within the slope above the slip surface, soil is forced to squeeze between the piles and shear stresses are developed by the relative displacement of the two masses in the transition zone between the moving and stationary masses. Since the shearing resistance pretends to keep the yielding mass on its original position by reducing the pressure on the yielding part and increasing the pressure on the adjoining stationary part (Bosscher and Gray, 1986; Adachi et al., 1989; Pan et al., 2000; Cai and Ugai, 2003; Zhao et al., 2008). This transferring process of forces is called soil arching which is a phenomenon of transfer of stresses from a yielding mass onto the adjoining stationary part of soil, which normally depends on soil properties, pile rigidity, spacing between piles, and relative movement between the soil and the pile, the fixity condition at the pile top (Chelapati, 1964; Ladanyi and Hoyaux, 1969; Evans, 1983; Iglesia, 1991).

The formation of the arch is described in terms of radial and tangential stresses of soil. As for isolated piles subject to lateral soil movement, radial stresses develop in front of grouped piles. The difference between isolated piles and grouped piles is that the directions of the major principal stresses from grouped piles do not extend radially from the pile centers, but rather form an arch (Thompson et al., 2005). The

arch is the path of the major principal stress, and the direction perpendicular to the arch is direction in which the minor principal stress acts. The major principal stress increase is still accompanied by a decrease in the minor principal stress.

One of the requirements to practicing soil engineers is to understand fully the factors influencing the development for the soil arching. Incorporating the arching mechanism into slope stability analysis and thereafter the stabilization design, however, requires a comprehensive investigation of the conditions of soil arching to develop (Poulos, 1995; Pan et al., 2002; Liang and Yamin, 2009).

The methods of analysis of piles and pile groups subjected to lateral loading from lateral soil movements are generally categorized into four groups (Stewart, 1992):
(1) empirical method, where the pile response is estimated in terms of maximum bending moment and pile cap deflection on the basis of charts developed from experimental data (2) earth pressure based method, where the distribution acting against the piles is estimated in a relatively simple manner and is often used only to calculate the maximum bending moment in the piles (3) displacement-based method, where the distribution of lateral soil displacement with depth is introduced and the resulting pile deflection and bending moment calculated and (4) finite element analysis method, where the piles are represented in the mesh and the overall soil-pile response is included. However, the empirical method needs empirical design chart and the design chart cannot be used if the specific site condition is different from the site condition from which the data was obtained. Furthermore, the empirical method cannot take into account of the effects such as the pile spacing, pile dimensions, and slope angle. The earth pressure based method involves the stability analysis of both the slope and pile. The major problem involved is the determination of lateral load acting on a drilled shaft. The displacement-based method is a half empirical method and accurate description of free field soil movements is a priori which is extremely difficult to do. Finite element analysis method is a better approach to analyze the interactive system of soil and pile, but it is usually expensive and sometimes proper representation of boundary conditions, the soil-pile interface, and the soil model may not be easy. A brief review of each method is given below.

2.2.1 Empirical Methods

Empirical methods have been proposed by several authors to estimate lateral pressure on piles induced by soil movement. All these methods were developed for piles in soft clay subjected to deformations generated from adjacent embankment construction. De Beer and Wallays (1972), Tchebotarioff (1973), Nakamura (1984) and Stewart et al. (1994) proposed similar approaches for estimating the lateral earth pressure on piles due to surcharge loads. They have proposed several empirical relationships on the basis of field and laboratory test results for estimating maximum bending moment and shear in the piles, and wide design envelopes for maximum bending moment and deflection were suggested. The advantage of this method is that it can provide a means for a quick and rough estimate of the likely behavior of a group of piles. The suggested earth pressure coefficients are based on observations from a limited number of field cases involving soft clay. On the other hand, the design chart cannot be used if the specific site condition is different from the site condition from which the data was obtained. Furthermore, it is very difficult to take into account of the effects such as the pile spacing, pile size, and slope angle when the empirical method is used.

2.2.2 Pressure Based Methods

These methods rely on the semi-analytical derived pressure distribution, or the resultant force, acting on the pile to determine the factor of safety (FS) of the piles stabilized slope.

The definition of FS of a slope with the stabilizing piles within the framework of limiting equilibrium slope stability analysis technique has not been well established. Limit equilibrium analysis in conjunction with the method of slices is the most widely used method for evaluating stability of slopes. The techniques can accommodate complex geometry and variable soil properties and water pressure conditions. The limit equilibrium analysis method can provide a global safety factor against sliding. Numerous limit equilibrium methods for slope stability analysis have been proposed by several investigators, including the celebrated pioneers Fellenius

(1936), Bishop (1955), Janbu (1954), Morgenstern and Price (1965), Spencer (1967), and Sarma (1973). These efforts, however, were related to a slope without piles. The analysis of a slope stabilized with the piles requires a development of an approach to account for the contribution of piles. Furthermore, the earth pressures applied to the piles are highly dependent upon the relative movement of the soil and the piles, which in fact is an indeterminate problem as the structural response of the pile depends on the earth pressure applied, which in turn, relies on the structural response (deflection) of the pile.

The current design practices for the design of slopes stabilized with a single row of piles often use the limit equilibrium method, where the soil-pile interaction is not considered, and the piles are assumed to only supply additional sliding resistance (Ito et al., 1975, 1979, 1981, 1982; Steward et al., 1994; Poulos, 1995; Lee et al., 1995; Chow, 1996; Chen and Poulos, 1997; Hassiotis et al., 1997). The key to the limit equilibrium method is an accurate estimation of the lateral pressure acting against the stabilizing piles, which is in turn, the reaction force from the piles against the slope sliding.

There are two steps involved in the determination of earth pressures acting on the piles constructed on a slope. The first step is to determine the earth pressure in the section of a slope where the piles will be installed; the second step is to determine the distribution of the calculated earth pressures onto each pile.

The limit state considered for the limit soil resistance is failure of the soil above the sliding surface by flow around or between the piles and limit soil pressure (P_u) can be defined as lateral pressure on the pile that will cause the soil to fail laterally at a particular depth. The total limit resistance based on failure of soil above the sliding surface is obtained by integrating the computed limit soil pressure over the pile length above the sliding surface. For stability analysis, this total limit resistance force is assumed to act at the sliding surface. The total resistance increases from a minimum value at the ground surface to a maximum value at the tip of the member. Since stability analyses are generally performed for cross-sections of unit width, the

total resisting forces computed by integrating the limit soil pressure are divided by the longitudinal spacing to produce values of the limit force per unit width of slope suitable for stability analyses.

Baker and Yonder (1958) calculated the pressure on the piles by the procedure of slices and considered the piles as cantilever beams, provided that they penetrate into a stable layer for one third of their total length (Figure 2.3). However, analyzing the pile group as a retaining wall can lead to very conservative design, since soil arching between the piles is not taken into account.

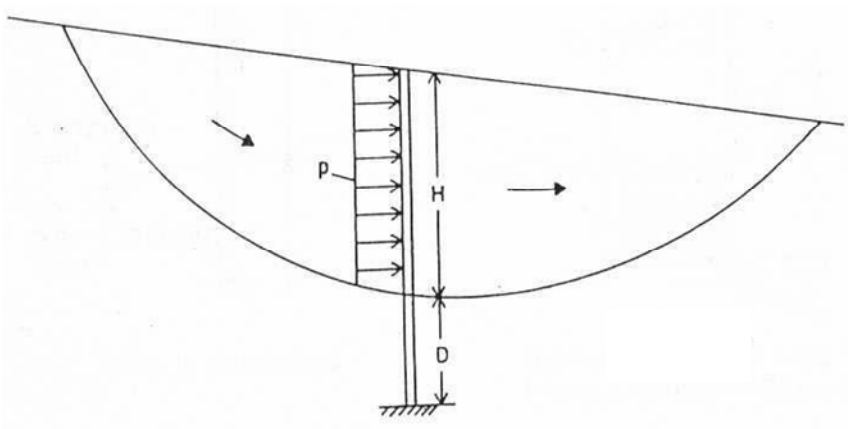

Figure 2.3 Design method of piles in landslide by Baker and Yonder (1958).

Piles should be penetrated into a stable soil by such an amount that the reaction should stop the movement which will develop. The depth of penetration should be estimated from the structural solution of the pile. The point of rotation should be within the depth of embedment, and also the negative pressures developed on the pile in the penetrated depth should be within allowable limits. To find the appropriate depth, a pile of infinite length is analyzed and the point at which the bending moment and shear forces approach zero is located. Embedding the pile deeper than this point will not increase its stability. The depth of penetration in the stiffer lower soil is usually less than half of the sliding upper depth.

Wang and Yen (1974) reported a design method based on a rigid-plastic soil arching. Their study comprises a classic infinite slope analysis where the soil behaves as a rigid plastic solid and into which piles are rigidly embedded in a single

row (Figure 2.4). The theory also indicates a relationship between slope length and arching potential while the necessary slope length to develop arching fully is approximately 6 fold inner distances between pile faces (s-d). The uniform soil pressure parallel to the ground surface, p(z), is a function of the soil unit weight, angle of internal friction, cohesion intercept of yielding layer and angle of internal friction, cohesion intercept of potential failure surface, coefficient of lateral pressure at rest, and slope angle. The load on each pile embedded in sandy slopes is the summation of two loads, one from the pressure at rest, acting on the pile, similar to the lateral pressure on a retaining wall. The other is the soil arching pressure transferred to the adjacent piles as if each pile is an abutment of an arc dam.

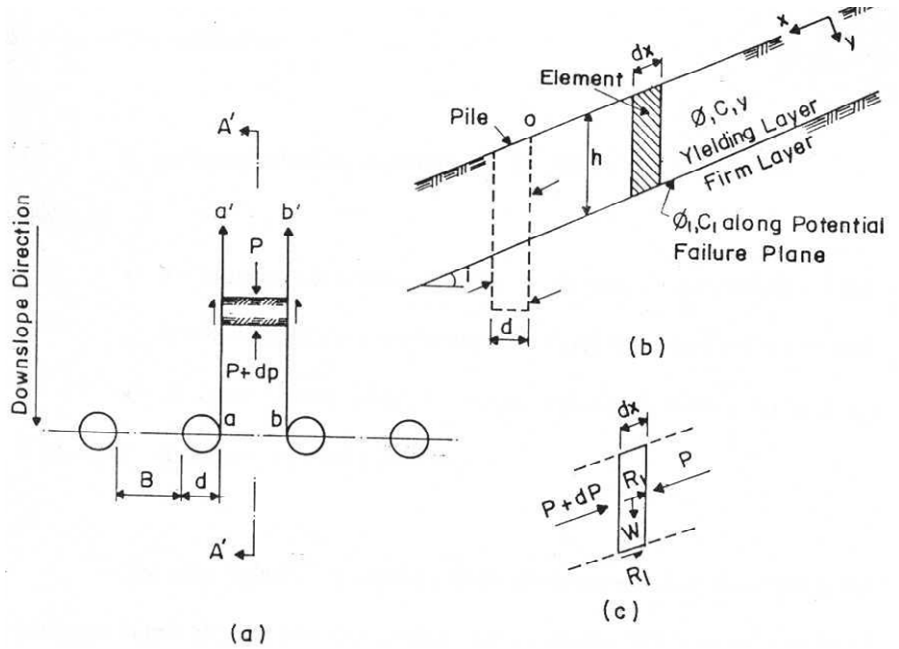

Figure 2.4 Views of piles on slope: a) Plan b) Cross-section c) Element (Wang and Yen, 1974).

Ito and Matsui (1975) proposed a method to predict the lateral force acting on stabilizing piles in a row when the soil is forced to squeeze between piles based on the theory of plastic deformation. They considered two types of plastic states in the ground surrounding the pile. One state, referred to as Theory of Plastic Deformation, satisfies the Mohr-Coulomb's yield criterion and the other state, referred to as Theory of Plastic Flow considers the ground as a visco-plastic solid. The lateral load can be estimated regardless of the state of equilibrium of the slope assuming that no

reduction in the shear resistance along the sliding surface has taken place. As the name indicates, the main assumption in this approach is that the soil is soft and able to deform plastically around the piles, while other assumptions are; the piles are rigid, the frictional forces between the pile and the soil are neglected, the active earth pressure acts on inner distance between pile faces, two sliding surfaces occur making an angle of (45+ϕ/2) with soil movement direction with the soil deformation (Figure 2.5). They also assumed that the normal stress on these planes is the principle stress.

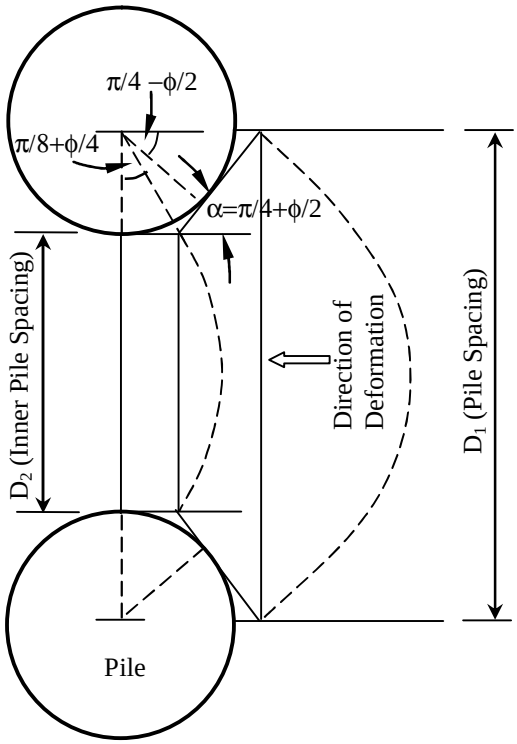

Figure 2.5 State of plastic deformation in the ground just around piles (after Ito and Matsui, 1975).

An equation (Eq. 2.7) was expressed as a function of the soil strength, pile diameter, spacing and location was derived to estimate the lateral load distribution acting on a row of piles caused by lateral soil movement (Ito and Matsui, 1975; Ito and Matsui, 1979; Ito et al., 1981).

$$p(z) = cD_1\left(\frac{D_1}{D_2}\right)^{(N_f^{1/2}\tan f + N_f - 1)}\left(\frac{1}{N_f \tan_f}\left(\exp\left(\frac{D_1 - D_2}{D_2} N_f \tan_f \tan\left(\frac{p}{8} + \frac{f}{4}\right)\right) - 2N_f^{1/2}\tan f - 1\right)\right.$$
$$\left. + \frac{2\tan f + 2N_f^{1/2} + N_f^{-1/2}}{N_f^{1/2}\tan f + N_f - 1}\right) - c\left(D_1 \frac{2\tan f + 2N_f^{1/2} + N_f^{-1/2}}{N_f^{1/2}\tan f + N_f - 1} - 2D_2 N_f^{-1/2}\right)$$
$$+ \frac{g\,z}{N_f}\left(D_1\left(\frac{D_1}{D_2}\right)^{(N_f^{1/2}\tan f + N_f - 1)} \exp\left(\frac{D_1 - D_2}{D_2} N_f \tan f \tan\left(\frac{p}{8} + \frac{f}{4}\right)\right) - D_2\right) \qquad (2.7)$$

where c is cohesion intercept; D_1 is center to center distance between piles; D_2 is opening between piles; ϕ is internal friction angle of soil; γ is unit weight of soil; z is depth from ground surface; and $N_\phi = \tan^2(\pi/4 + \phi/2)$

P (z) may vary from zero when there is no movement to limit pressure at large lateral deformations. Soil arching was not mentioned and the sloping ground was not taken into account either. The linear distribution of the calculated load is show in Figure 2.6. The limit soil pressure per unit area of pile face, P_z, is obtained by dividing the limit force computed from the equation by the length of the pile.

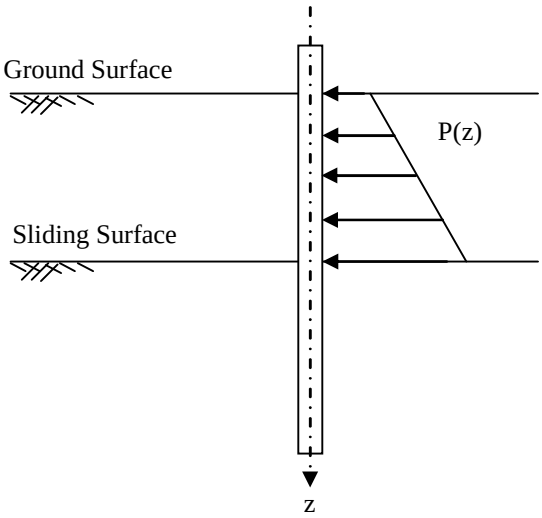

Figure 2.6 Load distribution of Ito and Matsui Method.

Ito and Matsui (1975) compared their results of the Theory of Plastic Deformation to field measurements in the landslide areas of Niigata in Japan. The comparison revealed that the forces estimated by the Theory of Plastic Deformation agreed for

the most part with the observed values. It was found that the closest agreement was for piles with restrained heads.

If a portion of that force is assumed to counter act the driving force of the slope, the safety factor of the slope stabilized with piles can be calculated as a function of pile size and position based on the limit equilibrium method. Although this approach appears useful, the model is derived for rigid piles, which may not represent the actual piles in the field as they are likely to be rigid. The model may also provide doubtful solutions when the piles are closely spaced. Although this method has been widely used, considerable uncertainty remains about group effects (Chen and Poulos 1994).

Ito and Matsui (1977) inspected the effects of conditions of pile head fixity on the stability of laterally loaded piles. The effects of the various conditions of pile head fixity on the pile stability was discussed for steel pipe piles in a row through plastically deforming ground assuming that the distributed lateral load acting on the piles above the sliding surface can be calculated using the equation, and that the reaction acting on piles below a sliding surface is proportional to the deflection of the pile. They have concluded that the safety factor for shear force are sufficiently larger than that for bending moment, and that the stability of piles can be judged by the latter. It was concluded that the smaller the deflection at the pile head is, the larger the safety factor on the pile stability becomes. Thus, in order to use the effects of piles in a row on preventing the slide of slope to the outmost limits, it may be generally considered to be more effective to restrain the deflection at the pile head, either as hinged or fixed. The distributions of deflection, shear force and bending moment of the pile with different fixity conditions of the pile head for Ito and Matsui (1977) case is given in Figure 2.7.

.

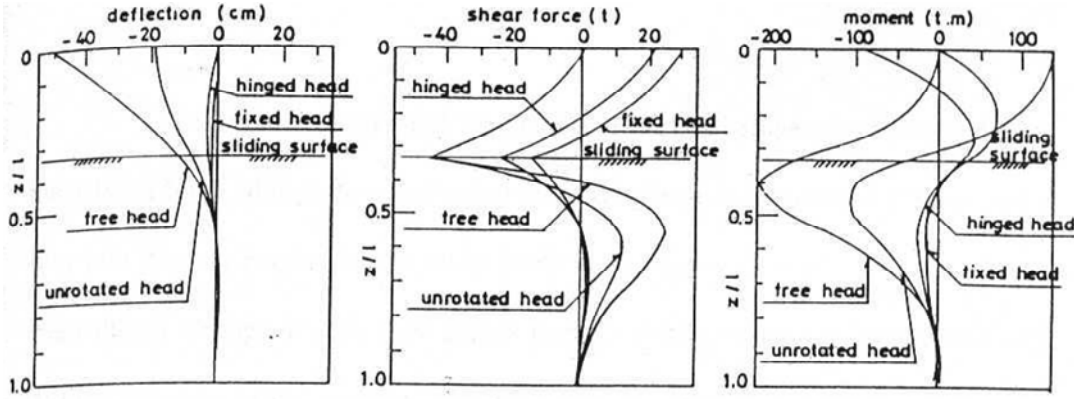

Figure 2.7 The calculated distributions of deflections of shear and bending moment acting on a pile (Ito and Matsui, 1977).

Ito et al. (1981) investigated the problem of piles placed in a row within a slope, which has a fixed sliding surface, as in the case of landslide, by considering piles and slope stability. Ito et al. (1982) investigated the problem of multi-row stabilizing piles placed in the soil mass with a fixed sliding surface.

To check the validity of their theoretical derivation of the lateral pressures on passive piles in a row, Matsui et al. (1982) used scaled modeling. An apparatus using air pistons pushed a block of soil through a row of model piles. In general, their theory was satisfactory in predicting lateral loads over a wide variety of cases. However, this modeling is not exactly applicable to real slopes since the soil was pushed perpendicularly to the piles. A more realistic model must allow for both the vertical and rotational movements of the soil mass. These are the factors which will have a significant effect on the stresses along a potential failure surface and must be accounted for when analyzing the stability of the slope (Oakland and Chameau, 1984).

Hassiotis and Chameau (1984) determined the pressure distribution against the piles; no concern was given to the changing stress distribution along the remainder of the failure surface and used the resulting forces in a limit equilibrium analysis of the slope. The strength of this approach is that the method used to determine the pressure distribution against the piles has been developed exclusively for this purpose, based on elastic-plastic theory, and has been shown to give good results in

models (Matsui et al., 1982). The Hassiotis and Chameau approach should be used to determine the factor of safety analysis of simple cases where piles are to primarily absorb lateral forces and the parametric relations of pile size and spacing for specific cases of gentle slopes supported laterally.

Popescu (1991) proposed a design procedure for preventing the movement of an existing landslide with concrete piles for the use of reinforcement of the unstable mass. In this design procedure both slope stability and pile stability was taken into account. The reaction force of piles was evaluated on the basis of Ito-Matsui theory (Ito and Matsui, 1977). The effect of pile diameter, pile spacing between piles and the fixity condition of pile heads on the slope and pile stability were investigated. Popescu stated that lateral pile force increases with increasing diameter. However, the relation between the safety factor of the slope and the interval ratio (s/d) is uniquely regardless of pile diameter. Figure 2.8 shows an example of the distribution of bending moment for the piles with 1m diameter and spacing ratio s/d of 1.7, with the fixity condition of the pile head as a variable parameter.

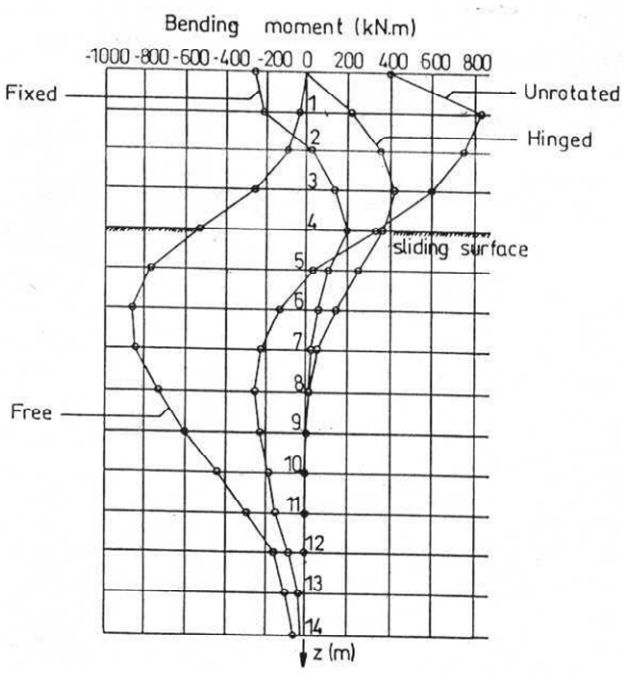

Figure 2.8 Distribution of bending moments for different pile head fixity conditions (Popescu, 1991).

Reese et al. (1992) presented a rational method for the analysis of drilled shafts used for slope stabilization. The method assumes a vertical shaft and considers only the horizontal forces imposed by the moving soil above the sliding surface. The method uses the *p-y* method, based on soil-structure interaction principles, to determine the horizontal forces acting on the shaft.

Zeng and Liang (2002) proposed a mathematical formulation based on interslice force equilibrium to predict the factor of safety for slope reinforced with piles. This approach would allow for not only the determination of the safety factor of the reinforced slope, but also the forces acting on the piles. The influence of pile location, size and spacing on the computed factor of safety can be examined utilizing this approach. As the soil mass moves through the piles, the driving force transmitted to the soil mass behind the piles is reduced by a reduction factor (R), which is related to both pile and soil parameters, leading to a higher stability of the slope as a result of soil arching. The cross-section of piled slope is illustrated in Figure 2.9.

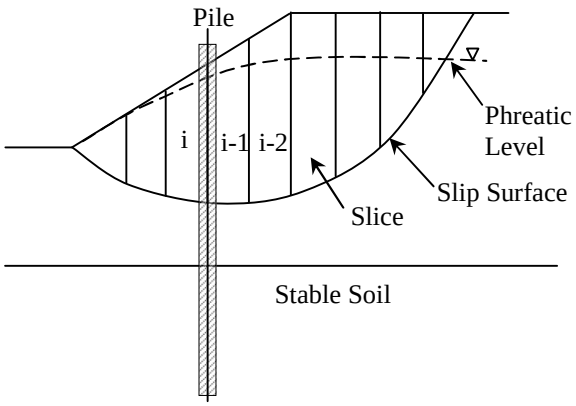

Figure 2.9 Cross section of slope with piles.

The forces acting on the slice are W_i, the weight of the slice; P_{i-1}, P_i, the resultant interslice forces on the $(i-1)^{th}$ and i^{th} interfaces, respectively; N_i, the normal force reaction on the base of the slice; and T_i, the shear force reaction on the base of the slices. Also, α_{i-1} and α_i are the average slopes of the bases of the slices i-1 and i, respectively. The resultant interslice force is assumed to be parallel to the base of the

previous up-slope slice, with the point of application located at one third from the bottom of the interface (Figure 2.10).

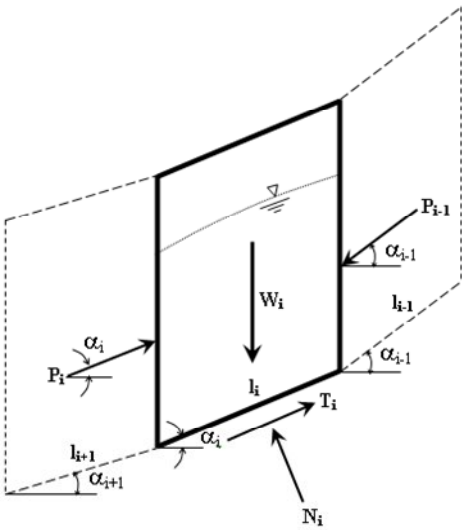

Figure 2.10 Forces acting on a typical slice.

The force equilibrium of slice i requires, in the direction parallel to N_i, and similarly perpendicular to N_i, and resultant interslice force can be computed with the equations given below.

$$P_i = W_i \sin a_i - \left[\frac{c_i l_i}{F} + (W_i \cos a_i - u_i l_i) \frac{\tan f_i}{F} \right] + k_i R P_{i-1} \quad (2.8)$$

where

$$k_i = \cos(a_{i-1} - a_i) - \sin(a_{i-1} - a_i) \frac{\tan f_i}{F} \quad (2.9)$$

P_i depends on the safety factor (F), thus an iterative computational scheme is required. Iterative computational process should continue until the calculated P_n at the toe slice matches zero. The development of soil arching was assessed by the degree to which the driving force was transferred to the piles. The soil pressure acting on the soil mass between the piles due to soil arching was calculated and normalized with respect to the initial pressure to obtain a percentage factor R_p and the variation of pile spacing ratio and internal fiction angle with this factor is given in Figure 2.11.

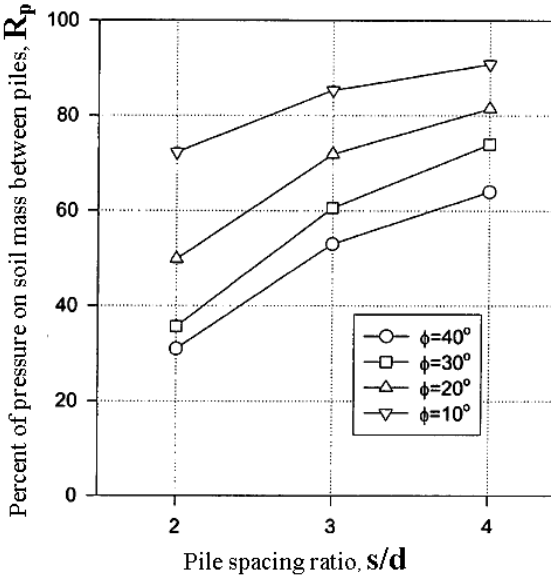

Figure 2.11 Effect of variation in angle of internal friction on R_p (after Zeng and Liang, 2002).

If the value of R_p is 100%, it means that no arching effect exists and all soil pressure would be fully transmitted to the soil mass downslope. The more net force would act on the pile while the value of R_p is smaller where the stronger the soil arching effects. Reduction factor (R) is given below in the expression with pile spacing and R_p.

$$R = \frac{1}{s/d} + (1 - \frac{1}{s/d})R_p \quad (2.10)$$

The net load acting on one pile is;

$$P_{pile} = \frac{(1 - R_p)P_{i-1}}{\frac{s}{d}} \quad (2.11)$$

For any reason, if there is no relative movement between soil mass and the piles, then there would be no arching effect and no net force acting on the piles.

2.2.3 Displacement Based Methods

In these methods, the magnitude and pattern of the lateral soil displacement are used to determine the resulting deflection and bending moment of the pile. Stewart et al. (1994) developed one of such methods. The particular situation considered was an embankment of soft clay foundation as an approach to a piled bridge abutment. They suggested two types of displacements based design methods. One was the proposed by Springman (1989), in which a simple soil deformation mechanism was used in deriving the relationship between the lateral earth pressure acting on a pile and the relative soil-displacement.

The other displacement based method was developed by Poulos (1973, 1995), in which the free field soil movement was used as input in a modified boundary element method to compute the axial and lateral response of piles subjected to these prescribed soil movements. The solution incorporates nonlinear soil-pile interface elements that can represent a hardening or softening response prior to reaching an ultimate state. The influencing factors such as position of piles, shear strength of soil, soil layer thickness, conditions of fix, and restraint at the pile head and the installation sequence of piles can be considered.

Lee et al. (1995) used the approach to determine the reaction force from the piles, and used Bishop's simplified method to study the most effective means of using piles for stabilizing slopes. The assumption that the pile tip is free to displace and to rotate limits the application of the results.

Chow (1996) presented a numerical model for the same purpose, where the piles are modeled using a hybrid method of analysis. The method simulates the soil response at individual pile using the subgrade reaction modulus, and the pile-soil-pile interaction using the theory of elasticity. Chow's approach is capable of predicting the behavior of the piles; including the magnitude and distribution of bending moments, shear forces, pile deflection and rotation.

Guo (2003, 2006) proposed a simplified approach for prediction of pile response due to lateral soil movement. This concept, which allows a correlation between an equivalent load and the magnitude of soil movement, is based on elastic-plastic solutions for either a free-head or fixed head pile. The response of this pile due to soil movement can be resolved into two-portions in the sliding soil and the stable soil, respectively. The portion in the lower stable layer may be treated as an imaginary free-head pile under an equivalent load P (Figure 2.12). The length of the imaginary pile is the difference between the pile length and the thickness of the upper sliding layer.

Generally speaking, the displacement based method is superior to the earth pressure based method, because it reflects the true mechanism of soil-pile interaction. However, it should be pointed out that accurate description of free soil movements is a priori condition to the accuracy of the calculated loads applied to the pile, and in most cases such description is difficult to gain.

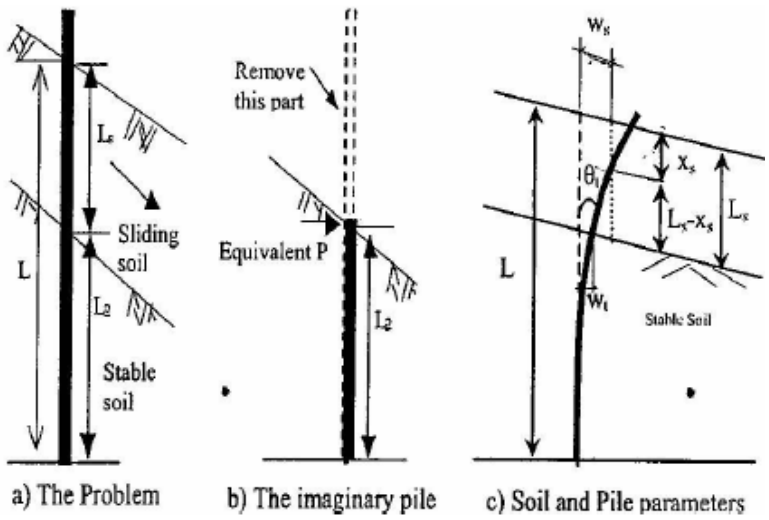

Figure 2.12 Simplified analysis of pile due to soil movement (Guo, 2003).

2.2.4 Finite Element Analysis

There have been numerous types of finite element representations for piles subjected to lateral soil movements. For example, some were axisymetric analysis with nonsymetric loading (Carter, 1984), some were plane strain analysis (Rowe and Poulos, 1979; Sirawardane et al., 1984; Stewart et al., 1993; Chen and Poulos, 1997; Liang and Zeng 2002), and some were three-dimensional analysis (Oakland and Chameau, 1984; Springman, 1989).

Rowe and Poulos (1979) have discussed the applicability of finite element technique to the analysis of slope stabilization incorporating passive piles. They employed a two-dimensional finite element model for soil structure interaction. It was concluded that the effect of piles upon slope stability increases very slowly with the stiffness and that it may be necessary to use very stiff piles to obtain any significant improvement in slope performance; and the effectiveness of piling is enhanced by provision of head and toe restraint, and is also enhanced where the soil stiffness and strength increases with depth.

The soil stratigraphy and embankment loading of a typical problem of this nature can often be depicted adequately by a cross-section parallel to the direction of soil movement. Representation of this cross-section with a finite element mesh is then relatively straightforward, and the piles could be modeled with similar to those used for the soil (Sirawardane et al., 1984), or beam elements incorporated into the soil mesh (Stewart et al., 1993).

Chen and Poulos (1997) investigated the behavior of single and group of piles using finite element methods. A plane strain analysis is applied to a horizontal plane within the soil mass. The effect of a row of pile can be considered by employing an equivalent sheet pile wall with appropriate properties assigned. It is obvious that, in a plane strain representation where the pile is explicitly represented in the finite element mesh, the soil cannot deform as much as it could flow around the pile. Thus, the FEM analysis results may be significantly in error. Piles are mostly used in

groups to support the imposed loads. The behavior of a group of piles is influenced by non-linear-soil-pile interaction and the group effect is mainly depending on spacing of piles with the applied load direction. In designing such piles, an understanding of the pile-soil interaction is desired, since as compared with single isolated pile, piles within a group may suffer some reduction in capacity due to interaction effects. They reported that, the ultimate lateral soil resistance is mainly governed by the pile adhesion (especially for piles with very smooth surfaces) and the properties of the interface between the pile and the soil. Analysis of pile groups show that, because of pile-soil-pile interaction, the ultimate soil resistance is generally lower for a pile in a group than that for a single isolated pile, contrary to slope stabilizing piles.

Liang and Zeng (2002) proposed a finite element analysis technique for quantitatively studying the soil arching mechanism associated with slopes reinforced with piles. Practical design tables developed to relate s/d ratio, pile diameter, and soil strength parameters after performing a series of numerical studies. FEM analysis results form a base for the development of a methodology to determine the force acting on piles considering soil arching. As a part of verification of the accuracy of numerical analysis, experimental measurements available in the literature were compared with the numerical predictions.

It is recognized that a finite element analysis of stabilization problem should make allowance for the soil-structure interaction effects, and also for three-dimensional effects such as arching between piles. To remedy this problem, Oakland and Chameau (1984) modeled the pile with eight node beam elements, in which the beam nodes are defined separately from those describing the soils. In this way, the relative soil movement around the pile was allowed, thus modeling more accurately the soil flow around the pile. It should be pointed out that this relative movement may be of minor importance for very flexible piles, but it can become very significant as the pile stiffness increases. Calculation results of the finite element method not only depend on the proper element representation of the soil and the pile,

but also on the proper representation of boundary conditions, the soil-pile interface, and the soil constitutive model.

Also important is interpretation of finite element analysis results for the purpose of design. It is well known that finite element methods are based on the model where the deformation compatibility and the force equilibrium are both required. Such model is qualified for representing slope deformation behavior under working condition and the finite element results are usually quite accurate and reliable during this state. For the slope stability analysis, however, the so-called safety factor is evaluated based on the critical or limit state where it is assumed the shear strengths on the slip plane are fully mobilized and only equilibrium conditions, precisely some of them, are required. Apparently, the critical state is significantly different from the deformation state under working condition and hence the finite element results have no direct link to safety factor. In brief, it is difficult to evaluate from the finite element results the slope stability for the critical state where limit analysis is required.

2.3 Experimental Studies

Laboratory tests performed by several investigators (Parakash, 1962; Oteo, 1972; Fukumoto, 1975; Ito and Matsui, 1982; Cox et al., 1983; Wang and Reese, 1986; Lieng, 1988; Carrubba et al., 1989; Shibata et al., 1989; Dağıstani, 1992; Kın, 1993; Barradas and Coreiga, 1995; Chen et al., 1997; McVay et al., 1998; Başaran, 1997; Nalçakan, 1999; Analay, 1999; Gültekin, 2001; and Özçelik, 2007) on both active and passive piles. Experimental studies conducted on a single pile or pile groups are summarized below. Test results have shown that, the maximum bending moment induced in the single pile and the group effect on the lateral response of a pile in a group depends on a number of factors, pile spacing, strength of the sliding soil, the amount of soil movements including pile head fixity condition, the ratio of the pile embedded length in the upper moving soil layer to the length in the lower stable soil layer, pile diameter, stiffness, and the position of the pile in the group.

2.3.1 Model Tests on Single Pile

Fukumoto (1975) set a model pile in soil filled in a rectangular iron box, and horizontal load was applied to the model pile by moving the soil in the box using a jack mounted onto the side frame of the box. Deflection of the model pile was measured by using wire strain gages already attached to the pile. Model pile was rectangular in section with different dimensions and was made up of steel and wood. It was concluded that the deformation of piles depends on the flexural rigidity of the pile.

Dagistani (1992) designed a large direct shear box with a cross section of 30x30 cm and a depth of 60 cm to simulate a landslide. The upper part of the box where the shear force was applied was movable and 15 cm deep. He investigated the behavior of a model rigid, a 30 cm long, steel passive pile with miniature stress cells in the clayey soil. Lateral earth pressure distribution was measured in front and at the back side of passive pile from stress cells and the pressure distribution and bearing capacity factors were determined. It was found that previously used methods of estimating the lateral pressure values are over conservative above the sliding surface. It was concluded that bearing capacity factors depend on the depth of penetration and consistencies of the moving and stabilizing soil.

Kın (1993) used the same large direct shear box of Dagistani in his study. Regarding the effect of a single pile on the shear resistance, the change in overall shear resistance due to different pile penetration depths and different consistencies of soil was investigated through displacements, stress distribution on the faces of the pile and total lateral force applied to the shear box. He reported the development of the pressure on a model rigid single passive pile for different penetration depths and different constancies of the soils.

Analay (1999) investigated the lateral resistance of a rigid socketed single model pile, fixed at head, under continuous movement, hence loading, in a cohesionless soil. For this purpose, a shear box with dimensions 20x20x15 cm was designed and constructed. It was a modified shear box, because, there was a rigid, stable steel base

instead of lower part of usual shear box and the upper part slides on that base by rollers. A 10 mm diameter brass pile was loaded laterally under different surcharges and the loading on the pile was measured at both ends by transducers. Limited numbers of tests are performed to study the effect of surface friction characteristics of the pile and shape of the cross-section of the pile. It was concluded that the resistance of the pile against movement of soil increases with increasing surcharge pressure. It was also stated that the increase is more clearly observed at one pile diameter displacement of the box.

Gültekin (2001) performed a laboratory model test to study the behavior of laterally loaded vertical pile in cohesionless soils. For this purpose, an aluminum model pile with a tubular cross-section of 0.022 m. diameter and 0.75 m. length was installed in a sand tank. By measuring the deformations and deflections under the applied lateral loads, some evaluations were made concerning the pile behavior. The test results obtained from the laboratory tests are compared with the theoretical calculation and the relations between them was tried to be determined. The behavior of the pile was observed by the strain-gages located at certain depths of pile and the deformation gages located at the upper part (outside the sand) of the pile.

2.3.2 Model Tests on Pile Groups

Prakash (1962), Oteo (1972), Cox et al (1983), Wang and Reese (1986), Lieng (1988), Shibata (1989) and Barradas and Corregia (1995) conducted experimental lateral loading tests on a group of piles to investigate the efficiencies of pile group and threshold values of pile spacing for group effect. The response of each individual pile within a group was compared with that of a single pile.

Test results indicated that, when the pile spacing was equal to or larger than threshold values, then the piles in a group behaved as if they were single piles. Their findings regarding the effect of pile spacing on the pile group behavior are summarized in Table 2.1.

Table 2.1 Effect of pile spacing on group behavior

Reference	Source of data	Threshold ratio (s / d)
Parakash (1962), Wang & Reese (1986), Lieng (1988)	Empirical curve derived from experimental studies, cited by Reese et al. (1992)	3.5 – 4.0
Cox et al. (1983)	Laboratory model test	3.0
McVay (1995)	Experience and centrifuge model	5.0
Shibata et al. (1989)	Laboratory model test	5.0
Oteo (1962), Barradas and Corregia (1995)	Laboratory model test	6.0

Başaran (1997) investigated the behavior of laterally loaded model single pile and pile groups in dry loose sand. Piles with 8 mm in diameter and 200 mm in length were driven into the sand in groups with 2.5d, 5d, and 10d center to center spacing. All tests were carried out in the box with the dimensions of 600 mm long, 300 mm wide and 300 mm high. The model piles were fixed at their tops to a 345x250x3 mm (width x length x thickness) steel cap. To obtain a frictionless system, the pile cap is supported by two wheels on each side of it. These wheels move on sharp rails attached to the sides of the equipment. Under the rails, there is a small wheel on each side of the cap to prevent any rotational effect. Results of the experiments show that, for the same displacement value, load carried by the group increases with increasing center to center spacing and number of piles in the group. It has been also observed that groups with the piles placed in rows perpendicular to the line of action of the load (side-by-side loading) carried more load than the groups with piles arranged in line with the load.

Chen et al. (1997) described a series of model tests on instrumented pile groups embedded in calcareous sand undergoing lateral movements. A number of tests were performed on a single and group of piles in the apparatus consisted of a testing vessel having internal dimensions of 450 mm wide by 565 mm long and by 700 mm height. Two vertical steel plates, consisting of two parts hinged at mid height, were placed inside the box. With a loading system attached to the steel vessel, the upper part of each steel plate could be rotated around its hinge, and consequently caused the upper part of the sand to move. During the test, the maximum soil movement was measured by transducer which was attached to the outside wall of the vessel. The model piles were made from aluminum tubes, and were 1m in length, 25 mm in

diameter and 1.2 mm in wall thickness. Pile head deflections were measured by displacement transducers.

The extent of the group effect on the lateral response of a pile in a group was found to be dependent on a number of factors, including the position of the pile in the group, the pile spacing, the number of piles, and the head fixity condition. For piles in a row, the maximum bending moment was found to decrease with decreasing pile spacing and was not significantly affected either the number of pile or the pile head condition. For the piles in a line, each pile behaved differently. A rigid pile cap was found to have a significant effect on the pile response, with a tendency to reduce the positive bending moment and develop a relatively negative bending moment in the upper pile portion. In order to investigate the effect of pile-soil-pile interaction on the pile behavior, the response of each individual pile within a group will be compared with that of a single pile. For investigating the effect of pile spacing on the pile response s/d ratio of 2.5, 5.0, 7.5 and 9.0 were adopted for free and fixed head conditions. The group effect was primarily assessed based on the measured bending moments. It was reported that no group action observed when the pile spacing exceeds 9d. The group factor for maximum bending moment (F^m) has been found to be smaller than unity for each case, and it decreases with a decreasing spacing for the both head conditions. The F^m is also smaller for the capped case than for the free-head case which may be attributed to the development of negative bending moment near the top of the pile for the capped case. Reductions of maximum bending moment of about 20% and about 30% as compared with that for the single pile was observed for a pile spacing of 2.5d for the free head case and the capped case, respectively (Chen et al, 1997).

Nalçakan (1999) investigated the loads on passive piles in a row due to sliding cohesive soils. The large shear box used by Dağıstani and Kın was modified and a computerized data accumulation system was designed. Two different types of clays with different undrained strength values were placed in the box. Tensile load transducers were used to measure the passive load on a pile in a group due to moving soil. Additionally, total loads on the piles were measured using a load cell attached to

the shear box. Interpretations were done for different pile spacing ratio (s/d) at the specified box displacements. Group action reduction factors depending on pile spacing, shear strength of sliding cohesive soils and amount of soil movements were recommended to be used in the design stage.

In the study of Ozcelik (2007), for the purpose of providing the slope stability and to observe the behavior of the vertical pile along the lateral soil movement, a large scaled shear box manufactured. Sand is considered with three different densities and case of the stability of slope with pile is studied for modeling. In the experiments empty aluminum pile with d=35 mm diameter is used and the thickness wall of the pile is t = 5.0 mm. Model pile length is 830 mm. Fixed head piles subjected to the lateral loading are in one row and include total 4 piles. Evaluation of the pile behavior under lateral movement can be observed from strain levels and displacements. Data derived from the laboratory tests were compared with the empirical correlations and LPILE program.

CHAPTER THREE
3D FINITE ELEMENT ANALYSES OF MODEL PASSIVE PILES

In this study, a series of numerical simulation study with the aid of finite element method (FEM) have been performed to evaluate load acting on passive pile groups and to determine the behavior of soil around piles due to soil arching mechanism. Firstly, a published experimental model test with a single pile was simulated in order to have a command of control in using the finite element analysis program. Secondly, the problem associated with the displacement effects of embankments sliding on a weak soil on passive piles was examined with a finite number of piles. In this part, model piles were set in a box over a weak layer. The box was forced by applying horizontal external load to make uniform horizontal soil displacement as in the previous experimental studies. Thirdly, the slope stabilizing pile case was simulated with a slice from a infinitely long row of piles. The parametric studies have been carried out to determine the effects of the ratio of pile spacing to pile diameter (s/d) and the angle of internal friction on the load transfer behavior in two different passive pile cases. The load acting on the piles and group behavior of the piles were determined by making use of the numerical results.

3.1 Finite Element Modeling Study

The finite element analysis program, PLAXIS 3D Foundation (Version 1.5) (Brinkgreve and Broere, 2006) was used for the analysis of load transfer process between moving soil and piles and the behavior of soil around piles. Published experimental model test results on soil arching were examined for verification of the numerical analysis (Matsui et al., 1982; Poulos et al., 1995; Goh et al., 1997; Chen et al., 1997; Pan et al., 2000). Following the validation, parametric studies were performed to determine the effects of the ratio of pile spacing to pile diameter (s/d) on the load transfer.

3.1.1 Finite Element Simulation of Single Passive Pile Case

3.1.1.1 Poulos et al. (1995) Laboratory Test and Results

Poulos et al. (1995) have presented laboratory tests, conducted on instrumented model single pile, the results of which are helpful for a better understanding of the pile behavior when subjected to lateral soil movement. A series of laboratory tests was carried out in order to understand the performance of pile subjected to lateral soil movement. In that experimental study, main part of the apparatus consisted of testing vessel having internal dimensions of 450 mm wide by 500 mm long and by 700 mm in height as shown in Figure 3.1.

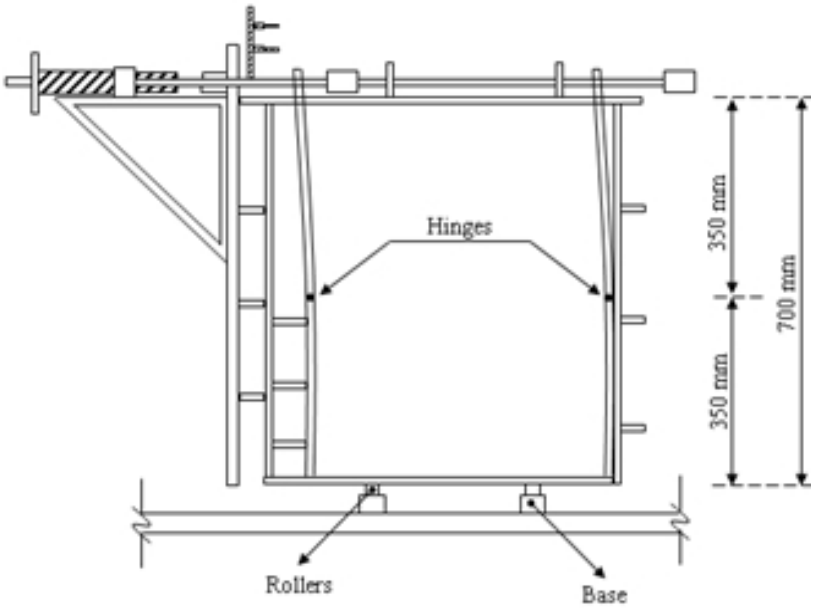

Figure 3.1 Elevation view of testing vessel (Poulos et al., 1995).

The vessel was filled with soil, Young's modulus of which was E_s = 0.025z (in MPa, where z is the depth below the soil surface) with Poisson's ratio of 0.30. The unit weight of soil was γ= 13 kN/m^3 and ϕ was measured as 30°. An aluminum tube of 25 mm in diameter and 675 mm in length, with a bending stiffness of 3.6 x 10^8 kN m^2, is used as a model pile. The side walls of the vessel were hinged at mid height. The lower parts were fixed with bolts while the upper parts were able to rotate about the hinges, thus the soil in the vessel was divided into two regions. The soil in the

lower part was stationary while that in the upper part was subjected to movement. A loading system was attached to the vessel and controlled by a thread. By turning the thread, the upper part was forced to rotate around its hinge and caused the upper part of soil to move. In the model tests, the resistance of pile against a triangular profile of lateral soil movement was determined and the bending moment–depth profiles for the definite soil surface displacements were given in Figure 3.2. The load that caused triangular soil movement, was increased until soil surface displacement (y) reached 65 mm, and it can be seen that the maximum bending moment on the pile increase when the soil surface displacement increased. However, increasing rate decreases after especially the displacements larger than 50 mm. Although the maximum moment cannot be measured exactly, it can be said that the maximum value would be the moment of the test that had 60 mm soil surface displacement as 44.2 kN mm because the moment profiles of 60 and 65 mm were very similar.

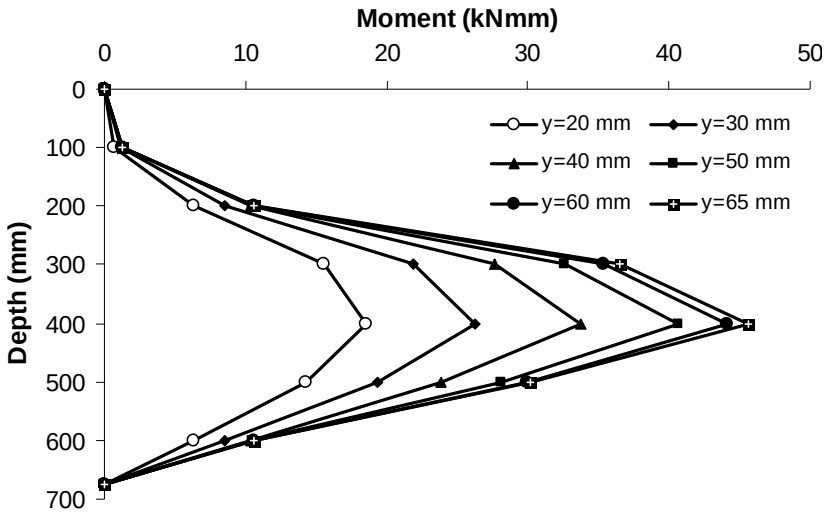

Figure 3.2 Bending moment profiles with respect to soil surface displacement (Poulos et al., 1995).

3.1.1.2 Finite Element Simulation and Verification

A typical test model was simulated and the FEM numerical predictions were compared with the experimental results. The parameters used in FEM analysis were taken directly from Poulos et al. (1995) for comparison purpose. The system used in the study, consists of seven main elements namely, five rigid walls, cohesionless

uniform soil and a model pile. The elevation and the plan view of finite element model simulated by PLAXIS 3D are shown in Figure 3.3a and 3.3b, respectively. In order to simulate the hinges in the mid height of the vessel, horizontal line fixities were used in the work plane of 350 mm.

The points and the positions in Figure 3.3b are selected in order to investigate the effect of pile–soil relative displacement on pile behavior. The point A shows the displacement of soil in front of the pile, the point B shows the displacement of the pile head, the points C and D show the displacement of soil just near the pile and enough far from the pile, respectively. The difference between the displacements of pile head (B) and the soil just near the pile (C) is defined as the relative pile–soil displacement (δ).

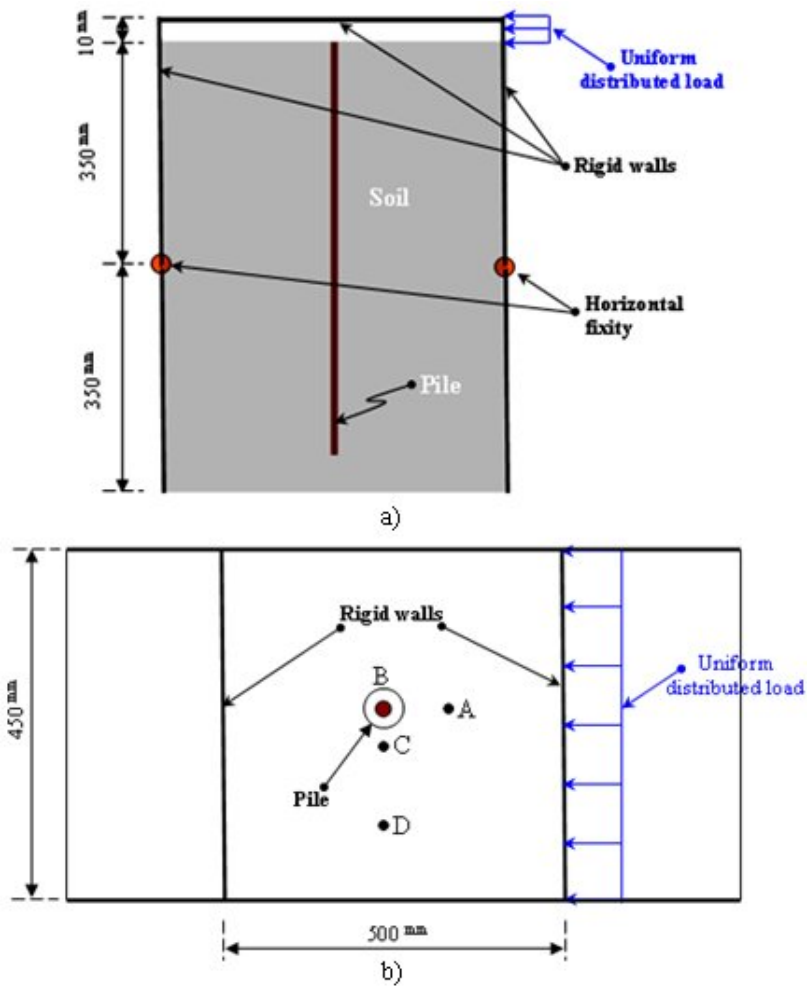

Figure 3.3 Views of model simulation: a) Elevation view b) Plan view

The rigid wall is forced to move by a uniform horizontal load after the removal (excavation) of soil clusters that are in the back and front positions of the box. A soil boundary, which enables displacements only in the horizontal direction, was used in order to simulate the horizontal soil displacement. Various numerical tests were performed on a free-head pile of 25 mm in diameter. Finite element simulation and the deformed shape of 3D mesh are shown in Figure 3.4.

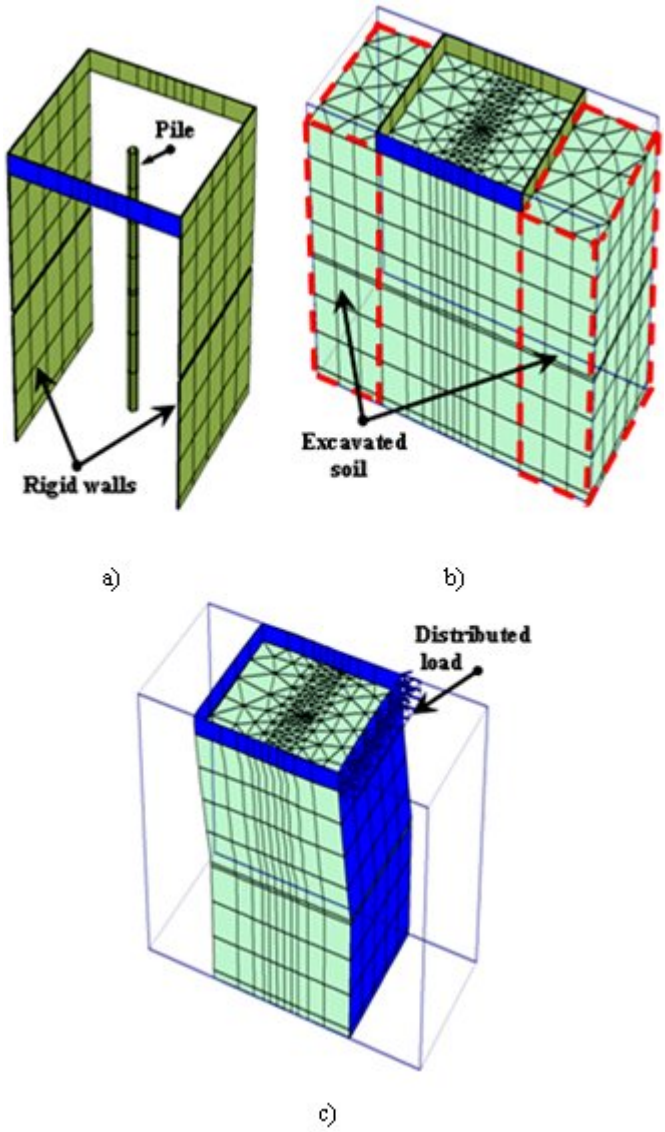

Figure 3.4 3D finite element model: a) Structural elements b) Structural elements in soil matrix c) Deformed shape of the system

It should be noted that the lateral loads on the piles varies during the soil movement. Reaction force on the pile depends on the relative displacement between pile and soil. Once the soil movements exceed the pile deflection, then driving forces start to generate on the pile. In order to examine the effects of the magnitude of the relative displacement between pile and soil (δ), the responses of the passive piles for δ = 0.2d, 0.35d, 0.6d, 0.85d, 1.0d, 1.2d and 1.4d were compared. Figure 3.5 shows the distribution of bending moment along the pile shaft at seven different values of relative displacements. It can be seen from Figure 3.5 that the maximum bending moment increases with the increase of relative displacement and also the point of maximum moment shifts to somewhat deeper depths.

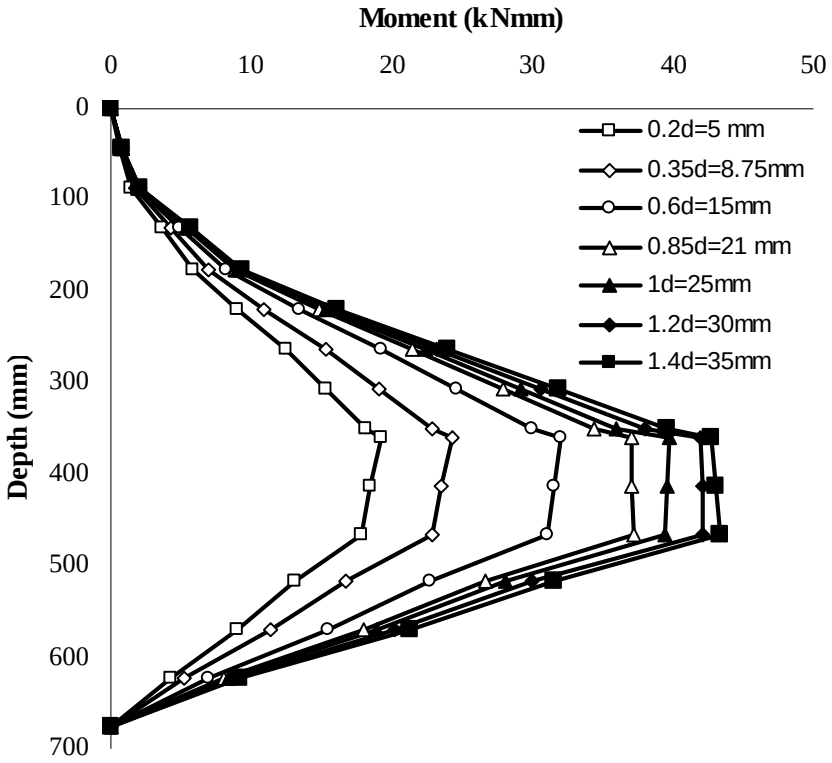

Figure 3.5 Bending moment distributions along pile with different relative displacement.

During the analyses the applied lateral force is increased until soil failure occurred. The lateral displacements of obtained at pile head (point B) and in the surrounding soil at points (A, C, and D) (Fig. 3.3) are given in Table 3.1.

The applied force is increased step by step and the bending moment variations in selected depths are also determined. Bending moments at different depths (D) versus the pile displacements along the pile shaft are also plotted in Figure 3.6.

Table 3.1 Lateral displacement of soil points and the pile head

Lateral Displacement (mm)				**Relative Displacement (d) (mm)**
A	**B**	**C**	**D**	**C - B**
23	20	42	43	22
34	30	53	54	23
45	40	64	65	24
56	50	75	76	25
67	60	86	87	26
73	65	92	93	27
78	70	98	99	28
89	**80**	**110**	**111**	**30 (1.2d)**
100	90	125	130	35

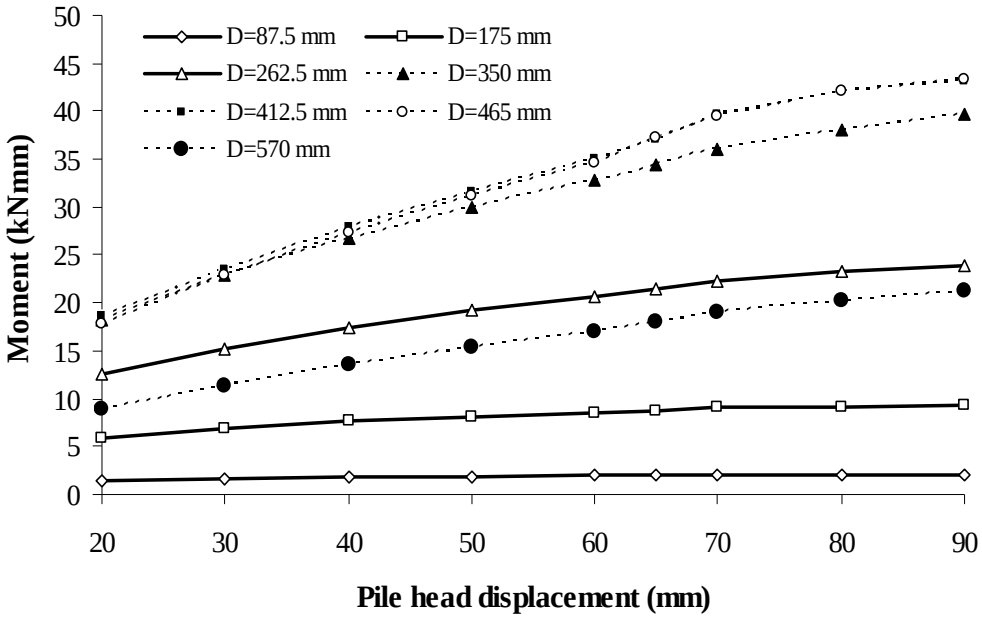

Figure 3.6 Bending moments at different depths along pile against pile head displacement.

Moment values increase parallel to increase with pile head displacement, and approaches to a limiting value after 80 mm pile head displacement. In spite of the pile head displacement increasing, moments at depths closer to ground surface

(D = 87.5 mm and D = 175 mm) are nearly the same. The relations between the pile and the relative displacements at different depths are determined and are given in Figure 3.7. As the soil is forced to move with linearly increasing displacement from hinge to upward direction, relative displacements have positive high values at the upper part but decrease at deeper depths and have negative values below the hinge.

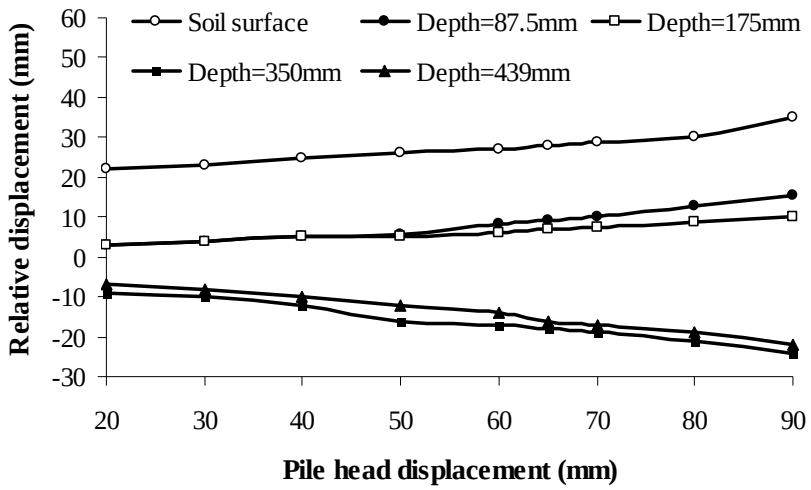

Figure 3.7 Pile head displacement-relative displacement relations at different depths.

One of the advantages of the Plaxis 3D analysis is the determination of lateral soil pressure distribution acting on the pile. Along the pile length, soil pressure distribution has been obtained from effective normal stress values that act on the pile–soil interface for the state of 80 mm pile head displacement ($\delta = 1.2d = 30$ mm). Active soil pressure on the pile increases with depth and reaches a peak value, and then, it decreases with depth and at deeper depths passive soil pressure can be observed. The values of interface pressure along the pile length are presented in Figure 3.8.

Various numerical analyses for different interface roughness values (R= 2/3, 4/5, and 1) have been performed in order to determine the effect of interface roughness on the value of force acting on pile. The effect of interface roughness on the bending moment at 30 mm relative displacement is shown in Figure 3.9.

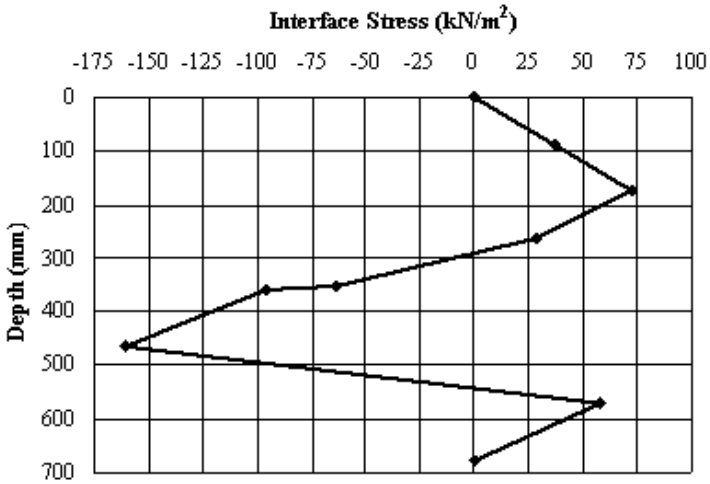

Figure 3.8 Interface stress distribution along pile at relative displacement of 1.2d (δ=30mm).

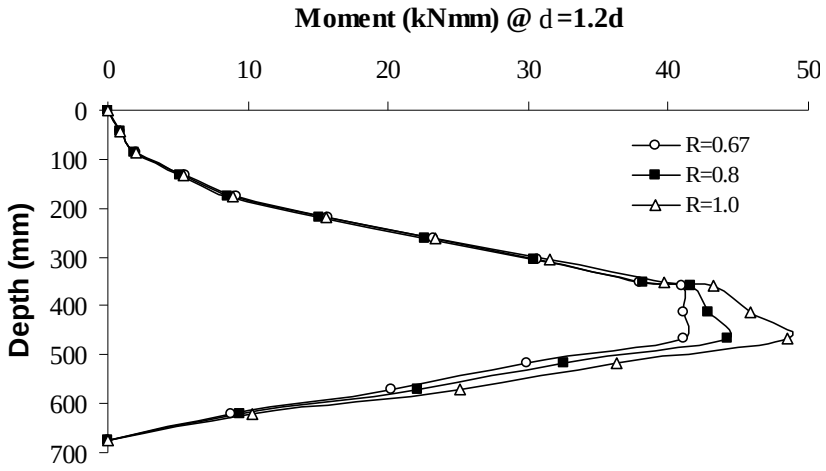

Figure 3.9 The effect of interface roughness on bending moment distribution.

The predicted and the measured moment values for the single pile test are presented in Figure 3.10. This figure presents the bending moment distributions for two different soil surface displacements of points very close to the pile, namely y = 20 mm and y = 60 mm.

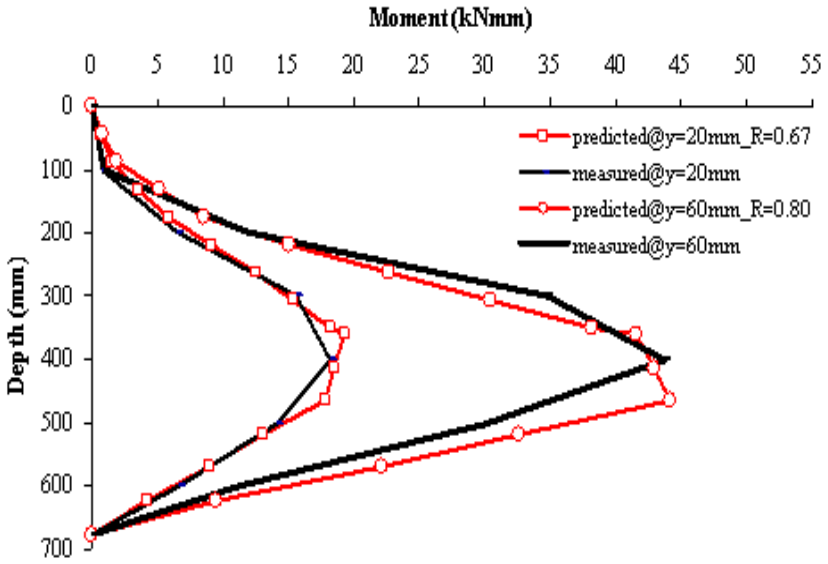

Figure 3.10 Predicted and measured moment values along pile for two different soil displacements.

In Figure 3.10, it can be clearly seen that the numerical predictions are in good agreement with the Poulos' experimental measurements for each case, particularly with regard to the trend of behavior. It can be seen that the predicted moment profile agrees fairly well with that measured at y = 60 mm, but the finite element simulation overestimates the maximum bending moment at y = 20 mm by about 5% more than the measured, although the shape of distribution and the position of the maximum are predicted very well. In order to represent moment distribution better, the interface rigidity factor values should be increased parallel to surface displacement increase.

3.1.1.3 Extend of Poulos' Test with two piles having different pile spacings

The numerical analyses were extended to two piles in a row in order to investigate the effect of pile spacing. Five numerical tests were performed on two free-head piles with five different spacings and the responses of the passive piles (s = 2.5d, 5d, 7.5d, 10d, and 12d) were compared. Bending moment distributions for 1.2d relative displacement at different pile spacing are plotted in Figure 3.11.

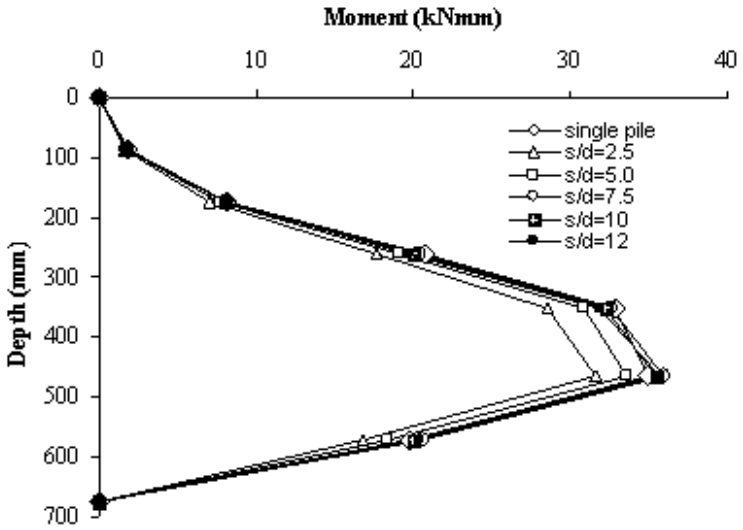

Figure 3.11 Bending moment profiles for two free head piles in a row at 1.2d relative displacement.

Figure 3.11 shows that the distributions are very similar in shape, including the position of the maximum bending moment. The bending moments acting on piles increases as the pile spacing increases. However, when s becomes larger than 7.5d, each pile behaves like a single pile.

The soil reaction at the interface between the soil and the pile along the pile length is also examined with different pile spacing. The effect of pile spacing on the soil reaction is plotted in Figure 3.12. It can be seen that with an increase of the pile spacing, the soil reaction increases while passive resistance of soil decreases.

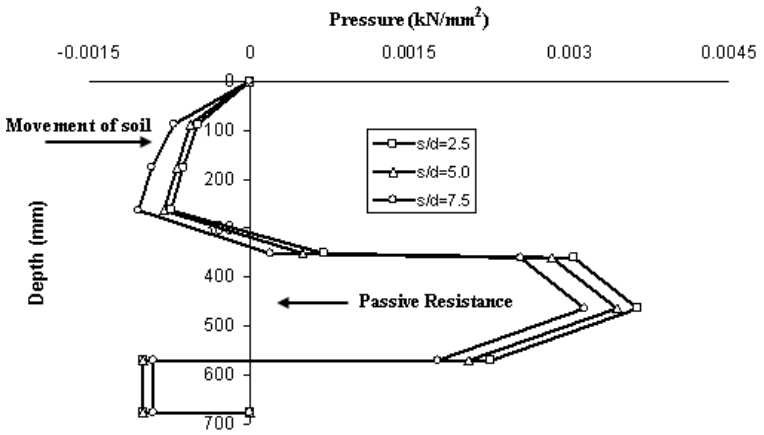

Figure 3.12 Soil reaction profiles for two free head piles in a row.

3.1.2 Finite Element Simulation of Finite Number of Passive Pile Case

The problem associated with the displacement effects of embankments constructed on soft soil on passive piles was examined with a model simulation study. The mobilization of resistance of finite number of piles subjected to lateral soil movement is discussed from the standpoint of the arching effect and the existence of an arching zone around pile groups for sandy soils. The formation of an arch is explained by stress transfer from moving soil to the piles. Loads on passive piles in a row due to sliding soils are also investigated.

The model used in this study consists of eleven main elements namely, large box, cohesionless soil, weak soil, concrete block, three model piles, and four springs. The dimensions and material properties used in the model simulation are given in Table 3.2.

Table 3.2 Material properties

Item	Thickness cm	Soil Properties						
		Material Model	γ kN/m^3	Stiffness		Strength		R
				E kPa	υ	c^* kPa	ϕ	
Sand	100	Mohr-Coulomb	17	5000	0.3	1	30	0.67
Weak Soil	5	Mohr-Coulomb	17	1000	0.3	1	5	0.67
Rigid Block	100	Linear-Elastic	25	$2x10^6$	0.15	-		1
Pile	5	Linear-Elastic	24	$3x10^7$	0.15	-		1

***** *for numerical stability purposes*

Analyses were conducted on a volume of 2 x 2 x 2 m as illustrated with the finite element mesh model in Figure 3.13. Numerical experiments with different number of elements in the mesh around the pile have been performed to investigate the model including mesh refinement. The FE mesh used for the parametric studies consists of 4867 elements and the computer time for each analysis was approximately 2 h of CPU time.

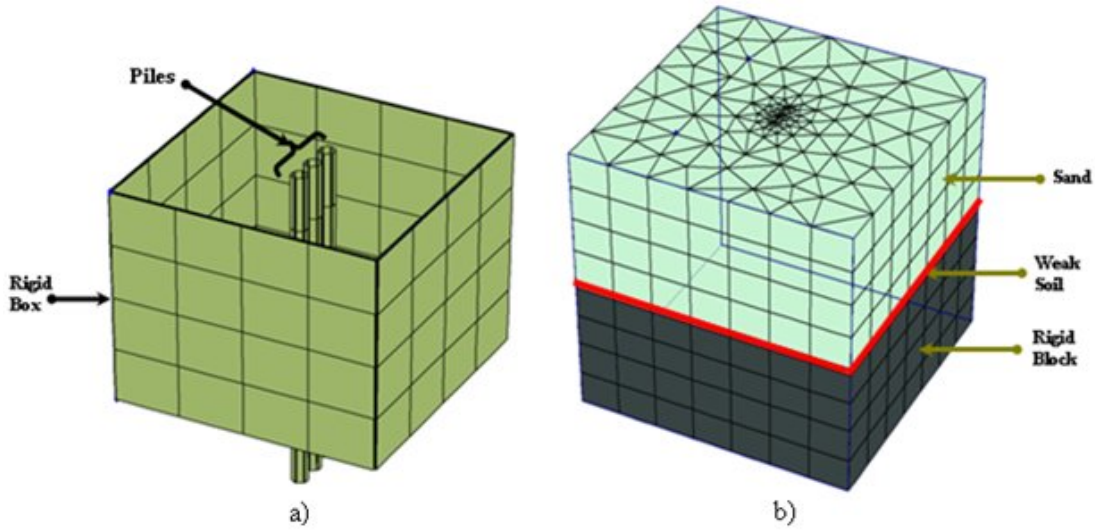

Figure 3.13 Soils and structure finite element simulation: a) Structural elements b) Soil matrix

The box, which has the dimensions of 100xBx100 cm, was modeled. The width of the box (B) is varied according to pile arrangement. Model piles, with a diameter of 5 cm, were inserted into this box, which was filled with cohesionless soil. In this study, the model was based upon a linear-elastic non-porous pile with a length of 0.5 m embedded in rigid block. For every case throughout the analyses, the pile was long enough to act as long and flexible. The Young's Modulus of the pile should be less than $1.4x10^{12}$ kN/m^2 to correspond to a flexible pile according to pile flexibility factor K_R (Poulos and Davis, 1980) which is defined as follows (Eq. 3.1):

$$K_R = \frac{E_p\, I_p}{E_s\, L^4} \langle 10^{-5} \tag{3.1}$$

where; E_p is the Young's modulus of the pile, I_p is the moment of inertia of the pile section, E_s is the secant modulus of the soil and L is the embedded pile length.

The friction between the cohesionless soil and the rigid block was minimized by placing a thin weak soil layer that enables sliding. Springs were attached to the four edges of the box on the opposite side of the load to measure load on box due to moving soil. The box is forced to move by a uniform horizontal load after the removal of soil clusters that are in the back and front positions of the box. In order to

determine the ratio effect of pile spacing to pile diameter on the pile response, the rigidity of the pile, the pile length, as well as the Young's modulus of the soils was accepted constant throughout the analysis, while only the pile spacing was changed. A uniform distributed load was applied on the right face which forced the soil move horizontally. Plan and three dimensional view of the model are given in Figures 3.14 and 3.15, respectively.

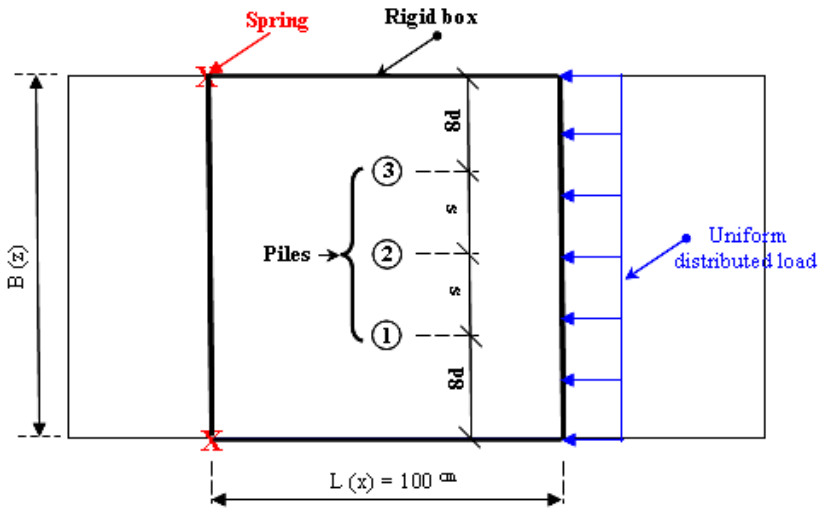

Figure 3.14 Plan view of model simulation.

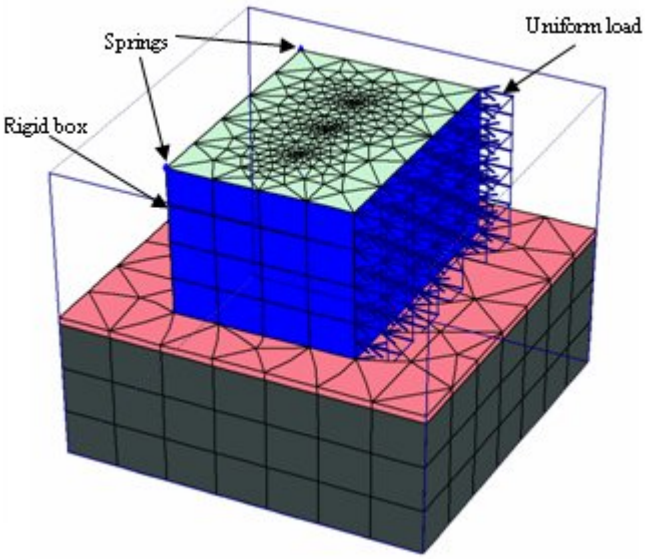

Figure 3.15 3D view of model simulation.

Firstly, the analysis without pile was performed to determine the friction load along the sliding surface (F_r) on weak layer. F_r was computed by subtracting the total loads on the springs (F_s) from the applied load (P) in. This friction load was considered in the interpretation of the analyses results. Then, single pile was positioned at the centre of the box width and single pile analysis was performed. The load carried by pile was determined by subtracting the load difference between P and F_r from F_s throughout the analyses.

An extensive parametric study was carried out to investigate the effects of variation of parameters on the arching behavior. Specifically, the parameter selected for the study was pile spacing. In this model study, five different pile spacing configurations (s = 2d, s = 4d, s = 6d, s = 8d and s = 10d) were examined in the box with different box width dimensions in each configuration. The pile spacing and the box dimensions used in the test series are summarized in Table 3.3. Here, spacing equal to or larger than two diameters was selected, because the ratios less than 2 are not usual. The relative displacement of 1.2d is found to be sufficient for the explanation of any behavior of passive load versus pile displacement.

Table 3.3 Box dimensions

s / d	**Box Dimensions (cm)**		
	L (x)	**B (z)**	**H (y)**
10	100	180	100
8	100	160	100
6	100	140	100
4	100	120	100
2	100	100	100

Interpretations are done for different pile spacing ratio, s/d, and for 1.2d (6 cm) relative displacement values. A series of analyses, in different pile spacing, have been performed in order to find the lateral applied load that causes 6 cm relative displacement between the soil and piles. By varying the spacing, s, and increasing the relative displacement, δ, the load acting on the piles were calculated. The calculated values of soil and pile displacements, maximum bending moments and shear forces on piles for different pile spacing in the test series are summarized in Table 3.4.

Table 3.4 Analysis results at 1.2d relative displacement

s/d	Pile Numbers					
	1		2		3	
	M (kNm)	T (kN)	M (kNm)	T (kN)	M (kNm)	T (kN)
2	2.746	30.61	2.674	30.43	2.909	30.75
4	3.047	34.57	3.115	34.31	3.204	34.62
6	3.485	37.07	3.444	36.34	3.470	36.81
8	3.623	39.02	3.571	38.10	3.701	38.82
10	3.626	39.06	3.574	38.18	3.708	38.85

Results of the analyses show that pile spacing has some effect on the pile response (shear force and moment distribution). As expected, the second pile in the middle has the minimum shear force and moment values. The calculated shear forces and moment values of the first and the third piles for 1.2d (6 cm) relative movement are a bit different although the system is symmetric. This ignorable difference is thought to be originated from numerical approach. The loads acting on the piles are determined by varying the spacing, s, and increasing the applied force to reach 1.2d relative displacement. The calculated loads acting on the center piles (pile #2) against pile spacing are plotted in Figure 3.16.

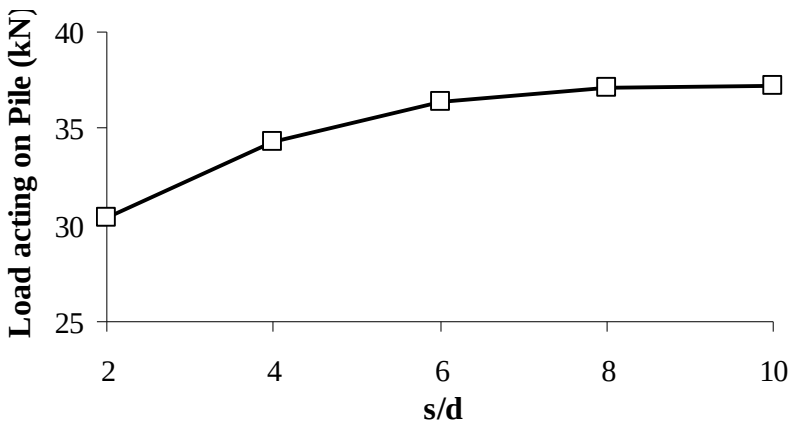

Figure 3.16 Loads acting on centre pile versus pile spacing.

It can be seen that the load acting on the piles increases, as the spacing increases, and approaches a limiting value. This indicates that arching is not as effective in large spacing as in small spacing.

Since the arching takes place within the soil, the soil properties such as angle of internal friction are expected to influence the soil arching mechanism directly (Liang and Zeng, 2002). Various numerical analyses have been performed with three different angle of internal friction (25°, 30° and 35°). Induced forces acting on piles are plotted in Figure 3.17. The variation of internal friction has a significant influence on the arching effect. It can be seen that the soil with higher friction angle is more likely to produce greater granular interlocking and develop stronger arching. Both the residual load acting on the soil mass between the piles and the displacement of soil between piles are evaluated. Figure 3.18 shows the variation of the displacement of soil between piles with different angle of internal friction values, when δ equal to 6 cm.

The soil with higher friction angle produces greater granular interlocking, and more loads will transfer to the piles and fewer displacements will occur in the soil between piles owing to the arching effect. It can also be seen that the displacement of soil between the piles increases as the spacing increases and approaches to a limiting value. The effect of variation of internal frictional angle on displacement of soil between piles becomes negligible when the pile spacing is 8d. This indicates that arching is not effective after larger spacing than 8d (Figs 3.17 and 3.18).

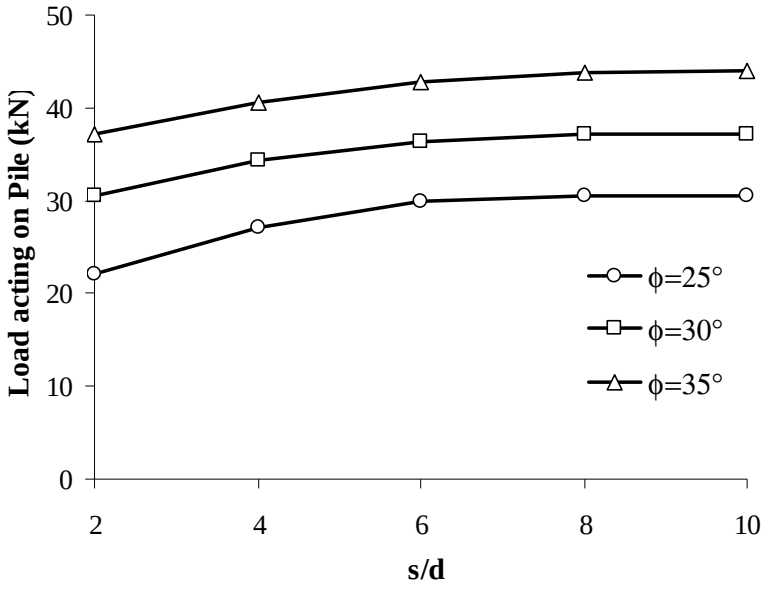

Figure 3.17 Effect of friction angle on load acting on pile.

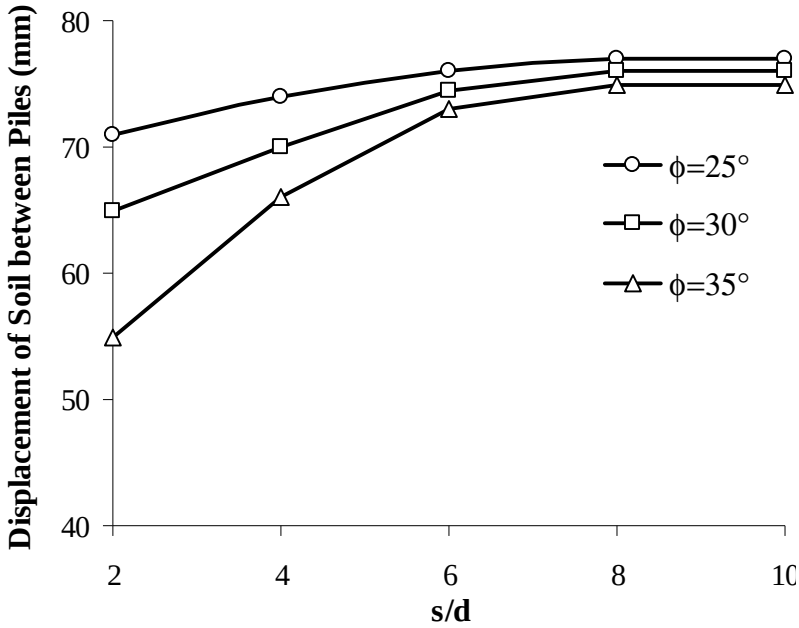

Figure 3.18 Effect of friction angle on displacement of soil between piles.

In order to investigate the effect of pile-soil-pile interaction on the free head pile behavior, the response of each individual pile within a group is compared with that of a single pile. Group effects may be assessed in terms of loads or moments for passive piles. Group factor can be determined by comparing the load acting on a pile determined from a pile group test with that of the single pile test (F_L) or comparing the maximum moment of the pile in a group with that of the single pile (F_M) at the same amount of relative displacement between pile and the soil (Chen et al., 1997; Jeong et al., 2003). In order to show the effect of pile spacing on the group factor, the group factors in terms of load and moment in finite number of passive pile case are given in Table 3.5.

Table 3.5 The effect of pile spacing variation on group factors

Pile Spacing (s)	**F_L**	**F_M**
2d	0.82	0.83
4d	0.93	0.91
6d	0.98	0.98
8d	1.00	1.00
10d	1.00	1.00

Group factor is really influenced by pile spacing that parallel to the decrease in pile spacing, group factor decreases. Therefore, group factor can be as group action reduction factor in finite number of passive pile case.

3.1.3 Finite Element Simulation of Infinite Number of Passive Pile Case

The problem associated with the displacement effects of sliding sandy soil mass on passive piles was also examined. The slope stabilizing pile case was simulated with a slice from infinite number of piles. Within this scope, plan view of model simulation established before was changed as given in Figure 3.19 while the other properties remained constant.

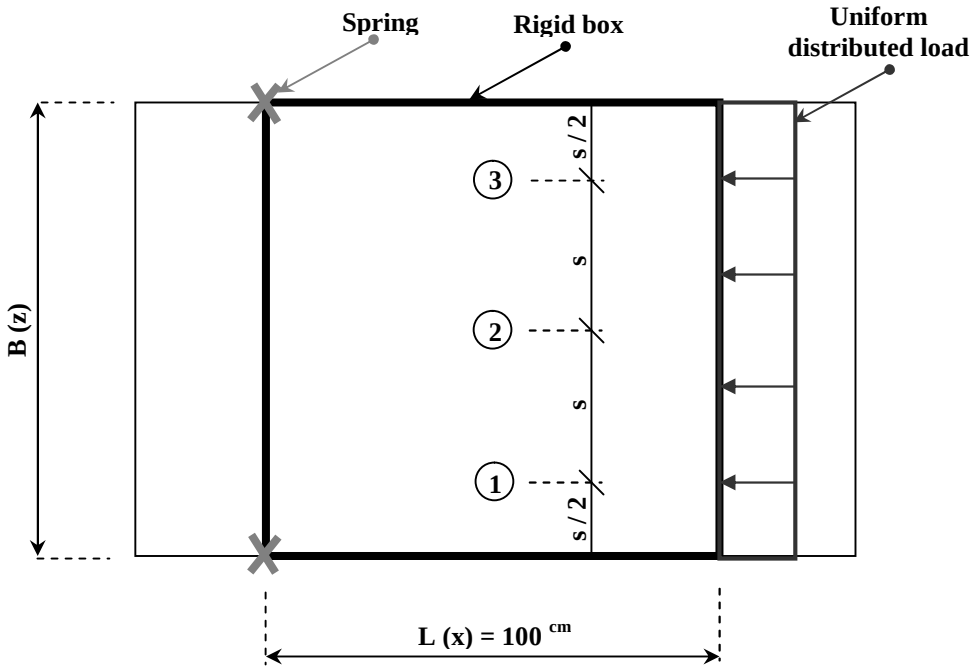

Figure 3.19 Plan view of slope stabilizing pile simulation.

In this slope stabilizing piles simulation study, five different pile spacing configurations (s = 2d, s = 4d, s = 6d, s = 8d and s = 12d) were again examined in the box which has different widths (B) in each configuration. The pile spacing and the box dimensions used in the test series are summarized in Table 3.6.

Table 3.6 Box dimensions

s / d	Box Dimensions (cm)		
	L (x)	B (z)	H (y)
12	100	180	100
8	100	120	100
6	100	90	100
4	100	60	100
2	100	30	100

Series of analyses with different pile spacings have been performed and the lateral loads cause 6 cm relative displacement have been determined. By varying the spacing, s, and increasing the applied force to get the state of 1.2d relative displacement, the loads acting on the piles are calculated. The calculated loads acting on the piles against pile spacing are plotted in Figure 3.20.

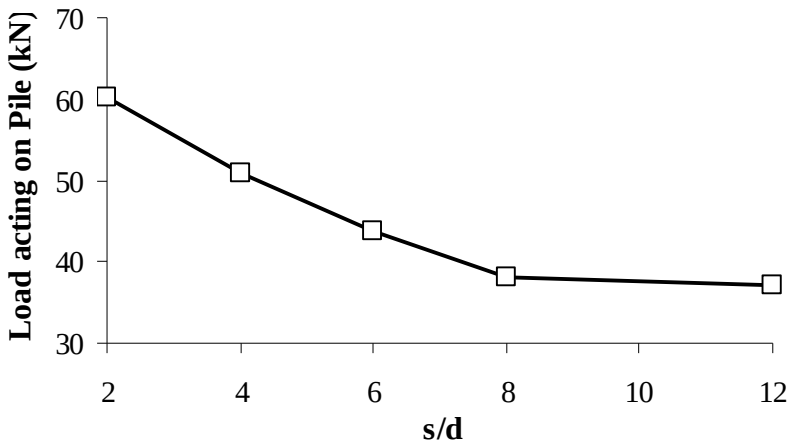

Figure 3.20 Force acting on pile versus pile spacing.

It can be seen that the load acting on the piles decreases, as the spacing increases. In other words, when pile spacing increases, a smaller amount of load would be transferred to the piles. This indicates that arching is not as effective at large spacing as in small spacing. Around 80% of load would be transferred to the piles if the piles are placed in a row with s/d=2. For a wide pile spacing with s/d=6, however, less than 40% load have transferred to the piles. Once the pile spacing becomes larger than 8d, there would be no arching effect so that each pile behaves like a single pile. This indicates that arching is not effective after larger spacings than 8d.

Various numerical analyses have been performed with three different angle of internal friction (25°, 30° and 35°). By varying the angle of internal friction (ϕ) and the pile spacing ratio (s/d) at the ultimate state, the loads acting on the piles are determined. The calculated loads acting on the piles induced by moving soil with different angle of internal friction are plotted in Figure 3.21.

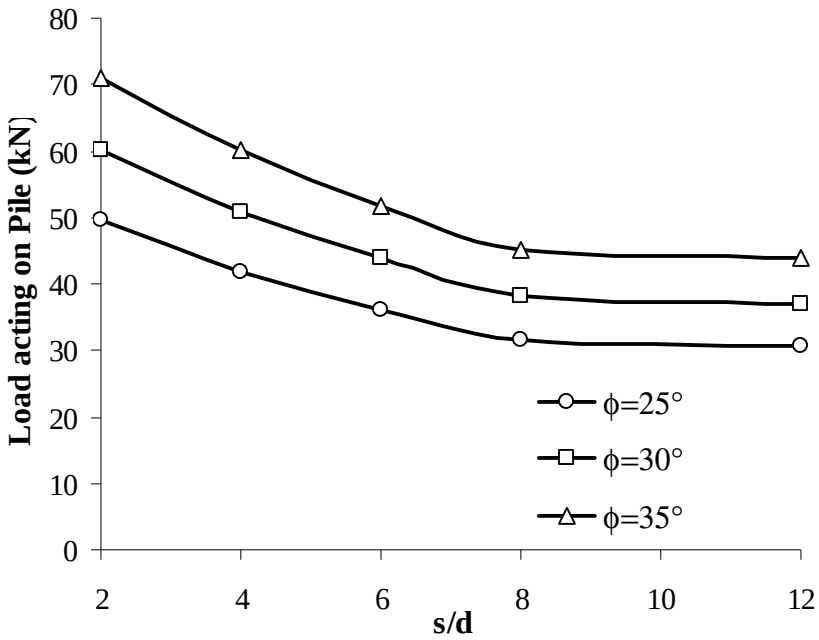

Figure 3.21 Effect of friction angle on load acting on pile.

Consequently, more loads will be transferred to the piles owing to the arching effect. The soil with higher friction angle produces greater granular interlocking, and more loads will be transferred to the piles.

In order to show the effect of pile spacing on the group factor, the group factors in terms of load and moment in infinite number of passive pile case are given in Table 3.7.

Table 3.7 The effect of pile spacing variation on group factors

Pile Spacing (s)	F_L	F_M
2d	1.72	1.70
4d	1.17	1.15
6d	1.08	1.07
8d	1.02	1.01
12	1.00	1.00

Group factor is really influenced by pile spacing that parallel to the decrease in pile spacing, group factor increases. It can be supposed that if the pile spacing increases, the amount of load would be transferred to the piles decreases in infinite number of passive pile case.

3.2 Determinations from Numerical Results

Various numerical analyses have been performed for five different pile spacing configurations (s = 2d, s = 4d, s = 6d, s = 8d and s = 12d) with three different angle of internal friction (25°, 30° and 35°). Some determination can be made from the results as follows:

- Laboratory tests can be successfully simulated with Plaxis 3D. As the results of finite element analyses are compared with the experimental results of Poulos et al. (1995), it can be seen that they are in good agreement. In spite of small differences of maximum moment values, moment distributions are determined successfully. Representing the moment distribution better, the interface roughness should be increased parallel to surface displacement increment.
- As relative displacement (δ) increases, the loads acting on the piles increase rapidly as a result of arching induced stress transfer. When the soil movement reaches a certain value, δ = 1.2d for cohesionless soils, the acting loads reach a maximum value and remain constant as the soil movement continues to increase. This indicates that the additional soil movement has no more influence on the load transfer mechanism.
- With an increase of the pile spacing, s, the loads acting on the piles increase for the case of piles adjacent to embankments, whereas for the case of piles used to

stabilize slopes, the load acting on the piles decreases. In other words, when the pile spacing decreases, a small amount of load would be transferred to the piles adjacent to embankments, whereas the amount of load would be transferred to the piles increases in the slope stabilizing piles case. However, when s becomes larger than 8d, each pile behaves like a single pile without arching effect for both two passive pile cases.

- The soil with higher friction angle produces greater granular interlocking and develops stronger arching. Consequently, more loads will be transferred to the piles and fewer displacements will occur in the soil between piles owing to the arching effect for both two passive pile cases.

CHAPTER FOUR
DESIGN OF EXPERIMENTAL SETUP

4.1 Introduction

Physical modeling in laboratory, an appropriate simplification of reality, is the primary tool used extensively by engineers and researchers for understanding soil behavior in spite of the high investment costs for experimental facilities and the contrasting decline in computing cost (Ladd et al., 1977; Jamiolkowski et al., 1985; Mesri and Choi, 1985; Ishihara, 1996).

Reduced scale physical models are fabricated and tested under controlled conditions, offers several advantages over full-scale models. The models are necessarily smaller and loading can be controlled accurately, so the tests duration are shorter and cheaper and data are more reliable than for full-scale models. All the details of the model can be fully controlled over and mechanical behavior of the soils can be characterized. The boundary and loading conditions of the model can be exactly known and many repeating observations can be performed. The effect of varying parameters can be studied. These advantages enable thorough parametric studies to develop better theoretical models.

The main concern with reduced-scale physical models is assuring their validity. Scaling effects must be minimized to ensure the behavior observed at a reduced scale and can be extrapolated to predict full-scale behavior (Wood, 2004).

If the model is not constructed at full scale then we need to have some idea about way in which we should extrapolate the observations that we make at model scale to the prototype scale. Many authors have discussed scaling factors for models in general and geotechnical models in particular (e.g. Krawinkler, 1979; Sabnis et al., 1983; Iai, 1989). If the material behavior is entirely linear and homogeneous for the loads that we apply in the model and expect in the prototype then it may be a simpler matter and to scale up the model may not be particularly important.

However, a lot of tests of physical models of piles have been reported in literature, and few of these include the slope stabilization application. An experimental work is needed to simulate the real behavior of flexible piles used for landslide remediation. In the reduced scale experiment, a large box filled with soil is slid on an inclined sliding surface against bottom fixed piles embedded through the box to the stable soil. Aluminum pipes with smooth surfaces are used to represent the small scale testing flexible piles having an outer diameter of 20 mm and 1.4 mm thickness with flexural rigidity (E_pI_p) as $2.49x10^5$ $kNmm^2$. The dimensions of the testing box were determined considering the scale effects.

4.2 Determination of Dimensions for the Testing Apparatus

A common problem in a physical model may be insufficient ratio between the minimum dimension of an embedded structure (e.g. pile diameter, d) and the soil particle size. With some exceptions, it is generally accepted that a minimum structural dimension of 20 to 30 times the mean particle size (D_{50}) of the soil is sufficient to avoid scaling effects (Ovesen, 1979; Nunez et al., 1988). To avoid scaling effects mean particle size of soil should be smaller than 0.67 mm because of the selected aluminum pile having 20 mm diameter. D_{50} is selected for sandy soil as 0.5 mm (D_{max}= 0.7 mm, D_{min}= 0.3 mm)

Modeling the load transfer between a pile and the surrounding ground is affected by several interrelated factors and the dominant one is the pile stiffness, which determines whether the pile behaves rigidly or flexible. Pile flexibility can be expressed with different factors the details of which were summarized in Table 4.1.

Firstly, pile embedded length reflecting the behavior of flexible piles in this model test box was determined (Table 4.2). Constant coefficient of subgrade reaction (n_h), coefficient of horizontal subgrade reaction (k_h), horizontal young's modulus (E_s) of loose sand were determined as 3200 kN/m^3 33000 kN/m^3 and 20000 kN/m^2, respectively (Soletanche, 1982; Navy Design Manual, 1986).

Table 4.1 Criteria for classification of pile behavior

Source	**Criterion for rigid behavior**	**Criterion for flexible behavior**	**Note**
Matlock and Reese (1962)	L < 2T	L > 4T	A
Poulos and Davis (1980)	$K_r > 10^{-2}$	$K_r < 10^{-5}$	B
Bierschwale et al. (1981)	L / d < 6	L / d > 6	C
Dobry et al. (1982)	$S_H < 5$	$S_H > 5$	D
Davies and Budhu (1986)	$L < 1.5\ d\ K^{0.36}$	$L > 1.5\ d\ K^{0.36}$	E
Poulos and Hull (1989)	$L < L_c / 3$	$L > L_c$	F
Carter and Kulhawy (1992)	$0.05\left(\frac{E_e}{G^*}\right)^{1/2} < \frac{L}{d} < \left(\frac{E_e}{G^*}\right)^{2}$		G
Hannigan et al. (1997)	$b_r L < 2.25$	$b_r L > 2.25$	H

A: $T = \sqrt[5]{\frac{E_p I_p}{n_h}}$; T = stiffness factor

B: $K_r = \frac{E_p I_p}{E_s d^4}$; K_r = flexibility factor

C: In some cases, may be rigid for L / d < 10

D: $S_H = \frac{L/d}{(E_p / E_s)^{0.25}}$; S_H = flexibility factor

E: $K = \frac{E_p}{E_s}$; K = stiffness ratio; for constant soil modulus with depth

F: $L_C = 4.44(\frac{E_p I_p}{E_s})^{0.25}$; L_c = critical pile length

G: $G^* = \left(\frac{E_s}{2(1+u_s)}\right)\left(1+\frac{3u_s}{4}\right)$; G^* = the equivalent shear modulus of soil

$E_e = \frac{E_p I_p}{\left(\frac{p\ d^4}{64}\right)}$; E_e = effective Young's modulus of the pile

H: $b_r = (k_h\, d / 4 E_p\, I_p)^{0.25}$; k_h = coefficient of subgrade reaction

where; d is pile diameter (m), L is pile length (m), E_p is pile elastic modulus (kPa), I_p is pile moment of inertia (m^4), E_s is soil elastic modulus (kPa), ν_s is poisson's ratio of soil, G_s is soil shear modulus (kPa), n_h is constant coefficient of subgrade reaction

Table 4.2 Calculation of required length for flexible pile behavior with different methods

Source	Criterion for flexible behavior	Required Length (L)
Matlock and Reese (1962)	$L \rangle 4 \times \sqrt[5]{\frac{E_p I_p}{n_h}}$	L > 0.6 m
Poulos and Davis (1980)	$L \rangle \sqrt[4]{\frac{E_p I_p}{E_s \times 10^{-5}}}$	L > 0.3 m
Bierschwale et al. (1981)	$L \rangle 6\, d$	L > 0.12 m
Dobry et al. (1982)	$L \rangle 5\, d \left(\frac{E_p}{E_s}\right)^{0.25}$	L > 0.41 m
Davies and Budhu (1986)	$L \rangle 1.5\, d \left(\frac{E_p}{E_s}\right)^{0.36}$	L > 0.31 m
Poulos and Hull (1989)	$L \rangle 4.44\, d \left(\frac{E_p}{E_s}\right)^{0.25}$	L > 0.37 m
Hannigan et al. (1997)	$L \rangle \frac{2.25}{\left(\frac{k_h\, d}{4\, E_p\, I_p}\right)^{0.25}}$	L > 0.45 m

The height of the box is selected as 50 cm regarding the necessary pile length embedded in the box in order to reflect the flexible pile behavior.

In order to determine the box length, piled slope on an inclined plane was examined via FEA program, PLAXIS 2D (version 8.2) (Brinkgreve and Vermeer, 2001). The system was comprised of a box open at top and bottom, flexible piles, moving soil in the box, stable soil under the box, linear elastic compressible soil, and prescribed sliding surface material.

The behaviors of moving soil (sand), inclined stable soil (rigid block), and the sliding surface material (weak soil) were simulated by an elastic perfectly-plastic model with Mohr-Coulomb yield criterion while linear elastic model, based on Hooke's Law, was selected to represent the behavior of the compressible soil (elastic soil) that enables the box movement. Soil elements were also assumed to be homogeneous and isotropic.

The 6-node triangle soil elements providing a numerical integration that involves three Gauss iteration points (stress points) is selected for displacement interpolations. 5-node beam elements were used to simulate the flexible piles and the experimental box with high flexural rigidity. Prescribed displacement process was used to simulate the displacement control. The box was forced to move by applying prescribed displacements on both right and left sides of the box.

The piles and the surrounding soil were discretized using a mesh consisting of 1631 elements. Numerical experiments with different numbers of elements in the mesh around the pile were performed to investigate the model including mesh refinement.

The soil-pile interface strength parameter is set to two-thirds (0.67) of sand and weak soil strength parameters for the box sliding, two-tenths (0.2) of rigid block and elastic soil strength parameters to provide and follow the box-soil displacements by means of the interface parameter (R_{inter}). So that strength reduction due to slippage of the soil around the pile is taken into consideration.

The input parameters of each soil layer and a typical model with the finite element mesh are given in Table 4.3 and Figure 4.1, respectively.

Table 4.3 Material properties

Item	**Soil Properties**					
	Material Model	**Stiffness**		**Strength**		**R_{inter}**
		E (kPa)	**υ**	**c (kPa)**	f (°)	
Sand	Mohr-Coulomb	10000	0.3	1	32	0.2
Weak Soil	Mohr-Coulomb	10000	0.3	1	5	0.2
Rigid Block	Mohr-Coulomb	$5x10^5$	0.15	150	50	0.67
Elastic Soil	Linear-Elastic	$5x10^5$	0.15	-		0.67

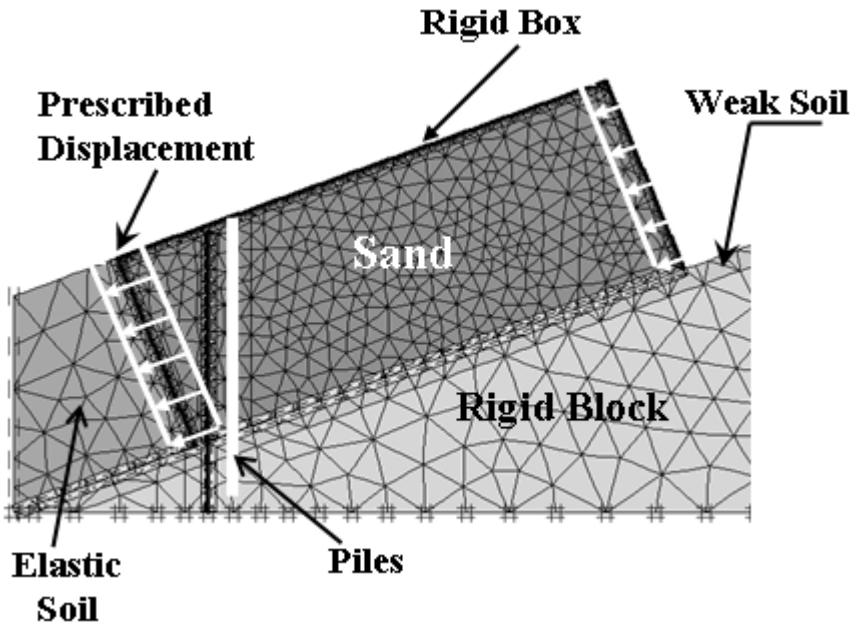

Figure 4.1 Section view of experimental simulation.

Box length is selected as 2 m initially and it is changed in the other analyses to determine its effect on the loads acting on the piles. No significant variation was found in the pile load for box lengths equal to or grater than 90 cm. The box length in front of the piles is selected as 1.0m. The inside dimensions of the box is selected as 1.2m long.

4.3 Failure Modes of Stabilizing Piles

The factors considered in the pile stabilization works are not only the development of lateral pressures on the pile above the slip surface and contribution of the piles to slope stability but also modes of failure of the soil-pile system. The failure modes of stabilizing rigid piles were examined by Viggiani (1981) who used the limit equilibrium method. Three kinds of failure modes were found in a rigid pile as shown in Figure 4.2.

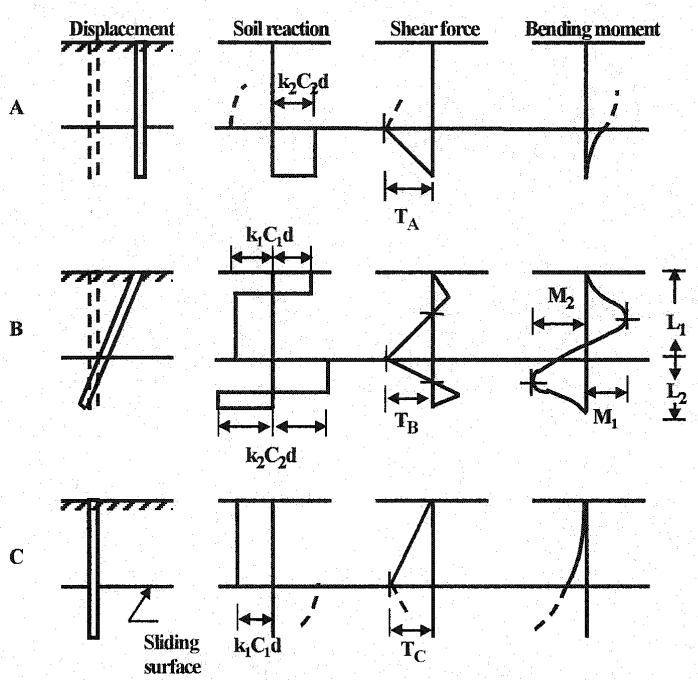

Figure 4.2 Failure modes of stabilizing rigid piles (Viggiani, 1981).

In mode A, the whole pile translates together with the sliding soil. Mode A occurs if;

$$\frac{L_2}{L_1} \langle \frac{P_{y1}}{P_{y2}} \times \left(\frac{\sqrt{2+2\times\frac{P_{y1}}{P_{y2}}}-1}{1+2\times\frac{P_{y1}}{P_{y2}}} \right) \tag{4.1}$$

where L_2 is the thickness of the stable layer with ultimate lateral soil pressure P_{y2} and L_1 is the thickness of a sliding clay layer with ultimate lateral soil pressure P_{y1}

Mode C occurs when the pile is fixed in the soil and the soil flows around the pile. The occurrence of mode C happens if;

$$\frac{L_2}{L_1} \rangle \frac{P_{y1}}{P_{y2}} + \sqrt{2\times\left(\frac{P_{y1}}{P_{y2}}\right)^2 + 2\times\frac{P_{y1}}{P_{y2}}} \tag{4.2}$$

In mode B, the piles are subject to a rigid rotation and soil failure above and below the slope surface. Failure mode B occurs when

$$\left[\frac{P_{y1}}{P_{y2}}\times\left(\frac{\sqrt{2+2\times\frac{P_{y1}}{P_{y2}}}-1}{1+2\times\frac{P_{y1}}{P_{y2}}}\right)\right]\leq\left[\frac{L_2}{L_1}\right]\leq\left[\frac{P_{y1}}{P_{y2}}+\sqrt{2\times\left(\frac{P_{y1}}{P_{y2}}\right)^2+2\times\frac{P_{y1}}{P_{y2}}}\right] \tag{4.3}$$

Although Viggiani (1981) provided valuable information about the failure modes of rigid piles on saturated clay soils, unfortunately, their applications are limited on the response of rigid piles. To overcome the shortcomings of the Viggiani (1981) method, Poulos (1995) presented an improved method using a simplified boundary element analysis. In the model, the pile was modeled as a simple elastic beam and the soil as an elastic continuum. The results of analysis are presented in Figure 4.3.

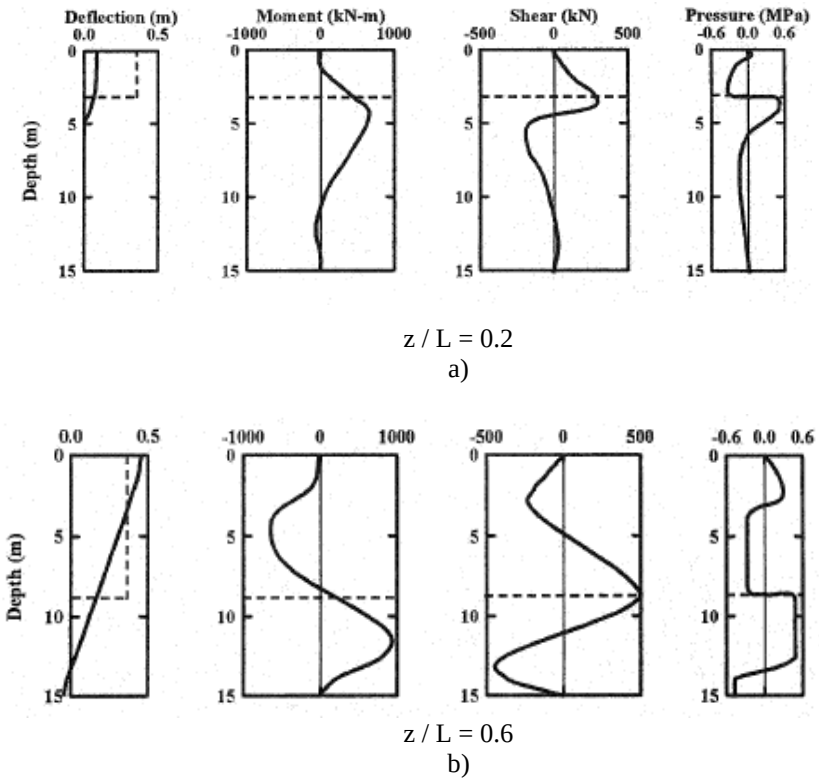

Figure 4.3 Modes of stabilizing piles (Poulos, 1995): a) Rigid pile mode b) Flexible pile mode

It is assumed that the upper portion of the unstable soil moves as a rigid body down slope. The possible existence of failure modes include:

1) Rigid pile mode; when shallow unstable soil becomes plastic and flows around the pile.
2) Flexible pile mode occurs in a deep slide length and a shallow stable length.

The following conclusions can be drawn from Figure 4.3;

- The maximum shear force in the pile occurs at the slide plane,
- In the rigid pile mode, the maximum moment occurs in the stable soil and the pile movement is obviously less than the soil movement,
- In the rigid pile mode, the pile has a similar displacement as the soil, the maximum bending moment is within the unstable layer, for the flexible pile mode, both stable and unstable soils show large moments, and the pile head movement is bigger than the soil movement near the soil surface.
- Figure 4.3 also reveals that the rigid pile mode failure mechanism will cause the least damaging effects from the unstable soil on the piles. Adjusting the embedded depth of piles in the stable layer the intermediate failure mode is expected and the largest shear force and bending moment can be developed.

4.4 Methods for Predicting Ultimate Lateral Soil Pressure

Several methods are available for determining the ultimate lateral resistance to piles in cohesionless soils (e.g., Brinch Hansen, 1961; Broms, 1964; Reese et al., 1974; Meyerhof et al., 1981; Borgard and Matlock, 1983; Fleming et al., 1994).

Brinch Hansen (1961) presented an expression for predicting the ultimate lateral resistance to piles in a general c–ϕ soil, where c and ϕ are, respectively, the cohesion and the effective internal friction angle of the soil. For a cohesionless soil, c=0 and the ultimate lateral resistance can be calculated by

$$P_u = K_q \, g \, z \, B \tag{4.4}$$

where P_u=ultimate lateral resistance in the unit of force per pile length; K_q=Hansen earth pressure coefficient which is a function of ϕ; γ=effective unit weight of soil; z=depth from the ground surface; and B=diameter or width of the pile.

Broms (1964) suggested the following expression for calculating the ultimate lateral resistance in cohesionless soils:

$$P_u = 3K_p\, g\, z\, B \tag{4.5}$$

where $K_p=\tan^2(45° +\phi'/2)$=passive earth pressure coefficient.

Using Eq. (4.5), Broms (1964) prepared charts in non-dimensional form giving the lateral capacity of piles in terms of the plastic moment and geometry of the pile.

Reese et al. (1974) suggested a more complicated, but nevertheless still approximate, variation of ultimate lateral resistance with depth, taking due account of the wedge type failure near the ground surface and plane-strain failure at a considerable depth below the ground surface. The value of P_u with depth can be determined from the lesser value given by Eqs. (4.6*a*) and (4.6*b*).

$$P_u = g\, z\left[B(K_p - K_a) + z(K_p - K_0)\sqrt{K_p}\tan a + z\,K_0\sqrt{K_p}\left(\frac{1}{\cos a}+1\right)\tan f'\sin b\right] \tag{4.6a}$$

$$P_u = g\, z\, B\left(K_p{}^3 + K_0\, K_p{}^2 \tan f' - K_a\right) \tag{4.6b}$$

where $K_a=\tan^2(45°- \phi'/2)$=active earth pressure coefficient; K_0=at rest earth pressure coefficient; $\beta=45°+ \phi'/2$; α=angle defining the shape of the wedge; and ϕ'=effective internal friction angle.

The plots of Eqs. (4.6a) and (4.6b) will intersect at a depth z_t. Above z_t Eq. (4.6a) is used to calculate P_u. Below z_t Eq. (4.6b) is used to calculate P_u.

Borgard and Matlock (1983) realized that some terms in the Reese et al. (1974) formulation of P_u can be taken as constant with little error. Then, they simplified Eq. (4.6) by grouping the terms to form factors that vary with ϕ'. The ultimate resistance P_u is taken as the lesser of

$$P_u = (C_1 z + C_2 B) g z \quad \text{(4.7a)}$$

(near ground surface)

$$P_u = C_3 g z B \quad \text{(4.7b)}$$

(well below ground surface)

The parameters C_1, C_2, and C_3 are functions of ϕ' and are presented by Borgard and Matlock (1980).

Fleming et al. (1994) assume P_u proportional to the square of the passive earth pressure coefficient, i.e.,

$$P_u = K_p^{\,2} g z B \quad \text{(4.8)}$$

For almost all naturally occurring cohesionless soils, K_p will be greater than 3. So Eq. (4.8) will give greater values than Eq. (4.5).

These studies have led to clear design concepts as far rigid piles are concerned. However, in practice, most of the prototype piles are flexible which bend under the action of external forces. Attempts have been made recently to relate the behavior of flexible piles in terms of equivalent rigid piles by introducing the concept of the effective depth for both ultimate and elastic stages of loading (Meyerhof et al., 1981; Sastry and Meyerhof, 1994).

A flexible pile of depth D can be considered as an equivalent rigid pile of ultimate effective depth D_{eu} for the computation of pile capacity and the maximum bending moment whereas it can be treated as a rigid pile of elastic effective depth D_e for the

estimation of deflections under working loads. The ratios D_{eu} / D and D_e / D are mainly controlled by the K_r value even though the variation of E_s with depth has some slight effect (Sastry and Meyerhof, 1994). In the absence of structural failure of the pile, the ultimate lateral capacity of a flexible pile of embedment depth D in homogeneous sand is obtained by considering the equilibrium of an equivalent rigid pile of depth D_{eu} so that

$$Q_u = 0.125g\, B D_{eu}^{\,2} K_b \tag{4.9}$$

where γ=unit weight of the soil, K_b=earth pressure coefficient for the pile (Meyerhof et al., 1981) and D_{eu} is given by

$$\frac{D_{eu}}{D} = 1.65 K_r^{\,0.12} \le 1 \tag{4.10}$$

The ultimate lateral capacity of the model pile used in this study is calculated with the above mentioned methods and listed below in Table 4.4

Table 4.4 Ultimate lateral capacity of model pile

Source	**Ultimate lateral capacity, P_u, kN**
Brinch Hansen (1961)	= 15 x 13.1 x 0.25 x 0.02 = 0.98
Broms (1964)	= 3 x 3.25 x 13.1 x 0.25 x 0.02 = 0.64
Reese (1974)	= 13.1 x 0.25 x 0.02 x [$(3.25)^3$+ 0.47 x $(3.25)^2$x tan32 - 0.308] = 2.43
Borgard and Matlock (1980)	= 0.76
Fleming et al. (1994)	= $(3.25)^2$ x 13.1 x 0.25 x 0.02 = 0.69
Meyerhof et al. (1981)	= 1.00

As a continuation of previous studies, the present investigation consists of instrumented model flexible piles buried in homogenous loose sand and subjected to lateral loads. The bending strain in the pile, the total load and the load carried by piles under each displacement increment were recorded. The recorded values were analyzed to predict the pile capacity, maximum bending moment and horizontal deflections of flexible piles under lateral loads. Some authors from their field measurements state that the measured soil-pile interactions are much smaller than the yield values, and that the creep movements have practically stopped at its 30≈40 %

(Fukumoto, 1976; Sommer, 1977; Allison et al., 1991). So the expected load acting on the model piles is approximately 30% of the ultimate lateral capacity (0.3 kN = 30 kg).

4.5 The Determination of Prototype Pile

The determination of the prototype pile representing the characteristics of model pile requires scaling principals for soil and structural elements. For example, the response of a pile under lateral loading is described by the following equation governing the deformation of the pile indicating a resistance to lateral displacement proportional to the shear stiffness of the soil.

$$EI\frac{d^4y}{dx^4} = -b\,G\,y \tag{4.11}$$

where x is the distance measured down the pile and y is the horizontal deflection of the pile, G is the shear modulus, of the soil.

Terms in the solution of this differential equation involve λL where L is the length of the pile and λ is a dimensionless pile deflection described in the following equation.

$$l^4 = \frac{b\,G}{4\,E\,I} \tag{4.12}$$

Hence $\frac{G\,L^4}{E\,I}$ is an appropriate dimensionless group to describe relative pile-soil stiffness. The soil quantity GL^4 has equivalence to the flexural rigidity, EI, of the pile in any case. Then it might be supposed that correct physical modeling will be obtained if the dimensionless ratio is maintained. To maintain the similarity of model and prototype, the scale factor is required for pile flexural rigidity. The scale factors, n_E and n_I for Young's modulus (E) and secant moment of area (I) of the pile can be deduced that

$$n_E\, n_I = n_L^{\,4} \tag{4.13}$$

with a length scale $n_L = \frac{1}{n}$

This leads to $n_E n_I = \frac{1}{n^4}$

It is needed to reduce the flexural rigidity of the pile by $1/\ n^4$ in order to maintain the dimensionless ratio.

For all models it is assumed that the same soil material has been used in the prototype and model so that the scale factor for density is to first order unity.

However it is decided that such a tubular model pile is rather delicate to manufacture and choose to replace the solid prototype pile with a tubular model pile.

$$\frac{I_{model}}{I_{prototype}} = \frac{\frac{p}{64}[d_m^{\,4} - (d_m - 2\times t)^4]}{\frac{p}{64} d_p^{\,4}} = \frac{1}{n^4} \tag{4.14}$$

The dimensions and the Young's modulus of selected prototype pile is determined and given in Table 4.5

Table 4.5 The design of prototype pile

	Aluminum Model Tube Pile (n=20)	**Concrete Prototype Pile**	**Aluminum Model Solid Pile (n=20)**	**Concrete Prototype Pile**
Young's Modulus (E_p) (kN/m^2)	$7x10^7$	$3.2x10^7$	$7x10^7$	$3.2x10^7$
Bending Rigidity (E_pI_p) (kNm^2)	0.249	39872	0.55	88000
Outer Diameter (d) (mm)	20	399	20	486
Wall Thickness (t) (mm)	1.4	-	-	-
Length in Sliding Soil (L) (m)	0.50	10.0	0.50	10.0

We have a length scale $n_L = 1 / n = 1/20$. As a result, the prototype length in sliding soil is 20 times greater than that of aluminum pipe used in the model. That is 10 m and corresponds approximately to a coarse prototype sand ($D_{50} = 0.5\sqrt{20} = 2.24$ mm). We need to reduce the flexural rigidity of the pile by $1/n^4$ in order to maintain the value of dimensionless ratio. This can be achieved by making the prototype concrete pile (C30) with 40 cm diameter for case of the flexible pile, and 50 cm diameter for the rigid pile.

CHAPTER FIVE
EXPERIMENTAL STUDY

5.1 Introduction

The complete testing system including the test box, test piles, load measurement, deformation measurement and data acquisition systems is presented in this section. The calibration procedure for the instrumentation is also discussed.

The unique experimental apparatus, used in this work to evaluate deformation and load transfer behavior of passive piles, consists of a box in which model tests are performed, a pluviation system to prepare homogeneous and uniform sand bed, model piles, and measurement systems.

Each of these components is described, along with the characteristics of the soil used in the testing program. Construction and testing procedures used for each model test are then presented.

In this setup, a slice from infinite number of piles in an inclined loose sand bed was simulated. A series of model pile tests in one and two rows is carried out in a large box filled with sandy soil. Moment and the lateral pressure distribution on the front faces of the model piles due to the moving soil mass are studied. The experimental apparatus was specially designed and manufactured for this purpose. Based on the experimental results, the behavior of soil around piles, pile spacing and pile rigidity effect on soil arching and the relation between the lateral soil pressure and moment acting on piles and the relative displacement, the difference of pile and soil displacement, and behavior of soil around pile are determined.

The dry uniform quartz sand was placed in the test box, the inside dimensions of which was 1200 mm long, 480 mm wide, and 500 mm high. The box is stiffened with steel frame to prevent it from bulging out when filled with sand. Two rollers were placed between the direct contact surfaces on two sides. Cylindrical aluminum

piles, with diameter of 20 mm, length of 750 mm were installed perpendicular to the ground and 7.5 times the pile diameter (7.5d) in front of box to minimize the end shear effects (Davie and Sutherland 1978).

In the previous experimental studies, researchers set model piles in boxes consisting of two parts. The upper part of the box was moved by using a jack to apply a horizontal load to the model pile. The fixity effect of the pile in the stationary part was obtained either by a steel frame or by a strong soil placed under the sliding surface. In the test setup, the sliding soil was forced to make uniform horizontal or triangular displacement. However, a landslide is generated by the own weight of sliding mass. As a contribution to the literature, the movement of the soil due to the box was planned to be controlled by an automatically operated loosening support. For the purpose of displacement control, the conventional direct shear box unloading function was used. By loosening the support, the soil mass starts to move to the downslope direction under its own weight. During the experimental study, the rate of 2.9 mm/min was used and maintained constant in all test series for loosening the support. The tests were continued up to 5 cm of box displacement.

In this experimental study, PC-based data acquisition system, which is capable of recording 32 channels of data at a 10 kHz sampling rate per channel, was used in order to record induced strain in terms of potential difference, ΔE. Voltage readings from analog signals were converted to digital signals. Three types of measuring devices were used. These are displacement transducers at the pile heads, strain gages along model piles, and load cell in front of the support. Strain gages were set in quarter bridge configuration, whereas load cell and displacement transducers were set in full bridge configuration.

For each experiment, sand deposition was carried out at the same fall height to get a uniform and homogeneous density all over the box. The sand was discharged from the base of the box following the completion of each test, and the box was refilled again for the next test.

Pile spacing and slope angle were chosen as variables in this experimental study. Single piles and pile groups with different configurations (such as pairs of piles and three, four and six piles in a group) were used in the experiments to understand the behavior of piles subjected to a soil movement over two different sloping angles of 10° and 20°. A total of 22 tests were conducted at different pile spacings (2d, 3d, 4d, 6d, 8d, 12d, and 24d) over two different slope angles (10° and 20°).

In addition to the flexible pile test series, some tests in 20° sloping angle with four rigid piles (s/d=6) were also conducted to determine the influence of pile stiffness on the pile behavior. The pile flexural rigidity (EI) was increased by using solid pile while keeping constant the diameter and the modulus of elasticity of the pile the same as before.

Both rigid and flexible piles (mixed pile tests) were also tested together in 20° sloping angle with s/d = 6 in order to understand the behavior of free head passive piles in bowl shaped landslide geometry. Simulation of bowl shaped landslide with the testing apparatus could be achieved by locating flexible piles in the inner and rigid piles on the outer.

Experimental studies were extended to two rows of pile groups. Four series of pile group tests were conducted on two different arrangements in 20° sloping angle, such as flexible piles in two rows in parallel arrangement, flexible piles in two rows in zigzag arrangement, rigid piles in two rows in parallel arrangement and rigid piles in two rows in zigzag arrangement for investigating the effect of pile rigidity and pile arrangement on the load transfer mechanism in pile rows.

5.2 Properties of Cohesionless Soil and Its Deposition

Quartz sand was used in the testing program to model the granular moving soil. The sand which was used throughout the experimental study is medium to fine sand.

Various testing procedures were carried out to determine grain size distribution curve, specific gravity, shear strength parameters and maximum and minimum dry unit weights. The tests results are described in the following sections. Moreover the calibration of the sand placement apparatus was discussed.

5.2.1 Grain Size Analysis

A sieve analysis was performed on the sand and the resulting grain size distribution is presented in Figure 5.1. The coefficient of uniformity, C_u, is 1.39 and the coefficient of curvature, C_c, is 1.01. Other characteristics that should be noted are the mean particle size D_{50}=0.50 mm, the effective size, D_{10}=0.38 mm, as well as D_{30}=0.45 mm and D_{60}=0.53 mm. This indicates that this uniform soil is classified as poorly graded sand (SP) in accordance with the Unified Soil Classification System.

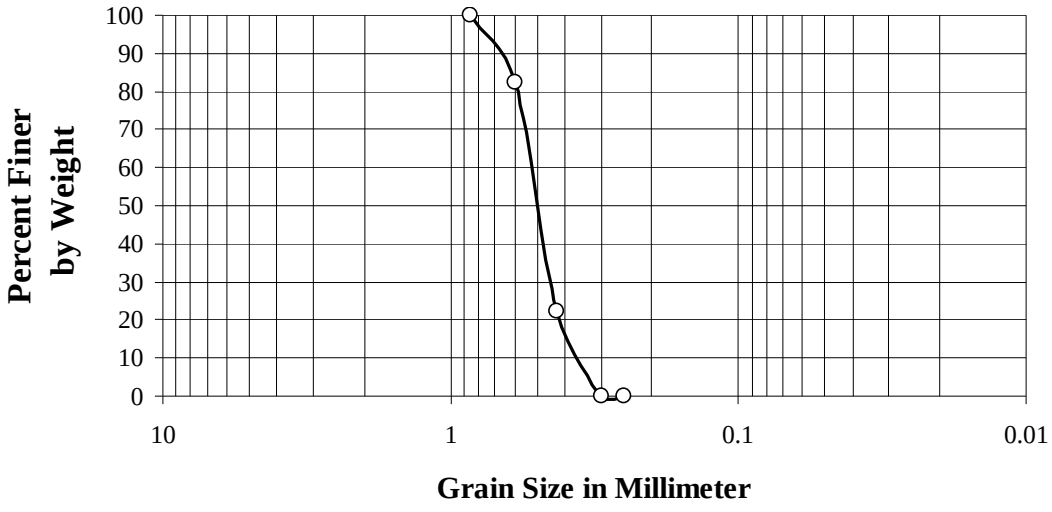

Figure 5.1 Grain size distribution of sand.

Specific gravity of the soil samples was determined. The average of four different samples of the oven dried sand was found to be G_s=2.65.

5.2.2 Maximum and Minimum Unit Weight Determination

The relative unit weight of a soil sample was obtained by relating the unit weight of the sample to the maximum and minimum densities of the material. The minimum and maximum densities of sand were calculated after performing two different tests.

Firstly, a method proposed by Adalier (1992) was used in order to determine the maximum and minimum void ratio of the soil. A standard compaction mold of 8.2 cm tall and 10.2 cm in diameter was used for both procedures. The oven dried sand was placed in the Proctor mold in 5 layers, and in order to gain the minimum void ratio, the side faces of the Proctor mold were hit with a hammer after the completion of each layer. In order to get the maximum void ratio the sand was poured in the same Proctor mold without compacting the already deposited soil from a 20 mm height with a spout. The procedures were described in detail in Bowles (1996). Each procedure was performed two times and the average was taken as the minimum or the maximum value. Table 5.1 contains the results for each trial as well as the means of trials.

Table 5.1 Maximum and minimum unit weights of sand

	Trial#1	Trial#2	Mean
Minimum Unit Weight (kN/m^3)	13.10	13.16	13.13
Maximum Unit Weight (kN/m^3)	16.07	16.05	16.06

In the second test to determine the minimum unit weight, a quantity of dry sand sufficient to fill a cylindirical mold with a diameter of about 10 cm and a height of 4 cm was placed with a funnel having a 0.9 cm diameter spout. Then the height between the mold and the spout of the funnel was kept constant as 2 cm until the mold overflows. The sand was then smeared level with the top of the mold and the minimum unit weight was calculated from measured masses and volumes as 13.13 kN/m^3. The maximum unit weight was determined by depositing the sand into this cylindrical mold through funnel from different heights and it was found as 16.06 kN/m^3. Relations between unit weight (γ) and void ratio (e) are given below.

$$g_{\max} = \frac{G_s g_w}{1 + e_{\min}} \tag{5.1a}$$

$$g_{\min} = \frac{G_s g_w}{1 + e_{\max}} \tag{5.1b}$$

The average index properties of the sand are given in Table 5.2.

Table 5.2 Average index properties of the sand

Property	Sand
Mineralogy	Quartz
Specific gravity, G_s	2.65
Mean particle size, D_{50} (mm)	0.50
Maximum and minimum particle size, $D_{max} - D_{min}$ (mm)	0.7 – 0.3
Coefficient of uniformity, C_u	1.39
Coefficient of curvature, C_c	1.01
Maximum dry unit weight, γ_{max} (kN/m^3)	16.06
Minimum dry unit weight, γ_{min} (kN/m^3)	13.13
Maximum void ratio, e_{max}	0.98
Minimum void ratio, e_{min}	0.62

5.2.3 Determination of Angularity of Sand using Digital Image Processing Techniques

The images of the sand particles have been acquired using a computer controlled microscope with a magnification factor of 60. The images have been stored directly to the computer's hard drive through USB connection as uncompressed bitmap images. Backlighting has been used in the acquisition process in order to have dark sand particles images on the white background. Thus, the contrast between the sand particles and background has been improved (Figure 5.2).

Figure 5.2 The raw microscope image.

In order to perform successful segmentation of the particles, the images of the sand particles have been processed by using a freeware digital image processing software called as ImageJ. The contrast of the particles has been improved by using contrast stretching operation (Figure 5.3a). Then, the borders of the sand particles have been sharpened by using an edge preserving smoothing filter (Figure 5.3b). Thus, the overall shapes of the sand particles have been refined for further image processing operations (Önal and Özden, 2006).

(a) (b)

Figure 5.3 Filter processes: (a) Contrast stretching (b) Edge preserving smoothing filter

A proper threshold value has been determined for each sand particle image (Figure 5.4a). The images have been converted to binary form using the determined threshold value (Figure 5.4b).

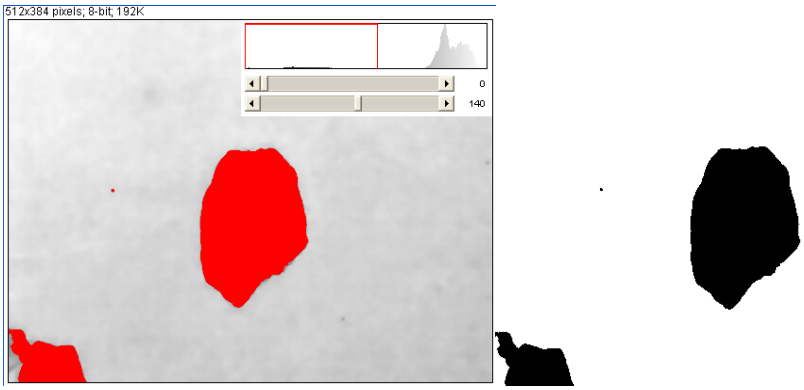

(a) (b)

Figure 5.4 Thresholding operations: (a) Histogram (b) Binary image

A total number of 79 particles have been processed and an image has been constructed which include all processed sand particles in order to perform shape analysis (Figure 5.5).

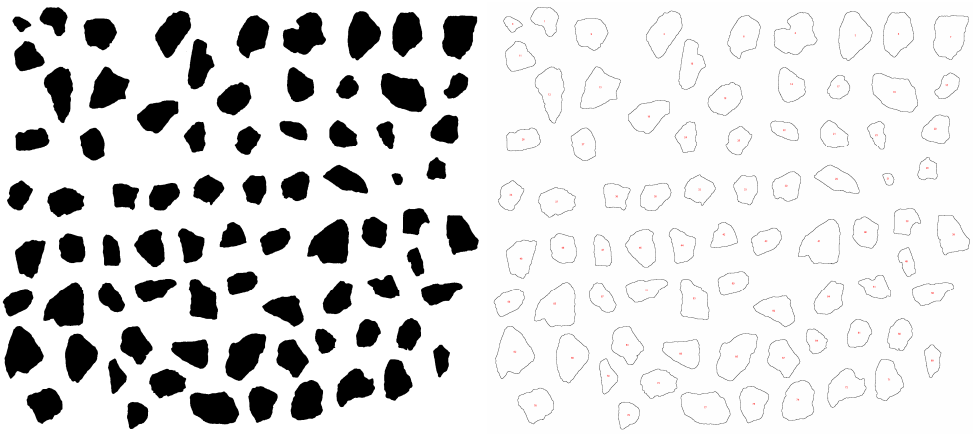

Figure 5.5 All particles used in shape analyses.

The roundness value which is defined as R = (4π area)/(perimeter)^2 has been calculated for each grain using the same image processing software. An average roundness value of 0.733 has been found with a standard deviation of 0.055. The same procedures have been performed to the grain groups which are presented as angular, subangular, sub rounded, rounded and well rounded in the literature (Lambe and Withman, 1969). The average values of 0.724, 0.737, 0.779, 0.801 and 0.852 have been found for each grain group, respectively. Thus, the inspected sand particles may be entitled as angular to subangular grains.

5.2.4 Pluviation of Sand

In model testing programs, the method used for the preparation of the soil beds is critical. It is necessary to place the soil in an easily repeatable manner such that the reconstituted sample is uniform and homogenous throughout. Also desirable is that the soil fabric of the sample reflects the actual in-situ conditions. The more popular techniques of sand placement are pluviation, vibration and tamping (Rad and Tumay, 1987; Lo Presti et al., 1992).

Pluviation (raining), which involves the free fall of sand grains through air, is generally considered the most effective and the easiest method because it is capable of producing a relatively homogeneous bed as well as simulating soil fabric as encountered in the field (Rad and Tumay, 1987). In addition, unlike the alternative techniques, pluviation generally produces little to no particle crushing or radial segregation (Lo Presti et al., 1992).

Many researches have been performed to determine the factors which affect the relative unit weight of specimen placed using pluvial deposition. It was theorized by Vaid and Negussey (1984) that it is the kinetic energy of the soil particles at the instant of impact during the raining that controls the relative unit weight of the sample. Several experimental testing programs identified several key factors as having a significant and direct influence on the relative unit weight of a sample. These are drop height, soil particle size, deposition intensity (Vaid and Negussey, 1984; Rad and Tumay, 1987; Lo Presti et al., 1992).

In general, the velocity (and therefore, the kinetic energy) at impact of a single soil particles is directly related to the height of drop, H_d. However, a soil particle leaving the nozzle will reach a constant (terminal) velocity after a specific falling height. Therefore, the kinetic energy at impact of a soil particle will increase as the height of drop is increased until the point at which constant (terminal) drop height is reached. An additional increase in drop height beyond this point has no effect on the kinetic energy on impact.

Both the velocity of falling particles and the constant falling height are also affected by the grain size. In general, for a given height, the impact velocity of larger soil particles is greater than the impact velocity of smaller particles. Also, the terminal velocity of the soil particles increases with an increase in particle size (Vaid and Negussey, 1984; Lo Presti et al., 1992).

The deposition intensity is defined as the amount (mass) of soil falling per unit area per unit time. This variable is primarily determined by the area of the opening through which the soil exits the hopper. The simultaneous fall of particles produces interferences in the falling sand which causes a loss in the kinetic energy of the particles and, therefore, a lower relative unit weight of the specimen. This obstacle increases with the increased deposition intensity thus producing an inverse relationship between deposition intensity and relative unit weight (Lo Presti et al., 1992).

In certain instances, pluviation may not be practical due to an inadequate apparatus or an irregular size and shape of the specimen. In these cases, it has been suggested that pouring the sand through the funnel directly into the specimen container may be a suitable approximation of the pluviation procedure.

A simplified procedure which omits the diffusing sieves and simply has the sand poured directly from the funnel into the collection pot has also been studied (Cresswell et al., 1999). A series of tests were performed by Cresswell et al. (1999) to determine the validity of this comparison. It was found that, at high deposition intensities, the poured sand tends to fall in a concentrated stream (rather than spreading out). This produces a conical pile of sand in the specimen container, shown in Figure 5.6, which results in lower densities and increased segregation.

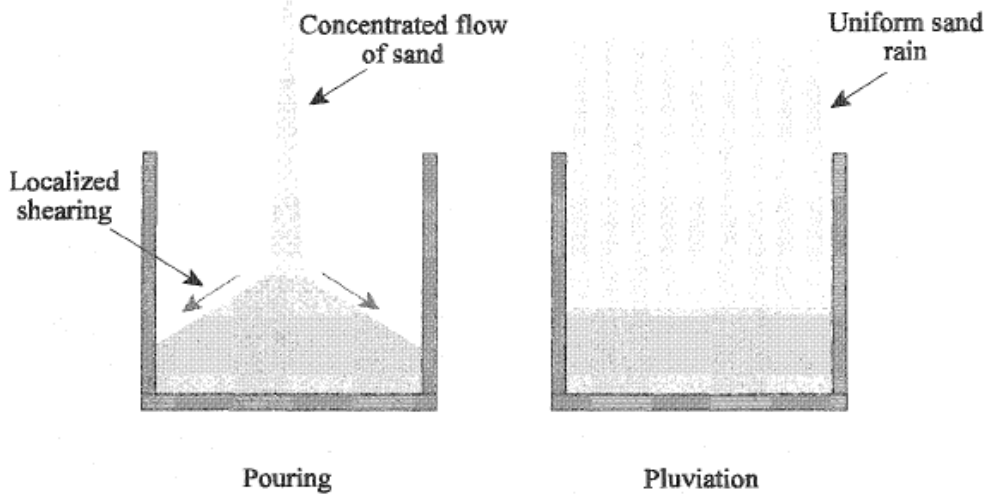

Figure 5.6 Pouring versus pluviation (Cresswell et al., 1999).

If several conditions are met, however, it was observed that specimens resulting from the pouring procedure can be reasonably comparable in terms of relative unit weight and uniformity to those specimens formed by pluviation. At lower deposition intensities and larger drop heights, the soil particles naturally tend to partially disperse into an even rain which reduces segregation such that it becomes negligible. Also the rate of sweep of the nozzle must be sufficient to prevent the formation of the segregating cone of sand. It has been concluded, therefore, that when these considerations are made, the pouring method is indeed a suitable approximation of pluviation. Experiments conducted to compare simple pouring without diffuser meshes with pluviation showed that at very slow rates of pour, pouring gives the same unit weight as pluviation (Cresswell et al., 1999).

5.2.5 Sand Placement Apparatus Calibration

In order to effectively create a repeatable and uniform sand bed so as to obtain a certain void ratio, a simple deposition device was designed accordingly with two basic parts as a reasonable approximation of pluviation method without diffuser meshes: Sand pluviation pan and flexible pipe are utilized to rain the sand into the box. A rectangular steel pan having dimensions of 600x600x150 mm with a diameter of 50mm aperture attached to the bottom. A photograph of the pluviation system positioned on the box can be seen in Figure 5.7.

Figure 5.7 Pluviation system, sand placement apparatus.

Several sets of trials were performed in order to determine an approximate drop height, H_d. All other variables reported in the literature to have an affect on specimen unit weight were kept constant.

Periodic checks of sand unit weight with several metal cans placed in the sand bed at different locations and depths during its deposition were done. The cans were subsequently excavated and weighted to determine the unit weight of the deposit. The volumes of the metal cans were determined accurately by filling them with distilled water. The weight of the sand retained in the cans was measured and the unit weight of the sand was determined as weight/volume. The average of the densities obtained by this method was accepted as the unit weight of sand in the rest of studies. Unit weights were also measured around the pile in order to know the effect of the presence of the pile. The overall unit weight was also measured by knowing the volume of the box and the weight of sand deposited. The results of the experiments are given in Table 5.3 and Figure 5.8.

Table 5.3 Summary of dry unit weight obtained using sand placement apparatus

Drop Height H_d (cm)	**Unit Weight, g (kN/m^3)**		
	Trial#1	**Trial#2**	**Mean**
2	13.05	13.15	13.10
40	14	14.3	14.15
80	14.85	15.05	14.95
120	15.25	15.55	15.5
160	15.8	16	15.9
240	16.05	16.15	16.1
280	16.1	16.2	16.15

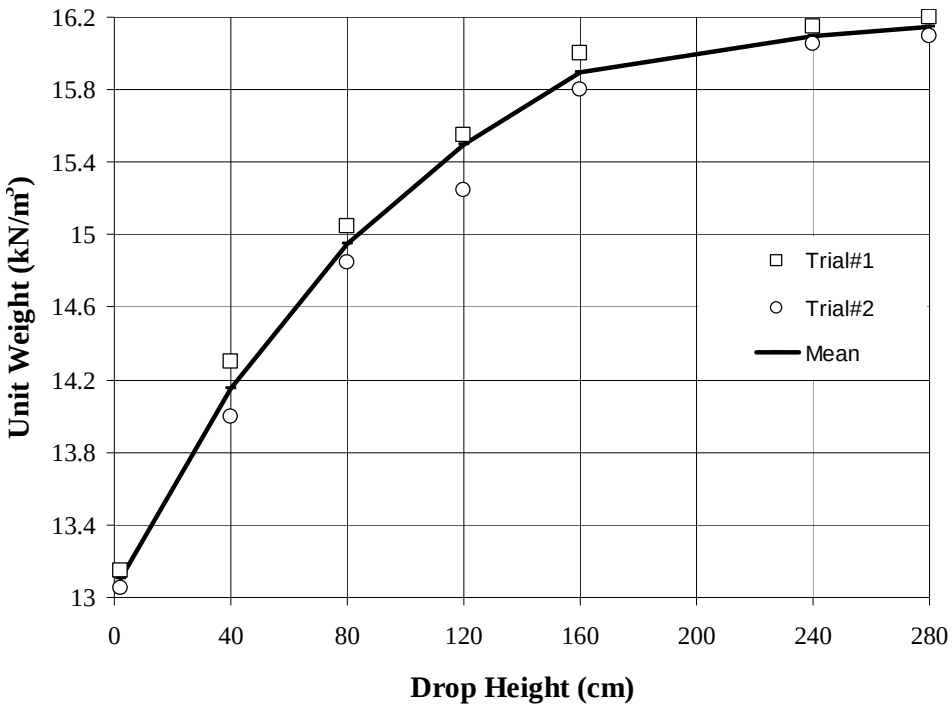

Figure 5.8 Results of sand placement apparatus.

It can be seen from Figure 5.8 that at H_d = 280 cm, the sand is approaching the terminal falling height. At this height the average dry unit weight is obtained as 16.15 kN/m^3 corresponding to a relative unit weight of 100%. Also, with a relatively large drop height, the sand particles have sufficient time to disperse, thereby increasing uniformity.

Direct shear tests have been performed on sand samples in three different relative unit weight, such as loose (39%), medium (66%) and dense (82%). The void ratio, the relative unit weight and the corresponding angle of internal friction of the sand are given in Table 5.4.

Table 5.4 The pluviation test results

Drop Height (cm)	**Unit Weight,** γ **(kN/m^3)**	**Void Ratio, e**	**Relative Density**		**Angle of Internal Friction,** ϕ **(°)**
			I_D	**Description**	
2	13.10	0.98	0		
40	14.15	0.84	39	Loose	32
80	14.95	0.74	66	Medium	35
120	15.50	0.68	82	Dense	39
160	15.90	0.64	93	Dense	
240	16.10	0.61	99	Dense	
280	16.15	0.61	100		

5.3 Experimental Set-Up

The unique experimental apparatus used in this work to evaluate load transfer in piles consists of seven main elements namely, a box in which model tests were performed, an automatically operated support to control the movement of the soil due to the box, flexible model piles, three types of measuring devices such as load cell in front of the support, displacement transducers at the pile heads, strain gages along model piles, and PC-based data acquisition system with 32 channel data logger to digitize and record the information data from measuring devices (Figure 5.9). Engineering drawing of the experimental setup is given in Appendix A.

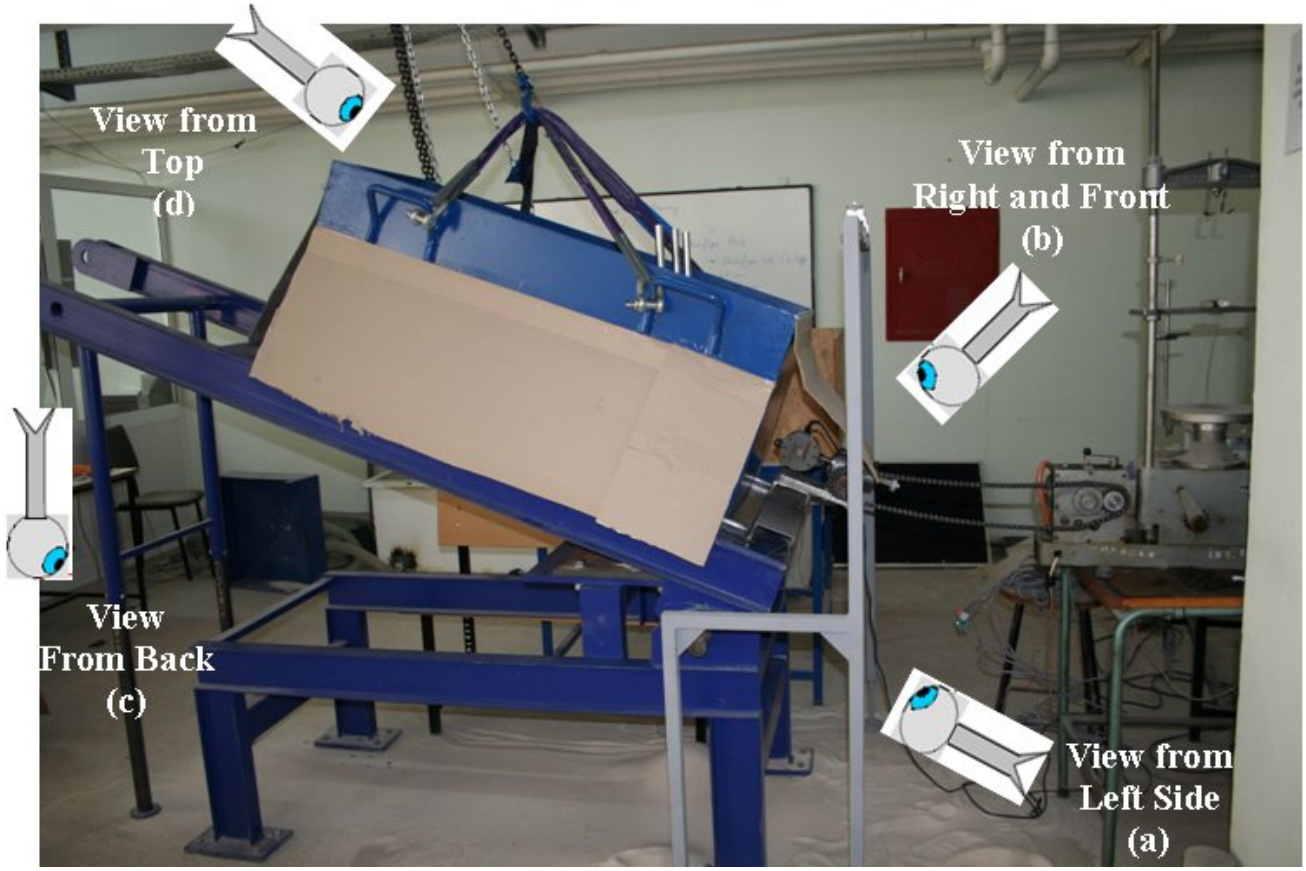

Figure 5.9 Photographs of test set-up: a) Left side view (b) Right side view (c) Back view and (d) Top (plan) view

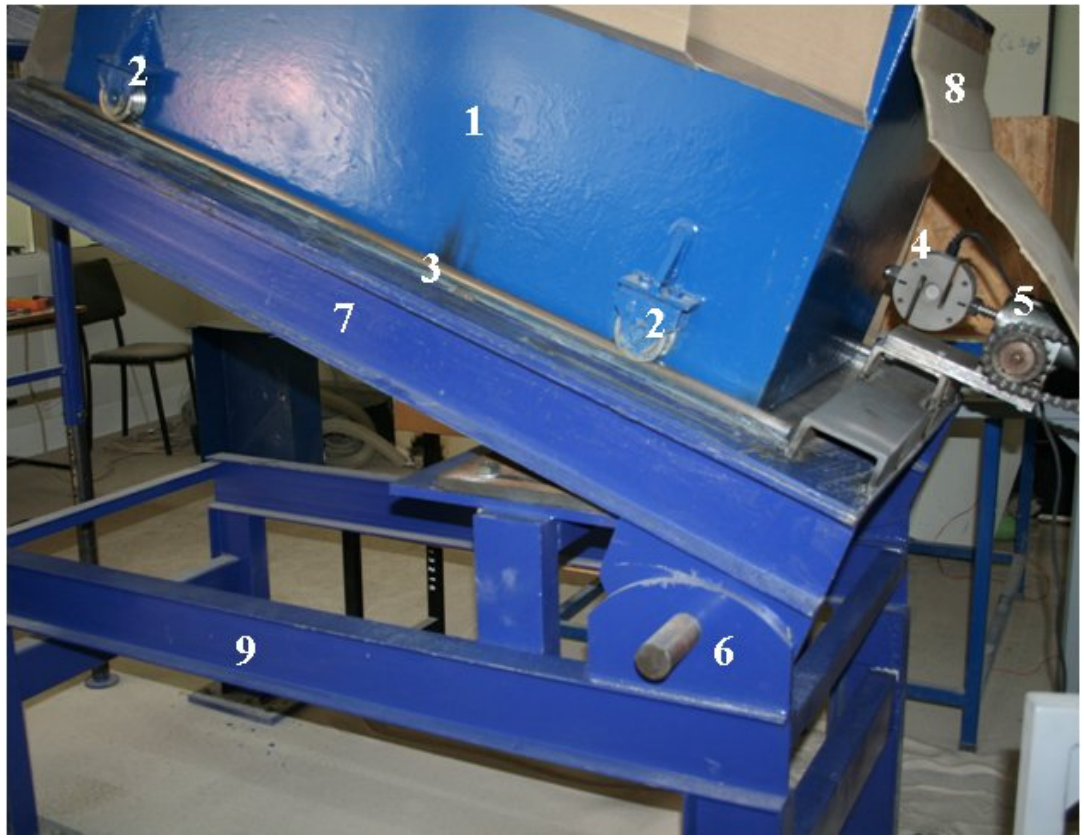

1. Box
2. Roller
3. Roller line
4. Load cell
5. Automatically operated support
6. Hinge
7. Supporter beam
8. Paper board
9. Supporter frame

Figure 5.9 (continued) (a) Left side view

1. Box
2. Roller
3. Roller line
4. Load cell
5. Automatically operated loosening support
6. Supporter beam
7. Hinge bar
8. Paper board
9. Protractor

Figure 5.9 (continued) (b) Right side view

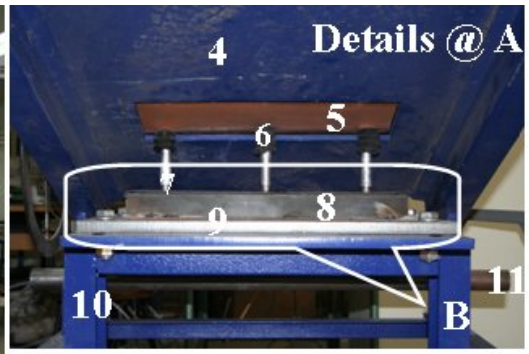

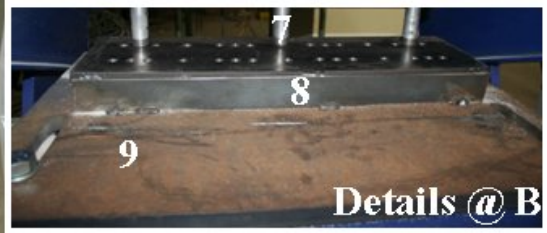

1. Supporter beam
2. Height adjusting column
3. Paper board
4. Box carrier sheet metal
5. Caoutchouc separator
6. Accordion bellow
7. Aluminum pile
8. Platform where piles are socketed
9. Steel plate adjusting the place of platform
10. Platform and plate carrier frame
11. Hinge bar

Figure 5.9 (continued) (c) Back view

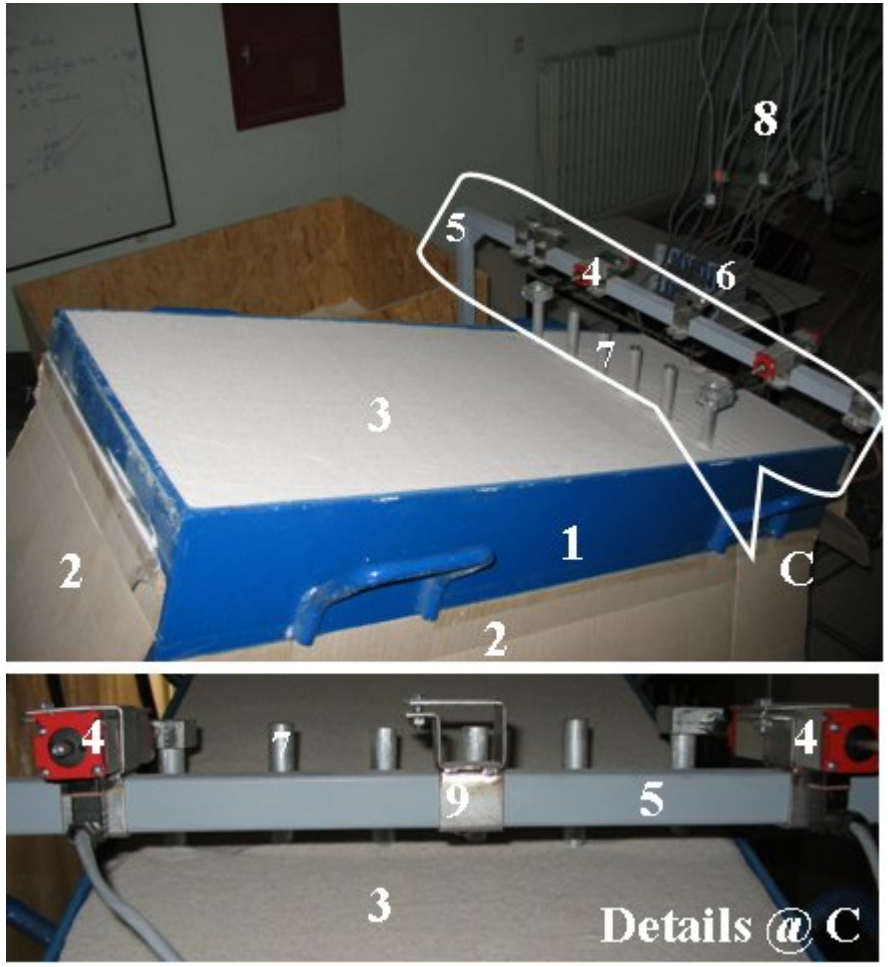

1. Box
2. Paper board
3. Sand
4. RLPT
5. Steel frame
6. Data logger
7. Aluminum pile
8. Data connecting cables
9. RLPT housing

Figure 5.9 (continued) (d) Top view

5.3.1 The Box

The aim of this study is to measure the moments and the soil pressure distribution developed on model piles due to the horizontal soil movements. In order to simulate the behavior of a sliding soil mass, a large box was designed and constructed. The experimental apparatus allows the movement of the sand in the box with two different sliding angles, and the sand mass moves by its own weight.

The inside dimensions of large box are 1200 mm long, 480 mm wide and 500 mm high. The box was made of rigid steel plates. It is desirable to reach as many combinations of pile spacing as possible. Two rollers were placed between the direct contact surfaces on two sides. The box was supported from both sides on two steel beams 240 cm long (I section of 120 mm width, bolts are used on each side to keep it still in the position). The beams were supported by four steel columns of 50 cm height at the four ends (Figure 5.10).

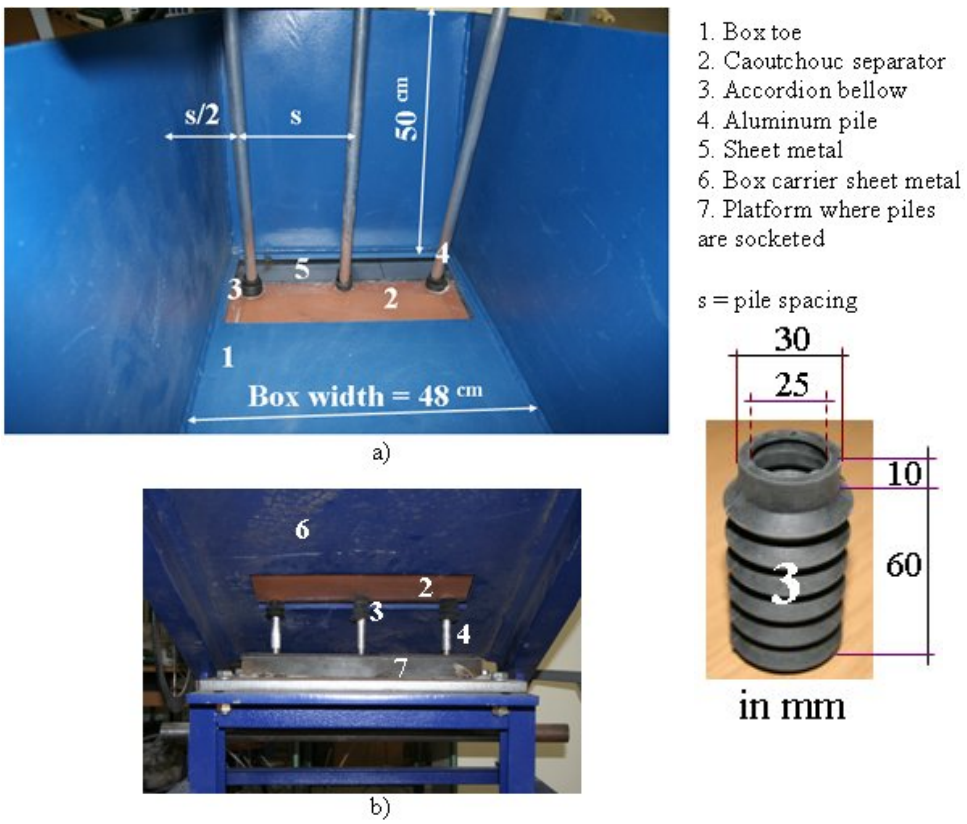

Figure 5.10 Photograph of model box with piles and placement apparatus: a) Inside view b) Bottom view

Sheet metal, the centre of which was remained open for pile installation was placed between the sliding plane and the box toe. The centre open part of the sheet metal was covered with caoutchouc separator having holes for pile installation. The diameter of holes was 25 mm and the number of holes was determined according to the pile configuration. The accordion bellows were placed in the holes as half length was in the box and the other half was under the box. Bellows heads were attached to the pile with clamps. These bellows ensured the pile free movement and prevent the sand to spill during pluviation.

5.3.2 The Model Piles

The model piles used in the tests were hollow cylindrical aluminum pipes with 20 mm outer diameter, 750 mm length, and 1.4 mm thickness. The surface of aluminum piles was sandpapered and roughed.

Tensile tests were conducted on a sample of these pipes according to ASTM-A370 at the Metallurgical and Materials Engineering Laboratory to determine the modulus of Elasticity (E). Two specimens of the material, used in the construction of the pile were tested. The modulus of elasticity is defined as the slope of the straight line from the origin to the proportional limit point. Table 5.5 shows the mechanical properties of the aluminum tubes used as model piles.

Table 5.5 Mechanical properties of aluminum material used for pile construction

Total Length (mm)	Outer Diameter (mm)	Wall Thickness (mm)	Elastic Modulus E (kN/mm^2)	Moment of Inertia I (mm^4)	Bending Stiffness EI ($kNmm^2$)	Yield Bending Moment (kNmm)
750	20	1.4	70	3557.8	2.49×10^5	80

5.3.3 Measurement Systems

Load cell with 1000 kg capacity was connected in series with the loosening support so as to determine the load-displacement relationships of the box. The load-displacement relationships for reinforced soil indicate the contribution of the pile to the shear strength of the system, assuming that the difference in load between reinforced box and unreinforced box, for an achieved lateral displacement, is that load carried by the pile elements. Details of load cell are given in Appendix B.

Deformation measurement system consisted of resistive linear position transducers (RLPT) and resistance type strain gages each were wired into a quarter Wheatstone bridge circuit. The response of the pile at each of the 7 strain gage locations was measured and stored. In addition to the strain gage measurements, RLPT measurements were also recorded at the pile tops. The properties of strain gages, linear position transducers and their measurement processes are described in detail in Appendix C.

In this experimental study, PC-based data acquisition system was used in order to digitize and record the deformation information of strain gages along piles, position transducers at the pile heads, and load cell connected in series with loosening support. The system consisted of a computer, a 32 channel data logger which are sequentially scanned and a computer program to monitor the test and allow readings to be taken and stored automatically. The details about the data acquisition system with the conversion from analog signal to digital signal are presented in Appendix D.

5.3.4 Instrumentation

A variety of instruments were used to measure the response of the pile. To ensure accuracy and reliability of data, checks were performed on the various instruments. The responses of the most interest in the research were the pile head deflection, pile bending moments and loads carried by piles.

The pile head deflections were measured by resistive linear position transducers (RLPT). An independent reference frame constructed a sufficient distance further the piles. The RLPT were attached to the reference frame at an elevation level of pile head. Data from the RLPT were digitally transferred to the data acquisition system.

The purpose of attaching strain gages directly to the model piles was to record the strain and moment behavior of the structure. The seven strain gages along the pile length were used to determine the bending moments corresponding to the same locations in both 10° and 20° slope angle series. Each strain gage was attached along the face of the pile against the soil movement. Instrumentation of pile series with the intervals of strain gages is given in Figure 5.11. Strain varies linearly over the cross section of an elastic material subjected to bending moments. This demonstrates the necessity of consistently placing strain gages along side of the pile subjected to soil pressure (Figure 5.12).

The relationship between output voltage and moment for the circuitry involved is as follows:

$$M = \frac{4xV_{out}xEI}{GFxV_i xGain\, x\frac{d}{2}} \tag{5.1}$$

Equation 5.1 described the relationship between bending moment and strain at this specific position on the cross section of the pile. This equation is only valid while the pile material remains within the elastic stress range.

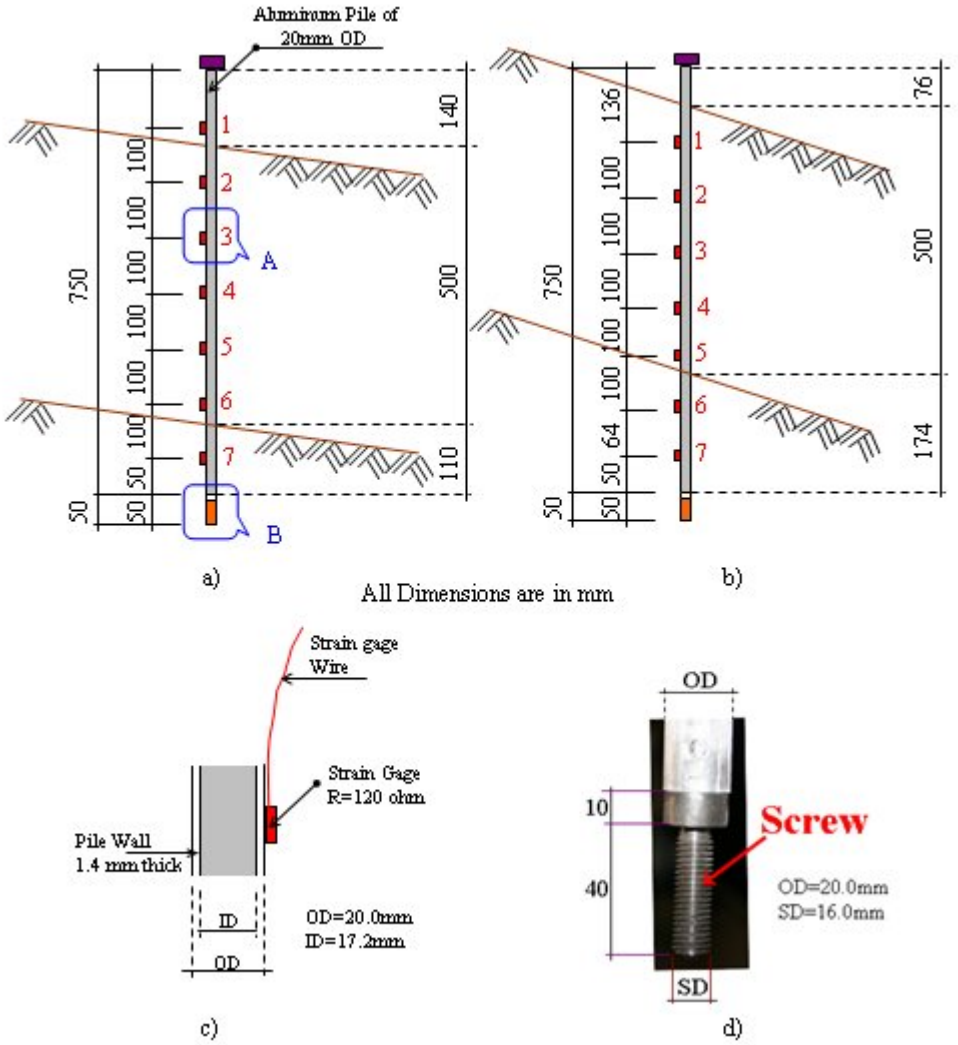

Figure 5.11 Instrumentation of pile series: a) Instrumentation of pile series in 10° slope angle b) Instrumentation of pile series in 20° slope angle c) Details @A d) Details @ B

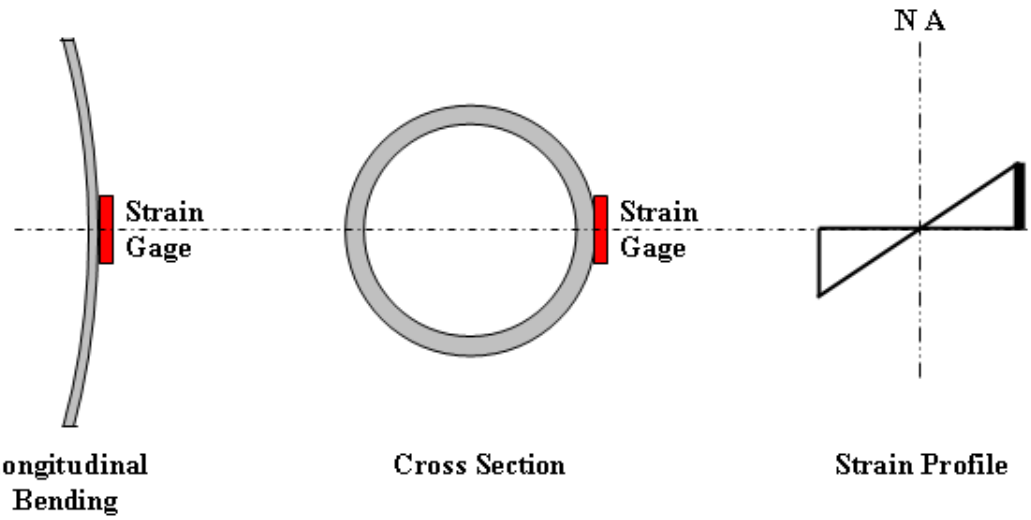

Figure 5.12 Cross section of elastic material subjected to bending moments

Before the installation of the gages, the gage locations were sanded smooth and rinsed with acetone to prevent the separation of the gages from the pile during testing. The gages were then glued to the pile with epoxy based glue. The gage resistances (120 ohm) were checked prior to installation. After the difficulties experienced during the single pile test, special precautions were taken during the instrumentation of the piles. After the installation of the gages, the shrink tubes were heated to wrap the pile tightly, covering the strain gages to protect them from damage during loading of the pile. The pile instrumentation is given in Figure 5.13.

Load cell was connected in series with the loosening support parallel to the inclined sliding surface to measure the load-displacement relationships of the box. Firstly, the load of the box filled with sand was measured as $F_{initial}$. Then the friction load along the sliding surface (F_r) was computed by subtracting the load measured by the load cell from the $F_{initial}$. For the determination of the loads carried by piles, the load difference between $F_{initial}$ and F_r was subtracted from the load measured by load cell throughout the test.

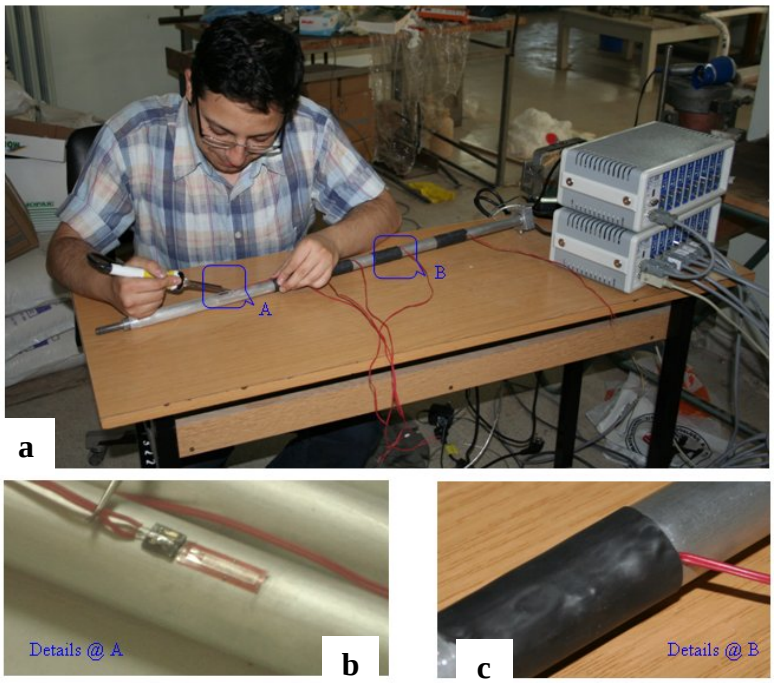

Figure 5.13 Pile instrumentation: a) Installation of gages b) Details of strain gage with connecting terminals and cable c) Precaution of gages with shrink tube

The load and deflection data has been adjusted to account for arbitrary initial values recorded by the instruments prior to soil movement. The results show that no anomalies took place during testing.

The instruments were set up and connected to the data acquisition system.

5.3.5 Calibration Experiment

Cantilever beam tests were performed on the instrumented piles to calibrate them before model tests. The calibration procedure consists of a series of three cantilever beam tests using 2, 5, and 7.5 kg weights. The pile was loaded in bending with a concentrated load at a point 100 mm far away from the pile tip (Figure 5.14). The calibration loads were chosen to ensure that the resulting stresses exceeded the anticipated stresses but remained less than the yield stress of the aluminum tube.

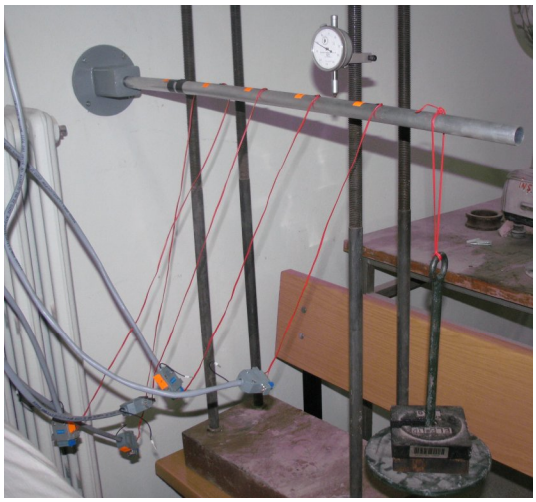

Figure 5.14 Calibration experiment of instrumented model pile.

Performing mechanics theory with known properties for the aluminum, the anticipated bending moment was calculated for each load at each gage location, and these moments were plotted against corresponding readings for each gage in Figure 5.15.

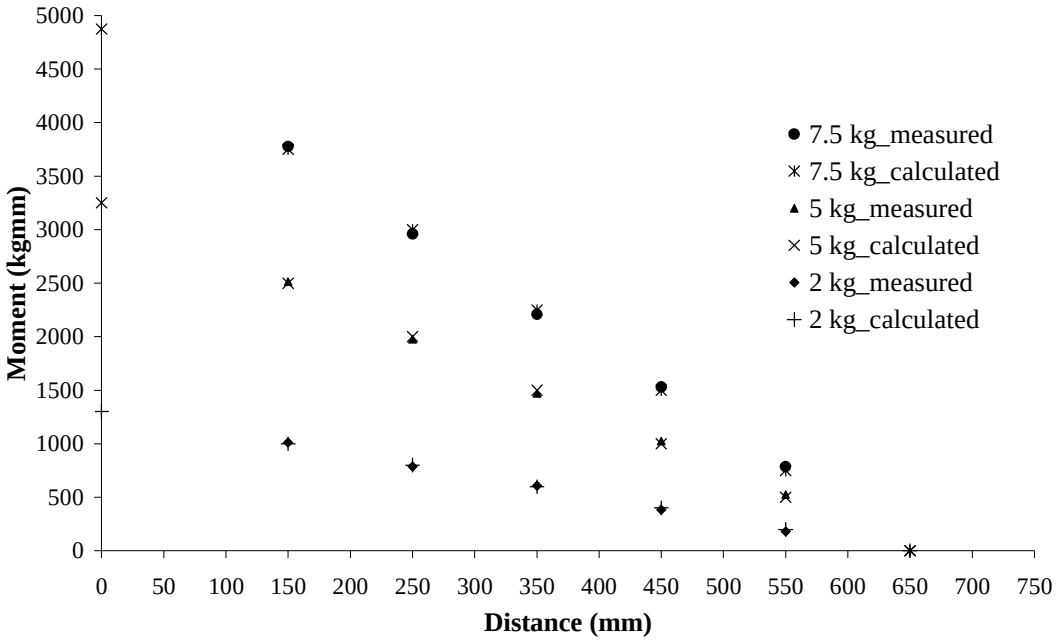

Figure 5.15 Comparison of measured and calculated moment values of calibration test.

A linear regression line, usually with a correlation coefficient of 0.99 or better, was created for the calculated and measured bending moment response of each gage as shown in Figure 5.16. This line was subsequently used to determine total bending moment during testing.

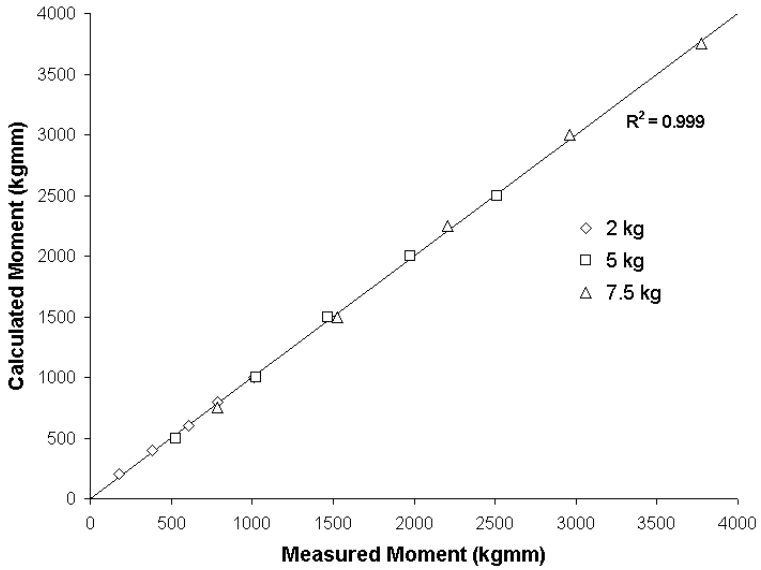

Figure 5.16 Best fit line of calculated and measured moments.

5.4 The Experimental Procedure

The testing procedure itself consisted of three phases. The first phase was the installation of aluminum model piles. Along one side of the piles 7 quarter bridge strain gages were attached at equally spaced intervals. Shrink tubes 30 mm in length were applied to the exterior surface of the pile to provide the strain gages with protection from mechanical damage. The second was the filling of homogeneous using sand placement apparatus. The third phase was the most critical portion of this research where motorized displacement control system was utilized to enable the box movement by its own weight at a constant rate of 2.9 mm/min. During the soil movement due to box movement, sensors including a load cell, displacement transducers and strain gages recorded the response of the pile. When the box displacement reached the displacement of 5 cm the system was stopped.

Pile spacing, pile rigidity and sloping angle are chosen as variables in this experimental study. A series of model tests were performed for one and two rows of piles with different pile spacing, including the tests without piles over two different sloping angles as 10° and 20°. For each experiment, the drop height of 2 cm was provided to get a uniform loose sand deposit. After the completion of instrumentation, all the instruments were set up and connected to the data acquisition system. The instruments were checked and the first test, without piles in 10° sloping angle, was performed. The load of the box filled with sand was measured as $F_{initial}$. Then the friction load along the sliding surface (F_r) was computed by subtracting the load measured by the load cell from the $F_{initial}$. This friction load was considered in the interpretation of the test results. The sand was discharged from the box. The centre open part of the bottom sheet metal was covered with Caoutchouc separator having a hole with 25 mm diameter for single pile installation. The accordion bellows was placed in the hole as half length was in the box and the other half was under the box. Bellows head was attached to the pile with clamps. A single pile was installed at the centre of the box width and 15 cm in front of the front wall of the box. Then the box was refilled again with sand by pluviation for the second test. Pile displacements at the pile head were continuously monitored during test by RLPT

attached to steel stand at a position of 140 mm above the box. By loosening the support in front of the box using the conventional direct shear box unloading function, the soil slid due to the box movement under its own weight. During the test the rate of 2.9 mm/min is maintained constant for loosening the support. In addition to a displacement measurement at the pile top, the response of the pile at each of the 7 strain gage locations was measured and stored during the box movement until the maximum allowable displacement of the box was reached (5 cm). The load carried by pile was determined by subtracting the load difference between $F_{initial}$ and F_r from the load measured by load cell throughout the test.

The same steps were performed as in the third and the following tests with the only three differences of the pile spacing, pile rigidity and sloping angles. The varied conditions including the pile spacing (s), and the sloping angle (α) were illustrated in Table 5.6.

Table 5.6 Model Test Program

Test No	**Sloping Angle (a)**	**Number of Rows**	**Pile Spacing (s)**	**Pile Rigidity**	**Number of Pile**
1	10	1	-	-	No pile
2	10	1	24d	Flexible	1
3	10	1	12d	Flexible	2
4	10	1	8d	Flexible	3
5	10	1	6d	Flexible	4
6	10	1	4d	Flexible	6
7	20	1	-	-	No pile
8	20	1	24d	Flexible	1
9	20	1	12d	Flexible	2
10	20	1	8d	Flexible	3
11	20	1	6d	Flexible	4
12	20	1	4d	Flexible	6
13	20	1	3d	Flexible	8
14	20	1	2d	Flexible	12
15	20	1	24d	Rigid	4
16	20	1	12d	Rigid	4
17	20	1	8d	Rigid	4
18	20	1	6d	Rigid	4
19	20	1	4d	Rigid	4
20	20	1	6d	Flexible Rigid	4
21	20	2	6d	Flexible (parallel)	8
22	20	2	6d	Rigid (parallel)	8
23	20	2	6d	Flexible (zigzag)	8
24	20	2	6d	Rigid (zigzag)	8
25	20	1	4d	Rigid	6
26	20	1	4d	Fixed head Rigid	6
27	20	1	4d	Fixed head Flexible	6

CHAPTER SIX
TEST RESULTS

This section presents the results of the response of the model piles to the lateral soil movement. Particular emphasis has been placed on the lateral deflection and bending moments experienced by the pile. In addition, the loads on piles during each test were carefully recorded and calculated in an effort to gain insight into the load transfer mechanism.

Tests were repeated two or three times under the same conditions in the 10° slope angle series and the results in each series were all found to be very close, with a variation of maximum 5% in total load cell recordings, 8% in transducer recordings and %12 in the strain gage recordings, demonstrating the repeatability of the tests. In the 20° slope angle series, no pile tests were repeated three times and the other tests were performed only once or twice since the discrepancy in the load cell, transducer and strain gage measurements were less than 5%. The pile spacing ratio (s/d) and the number of repeated test series are shown in Table 6.1.

Table 6.1 Pile spacing ratio and the number of piles used in tests

Pile Spacing Ratio (s/d)	**Pile Stiffness**	**Number of Pile Rows**	**Number of Pile in Tests**	**Number of Repeated Tests @ Slope Angle**	
				10°	**20°**
No pile	-	-	-	3	3
24	Flexible	1	1	3	2
12	Flexible	1	2	2	1
8	Flexible	1	3	3	2
6	Flexible	1	4	2	2
6	Rigid	1	4	-	2
6	Mixed	1	4	-	2
6	Flexible	2	8	-	2
6	Rigid	2	8	-	2
4	Flexible	1	6	2	2
3	Flexible	1	8	-	1
2	Flexible	1	12	-	1

6.1 Load-Displacement Relationship of Flexible Piles

Load cell measurements include the soil load, the frictional force between the soil and the base of the box and the load on the piles. The load-displacement relationships for piled soil indicate the contribution of the pile to the shear strength of the system, assuming that the difference in load between reinforced box and unreinforced box for an achieved lateral displacement is the load carried by the piles. The bending strain and head displacement values of all piles in a row are the same during the tests so each pile has similar elastic curves. The interpretations about load-displacement relationship have been made for the pile in the central position. Total load read from the load cell and the load carried by the piles for different pile spacing ratio for both 10° and 20° slope angle series are given in Figures 6.1 to 6.4.

In order to explain the group effect, it is needed to interpret the load per pile in the group from the load cell measurements. Therefore, the averages of total load carried by piles given in figures 6.3 and 6.4 are used and divided by the number of piles in the group. The average loads per pile versus box displacement (Δ) graphs are drawn for different pile spacing ratio for both 10° and 20° slope angle series in Figures 6.5 and 6.6, respectively.

Figure 6.7 shows plots of the loads at each box displacement for all tests. It is readily observable from Figure 6.7 that the increasing the slope angle didn’t really affect the lateral strength of the pile-soil system. In addition, at large deflections the load-displacement curves for all tests are very similar.

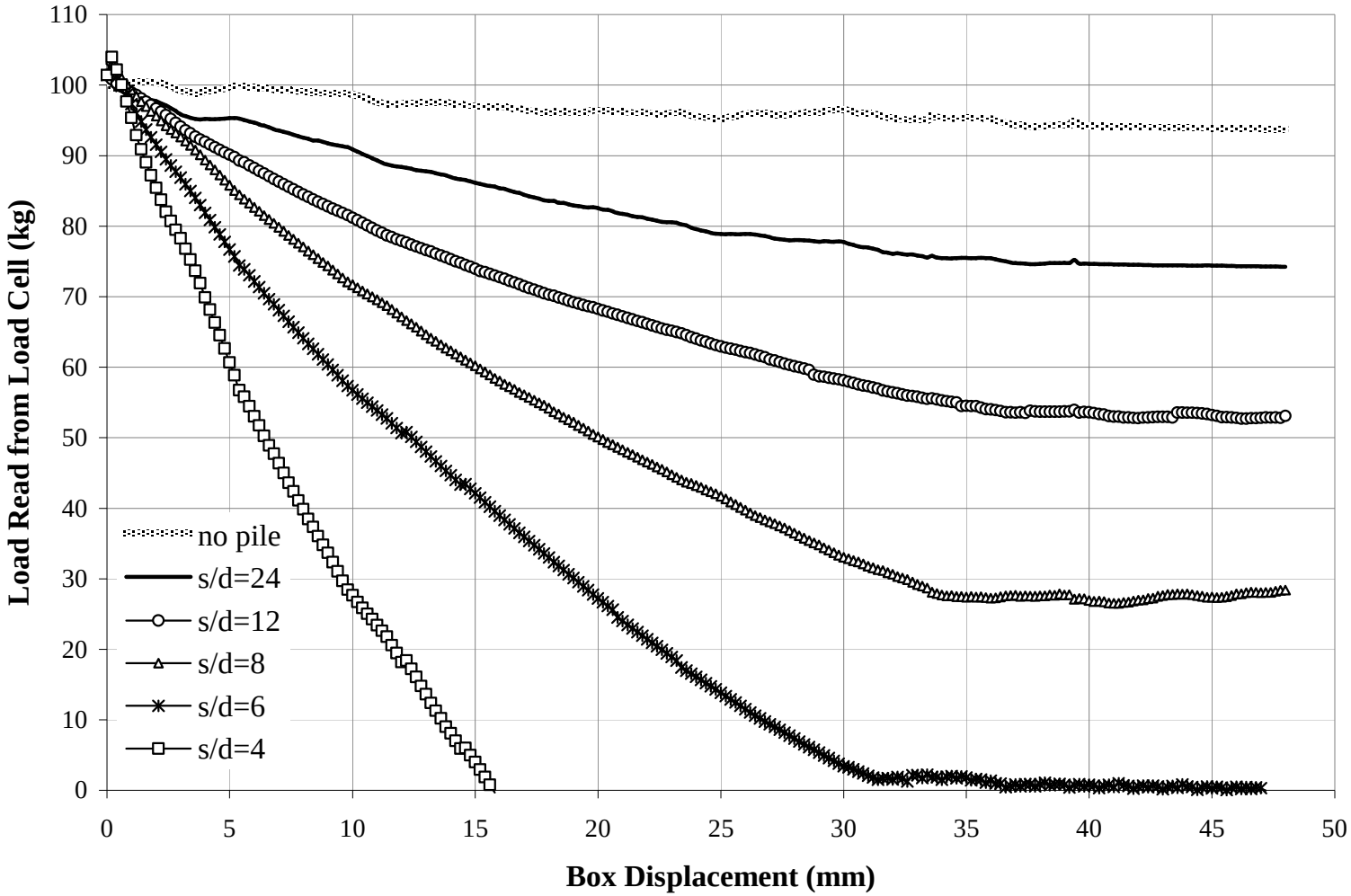

Figure 6.1 Total load from load cell versus box displacement in 10° slope angle series.

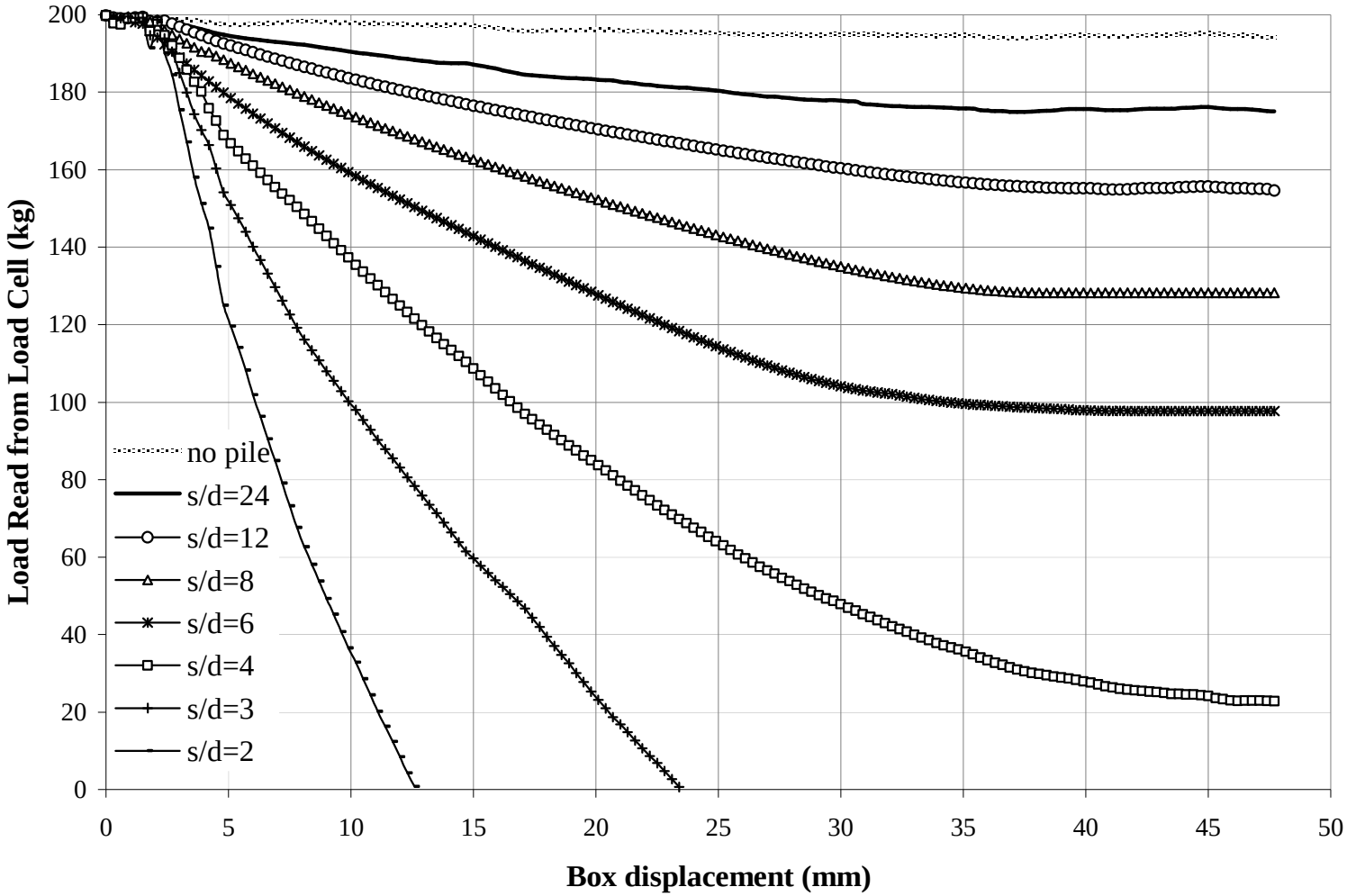

Figure 6.2 Total load from load cell versus box displacement in 20° slope angle series.

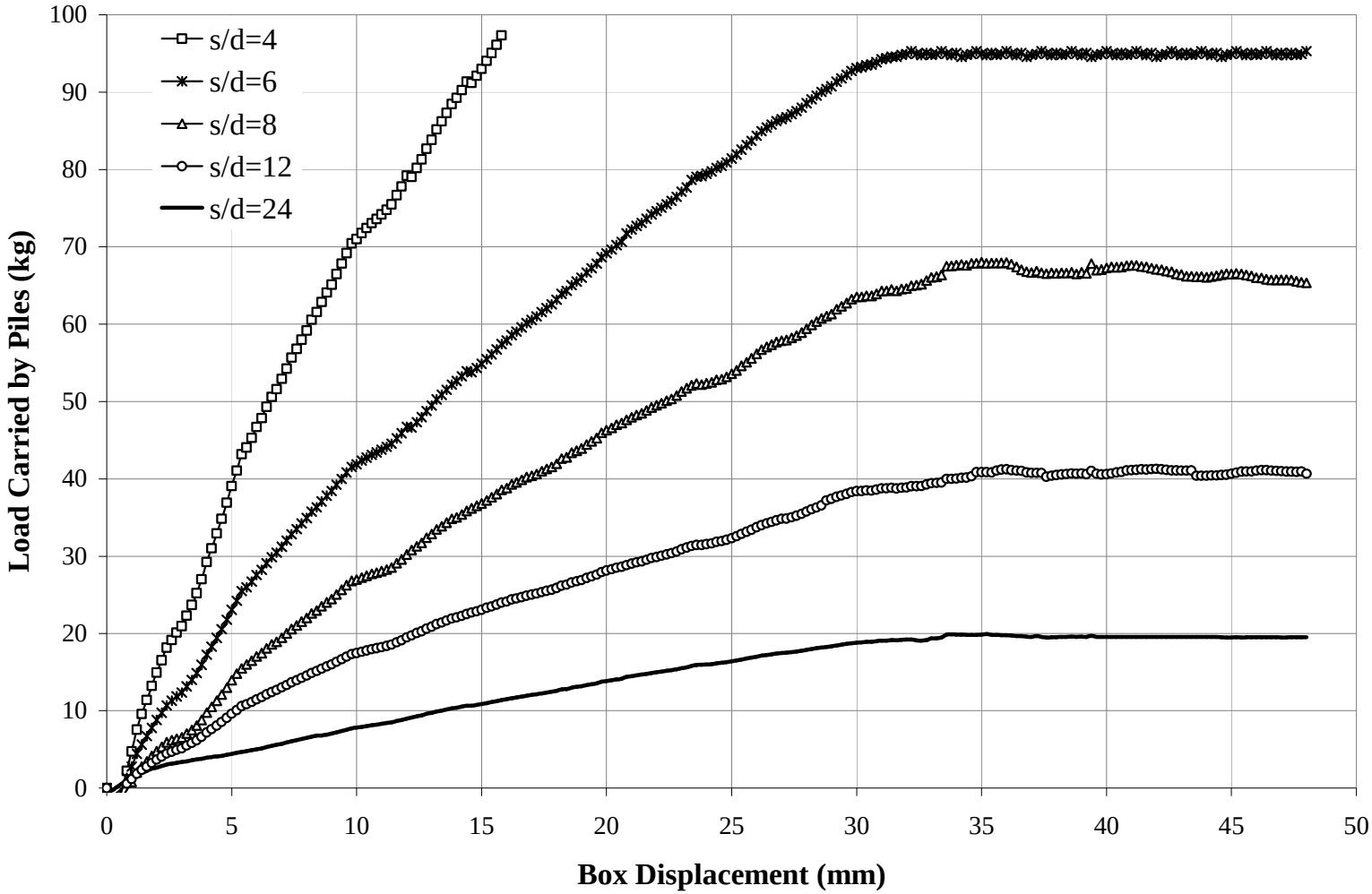

Figure 6.3 Load carried by piles versus box displacement in 10° slope angle series.

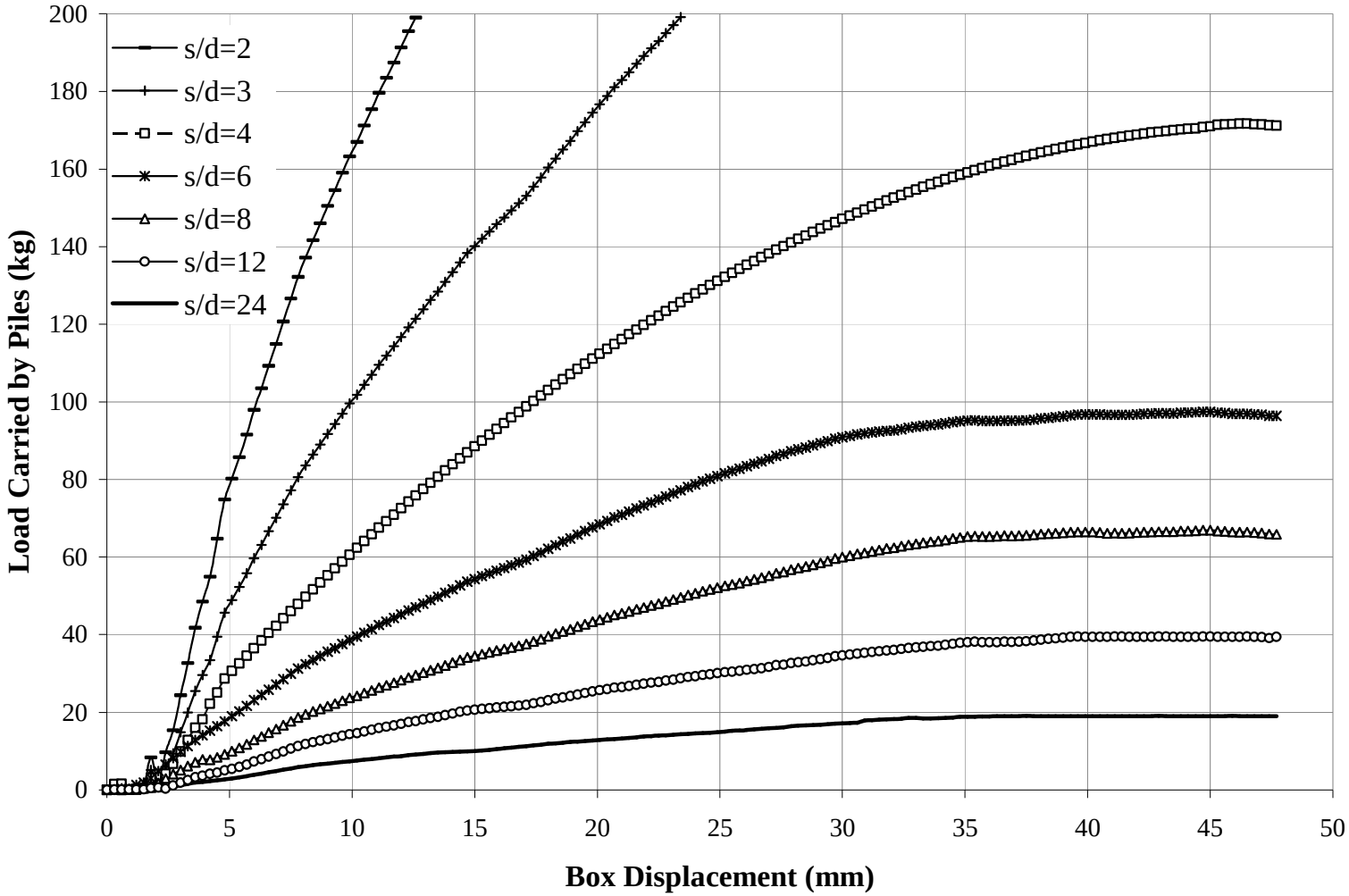

Figure 6.4 Load carried by piles versus box displacement in 20° slope angle series.

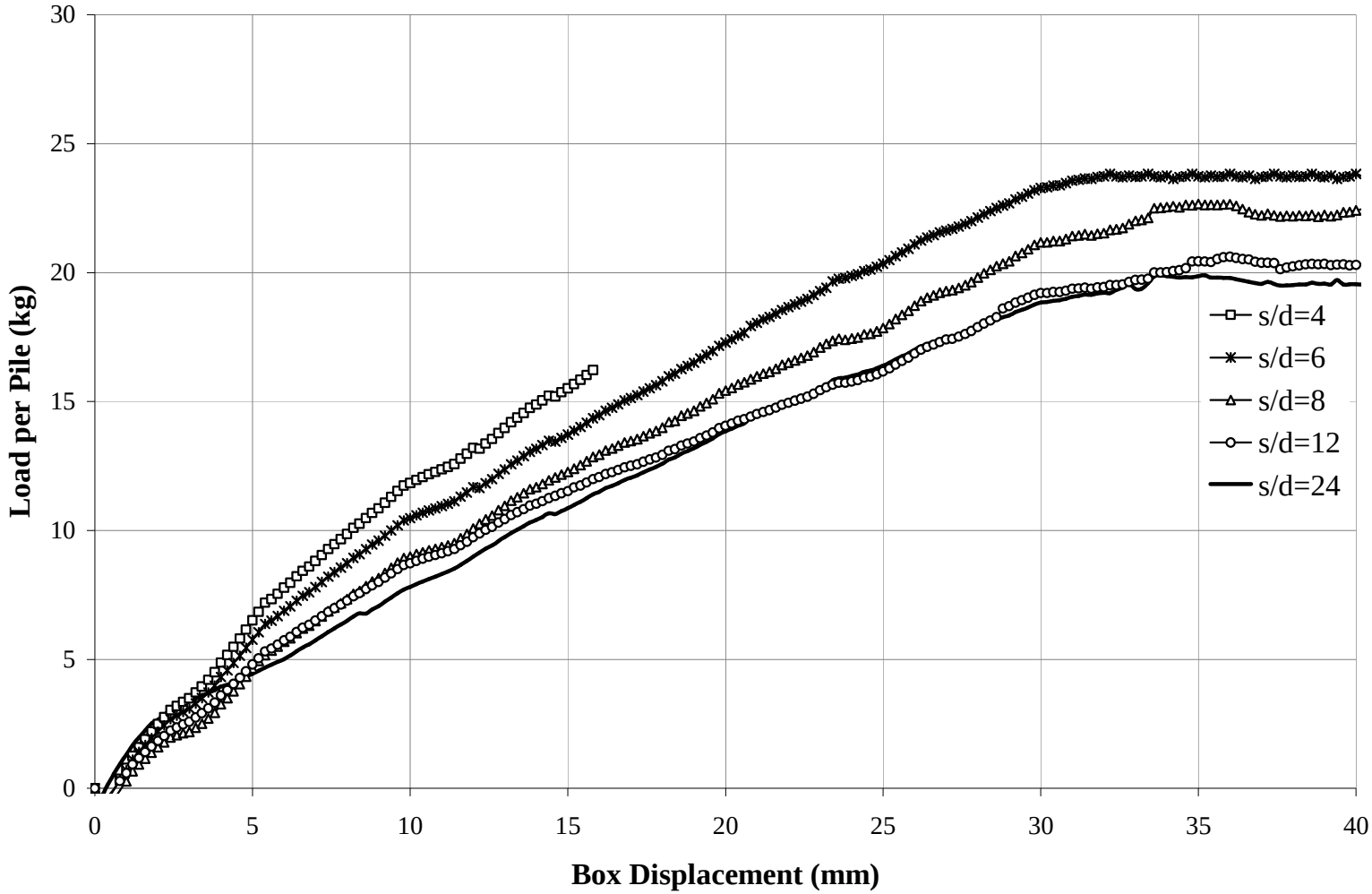

Figure 6.5 Load per pile versus box displacement in 10° slope angle series.

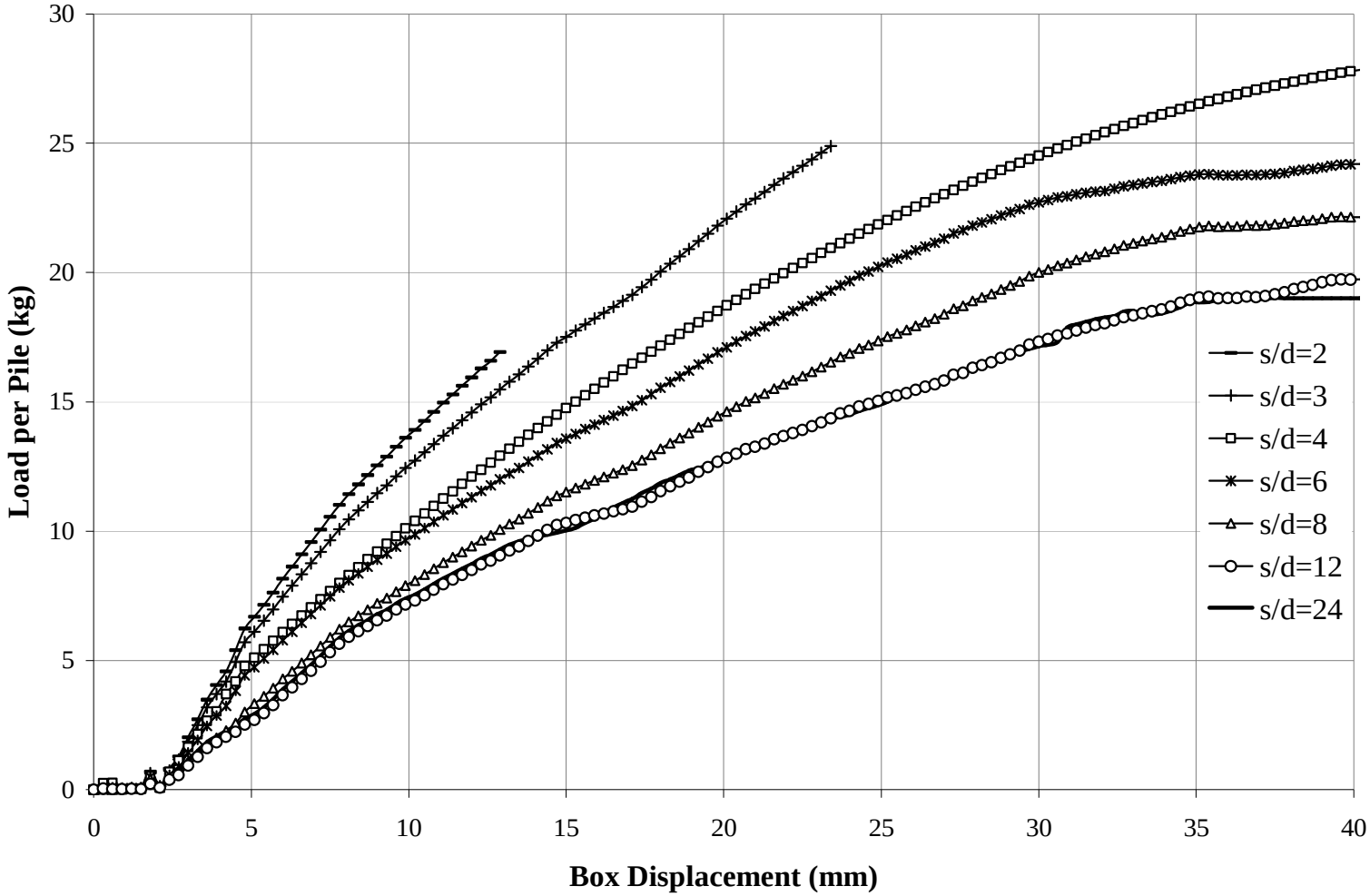

Figure 6.6 Load per pile versus box displacement in 20° slope angle series.

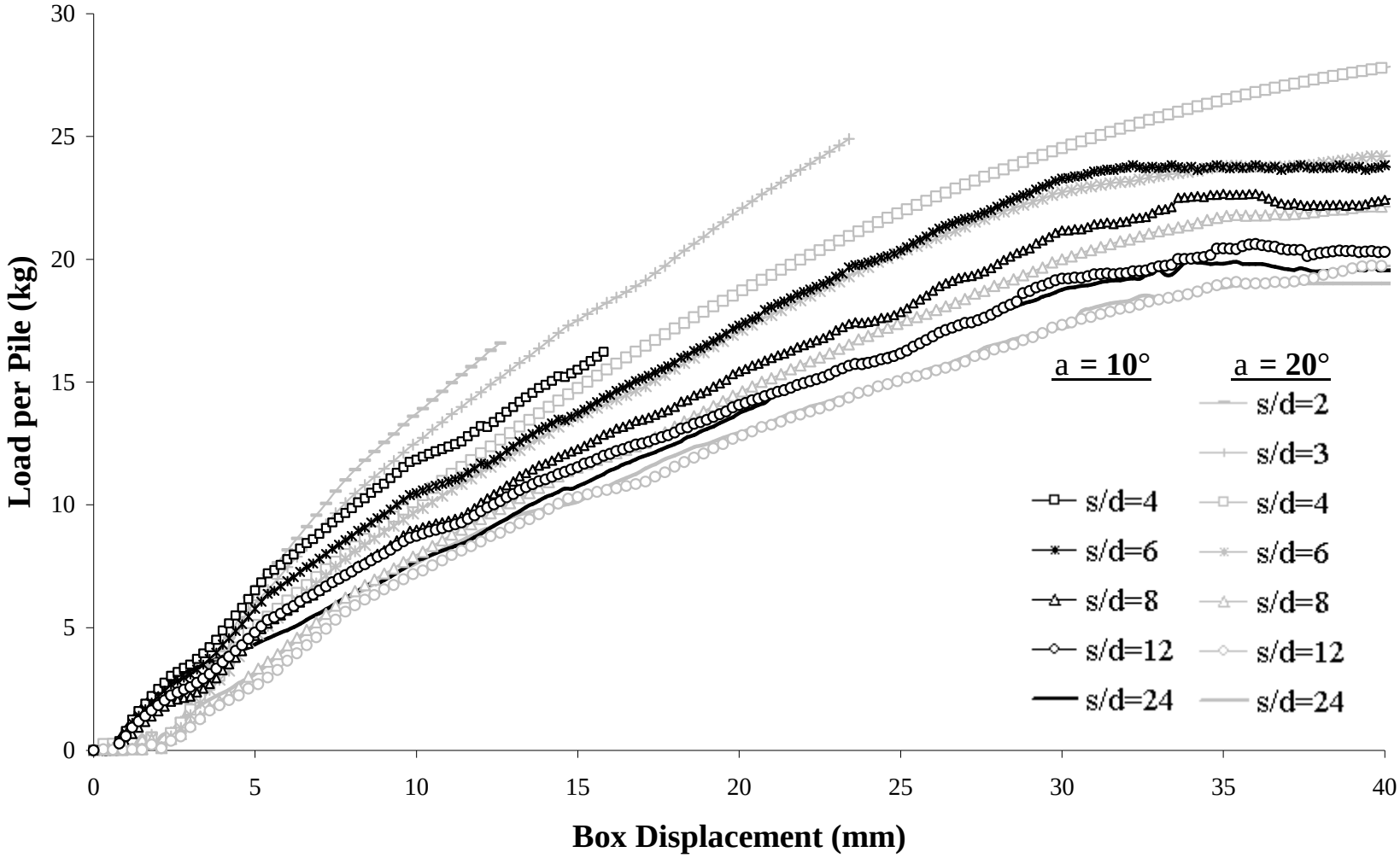

Figure 6.7 Load per pile versus box displacement in both 10° and 20° slope angle series.

The results show that no anomalies took place during testing as expected. Three different parts of a load displacement curve obtained from a pile loading can be distinguished. A very short initial linear part up to a deflection of about 2 mm (10% pile diameter), a second linear part up to a deflection of about 15 mm (75% pile diameter) and a horizontal linear part following the second linear portion up to a deflection of about 30 mm (150% pile diameter) at ultimate failure.

In using pile loads for evaluating the group effect on the lateral pile response, a group factor (F_L), which was explained previously, compares the load acting on a pile from a pile group test with that of the single pile test at the same amount of box displacement.

Representative group factor values, F_L versus box displacement (for different pile spacing ratios (s/d) are shown in Figure 6.8 for 10° slope angle series and in Figure 6.9 for 20° slope angle series. The values of group factor versus pile spacing ratio (s/d) for both 10° and 20° slope angle series are plotted together in figures 6.10 and 6.11, respectively.

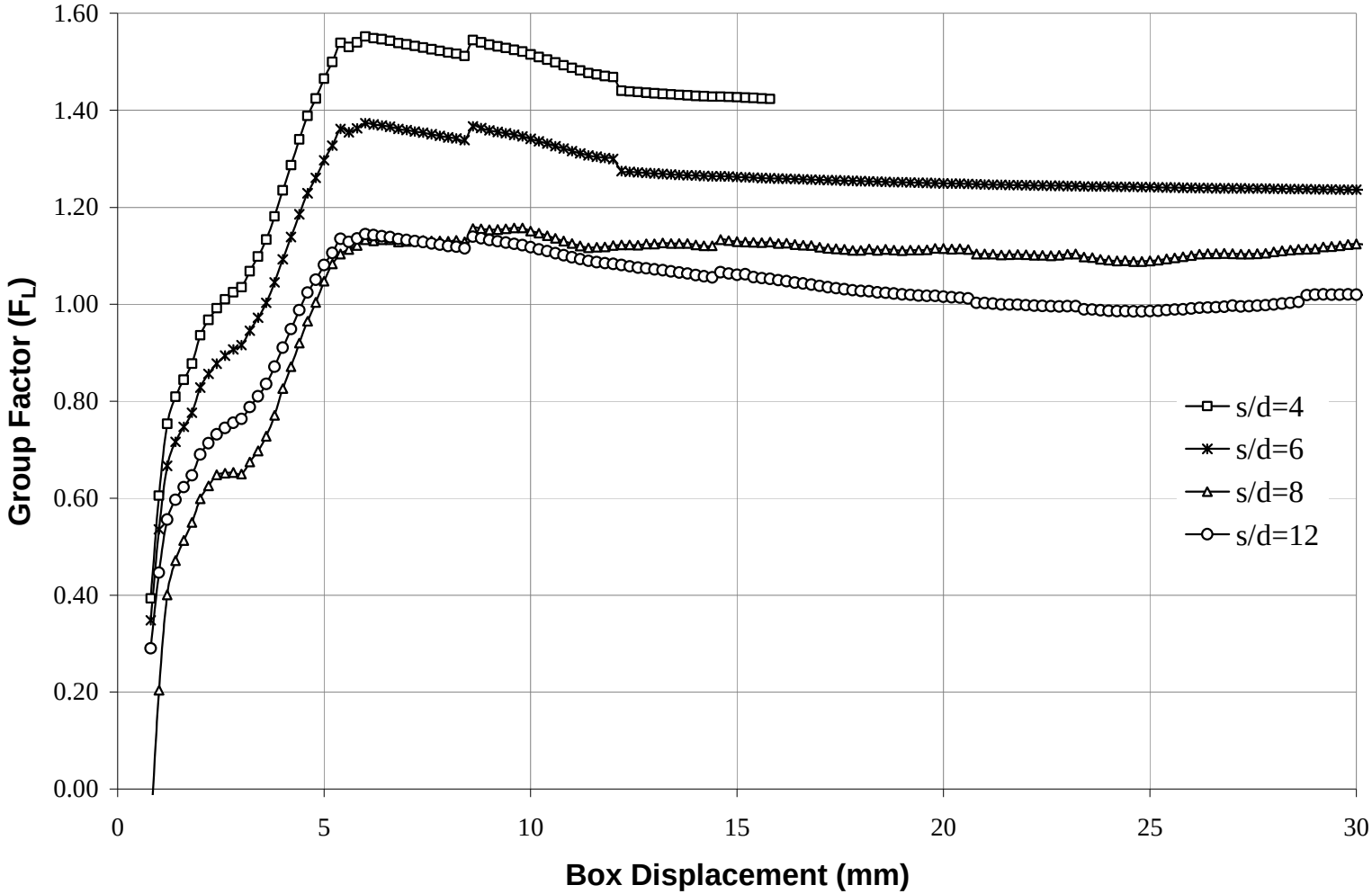

Figure 6.8 Group factor versus box displacement in 10° slope angle series.

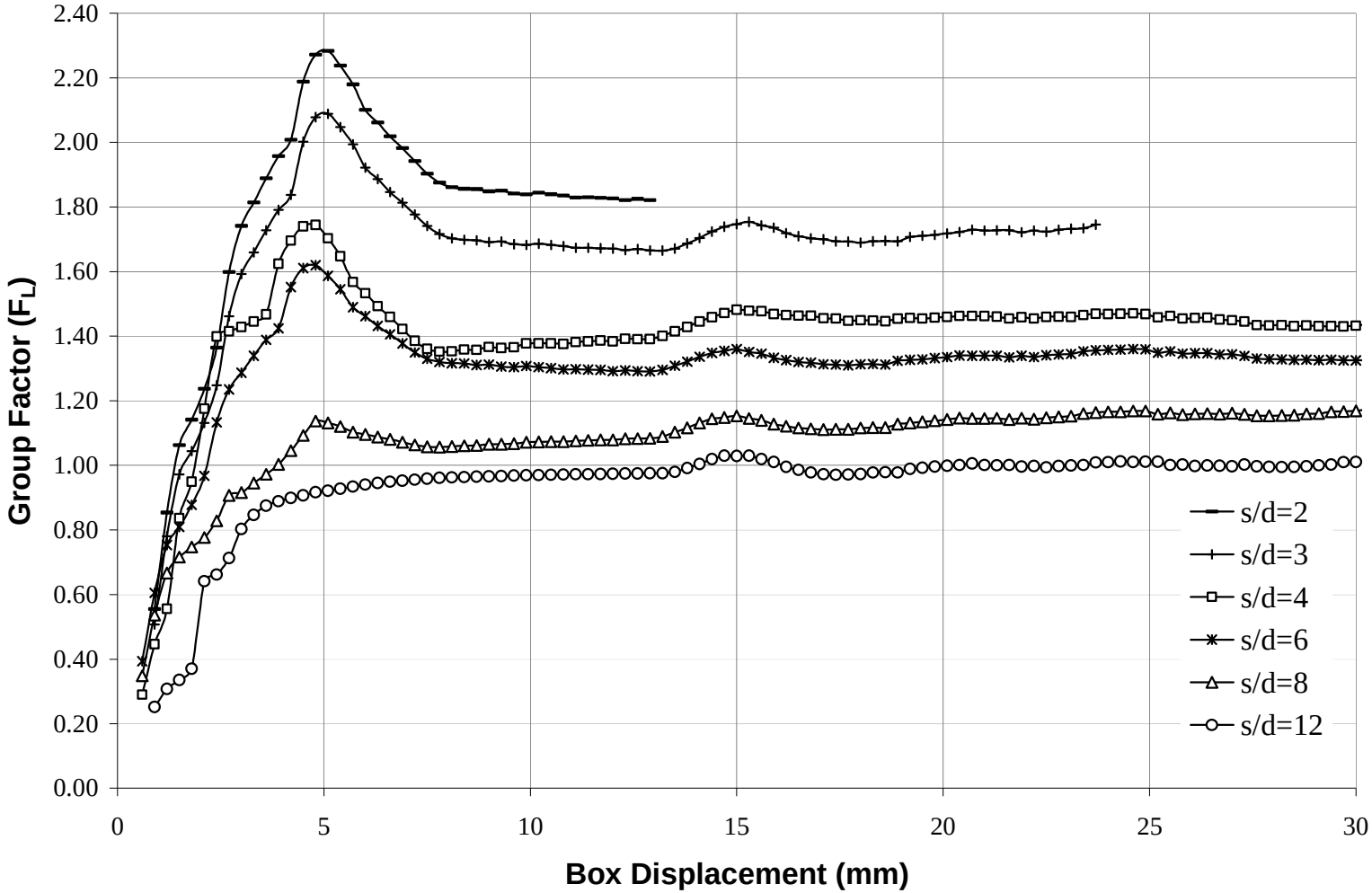

Figure 6.9 Group factor versus box displacement in 20° slope angle series.

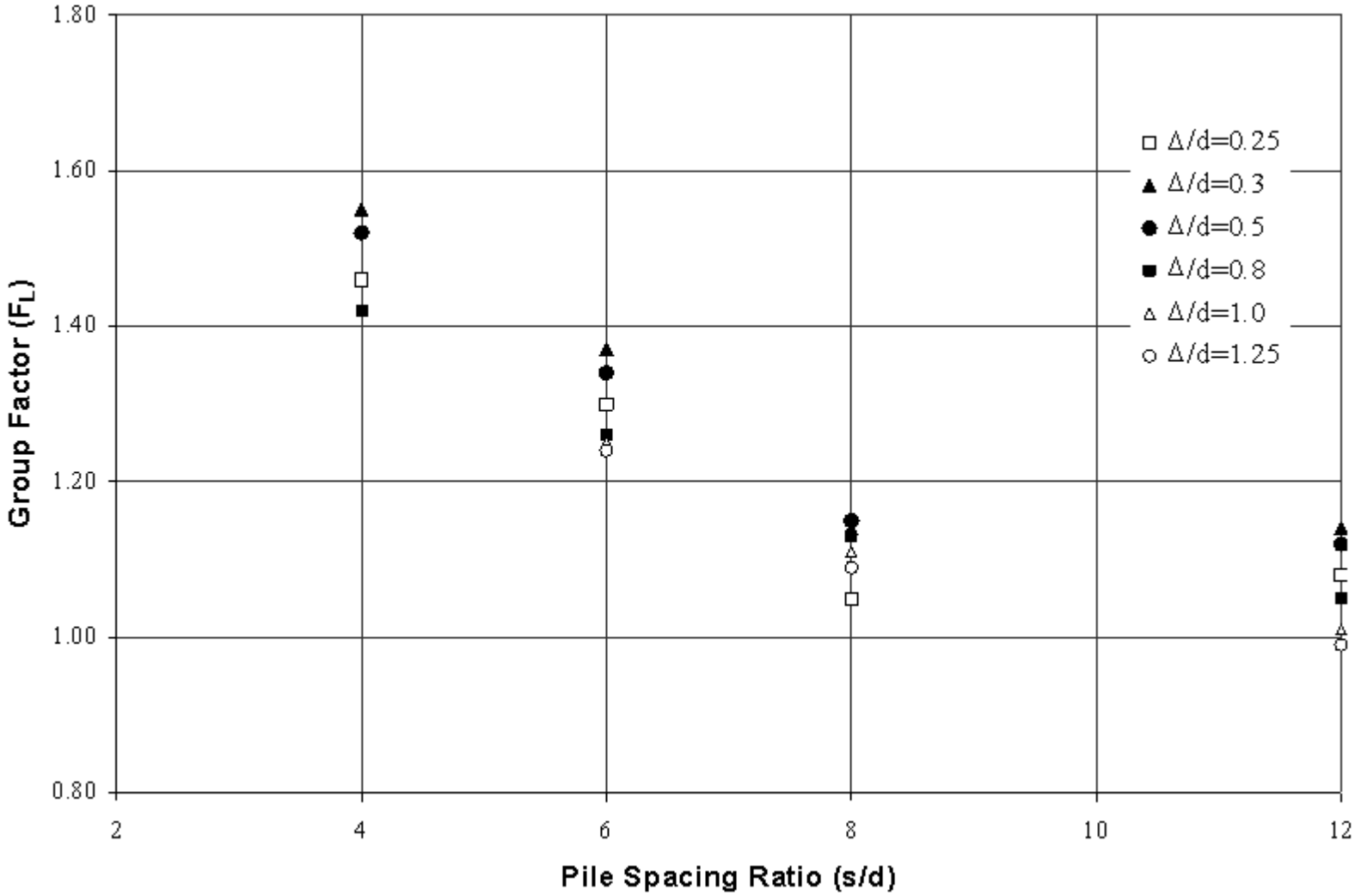

Figure 6.10 Group factor versus pile spacing ratio in 10° slope angle series.

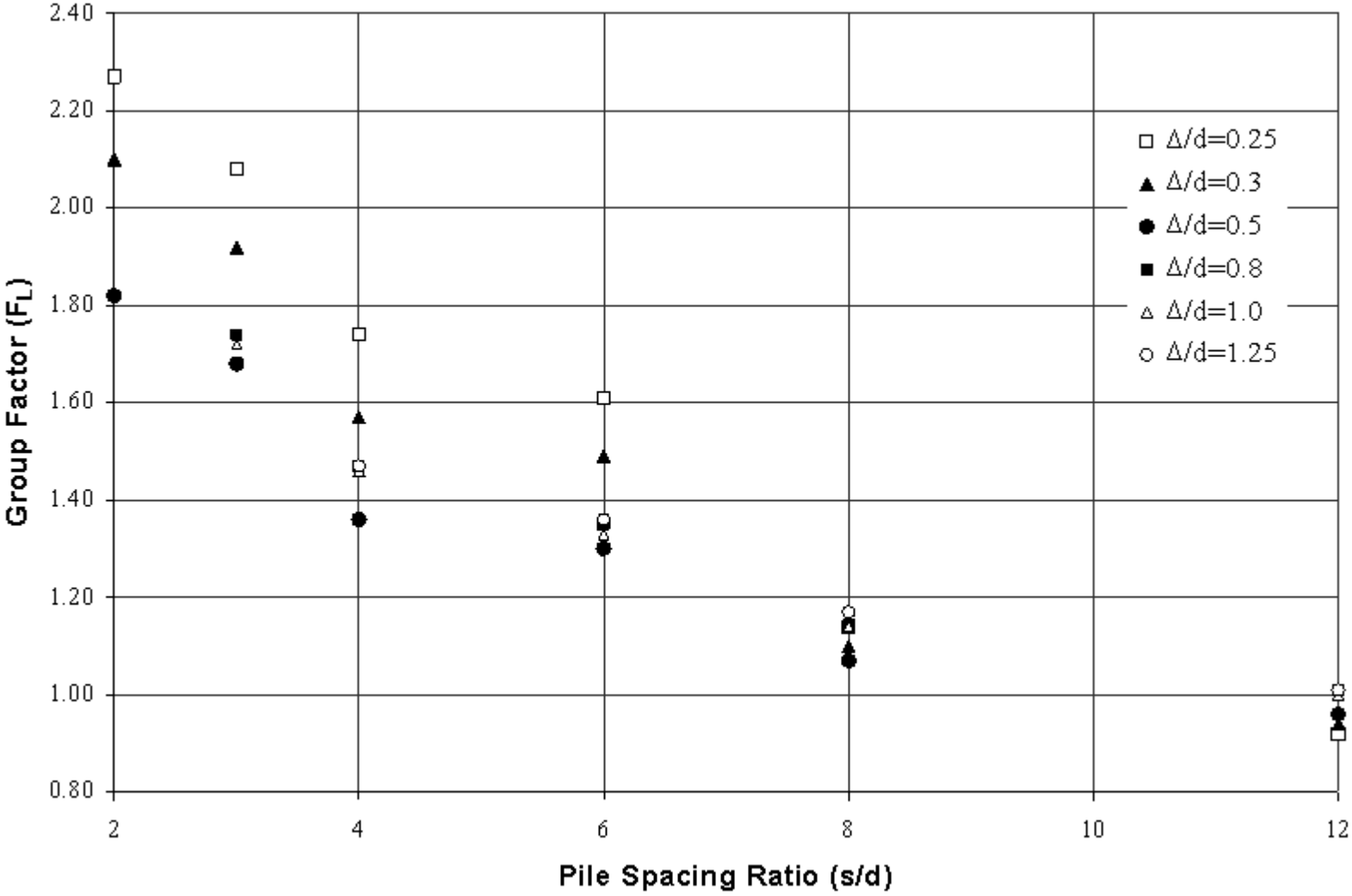

Figure 6.11 Group factor versus pile spacing ratio in 20° slope angle series.

As it is clearly seen in figures 6.8 and 6.9, the group factor is increased up to 5~6 mm box displacement for all s/d, and decreases up to 25 mm box displacement and then becomes constant. 10 mm box displacement is sufficient for the development of group factor values.

The maximum loads for all tests and the group factors, F_L, are summarized according to slope angles in Table 6.2. It is interesting to note that the slope angle has a very little effect on group factors.

Table 6.2 Maximum Load carried by Piles and Group Factors for all test series

	10° slope angle series			**20° slope angle series**		
Pile Spacing Ratio	**Load $_{max}$ (kg)**	**F_L @ Δ/d=0.30**	**F_L @ Δ/d=1.05**	**Load $_{max}$ (kg)**	**F_L @ Δ/d=0.30**	**F_L @ Δ/d=1.15**
s/d = 24	19.52	1.00	1.00	19.01	1.00	1.00
s/d = 12	20.52	1.14	1.04	19.73	1.12	1.04
s/d = 8	21.90	1.14	1.11	21.81	1.14	1.15
s/d = 6	23.76	1.37	1.22	24.05	1.61	1.26
s/d = 4		1.55	1.42 @15.8 mm	28.54	1.74	1.50 (1.47 @15.8 mm)
s/d = 3		-	-		2.08	1.73 @13.4 mm
s/d = 2		-	-		2.27	1.82 @12.9 mm

6.2 Bending Moment Distributions of Flexible Piles

In the design of pile cross-section, it is important to know the value and position of maximum bending moment developed in the pile. To determine the effect of pile spacing and the slope angle on the location and magnitude of the maximum bending moment, bending strain data from gages attached along the pile length were used to generate bending moment vs. depth curves for all tests. These curves provide bending moment distributions at successive increments of box displacements. Bending moment measurements provide valuable descriptions of a pile response and may be used to create load-transfer functions.

Figure 6.12 and Figure 6.13 show the bending moments at different positions (corresponding to the locations of strain gages) against the box displacement for single piles in both 10° and 20° slope angle series. The bending moment distributions of all tests for different box displacements are given in figures in Appendix E. The maximum bending moment is developed under the sliding surface at the tip of the pile. It should be noted that due to the interval of 100 mm between two adjacent strain gages, the location of the recorded maximum bending moment in the may not necessarily coincide with the actual location of the maximum.

It can be seen that the bending moment on the pile increase with the box displacement. However, rate of increase diminishes after displacements larger than a certain value (the ratio of between box displacement and pile diameter). It can be said that the maximum moment value for 10° slope angle series is at 21 mm box displacement ($\Delta/d=1.05$). For 20° slope angle series, the maximum moment value is at $\Delta/d =1.15$.

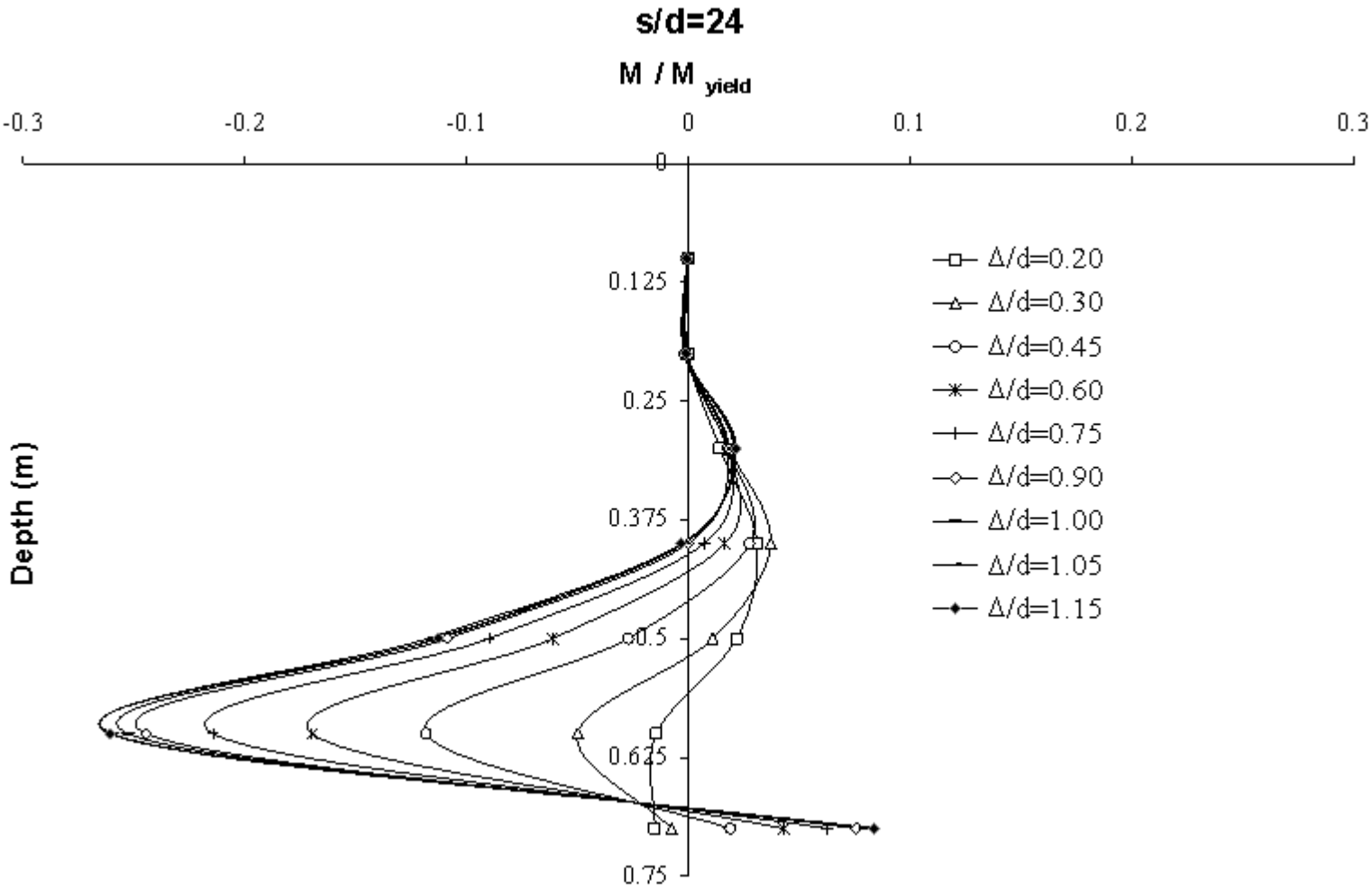

Figure 6.12 Normalized moment (M / M $_{yield}$) profile for s/d=24 in 10° slope angle.

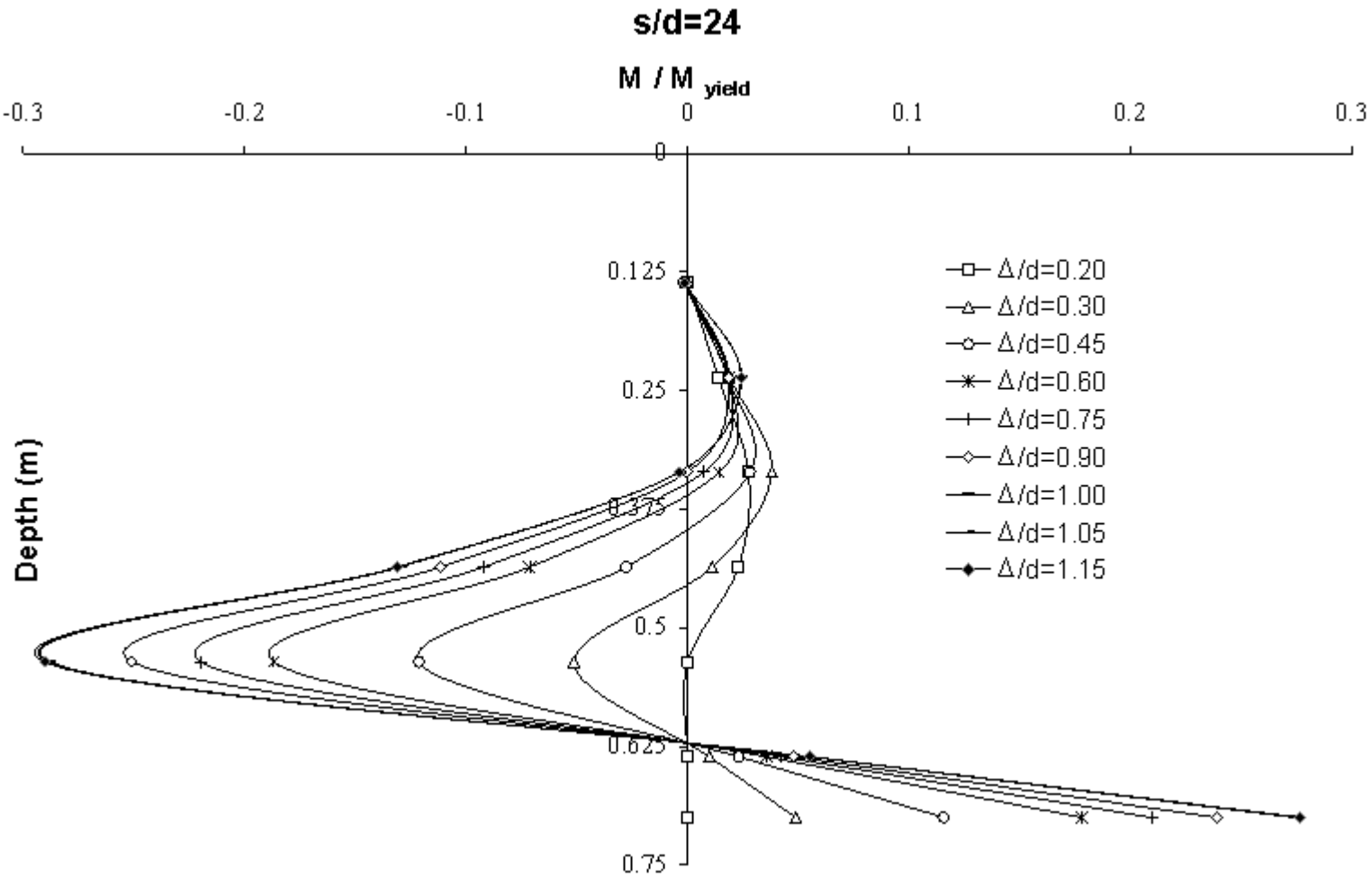

Figure 6.13 Normalized moment (M / M $_{yield}$) profile for s/d=24 in 20° slope angle.

A group factor (F_M) was also introduced for comparing the maximum moment of the pile in a group with that of the single pile at the same amount of box displacement.

The maximum moments for all tests and the group factor, F_M, is summarized in Table 6.3 which also indicates the effect of slope on the response of the pile. It is interesting to note that the slope angle had very little effect on the location and the magnitude of maximum bending moment at a target box displacement.

Table 6.3 Maximum moments and group factors of all test series

	10° slope angle series		**20° slope angle series**	
	F_M		**F_M**	
Pile Spacing Ratio	**Δ/d=0.30**	**Δ/d=1.05**	**Δ/d=030**	**Δ/d=1.15**
s/d = 24	1.00	1.00	1.00	1.00
s/d = 12	1.02	1.03	1.02	1.04
s/d = 8	1.10	1.11	1.08	1.11
s/d = 6	1.20	1.21	1.17	1.20
s/d = 4	1.39	-	1.40	1.42
s/d = 3	-	-	1.70	-
s/d = 2	-	-	1.86	-

6.3 Soil Pressure Distribution of Flexible Piles

The ultimate bending moment data at the strain gage locations were used and best fitting curves along the pile using Matlab cubic spline interpolation were determined in order to come up with the ultimate bending moment curvature defined as piecewise polynomials.

Distributions of shear force and soil resistance, however, were obtained by successive integration and differentiation of the ultimate bending moment curvature using Matlab cubic spline toolbox. Using spline toolbox, boundary condition can be applied to the first and second derivative of the spline function. Bending moment

values set as zero at the pile head in the free head pile case, and the soil pressure values set as zero at the soil surface in both free and fixed head pile cases as boundary conditions.

The influence of pile spacing on bending moment, shear force and soil pressure are shown in Figures 6.14 to 6.19 for both 10° and 20° slope angle series.

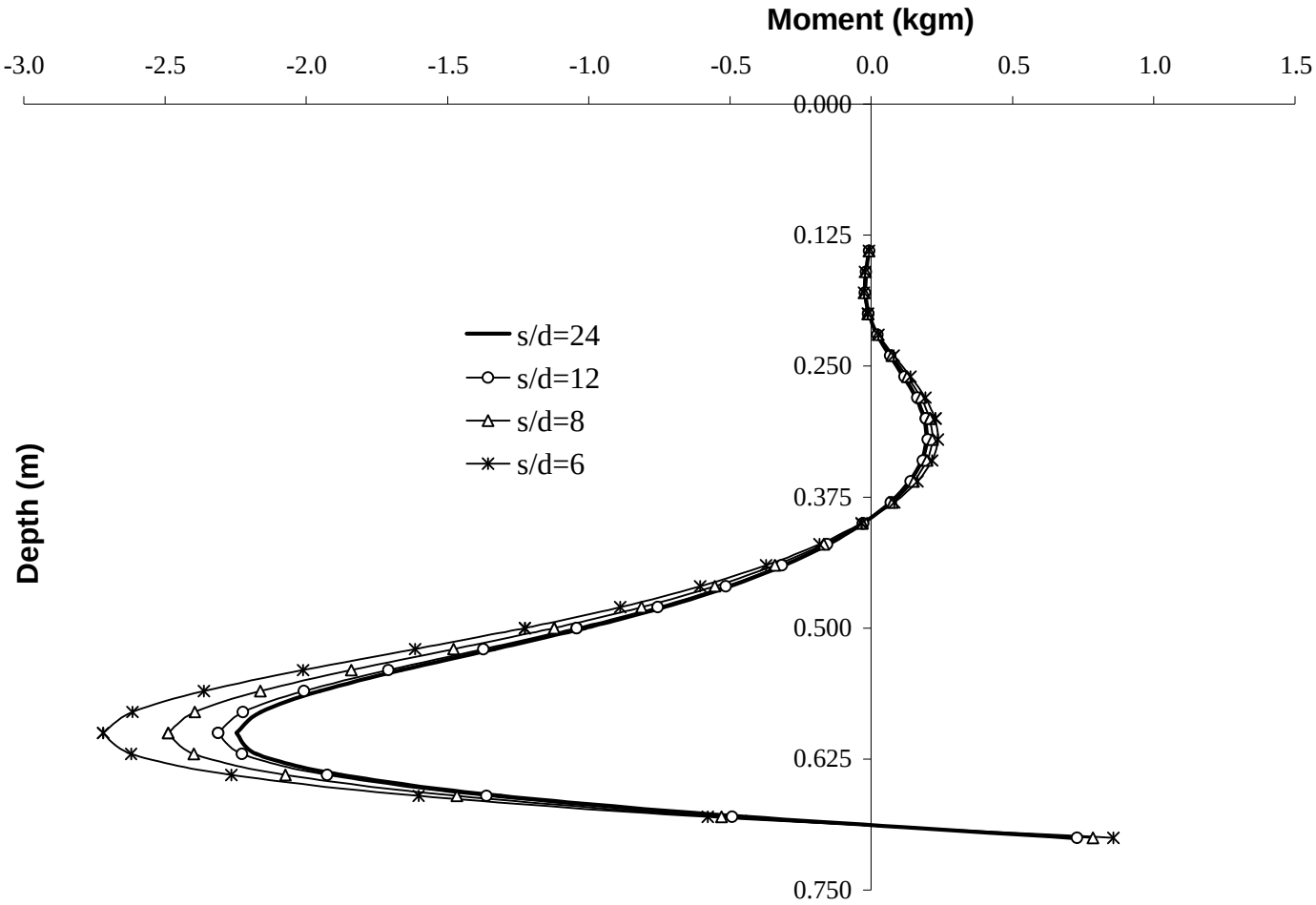

Figure 6.14 Moment profile for different pile spacing ratio in 10° slope angle.

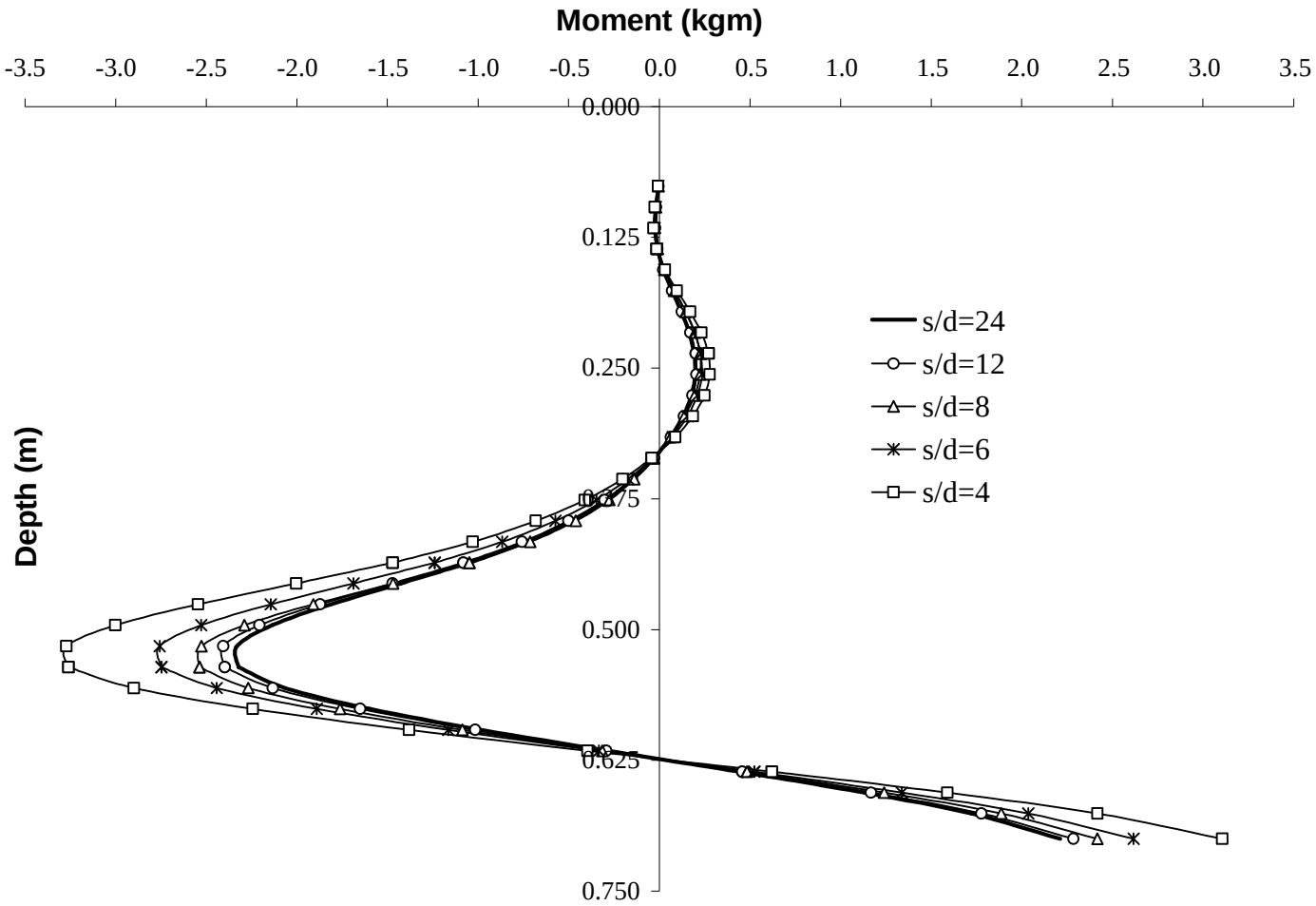

Figure 6.15 Moment profile for different pile spacing ratio in 20° slope angle.

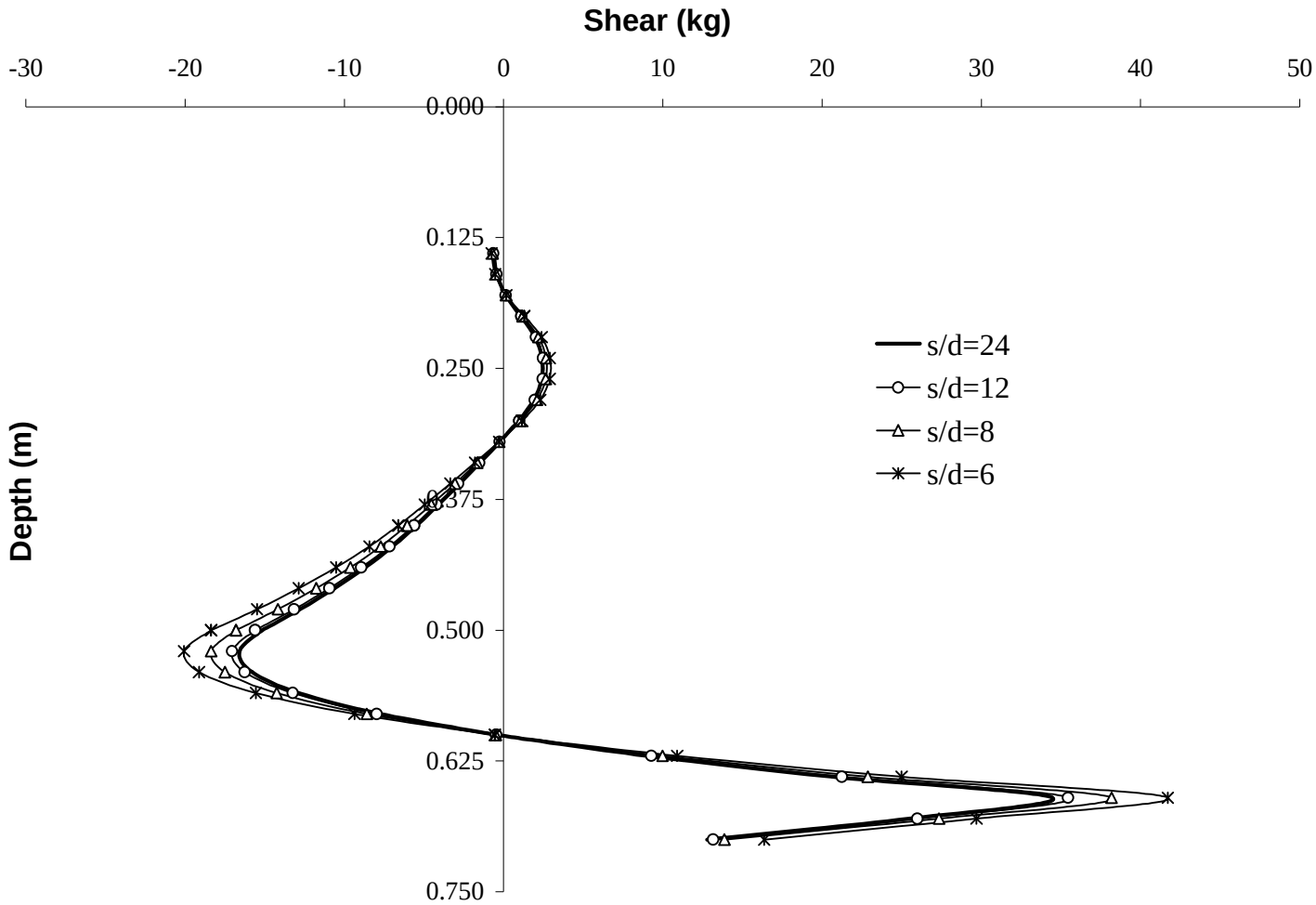

Figure 6.16 Shear force profile for different pile spacing ratio in 10° slope angle.

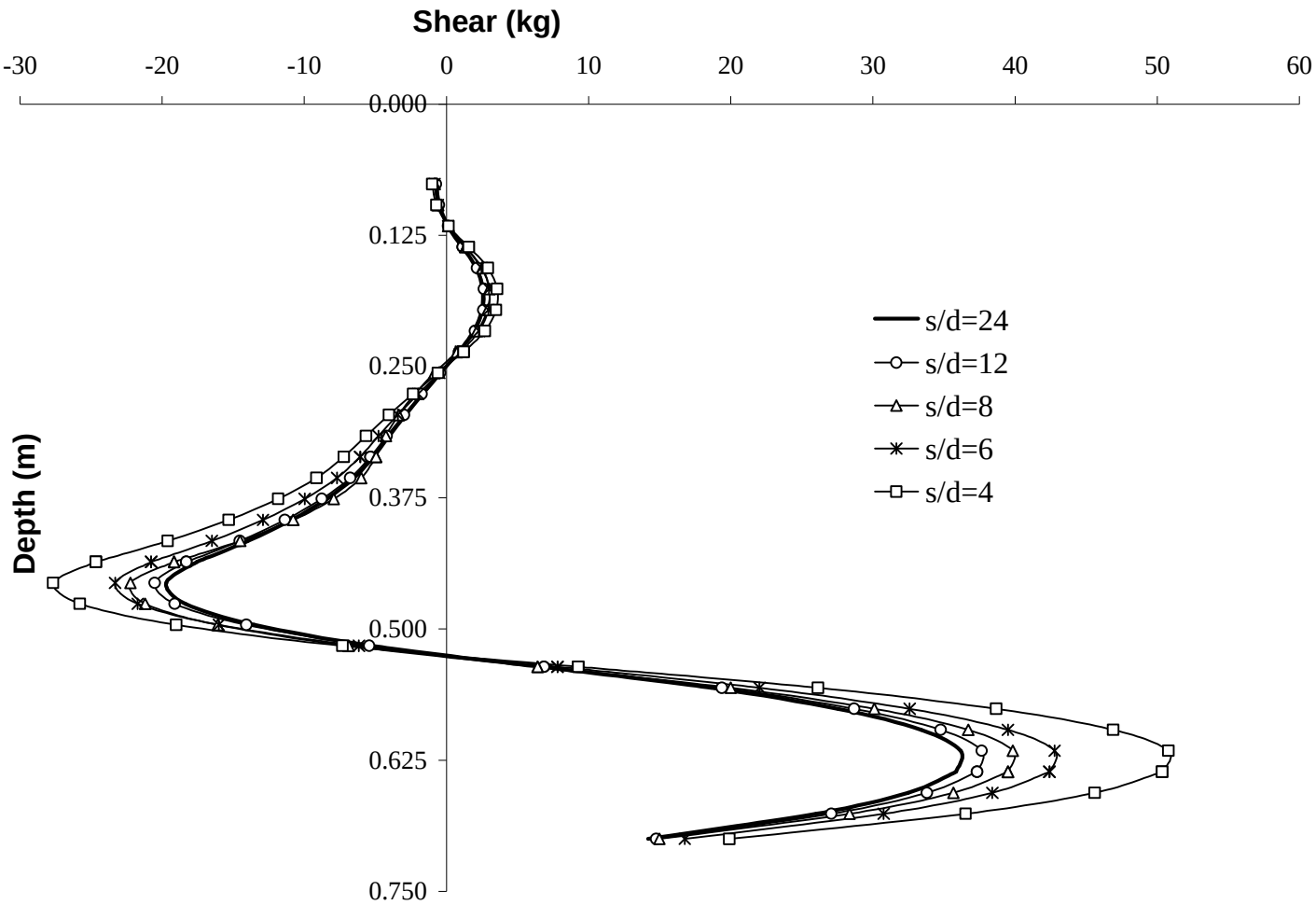

Figure 6.17 Shear force profile for different pile spacing ratio in 20° slope angle.

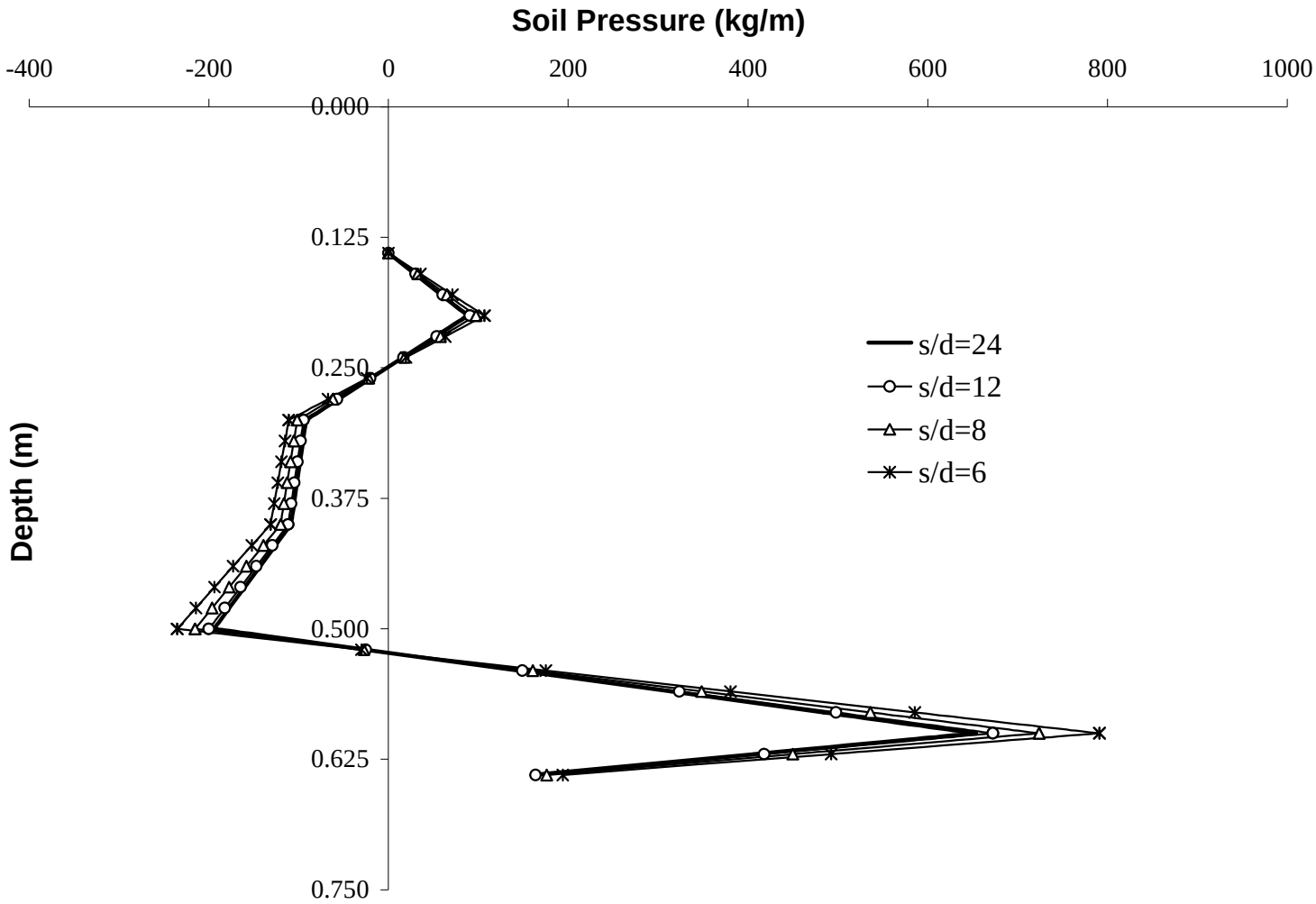

Figure 6.18 Soil pressure profile for different pile spacing ratio in 10° slope angle.

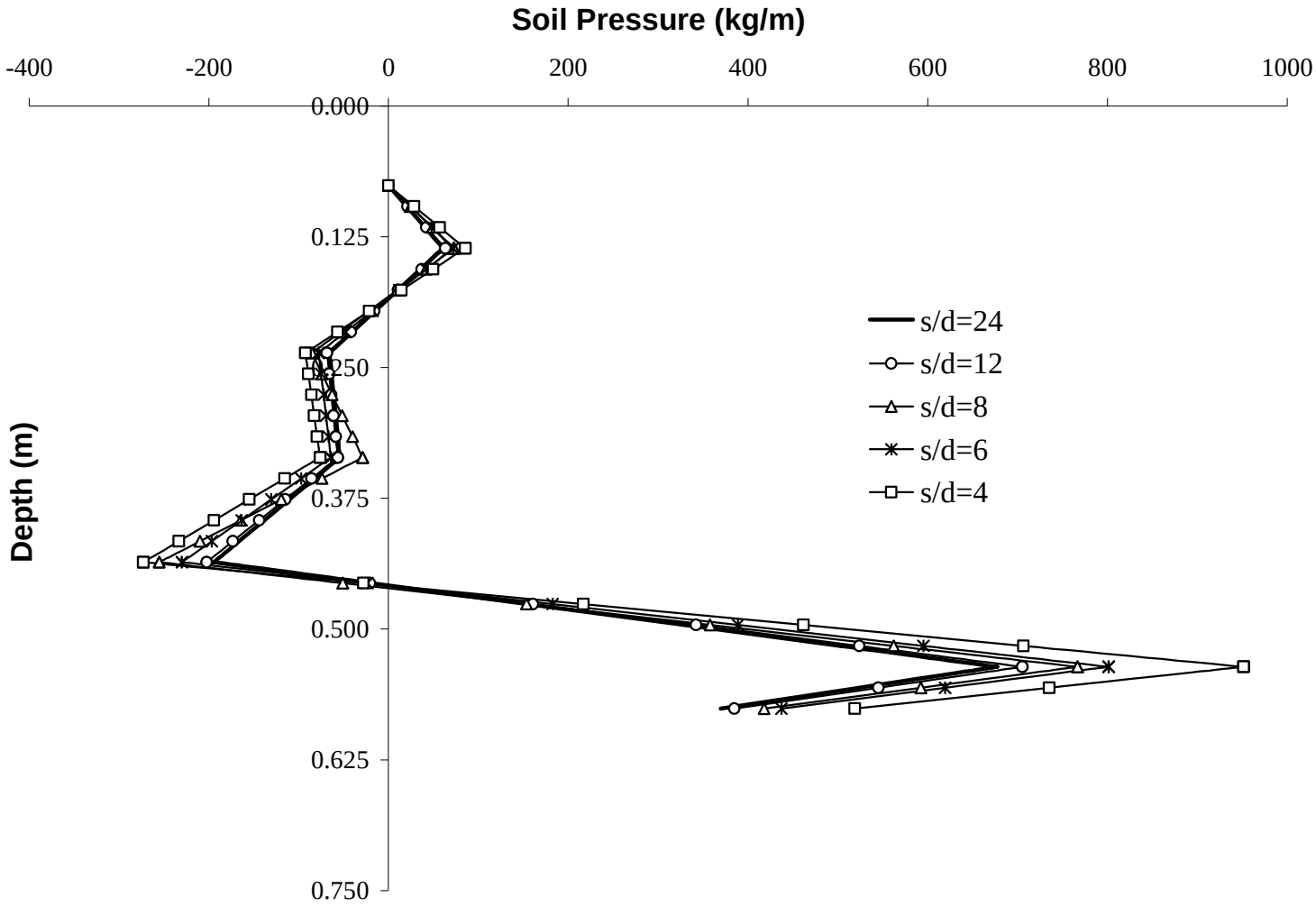

Figure 6.19 Soil pressure profile for different pile spacing ratio in 20° sloping angle.

Soil pressure distribution along the pile length, has been obtained from measured bending moments for the ultimate state. It can be seen from figures that the maximum values of moment, shear force and soil pressure are increased with the decrease of pile spacing ratio (s/d).

I can be seen from the Figures 6.18 and 6.19 that the soil pressure distributions are very similar in shape. The soil pressures acting on piles increased as the pile spacing decreased. However, when s becomes larger than 12d, each pile behaves like a single pile. For the pile series in 10° slope angle, pile head movement exceeds the soil movement, resulting in negative pressure on free head flexible piles over a certain depth approximately 20% of the sliding soil thickness. Below this depth, positive pressure occurs up to approximately 80% of the sliding soil thickness, and below this depth negative pressure starts to develop. Similar behavior was observed for the case of pile series in 20° slope angle. The determined maximum negative pressure is nearly three fold maximum active pressures.

6.4 Tests on Rigid Piles

The pile flexural rigidity (EI) was changed by using solid pile keeping the pile diameter and the modulus of elasticity values of the flexible piles. Table 6.4 shows the properties of the aluminum solid piles.

Table 6.4 Properties of Aluminum Solid Piles

Total Length (mm)	Diameter (mm)	Elastic Modulus E (kN/mm^2)	Moment of Inertia I (mm^4)	Bending Stiffness EI ($kNmm^2$)
750	20	70	7854	5.5×10^5

The solid pile is considered as rigid according to calculated pile flexibility parameter, βL, as 2.08 which is defined by Eq. 6.1 (Hannigan et al., 1997).

$$b\,L = \left(\frac{k_h d}{4 E_p I_p} \right)^{1/4} < \quad 2.25 \tag{6.1}$$

where E_pI_p is the bending stiffness of the pile (5500 kNmm2), k_h is the modulus of horizontal subgrade reaction ($3.3x10^{-5}$ kN/mm^3), d (20 mm) and L (500 mm) are the diameter and embedded length of the pile, respectively.

In addition to the test series of flexible piles, tests for 20° slope angle with 4 rigid piles (s/d=6) were conducted in order to determine the influence of pile stiffness on the pile behavior. Representative total load versus box displacement, load carried by piles, load per pile and pile displacement versus box displacement graphs for rigid and flexible piles in 20° slope angle with s/d = 6 are shown in Figures 6.20, 6.21, 6.22 and 6.23, respectively.

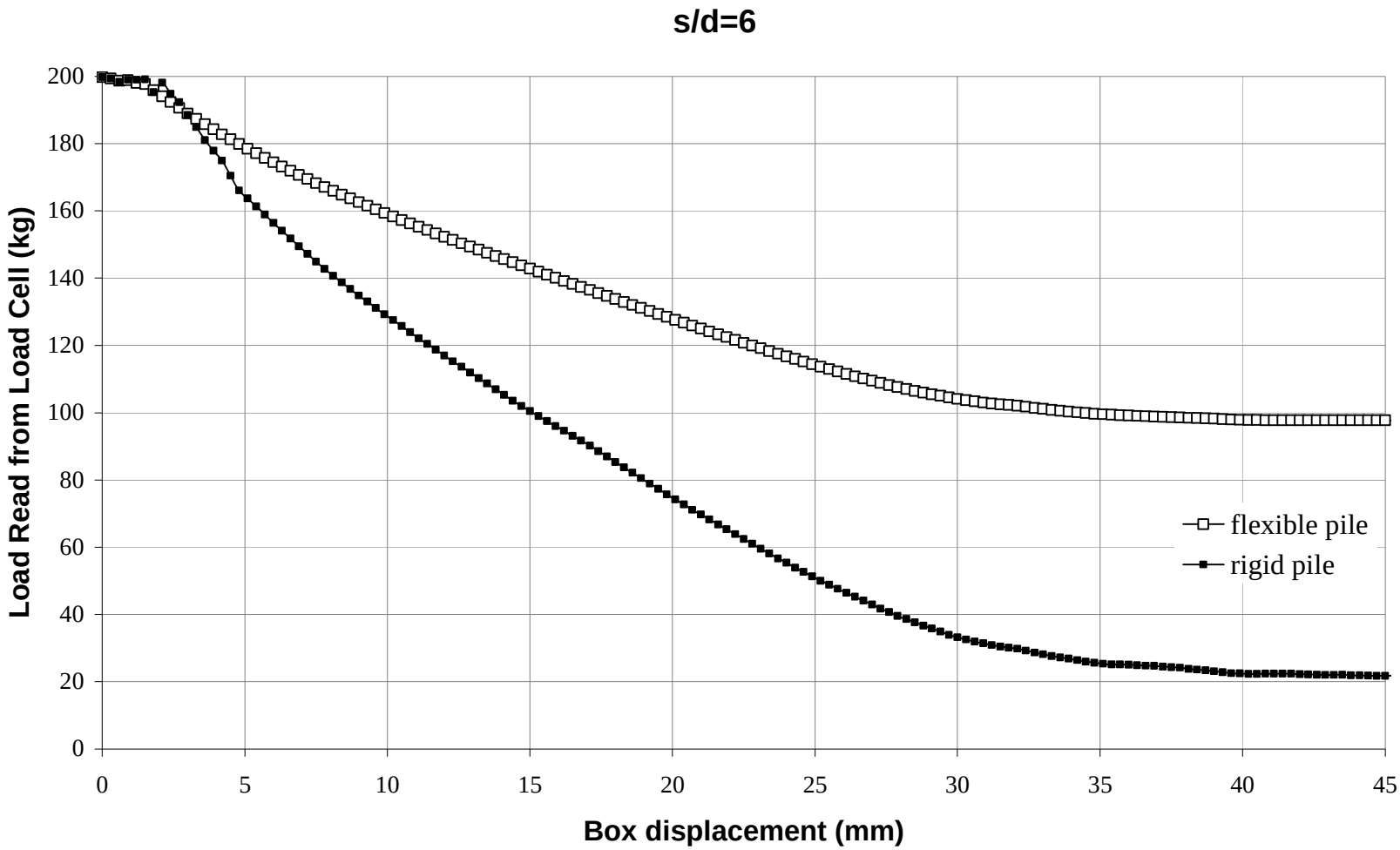

Figure 6.20 Total load read from load cell versus box displacement in 20° slope angle.

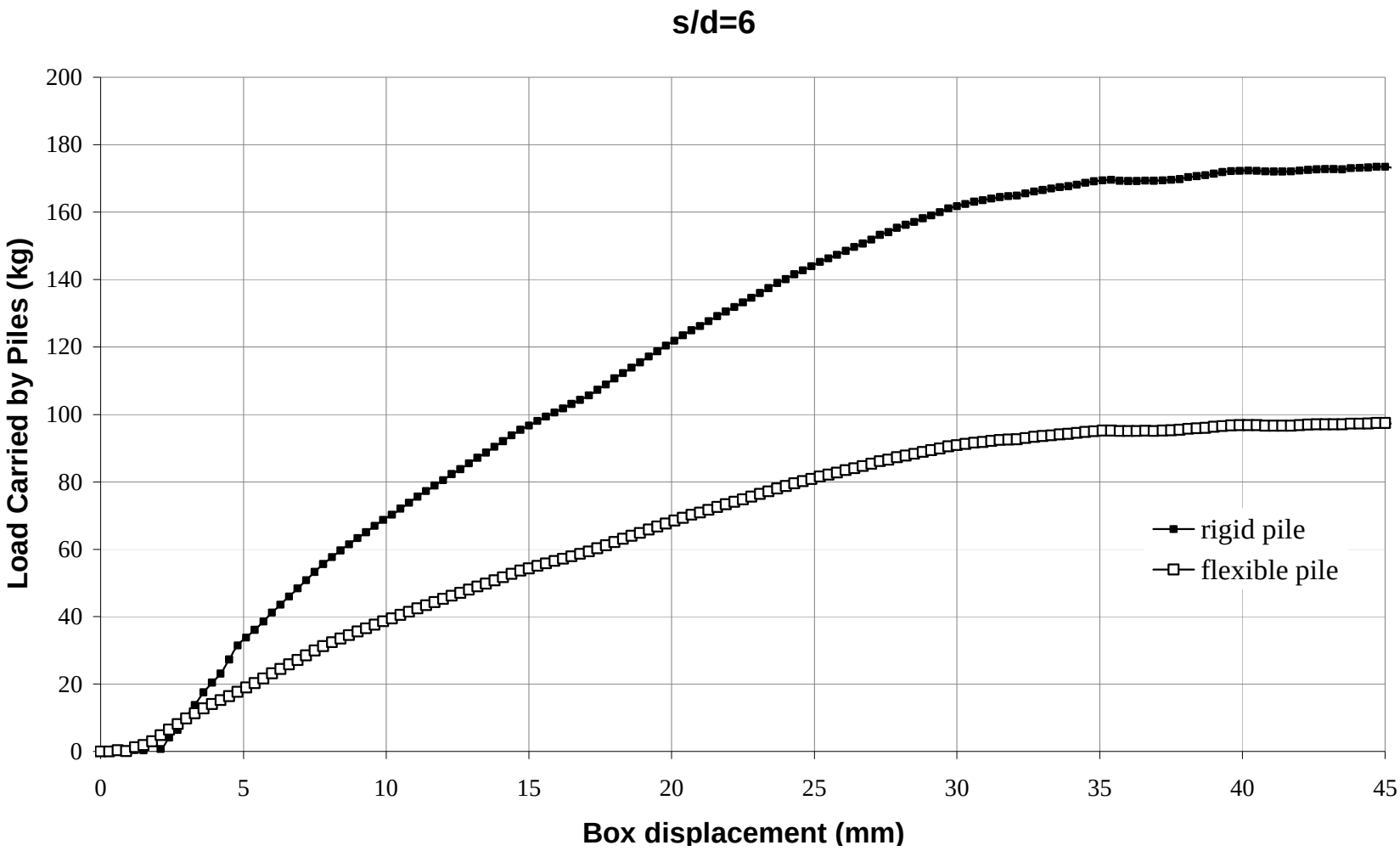

Figure 6.21 Load carried by piles versus box displacement in 20° slope angle.

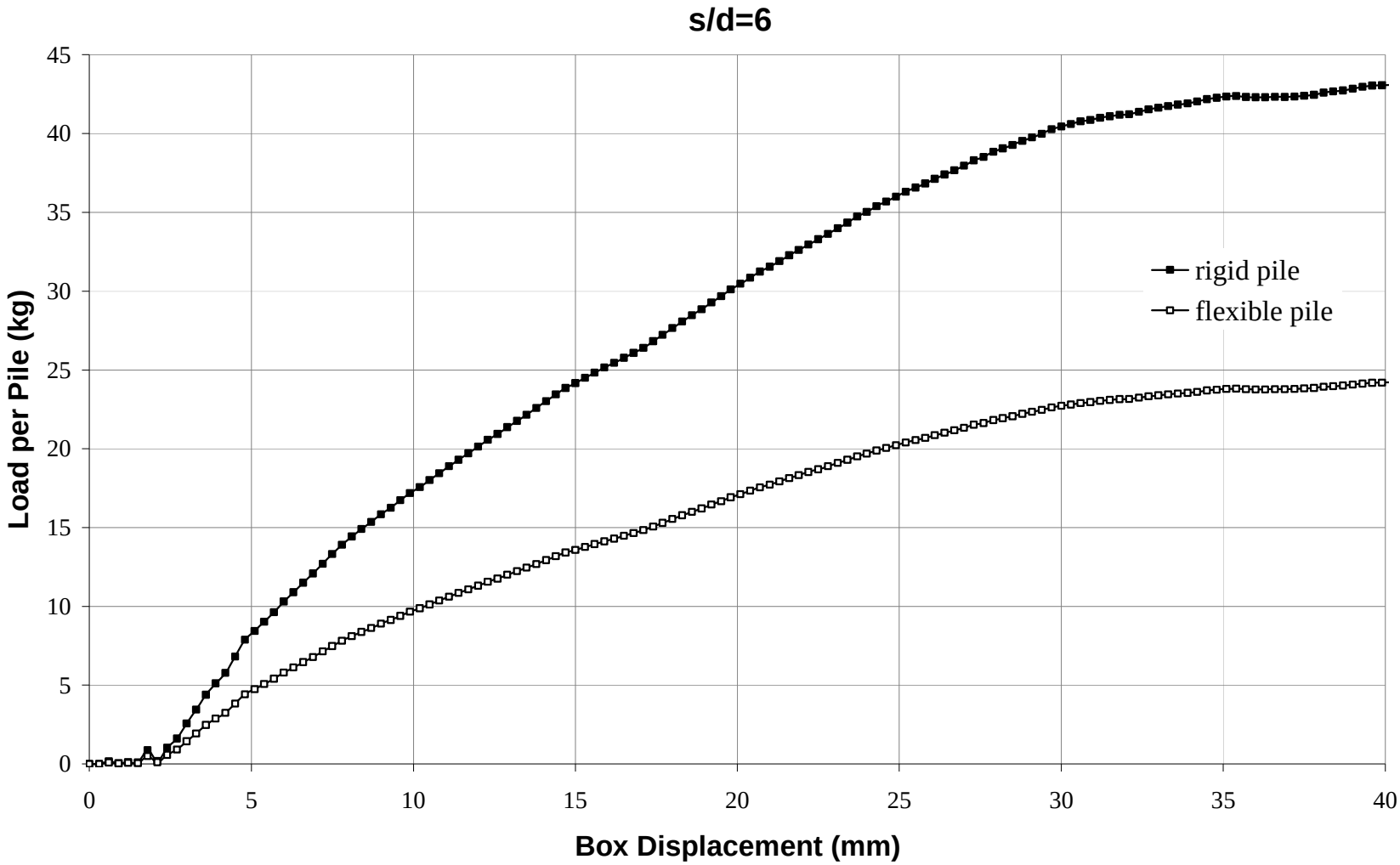

Figure 6.22 Load per pile versus box displacement in 20° slope angle.

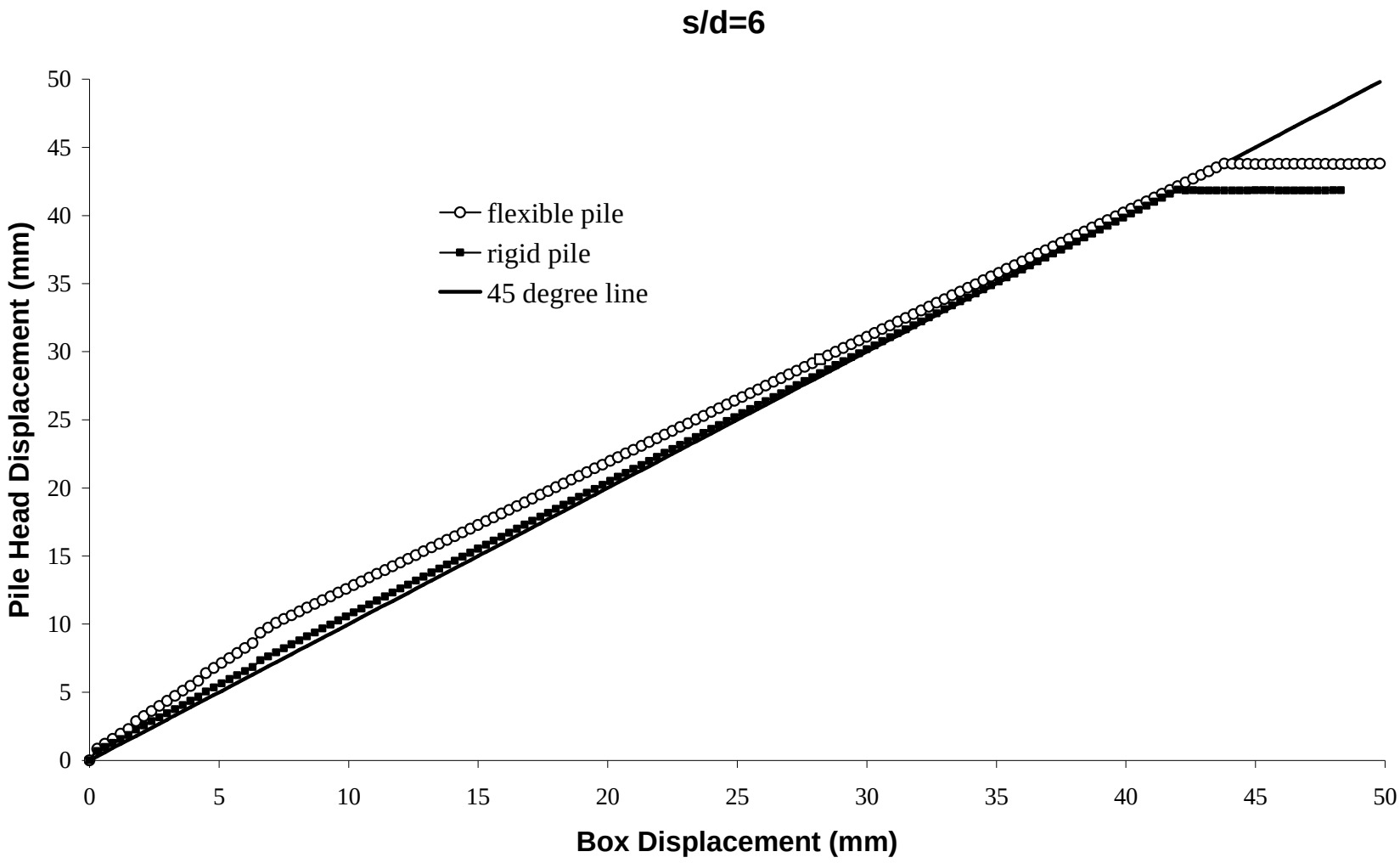

Figure 6.23 Pile head displacement versus box displacement in 20° slope angle.

The load carried by the piles increased as the pile stiffness increased. Rigid piles carry nearly 1.8 times the load carried by flexible piles.

The normalized bending moments for both rigid and flexible piles in 20° slope angle is shown in Figure 6.24. As expected, maximum moment increased as the pile stiffness increased. The moment acting on rigid piles is ~1.8 times higher than that on flexible piles.

Cubic polynomials were successively fitted to bending moment data points using cubic spline method. Using spline toolbox, same boundary conditions for flexible pile case were applied to the first and second derivative of the spline function. The soil resistance profile p (z) is evaluated by differentiating the bending moment profile M (z) twice with respect to depth z. The influence of pile stiffness on bending moment, shear force and soil pressure distribution are shown in Figures 6.25, 6.26 and 6.27, respectively. It can be seen from figures that the maximum shear force and soil pressure values increased with the increase of pile stiffness. However, the shape of pressure distribution is similar.

It is interesting to note that in this case, where no head restraint is provided, the movement of the top of a rigid pile is substantially greater than the surfacial soil movement, so that negative pressure occurs along a certain depth like in the case of flexible piles. However, the magnitude of negative pressure is larger than flexible piles.

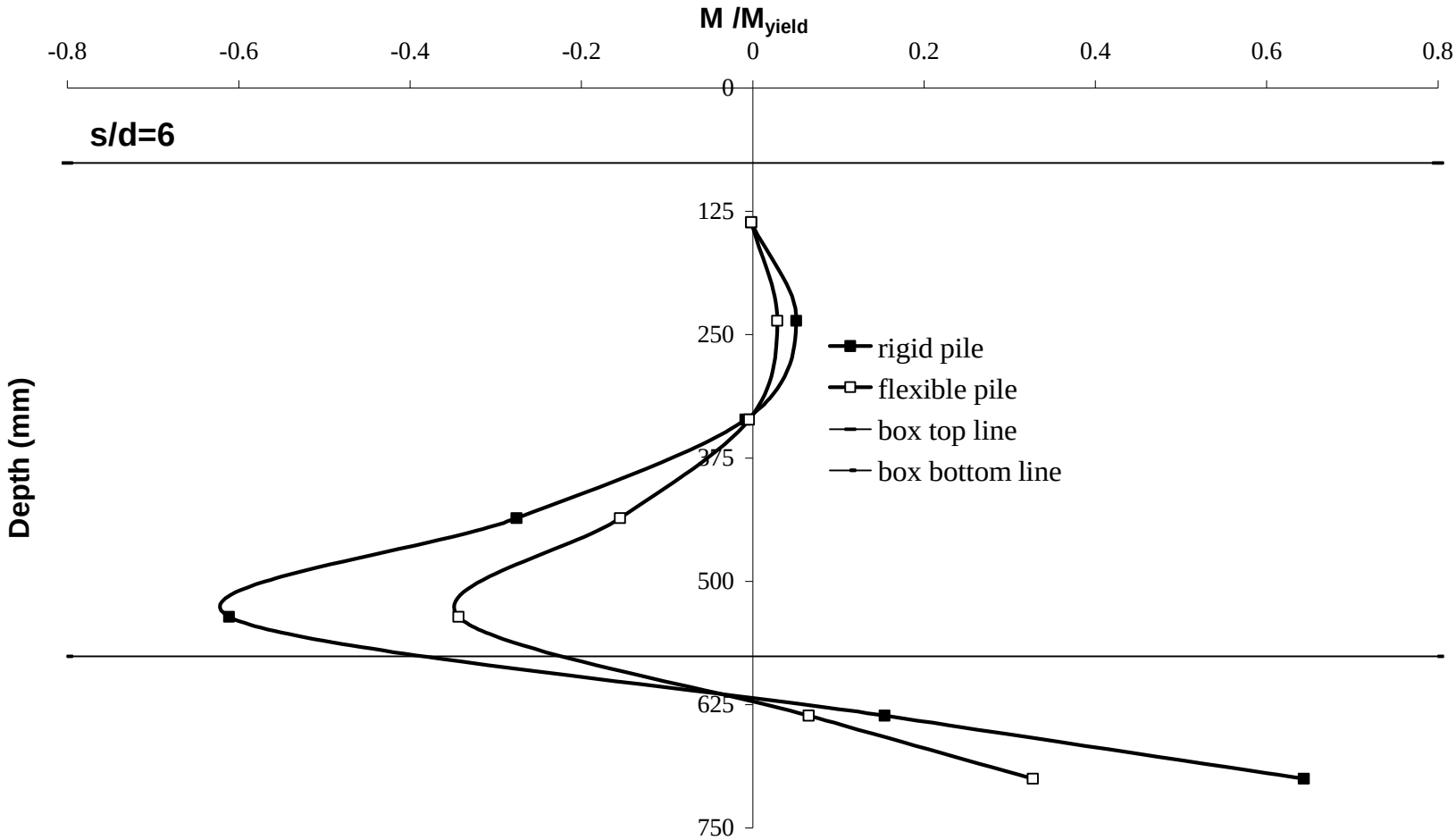

Figure 6.24 Normalized moment (M / M $_{yield}$) versus depth in 20° slope angle.

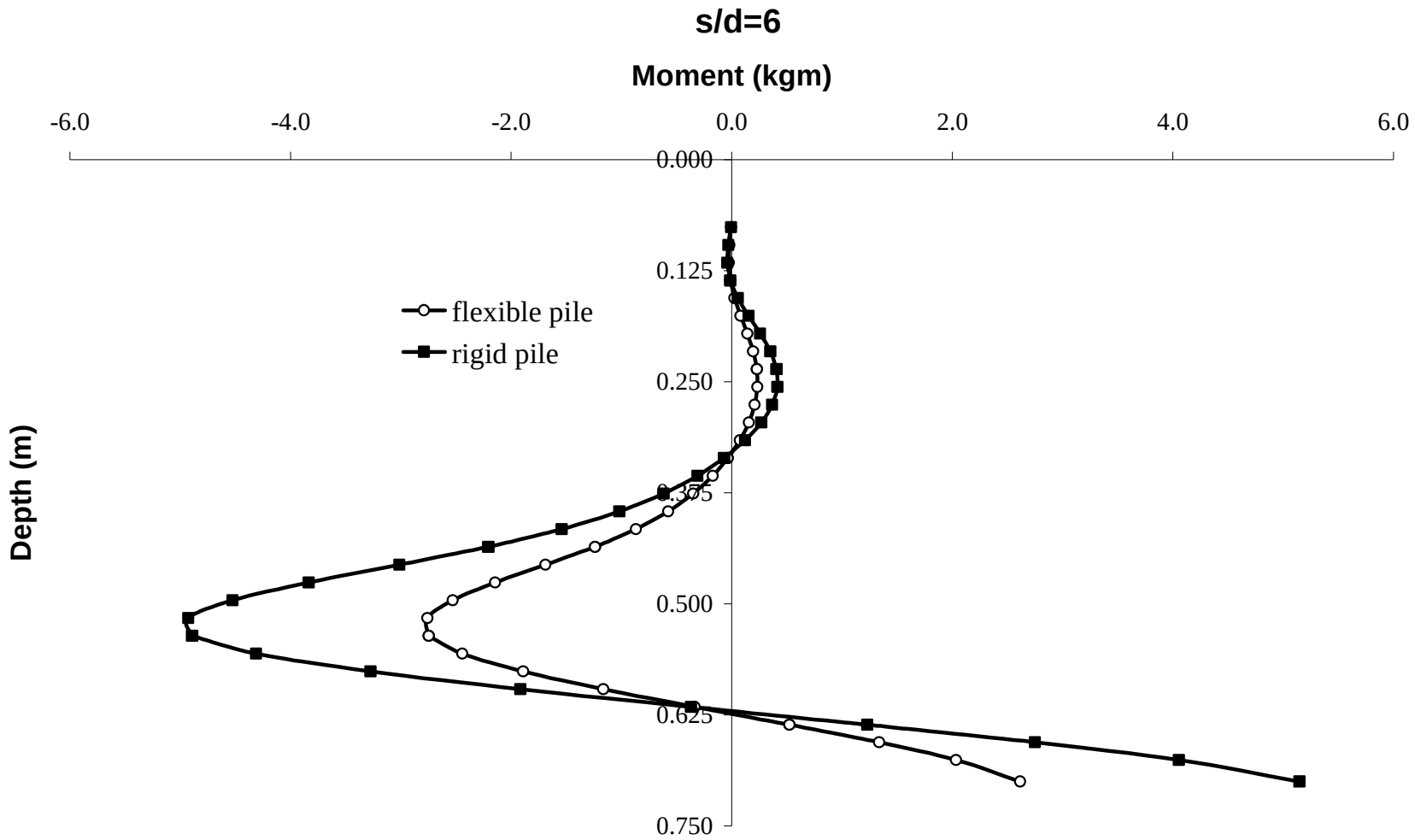

Figure 6.25 Moment profiles in 20° slope angle.

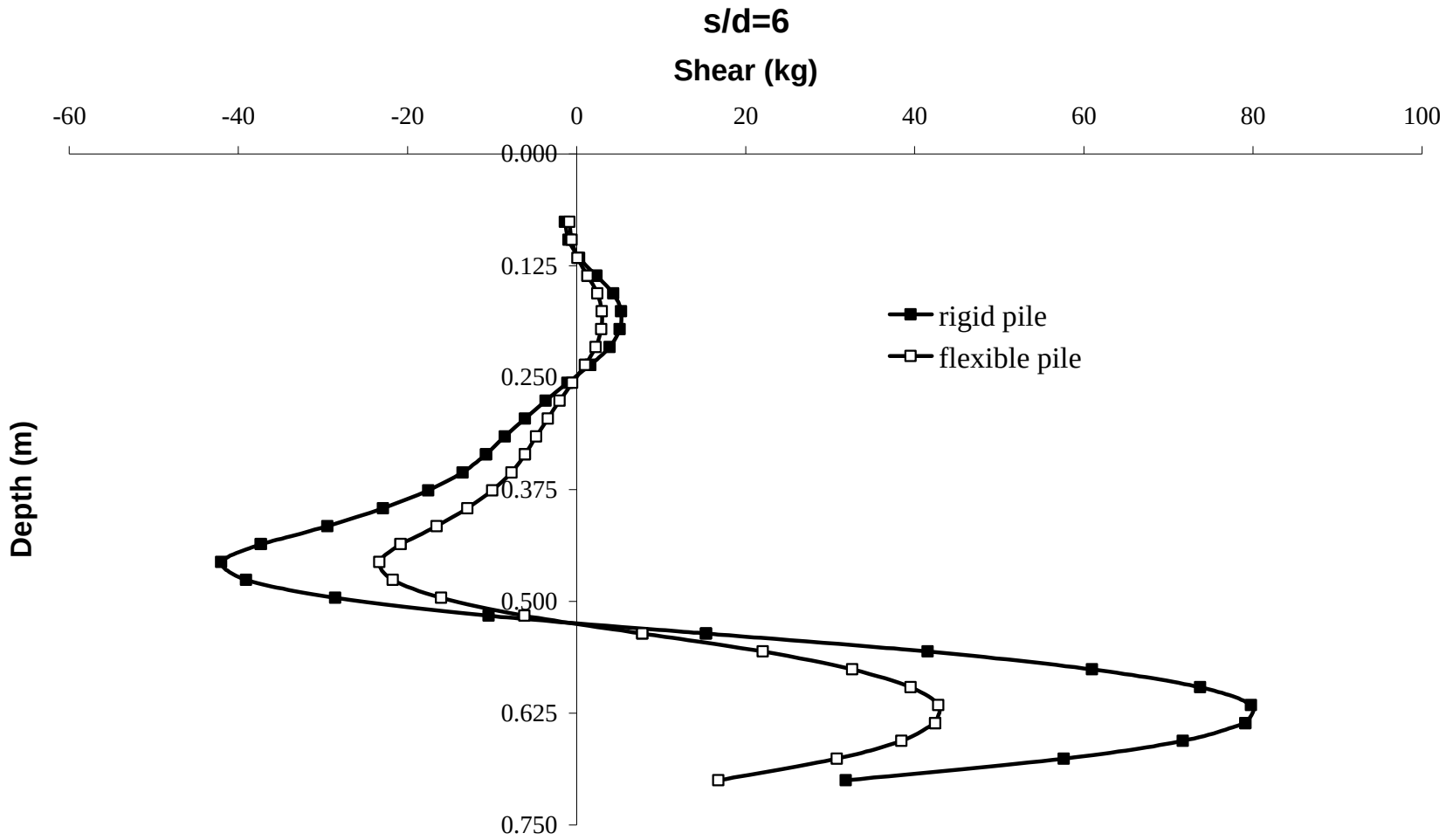

Figure 6.26 Shear force profiles in 20° slope angle.

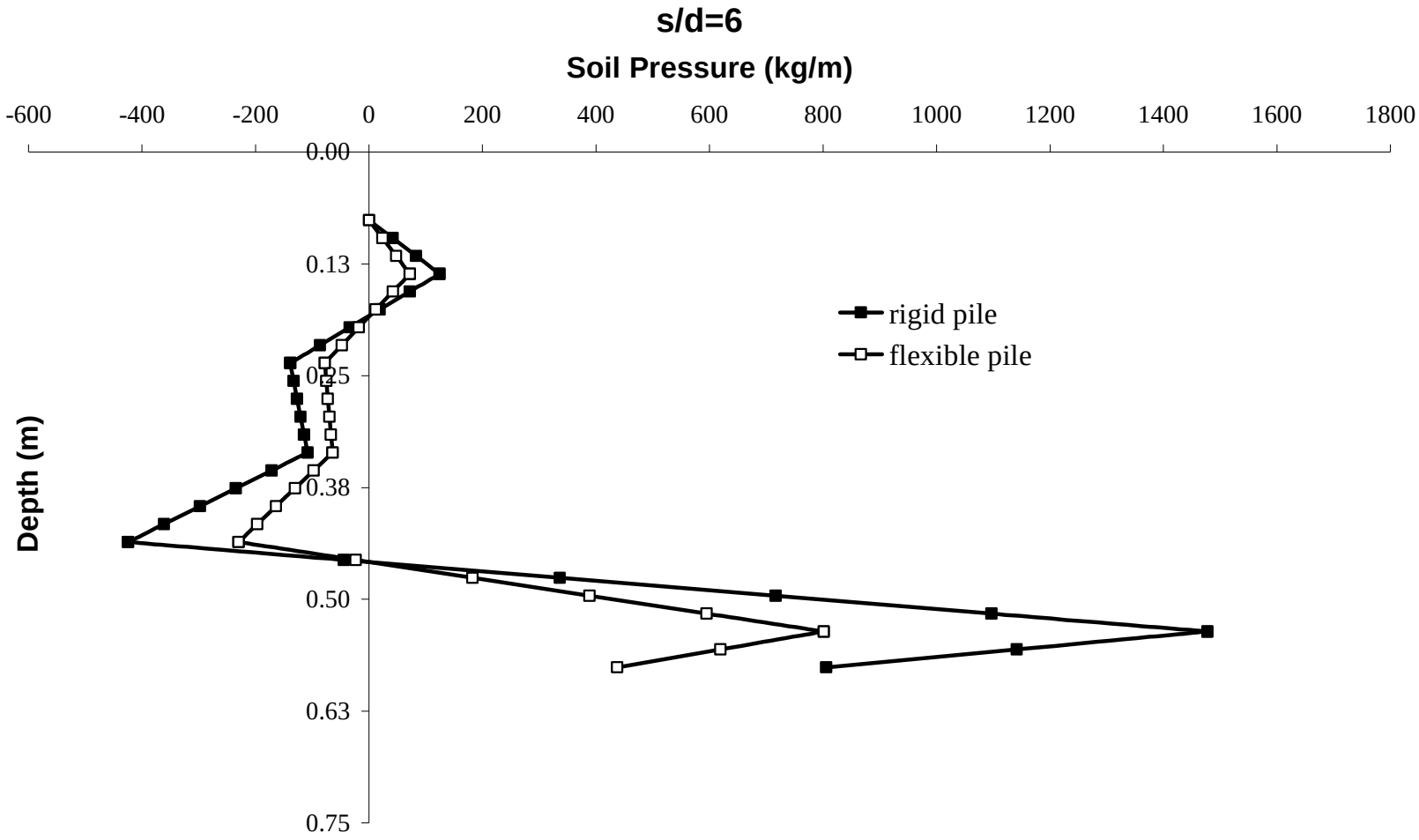

Figure 6.27 Soil pressure profiles in 20° slope angle.

6.5 Mixed Pile Tests

Deep sliding mass in the middle on account of bowl shaped landslide compels the inner pile to act as flexible pile, while the pile on the outer behaves as rigid due to shallow sliding mass. Accordingly, simulation of bowl shaped landslide with the testing apparatus could be achieved by locating flexible piles in the inner and rigid piles on the outer. Mixed type pile tests including both rigid and flexible piles together in 20° slope angle with s/d = 6 were performed in order to describe the behavior of free head passive piles in bowl shaped landslide geometry. Cubic polynomials were successively fitted bending moment data points using cubic spline method. Using spline toolbox, same boundary conditions for flexible and rigid pile cases were applied to the first and second derivative of the spline function. To determine the effect of landslide geometry on the behavior of piles, bending moment, shear force and soil pressure distributions along the pile length were used. These curves provide valuable descriptions of pile response and may be used to choose different pile length and cross-sections in bowl shape sliding mass cases.

Representative pile head displacement versus box displacement, normalized moment, cubic spline moment, shear force and soil pressure graphs for both outer piles (rigid) and inner piles (flexible) in 20° sloping angle with s/d = 6 are shown in figures 6.28, 6.29, 6.30, 6.31,and 6.32, respectively. Pile head displacement versus box displacement, the moments, shear forces and soil pressures acting on flexible piles, rigid piles, mixed piles with 6d pile spacing in 20° slope angle, were given together in figures 6.33, 6.34, 6.35 and 6.36, respectively.

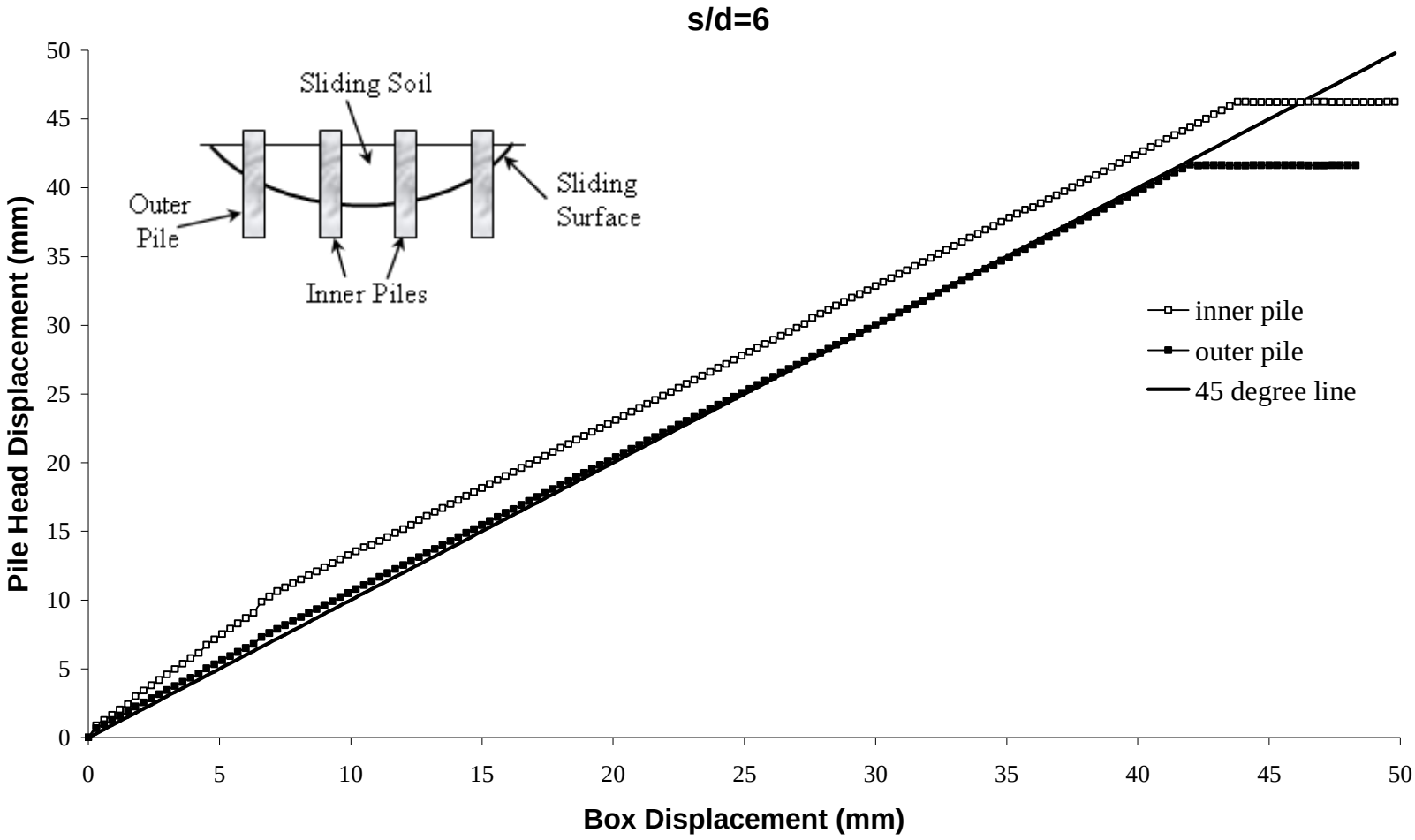

Figure 6.28 Pile head displacements versus box displacement in mixed pile test series.

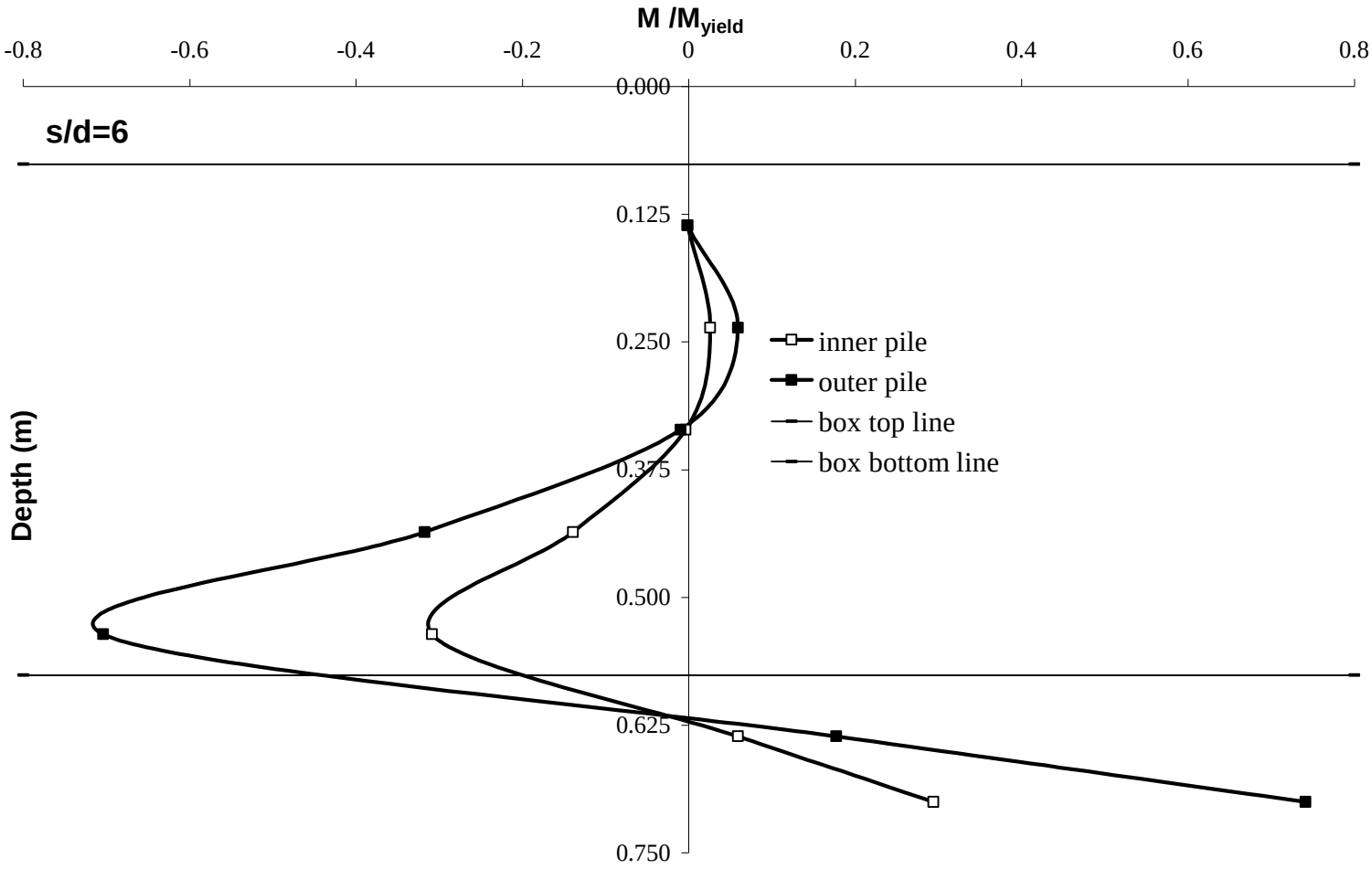

Figure 6.29 Normalized moment (M / M $_{yield}$) versus depth in mixed pile test series.

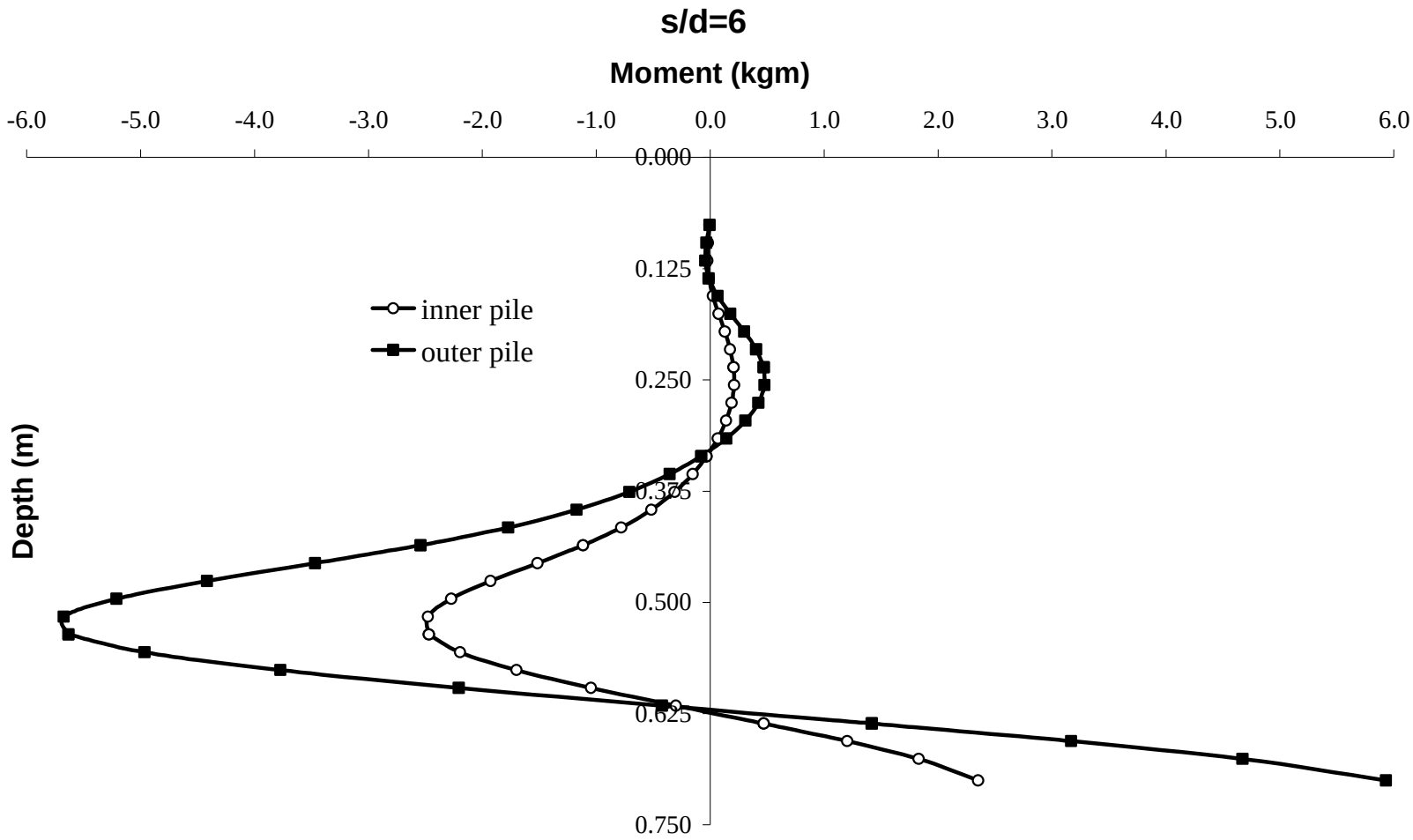

Figure 6.30 Moment profiles in mixed pile test series.

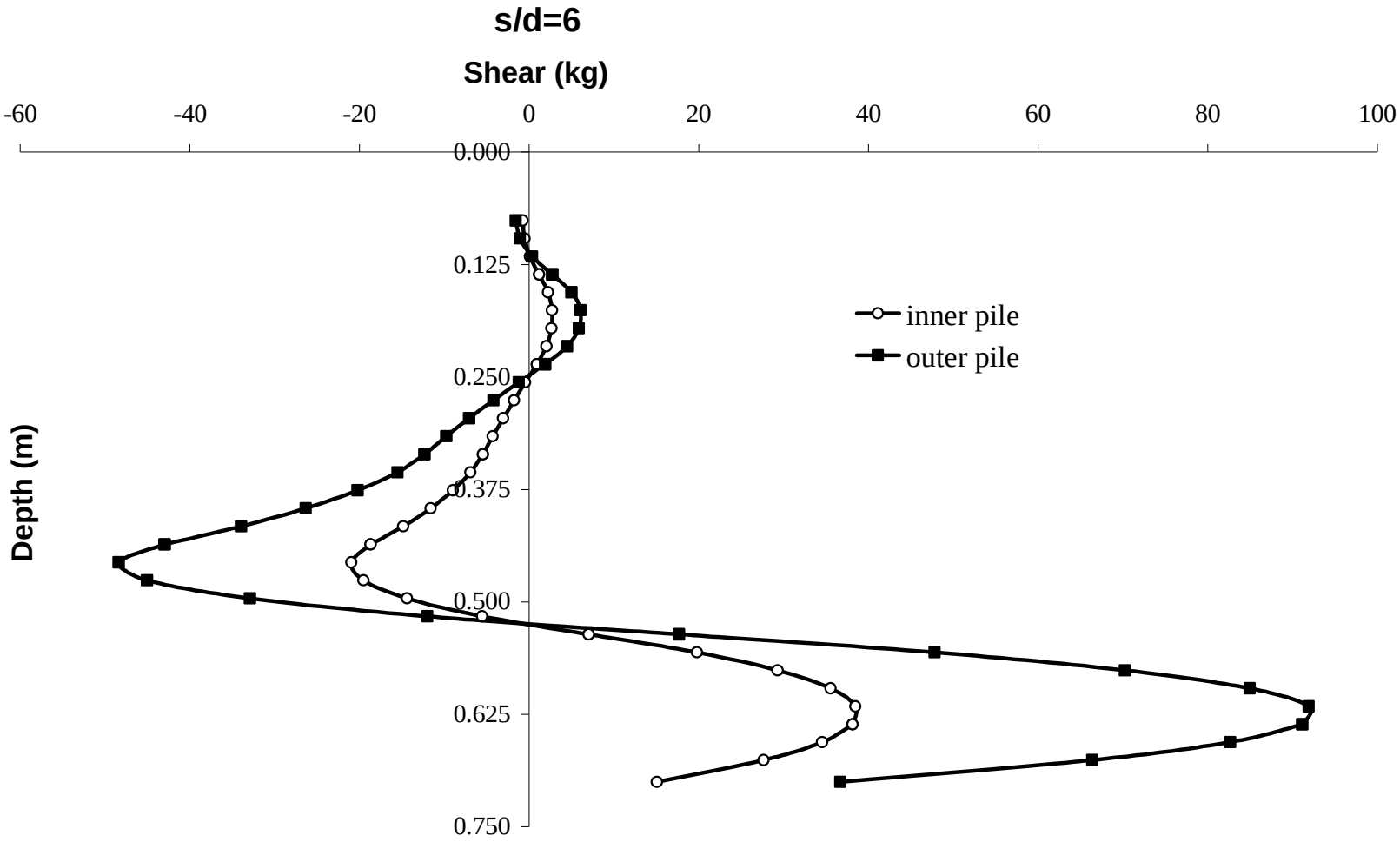

Figure 6.31 Shear force profiles in mixed pile test series.

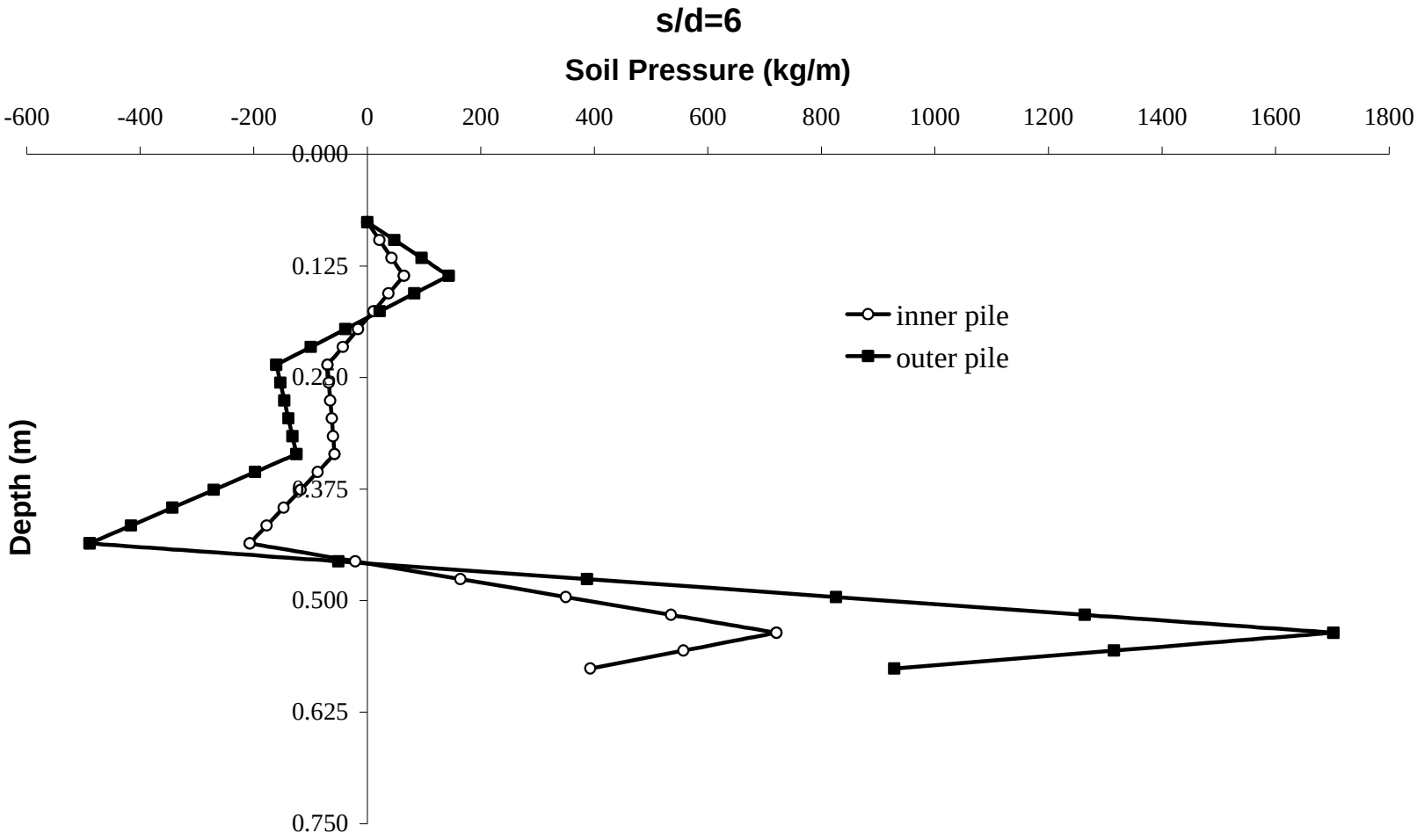

Figure 6.32 Soil pressure profiles in mixed pile test series.

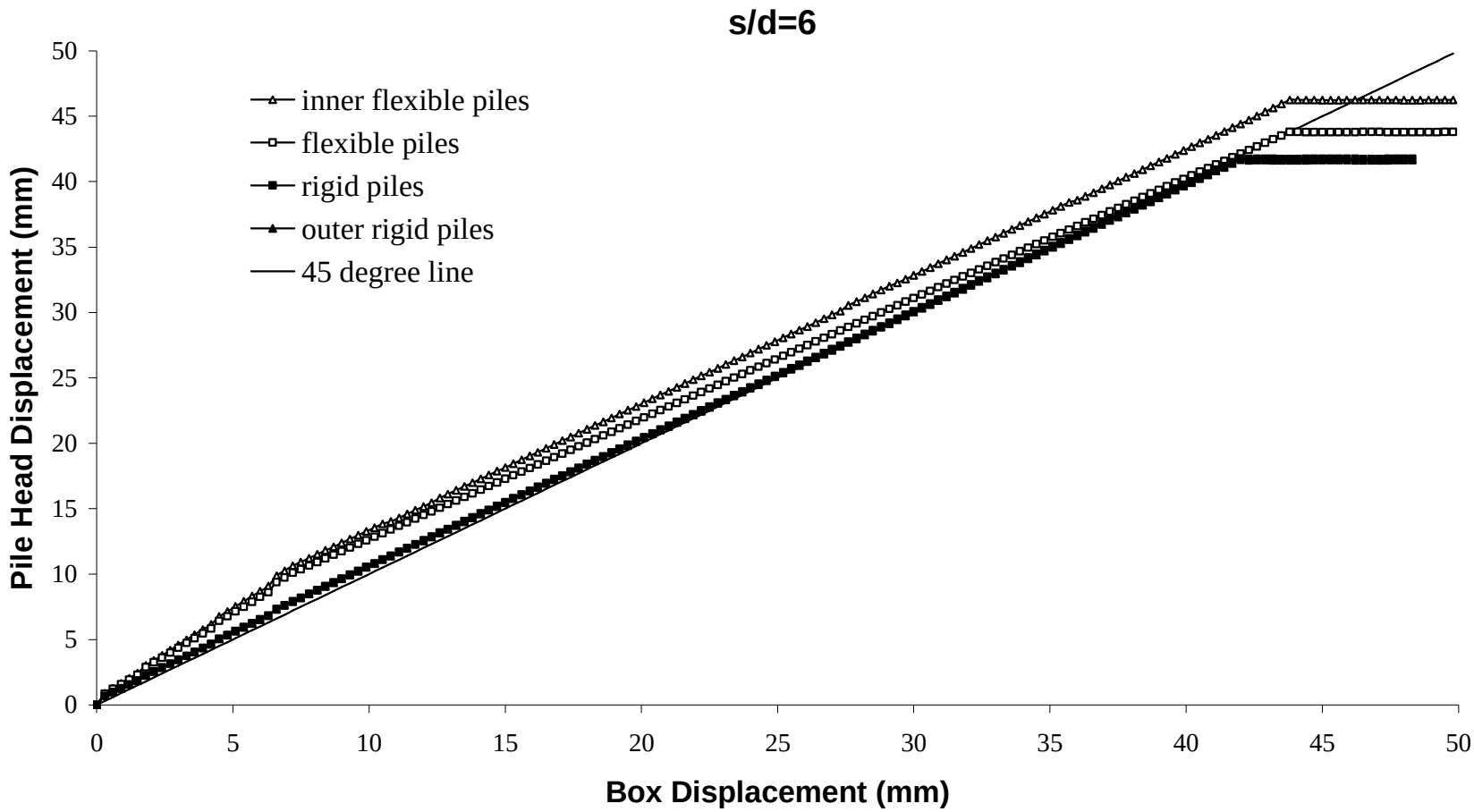

Figure 6.33 Pile displacements versus box displacement in 20° slope angle.

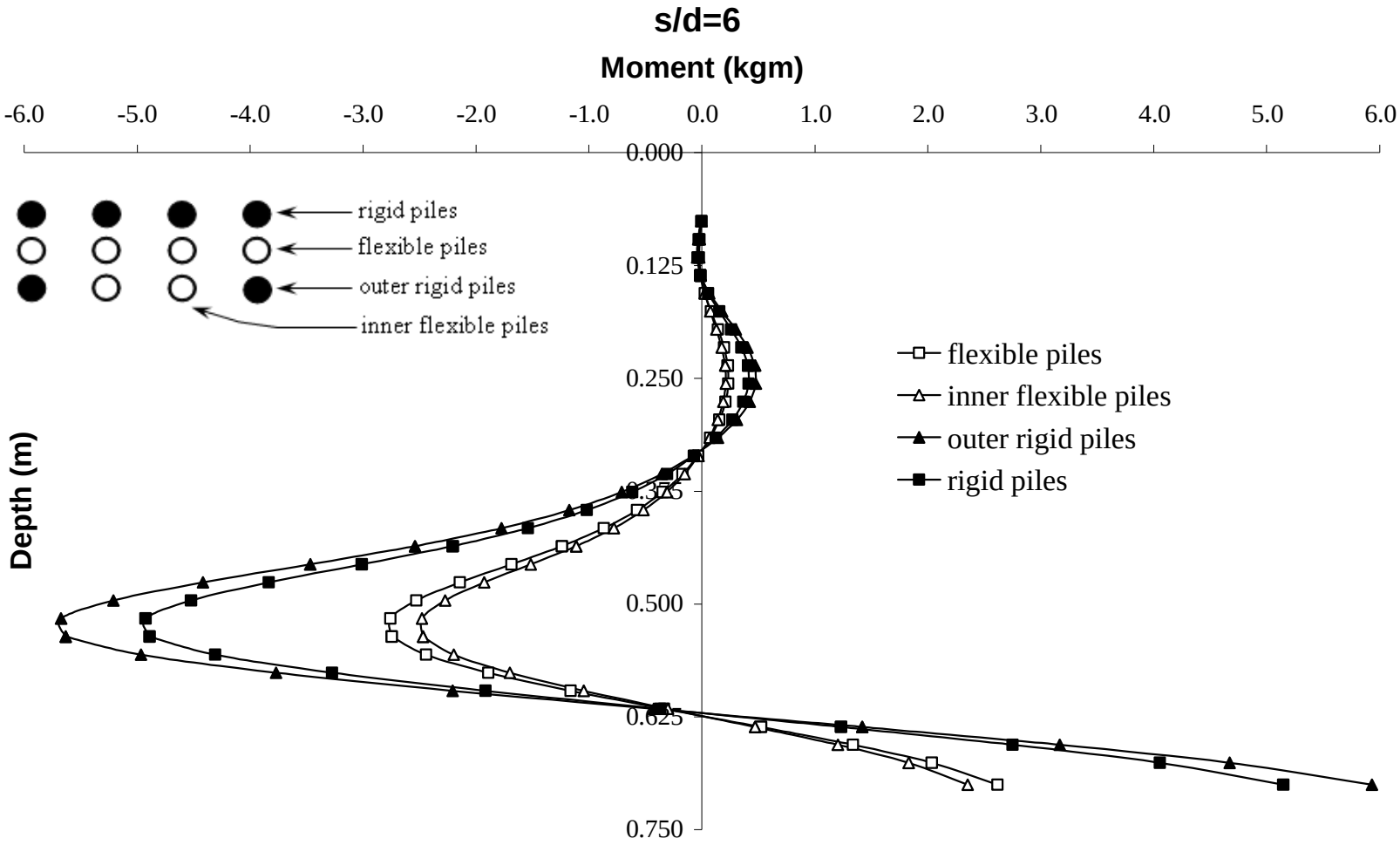

Figure 6.34 Moment profiles in 20° slope angle.

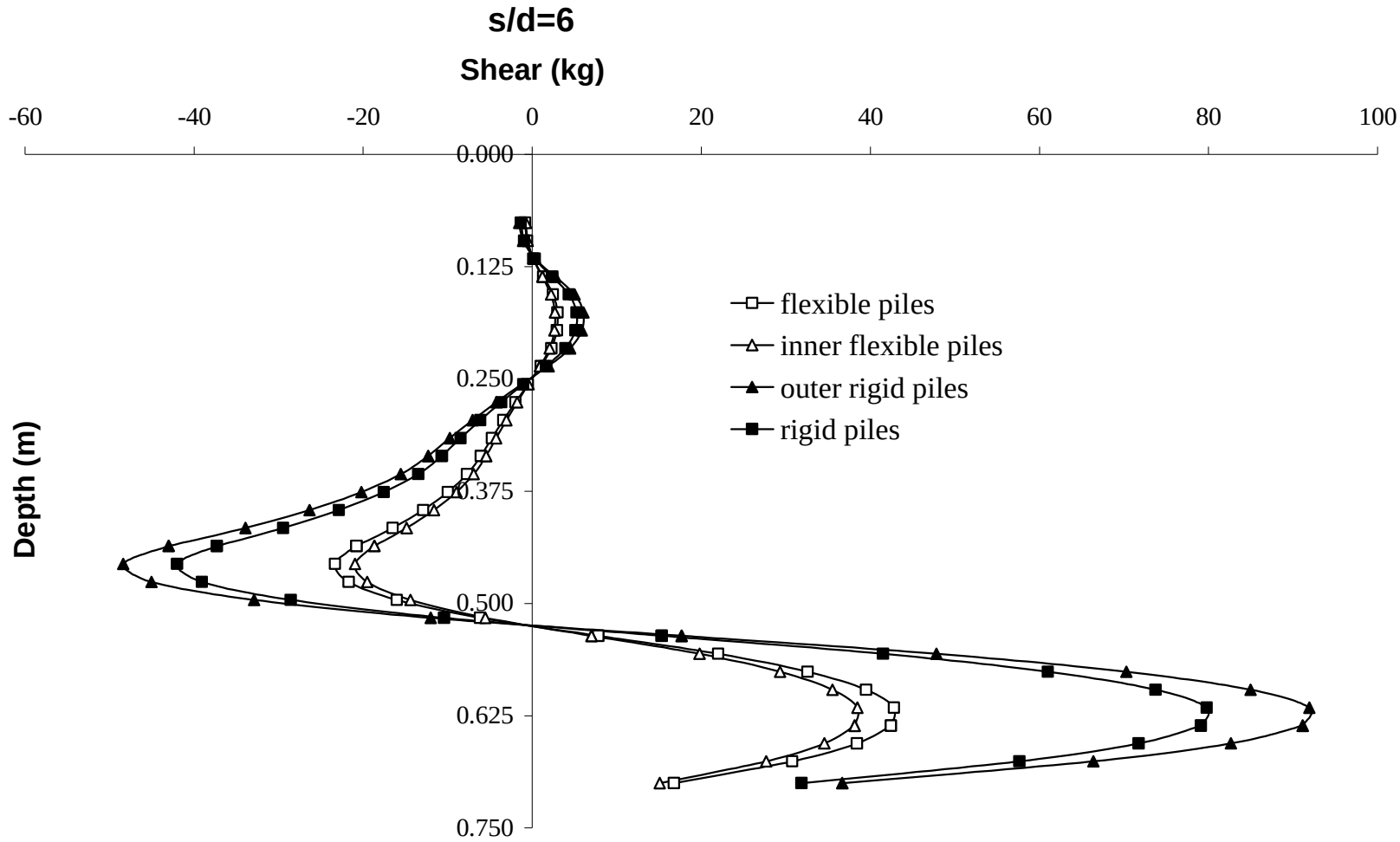

Figure 6.35 Shear force profiles in 20° slope angle.

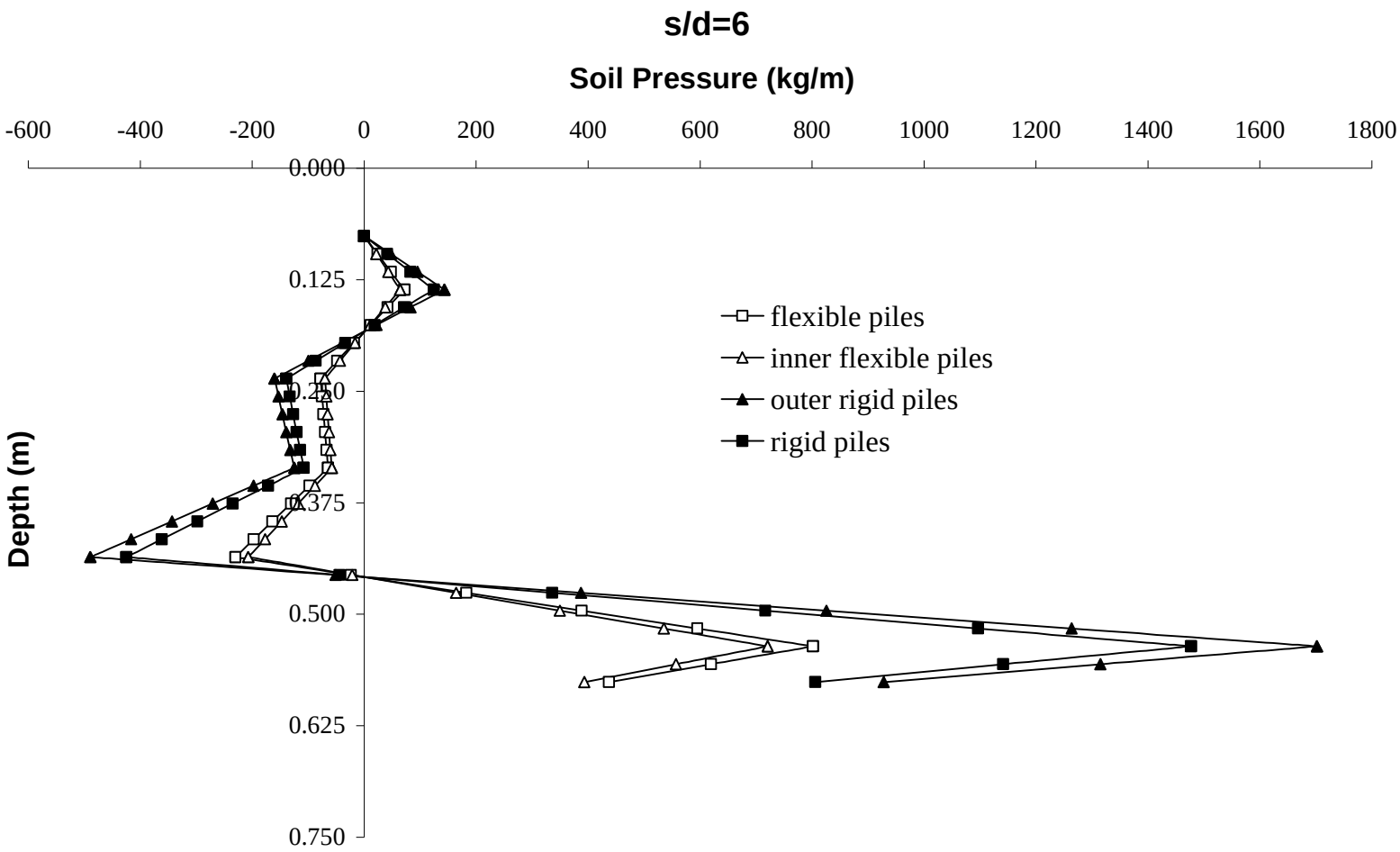

Figure 6.36 Soil pressure profiles in 20° slope angle.

It can be clearly seen from the figures that inner flexible piles displaced more than the outer rigid piles and they transferred their loads to the outer piles owing to arching mechanism. So, outer rigid piles were subjected to more soil pressure, therefore more moment and shear force.

It can be also said that the displacements of inner flexible piles were highest, and so they were subjected to the least soil pressure. On contrary, outer rigid piles have the least displacement and they were subjected to the highest moment and shear force due to highest soil pressure.

6.6 Tests on Two Rows of Piles

Experimental studies were extended to two rows of pile groups. Four series of pile group were conducted on two different arrangements in 20° sloping angle, such as flexible piles in two rows in parallel arrangement, flexible piles in two rows in zigzag arrangement, rigid piles in two rows in parallel arrangement and rigid piles in two rows in zigzag arrangement for investigating the effect of pile rigidity on the load transfer mechanism for pile in rows. The piles were set up in two rows at 6d intervals, and the interval between rows was 3d (Figure 6.37).

Representative total load versus box displacement, load carried by piles for flexible piles in two rows in both parallel and zigzag arrangement are shown in Figures 6.38, and 6.39, respectively. Figure 6.40 shows the normalized bending moment distributions in front and rear pile rows at different the box displacements.

For the case of two rows of rigid piles in both parallel and zigzag arrangement, total load versus box displacement and load carried by piles graphs are shown in Figures 6.41 and 6.42, respectively. Figure 6.43 shows the normalized bending moments distributions in front and rear rows at different box displacements.

For flexible pile case, it was determined that the moments acting on the front row of piles and the moments acting on the rear row of piles were approximately the

same. While the pile stiffness was increased, the moment on front piles was increased up to 3 times of moment on rear piles. Pile moments determined in the zigzag arrangement are approximately 5% higher moments in parallel arrangement. Therefore, multi soil arching effects for a zigzag arrangement of piles provide piles more restraint to soil movement.

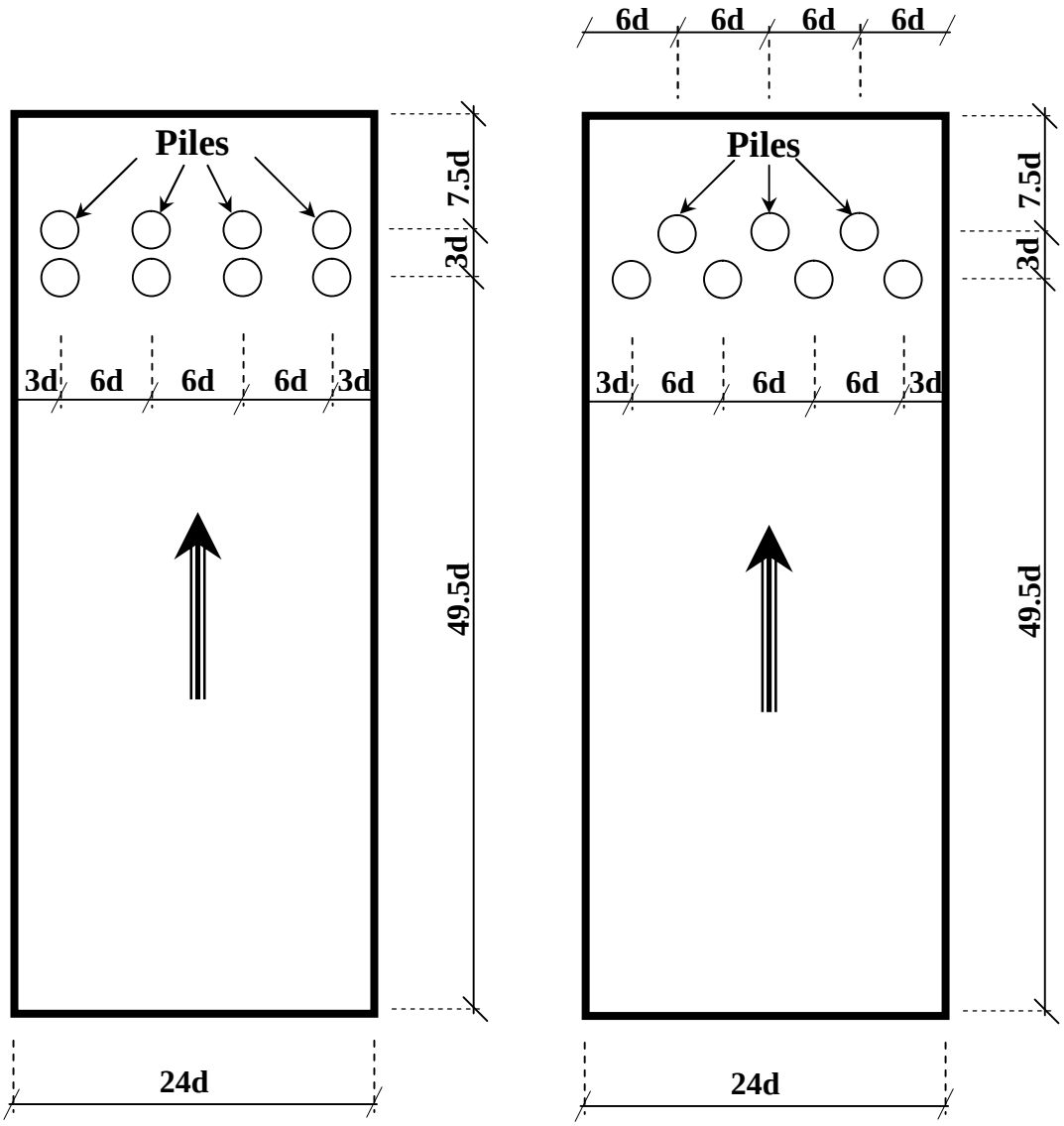

Figure 6.37 Pile arrangements for two rows of piles: a) Parallel arrangement b) Zigzag arrangement

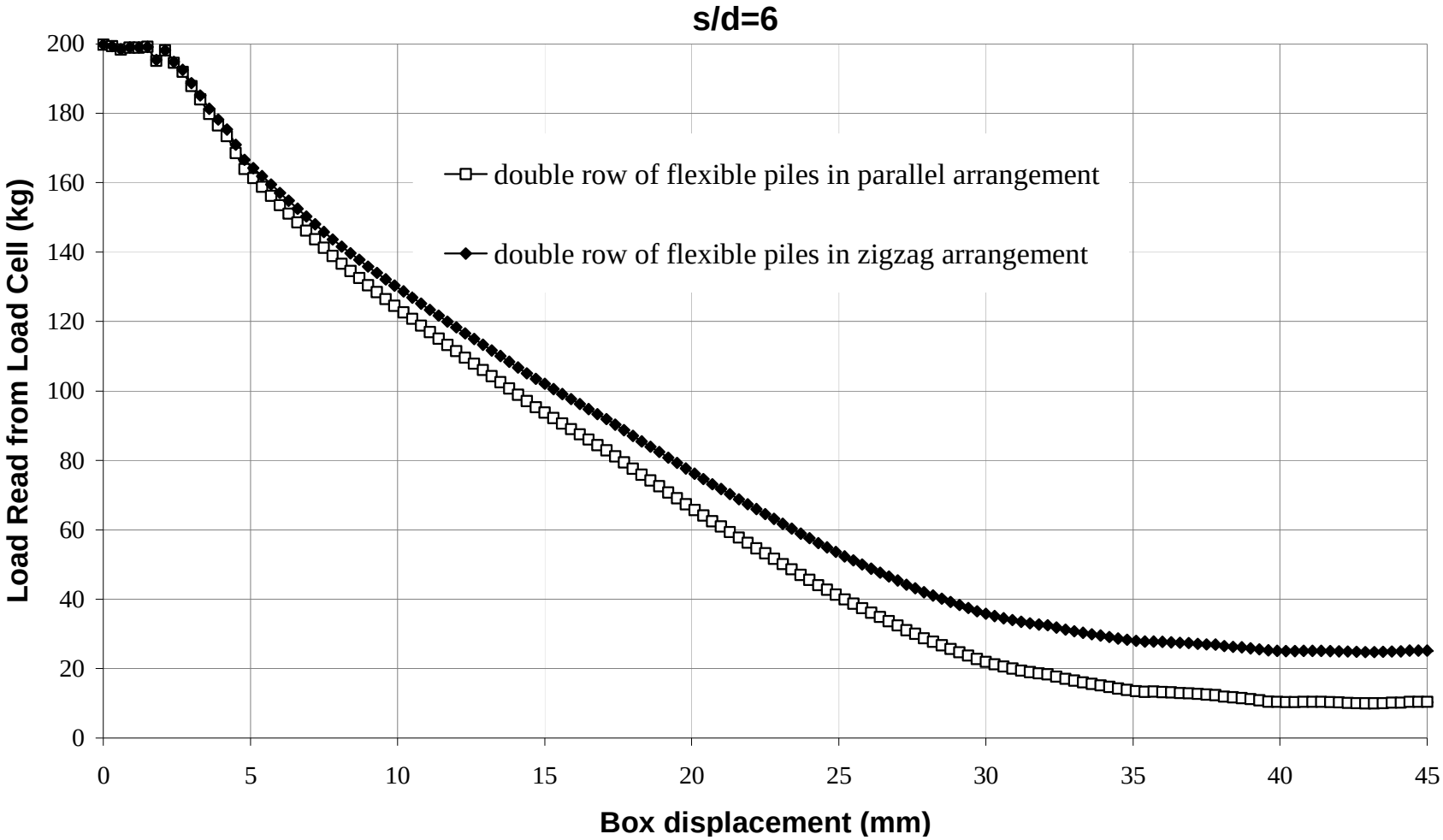

Figure 6.38 Load from load cell versus box displacement in double row of flexible piles in parallel and zigzag arrangements.

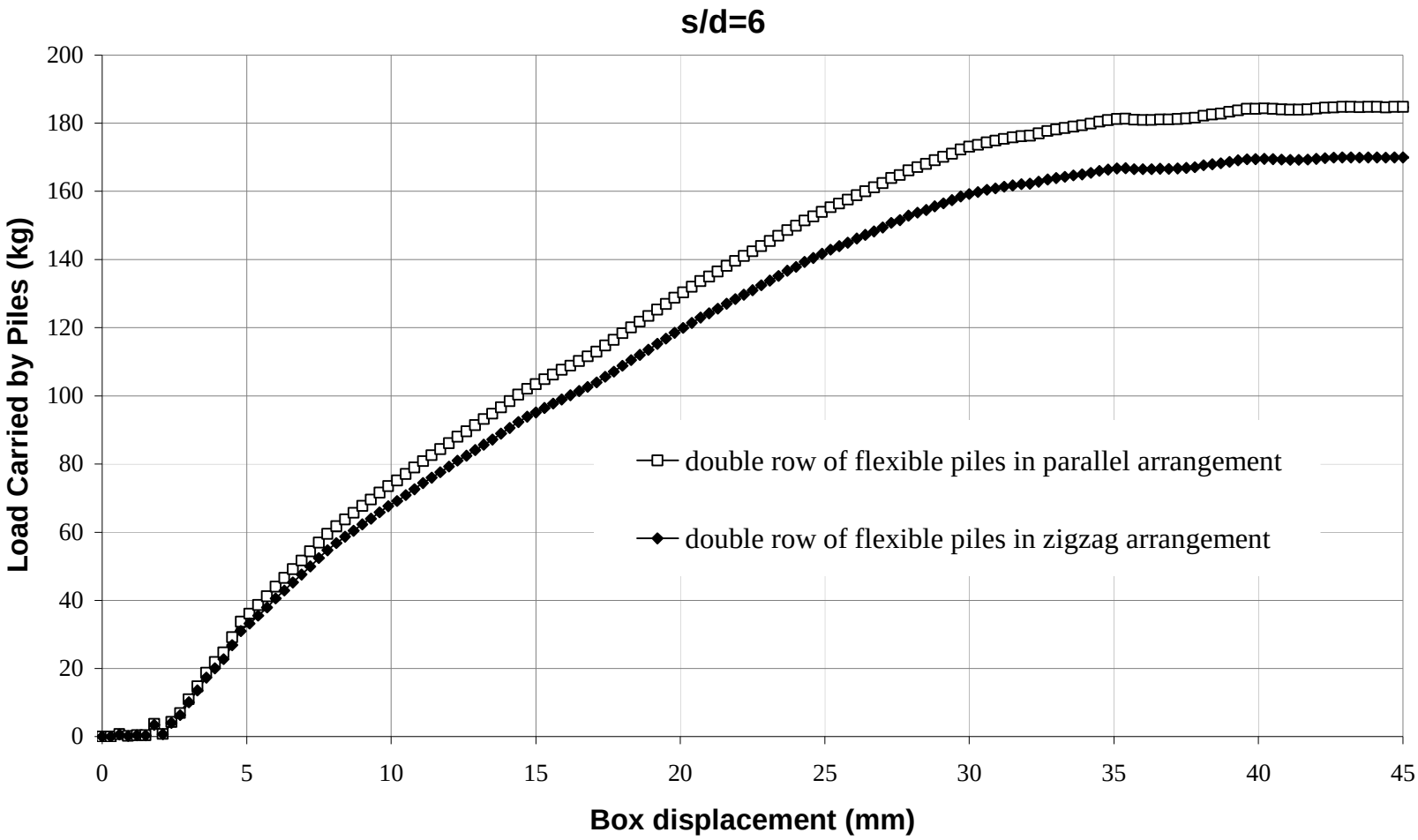

Figure 6.39 Load from load cell versus box displacement in double row of flexible piles in parallel and zigzag arrangements.

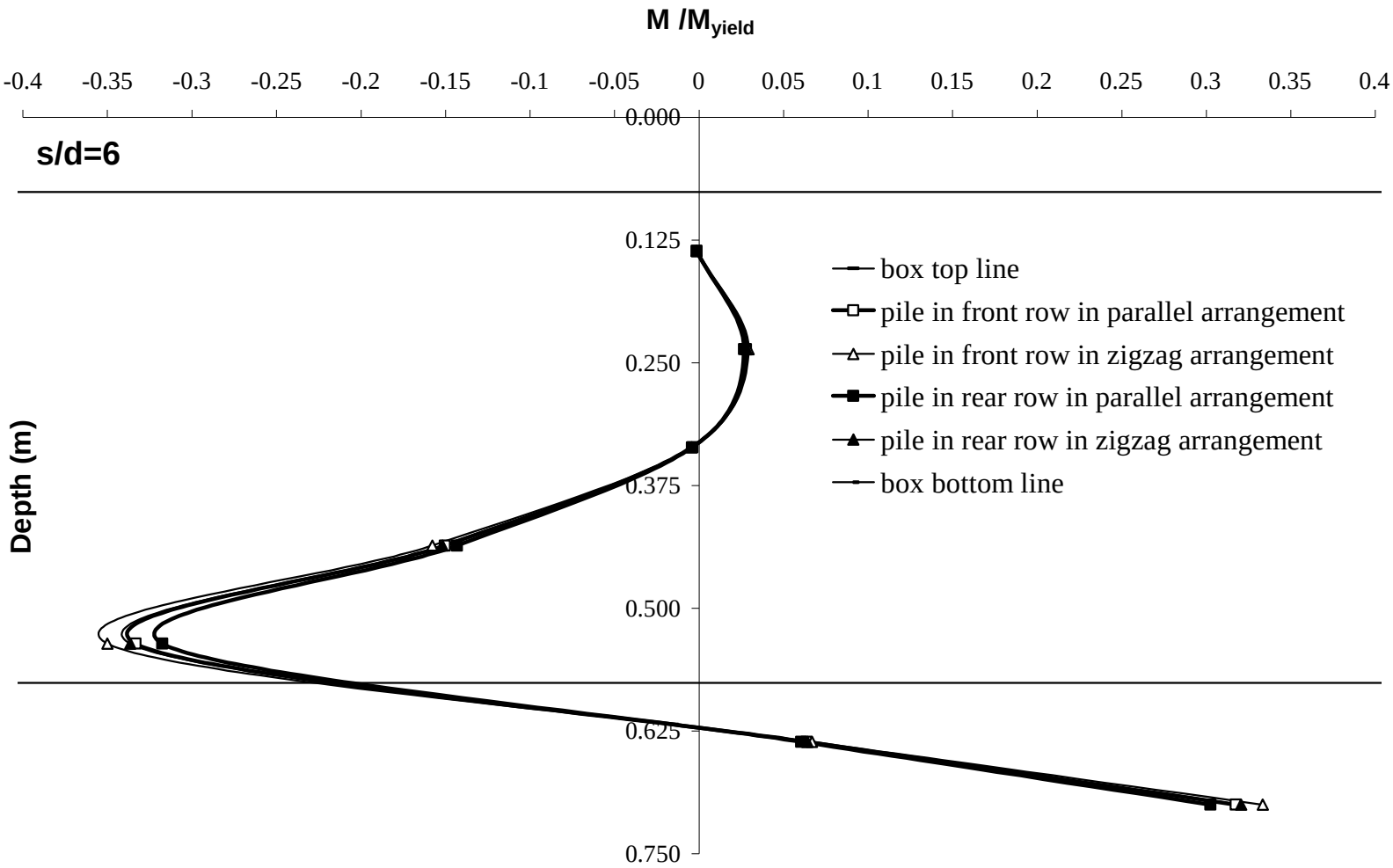

Figure 6.40 Normalized moment (M / M $_{yield}$) versus depth for s/d=6 in double row of flexible piles in parallel and zigzag arrangements.

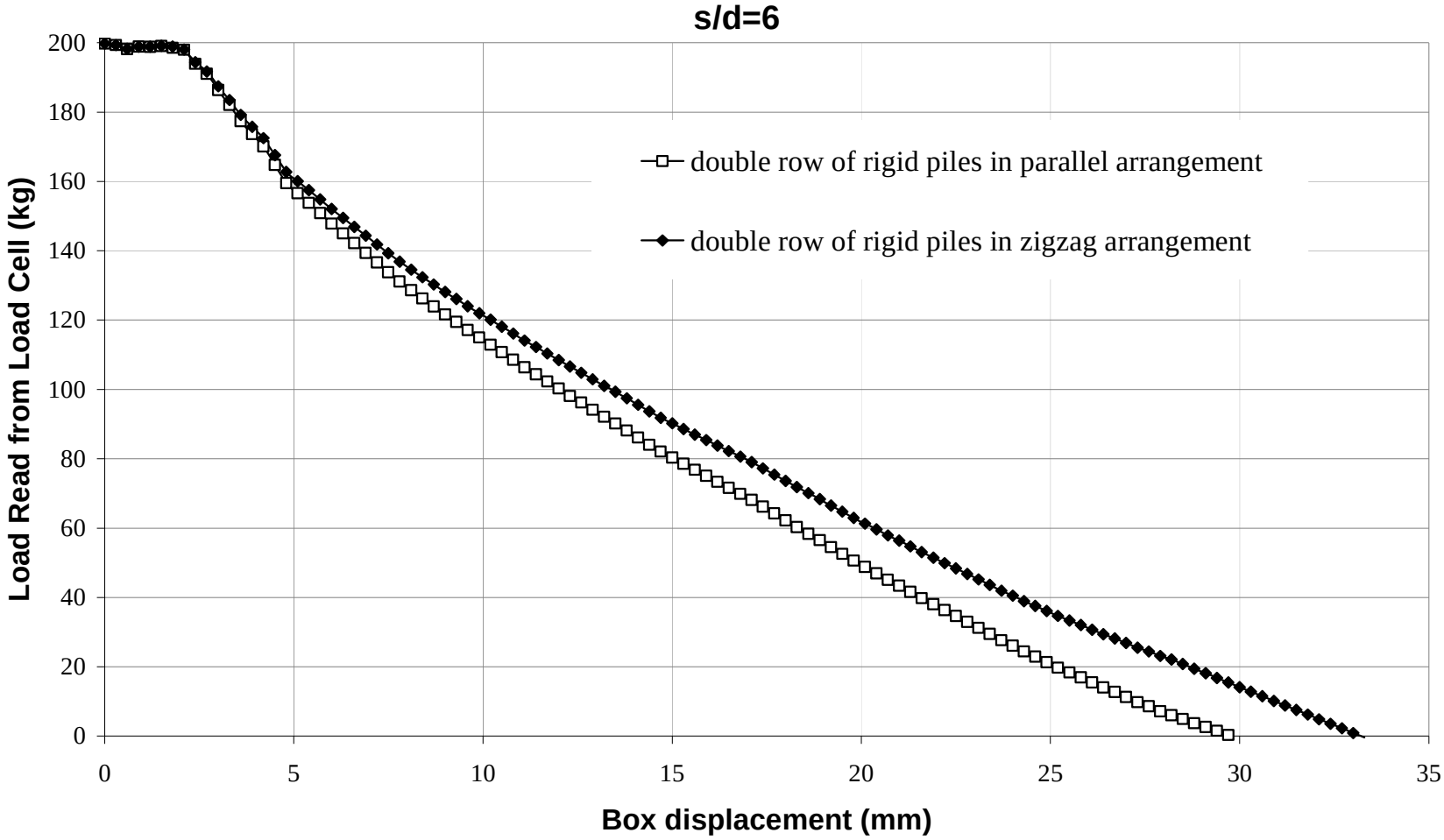

Figure 6.41 Load from load cell versus box displacement in double row of rigid piles in parallel and zigzag arrangements.

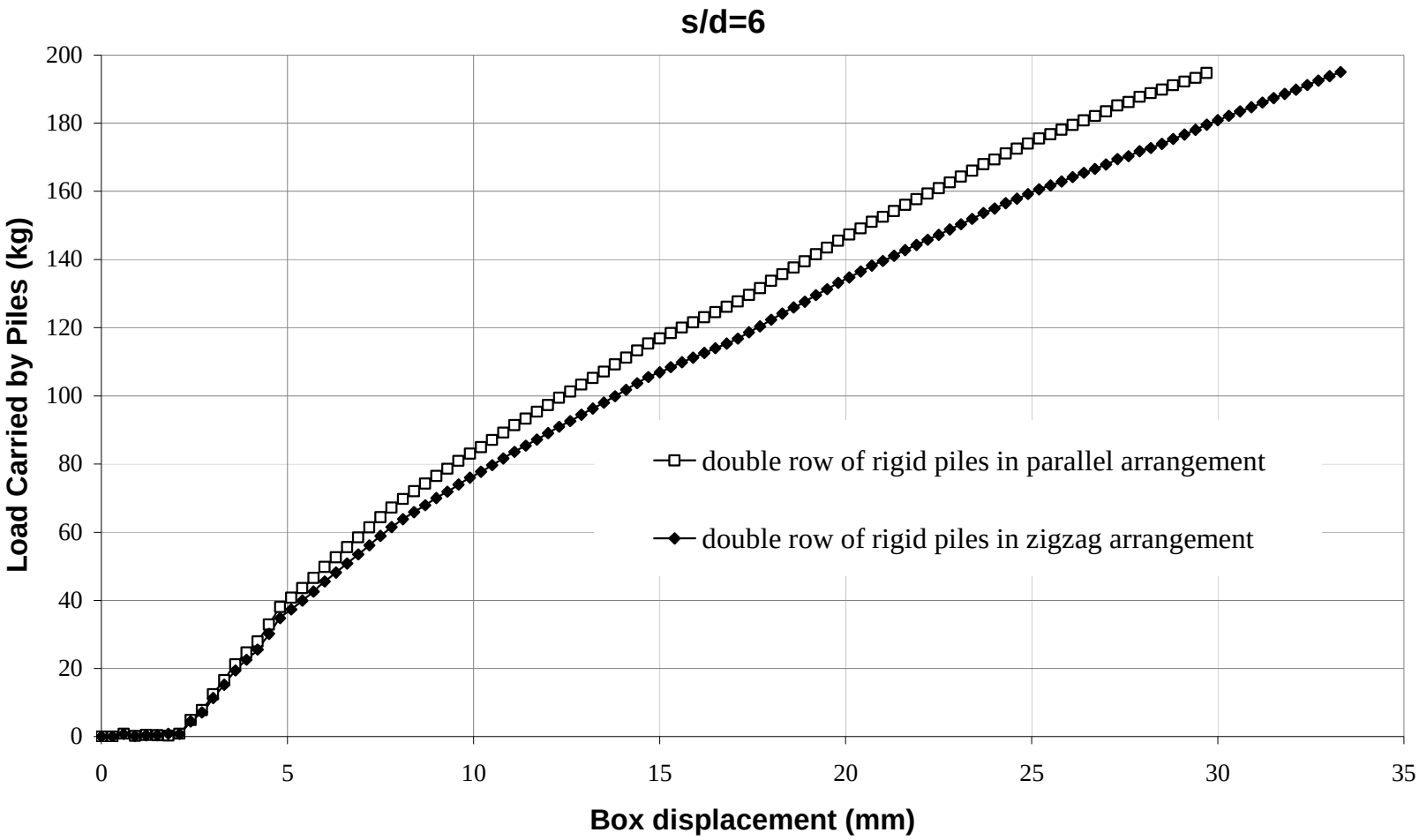

Figure 6.42 Load from load cell versus box displacement in double row of rigid piles in parallel and zigzag arrangements.

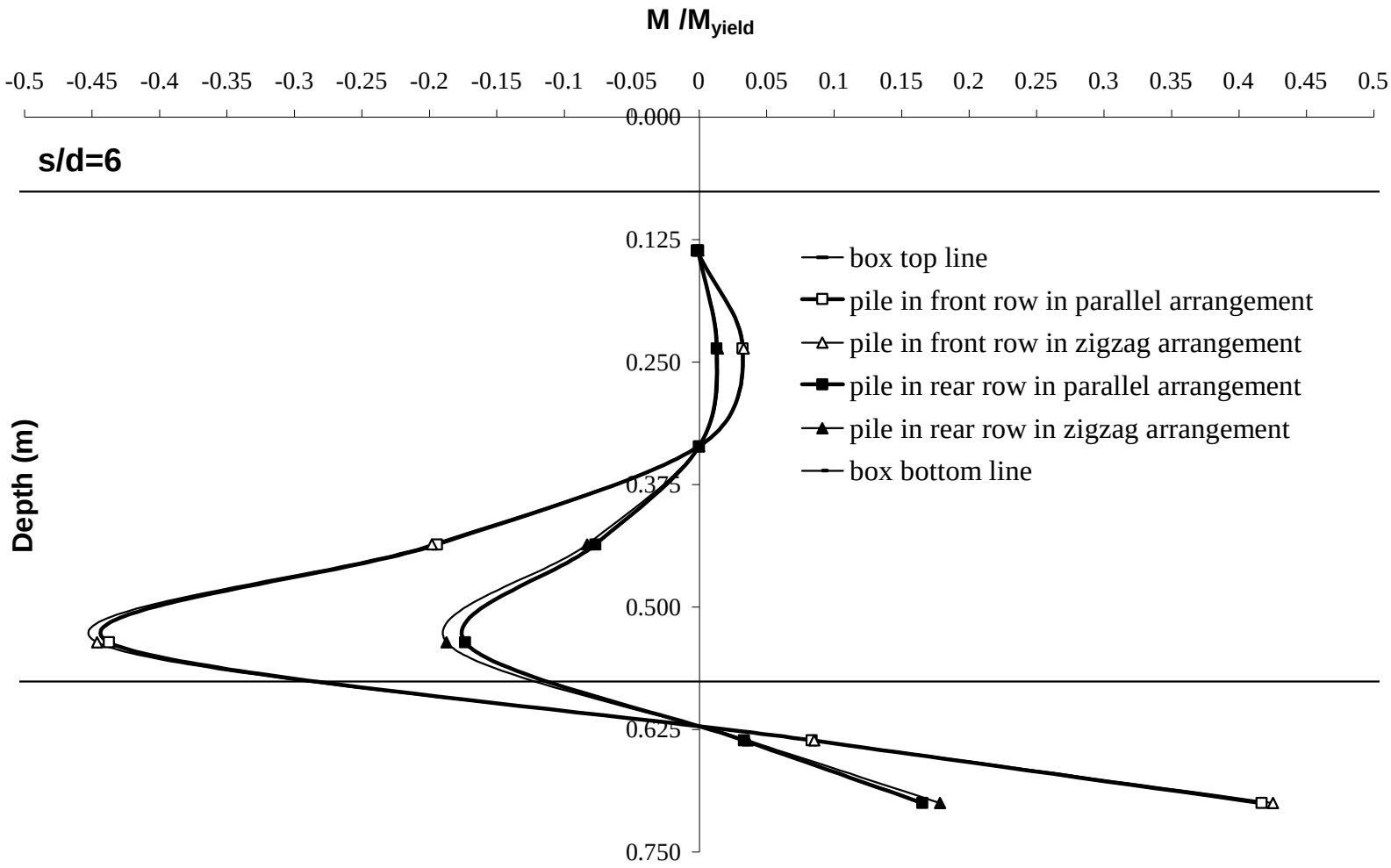

Figure 6.43 Normalized moment (M / M $_{yield}$) versus depth for s/d=6 in double row of rigid piles in parallel and zigzag arrangements.

CHAPTER SEVEN
DETERMINATION OF THE SOIL SURFACE DISPLACEMENTS USING DIGITAL IMAGE ANALYSIS TECHNIQUES

7.1 Arrangements to Establish Monitoring Setup

Since the soil load transfer to the piles by the soil arching mechanism has been measured during the several laboratory tests, the existence of this mechanism was investigated by monitoring the soil displacements using digital image analysis techniques. However, since only the top soil surface can be imaged by the camera, the movement of the soil particles below the surface can not be determined while evaluating soil arching by this method. A digital camera was mounted on the testing box, which has the same movement with the box and the soil surface to determine the relative surface displacements. The SLR camera Canon 350D with 18-55mm lens controlled by a laptop computer remotely via USB connection was aligned perpendicular to the inclined surface of the soil (Figure 7.1). The soil surface was equipped with specks having a diameter of 1 mm, in order to measure the relative displacements by monitoring these points (Figure 7.2).

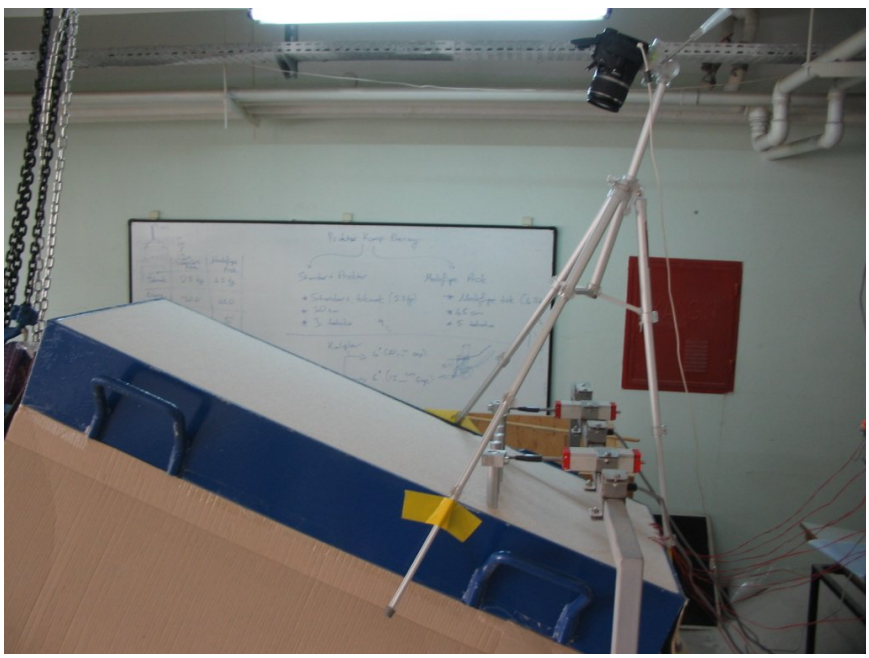

Figure 7.1 The position of the digital camera.

Figure 7.2 The installation of the displacement measurement points.

The specks were positioned denser around the piles and become coarser away the piles. Thus, relative displacements between the soil particles were determined by recording time-lapse images throughout the test. Time-lapse photography involves taking many pictures of the soil surface over the entire test period and then analyzing them together in order to determine relative soil displacements on the soil surface. Time-lapse photos were automatically captured at 20 seconds time intervals for the entire test period. The test period was divided into three intervals from the beginning to the end of the tests and four images were chosen for the image analysis, in order to reduce the computational efforts.

The calibration of the camera was performed by imaging a grid paper laid on the soil surface. On the calibration images, 10 mm corresponded to 65 pixels both in vertical and horizontal directions and negligible telecentricity effect was observed. Namely, the resolution of the system was determined as 1/6.5 mm. The frame of the camera was so arranged to capture the zones where soil arching is expected to take place (Figure 7.3).

Figure 7.3 The camera view of the testing box surface.

7.2 Digital Image Processing Operations by DEU Laboratory Team

The image processing and data visualization operations were performed by using MatLab Technical Computing Language and ImageJ image analysis software. The relative and final displacements of the monitoring points were marked into the original soil surface images in order to have a visual explanation of the soil arching phenomena.

The captured images were reduced to 8-bit gray scale images, in order to apply thresholding operation for the segmentation of the displacement tracking points (Figure 7.4a). The color of the specks was deliberately chosen as black, resulting relatively low gray values compared to sand particles after gray scaling. However, the contrast between the specks and soil particles was improved by using contrast stretching operation in order to get better segmentation results from the thresholding process (Figure 7.4b). The segmentation of the tracking points has been performed by choosing a proper threshold value and then applying the thresholding operation (Figure 7.4c). The threshold value was determined by using Otsu method (1979), which calculates an automated threshold value by using the histogram of the image being used. Thus, pixels having the gray value below the threshold have been converted to black and pixels having the gray value above the threshold converted to white (Figure 7.4d).

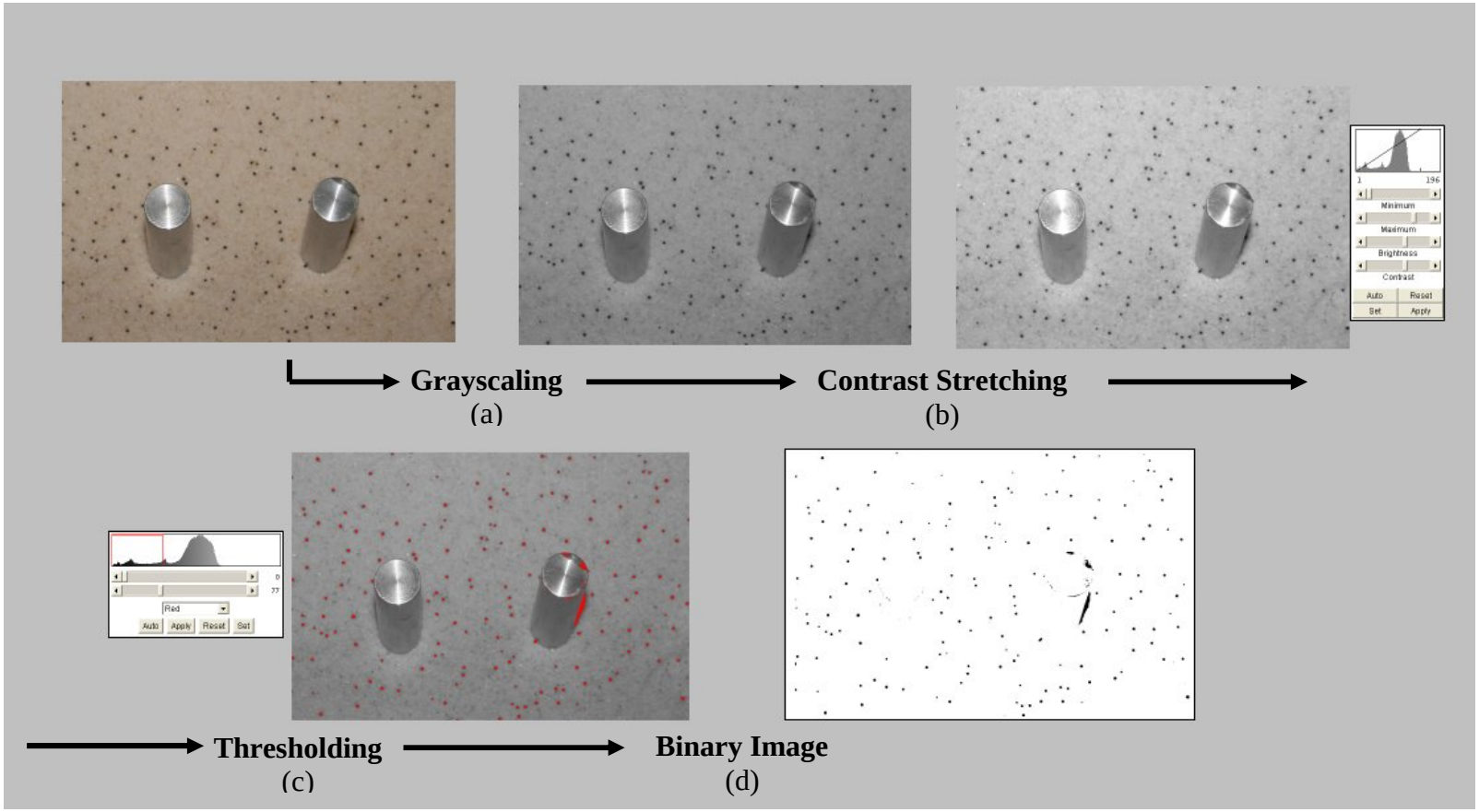

Figure 7.4 Digital image processing sequence.

After the image processing stage, the resulting binary images have been stored for the image analysis in order to determine the coordinates of the segmented tracking points.

7.3 Digital Image Analysis by DEU Laboratory Team

The area and circularity of the segmented tracking points was used as the elimination criteria at the analysis of the binary images. The segmented tracking points were analyzed in the binary images and a discrepancy between the speck areas, varying in a close range interval, was observed. The pixel blocks, having larger area than the speck area interval, was eliminated. Thus, piles, the borders of the box, the tripod were not considered at the analysis. Also, pixel blocks, having less area than the speck area interval, have been eliminated, which ensured the elimination of the mis-threshed pixels and remains of the eliminated big pixel groups. However, the area elimination criteria did not successfully segmented the touching specks alone. Therefore, the circularity of the segmented points was examined. The circularity presents a quantitative value which is defined as $C = (4\pi \text{ area})/(\text{perimeter})^2$. A perfect circled speck will have the circularity value of unity, where this value is decreasing according to the distortion of the shape. Since the touching specks have significantly lower circularity values, this pixel blocks were not considered as displacement tracking points in the analysis of the binary images. The centroidal coordinates of the remaining tracking points in each image were determined and stored for the visualization process.

7.4 Laboratory Tests

The time–lapse photo technique was performed for the entire test period. The test period was divided into three intervals from the beginning to the end of the tests and four images were chosen for the image analysis, in order to reduce the computational efforts.

7.4.1 Free head rigid piles

The pile head displacement versus box displacement graphs for free head piles with s/d = 6 and s/d = 4 are shown in Figure 7.5. It can be observed from this figure and time lapse images that pile head movement exceeds the soil movement throughout the tests. The relative displacements of the tracking points for free head piles with s/d = 6 and s/d = 4 were shown in Figure 7.6 and 7.7, respectively. For the case of piles with both s/d = 6 and s/d = 4, relative soil movements are seen in the downslope direction. Since the pile pushed the surrounding soil to displace to the down slope direction rather than resisting against sliding. This behavior appears to be distinct in the case of piles with s/d = 4 due to the excess number of piles in the same slice. As seen in Figures, the relative displacements of soil particles decreased with distance from the piles to the upslope direction. One can notice that, if there were no piles, there would not be any relative displacements between the soil particles on the soil surface. The existence of the relative displacements on the soil surface was attributed to the presence of the piles (pile effect). The pile effect became negligible after approximately eight pile diameter (8d) far away from the piles. Hence, no relative displacements were determined above this zone during the test.

The measured load carried by a single pile in a group is shown in Figure 7.8. As the displacement of the soil increases, the loads acting on the piles increase rapidly as a result of load transfer mechanism by means of shear. The acting loads reach a maximum value and remain constant as the soil movement continues to increase, when the soil movement reaches a certain value. This indicates that the additional soil movement has no more influence on the load transfer mechanism. It has been obtained that the decrease in pile spacing causes an increase of the carried load per pile. This behavior can only be explained by soil arching existed between the piles along the box depth.

The bending moment and soil pressure distributions along the pile length evaluated from the bending strain data are given in Figure 7.9 and Figure 7.10, respectively. It can be seen from figures that the maximum values of moment is

increased with the decrease of pile spacing (Figure 7.9). Soil pressure distribution obtained from the bending strain data confirms the existence of negative pressure zone. It is also observed that pile head movement exceeds the soil movement, resulting in negative pressure on the piles over a certain depth (i.e. approximately 20% of the sliding soil thickness). Below this depth, active pressure occurs up to approximately 80% of the sliding soil thickness, and again negative pressure starts (Figure 7.10). The maximum negative pressure has been observed to be nearly three fold the maximum active pressure. The pressure distribution increases with the decrease in pile spacing.

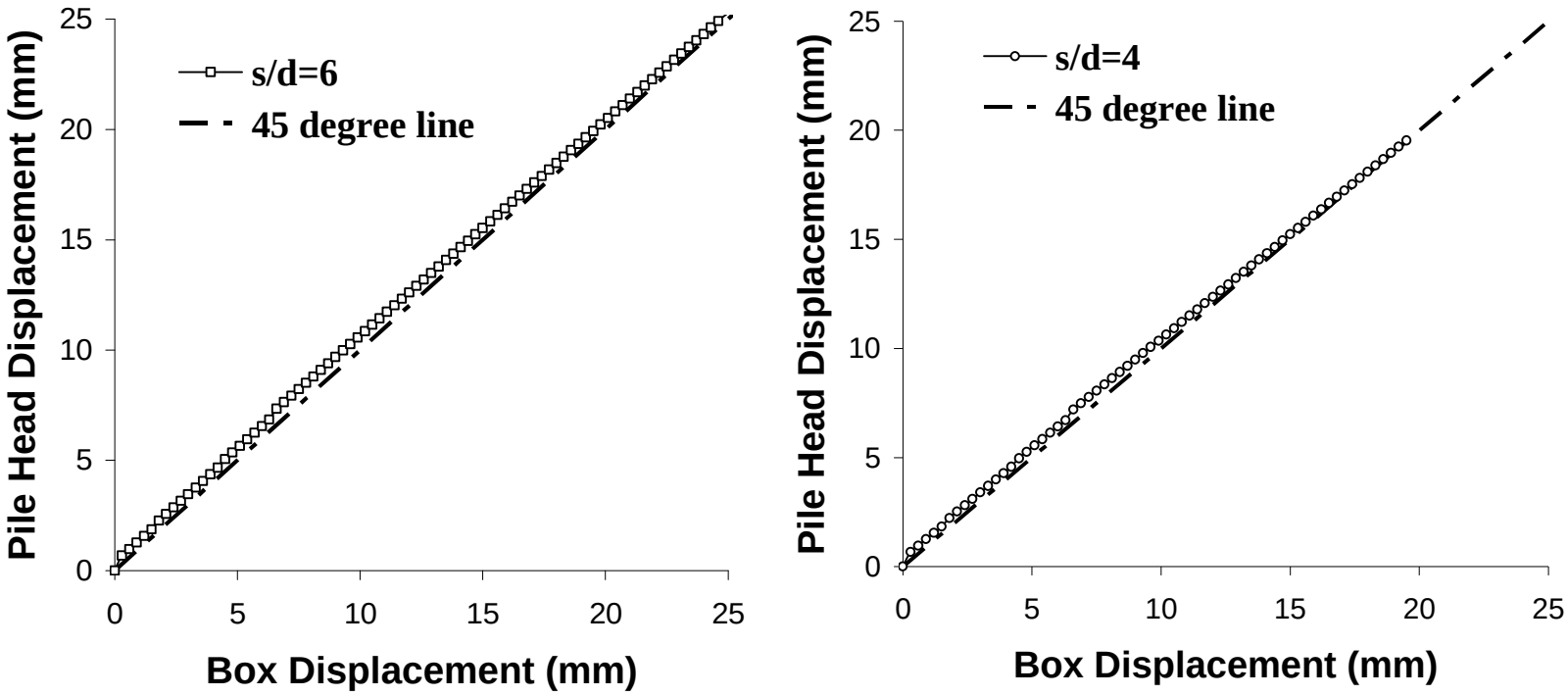

Figure 7.5 Pile head displacements versus box displacement.

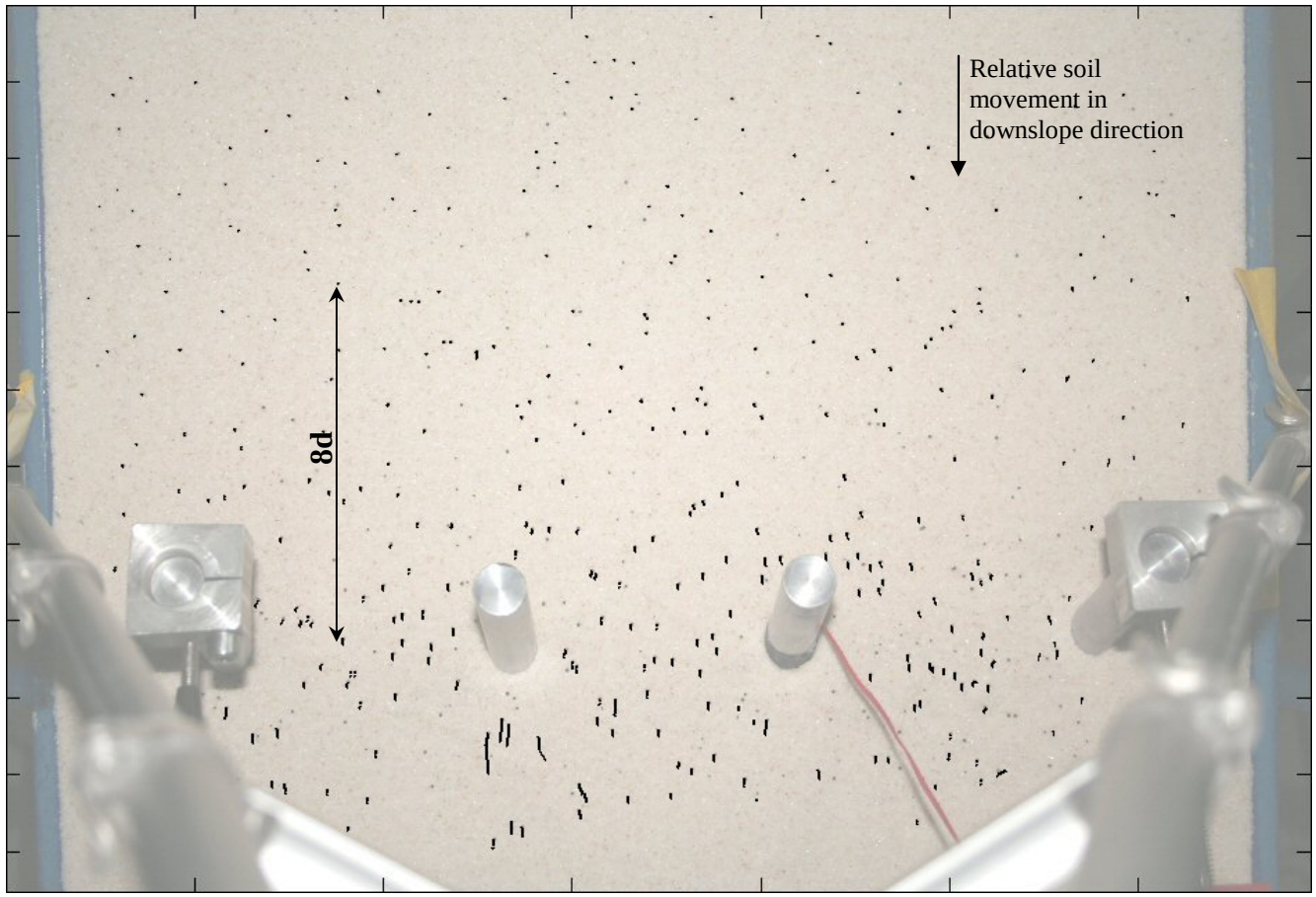

Figure 7.6 The overall relative displacements of data tracking points throughout the free head pile test with s/d=6.

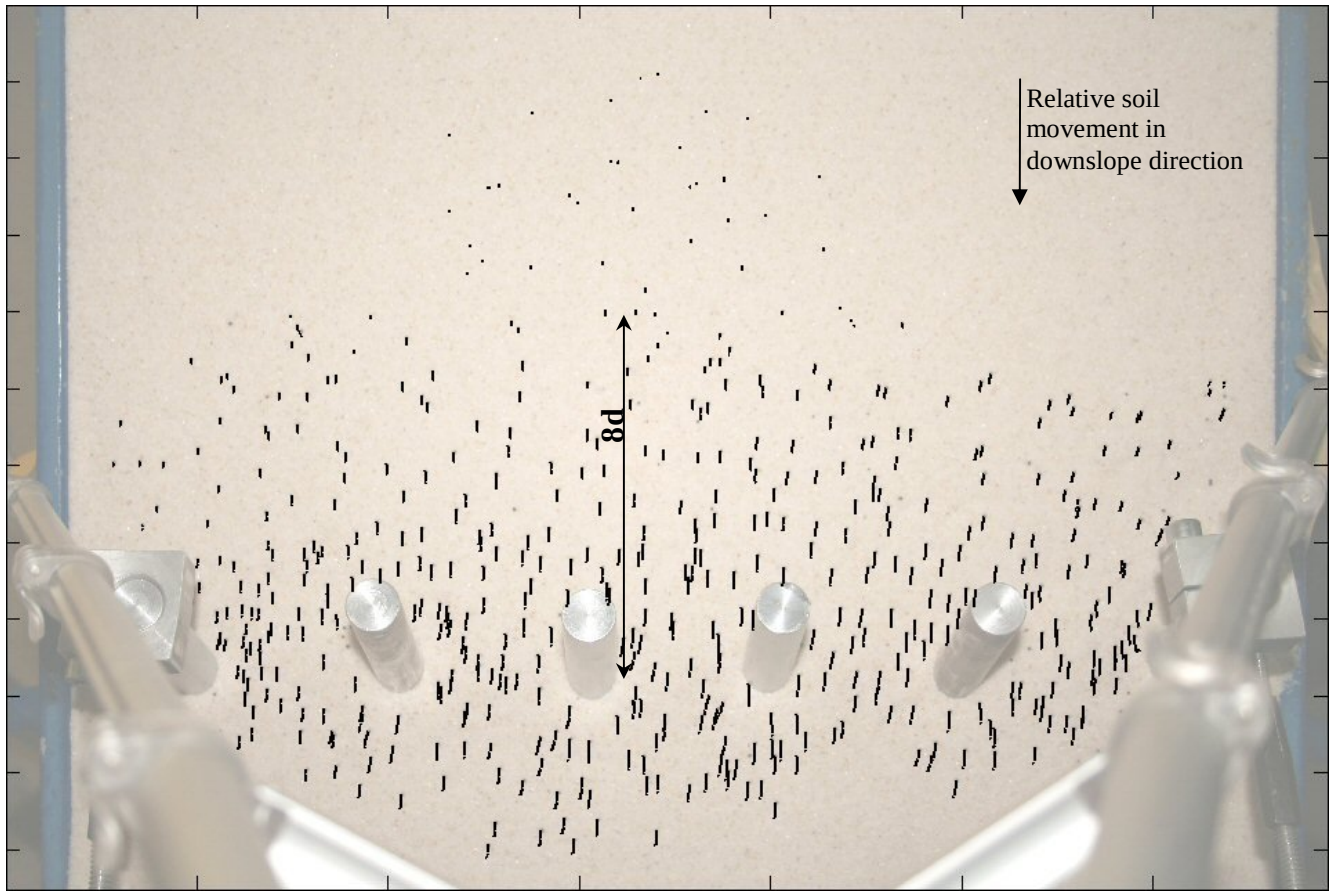

Figure 7.7 The overall relative soil surface displacements throughout the test the free head pile test with s/d=4.

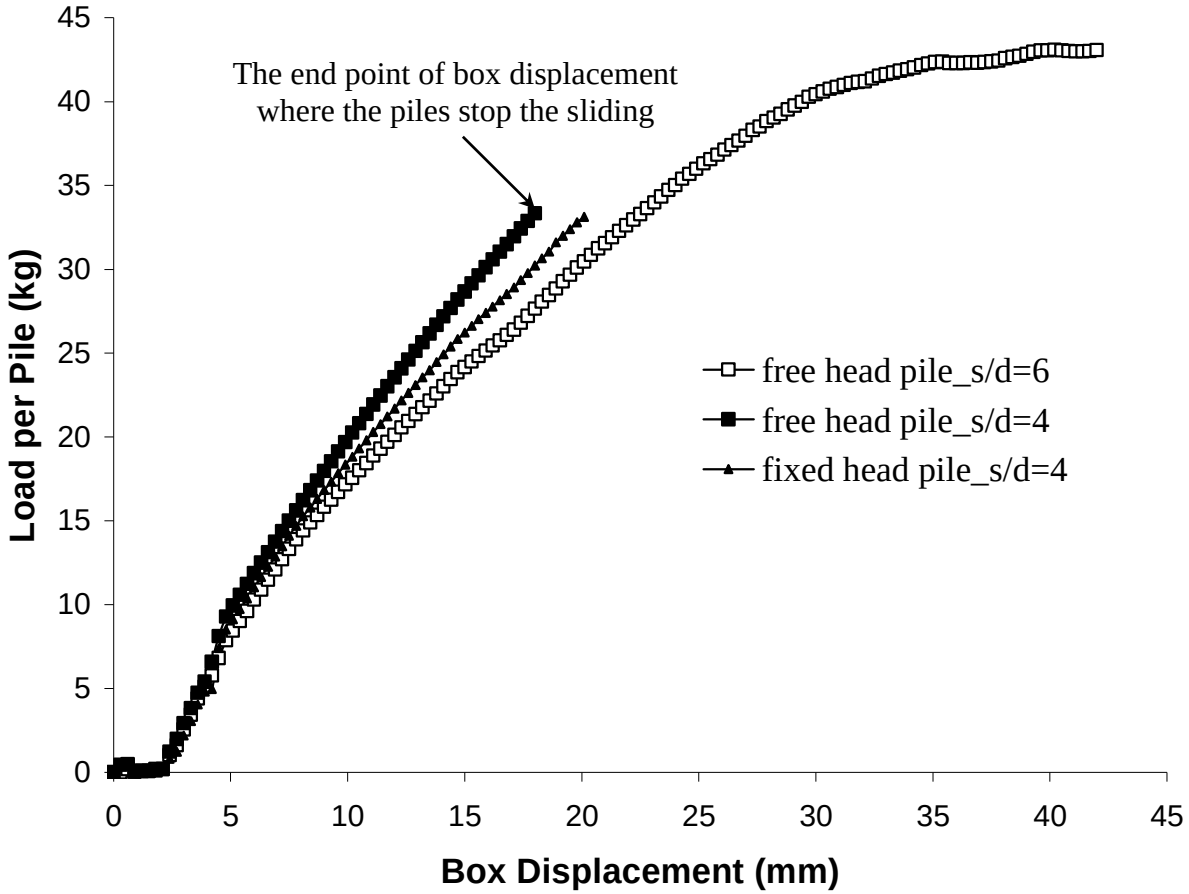

Figure 7.8 Load per pile.

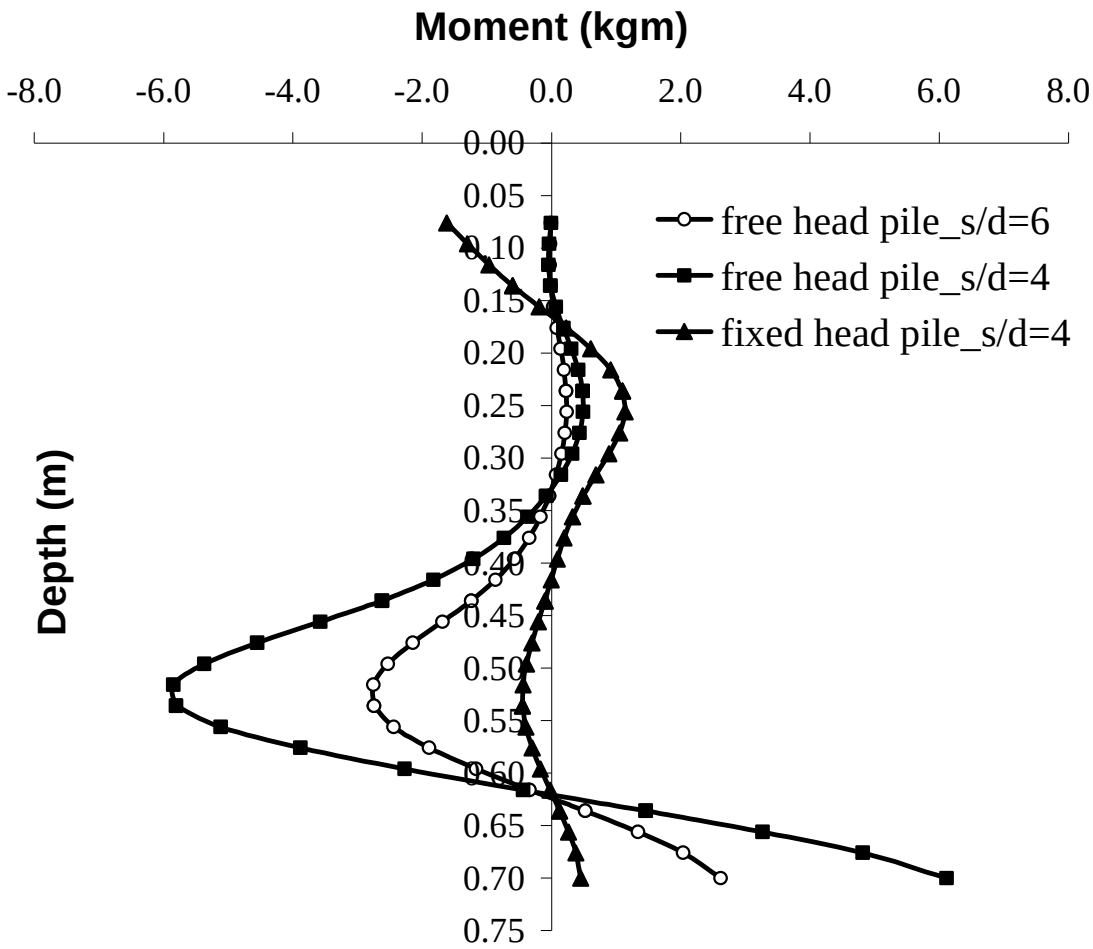

Figure 7.9 Bending moment distributions at the 18 mm box displacement.

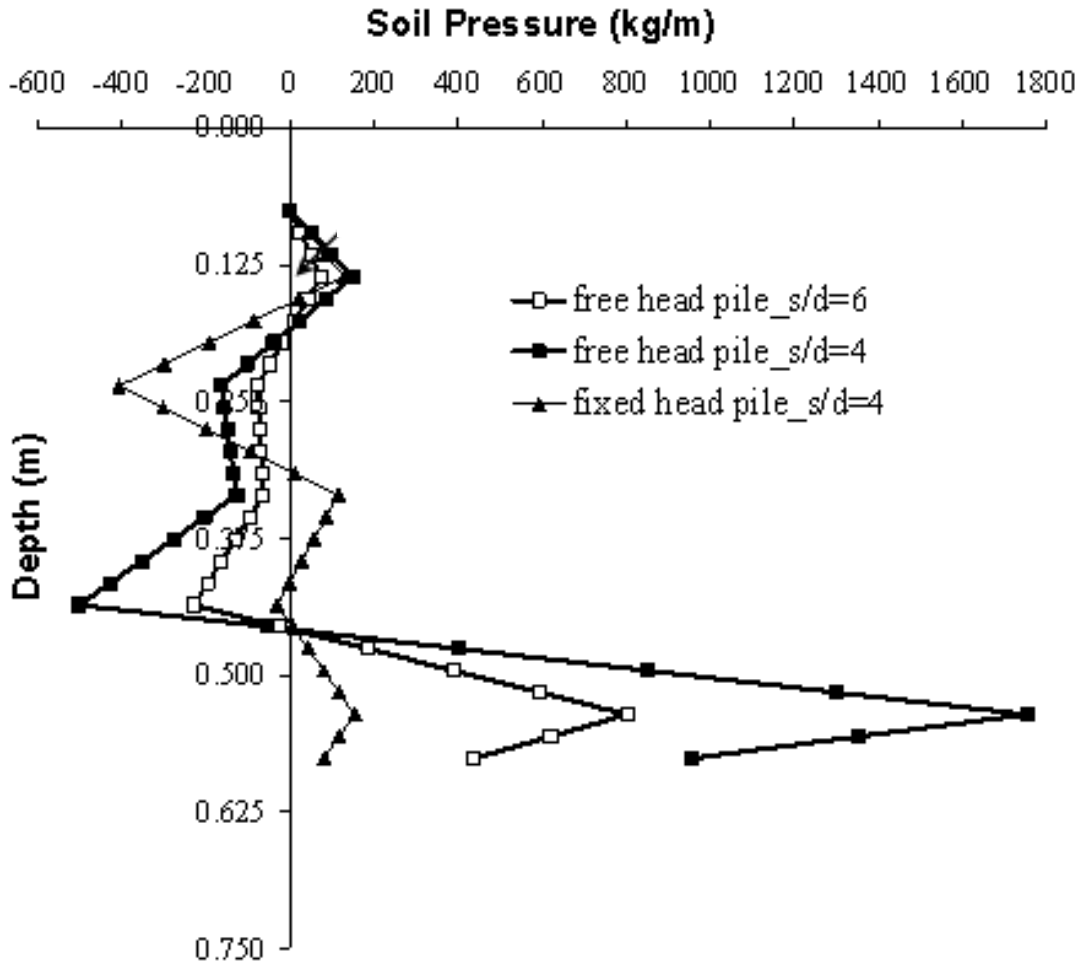

Figure 7.10 Soil load distributions at the 18 mm box displacement.

7.4.2 Fixed head rigid piles with s/d=4

It was decided that pile head movement should be restrained in order to succeed in observing soil arching on soil surface. Therefore, the experimental setup was improved with equipments so as to enable restrained pile head with by fixed head condition. The improved experimental setup was shown in Figure 7.11.

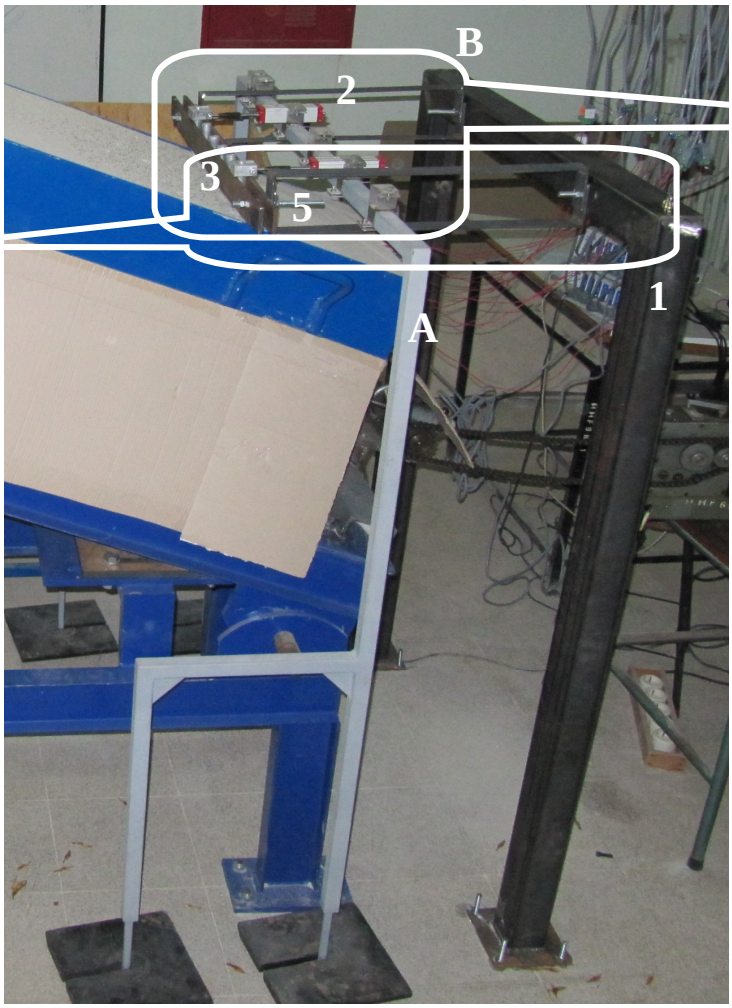

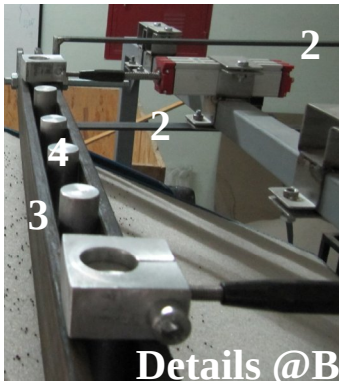

1. steel frame
2. metal sheet
3. steel plate
(pile head fixity)
4. pile
5. bolt

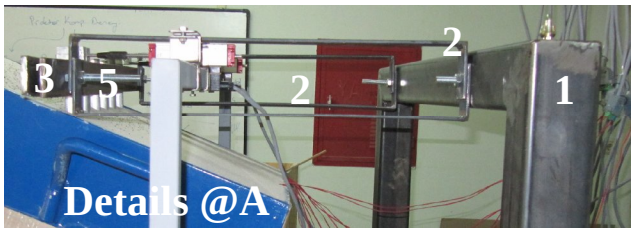

Figure 7.11 Improved experimental set up for fixed head pile tests.

As the displacement of the soil increases, the loads acting on the fixed piles increase rapidly as a result of load transfer mechanism like in the case of free head piles (Figure 7.8). It was also revealed that the restrained pile head condition causes a decrease of the carried load per pile. It can be noticed from the Figure 7.9 that the fixed head condition results in the smallest bending moment in the piles. The maximum bending moment in free head piles is about two times that in fixed head piles. It can be seen from Figure 7.10 that the maximum value of soil pressure in the case of fixed head is less than that in free head piles. The relative displacements of the tracking points for fixed head piles with s/d = 4 were shown in Figure 7.12. In the case of fixed head piles, piles resist against sliding and reduce the surficial soil displacements in contrast to the case of free head piles. Therefore, soil particles in the pile affected zone have less surficial displacements than the box displacement. Soil particles having less displacement than the box appear to displace towards the upslope direction in the time lapse images due to the resisting against sliding. The relative displacements of soil particles decreased with distance from the piles to the upslope direction.

The measured relative displacements are added to the box displacement in order to determine the magnitude and the direction of soil particle movement (Figure 7.13). By connecting the soil particles having the same and the minimum surficial displacements, paths resembling arches can be established. The surficial displacement of soil particles located over the developed arches increased towards the upslope direction, similarly that below the arches increased towards the downslope direction as shown in Figure 7.13.

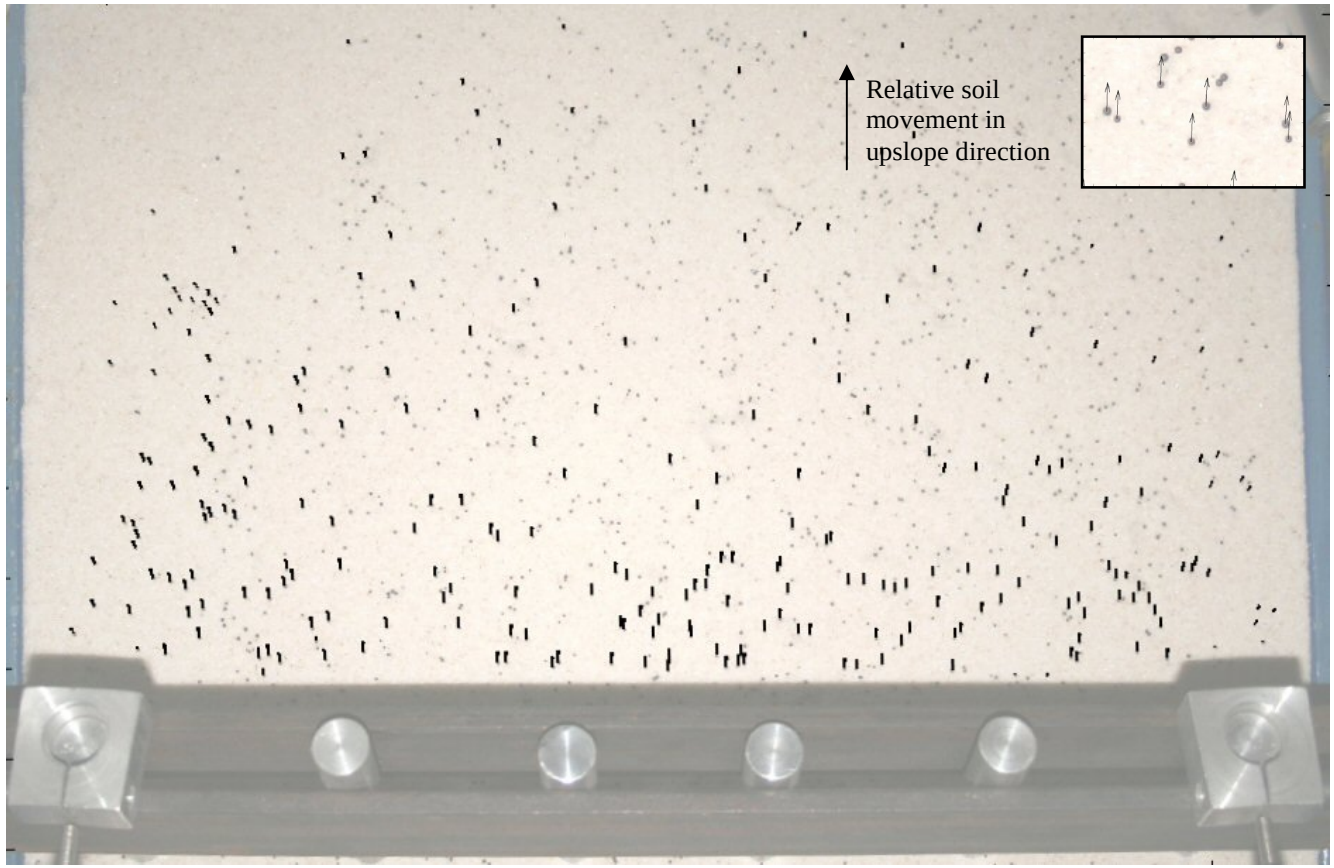

Figure 7.12 The overall relative soil surface displacements throughout the test.

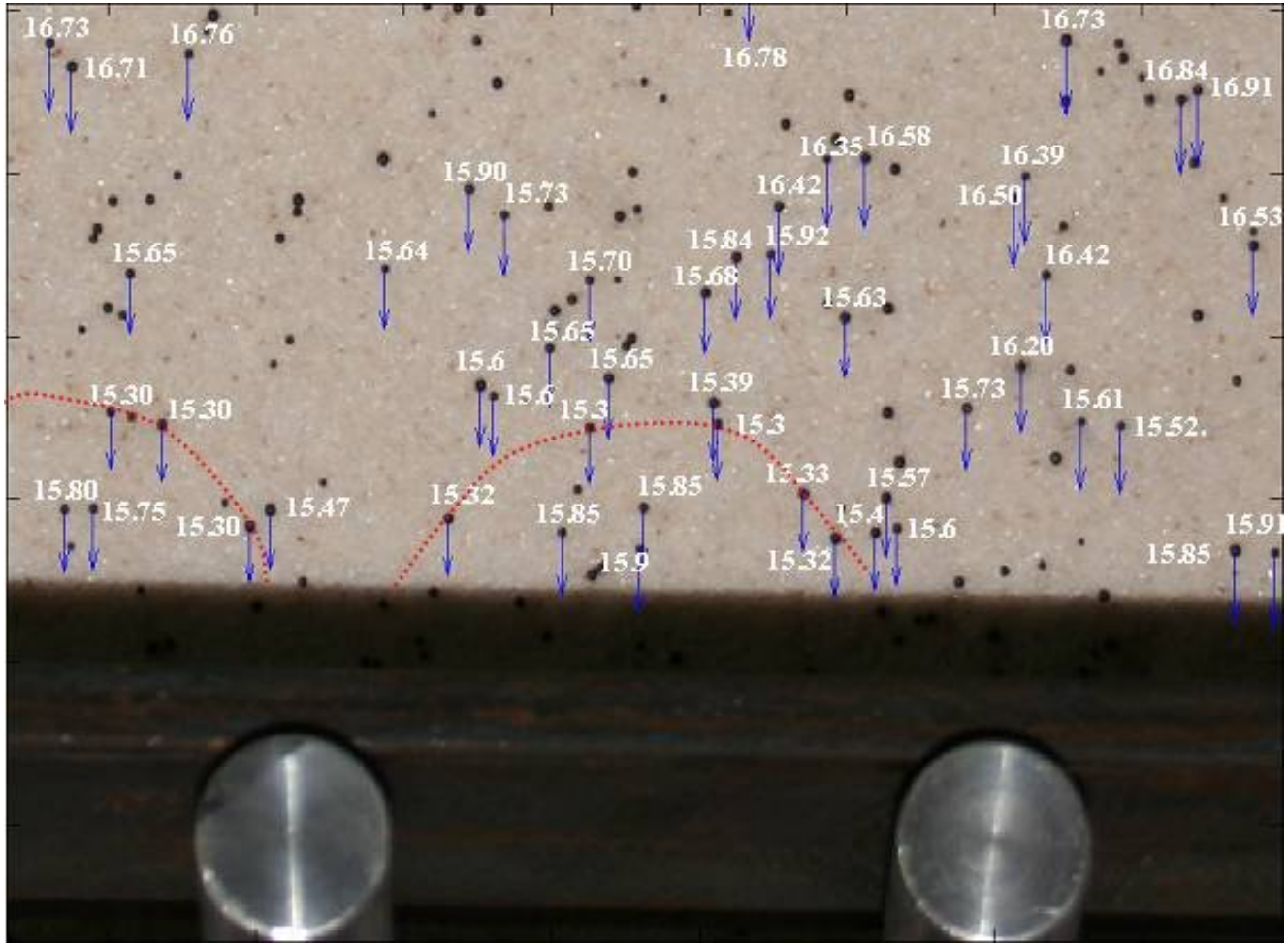

Figure 13 Total soil surface displacements in mm due to soil arching with 18 mm box displacement.

7.5 Discussion on Test Results

The soil surface displacements on three tests, containing free head rigid piles with s/d=6 and s/d=4, and fixed head rigid piles with s/d=4, were monitored and evaluated via digital image analysis techniques. Relative displacements between the soil particles were determined by recording time-lapse images throughout the tests.

It has been observed that for the free head pile cases, pile head movement exceeds the soil movement, resulting in negative pressure on the piles over a certain depth. This part of the pile with the negative pressure pushed the surrounding soil to the downslope direction and induced the soil particles to be displaced to the gaps. Closer pile spacing increases developed negative pressure and surface displacements of soil particles. The pile effect became negligible after eight pile diameter (8d) away from the piles. Hence, no relative displacements were determined at this zone during the tests. For the free head pile cases, the soil arching, which was determined from the load-displacement relations measured experimentally, was not observed on the soil surface due to larger pile head displacements than surficial soil displacements.

In the fixed pile case, no pile head movement was measured due to the restrained pile head condition in contrast to the free head cases. The displacement of surficial soil particles located over the developed arches increased towards the upslope direction, similarly the surface displacement of soil particles located below the developed arches increased towards the downslope direction. Hence, the arches can be established by connecting the soil particles having the minimum soil surface displacements. This displacement behavior of soil particles are the evidence of the existence of soil arching mechanism.

The fixed head condition results in the smallest bending moment in the piles (Figure 7.9). The maximum bending moment in free head piles is about two times that in fixed head piles.

CHAPTER EIGHT
BACK ANALYSIS OF A LANDSLIDE REMEDIATION PROJECT WITH DOUBLE-ROW STABILIZING PILES

Analysis of a case study where double-rows of passive piles were used to stabilize sliding Neogene aged soil mass is presented herein with an emphasis on the influence of arching mechanism on the transfer and distribution of the soil load between the front and rear pile rows. Constructed piled retaining system was back analyzed by means of three dimensional finite element models. In this respect, two different models were established. One of the models targeted structural analysis of the double row system whereas the second one was a full three dimensional model including piles and the surrounding soil. Measured displacements of piled retaining system were also compared with the back calculated displacements. In the light of back analyses, the loads acting on pile rows, considering the loads calculated by theories based on plastic deformation are determined and the importance of pile socket length and third dimension effects are decided.

8.1 Investigation of Landslide Mechanism

Several landslides took place in a narrow band of the coastline between İzmir and Söke causing frequent economic loss especially following rainy seasons. The study area is located in the backyard of a five storey high school building in Söke where landslide prone Neogene aged geological formations generate the soil profile (Figure 8.1).

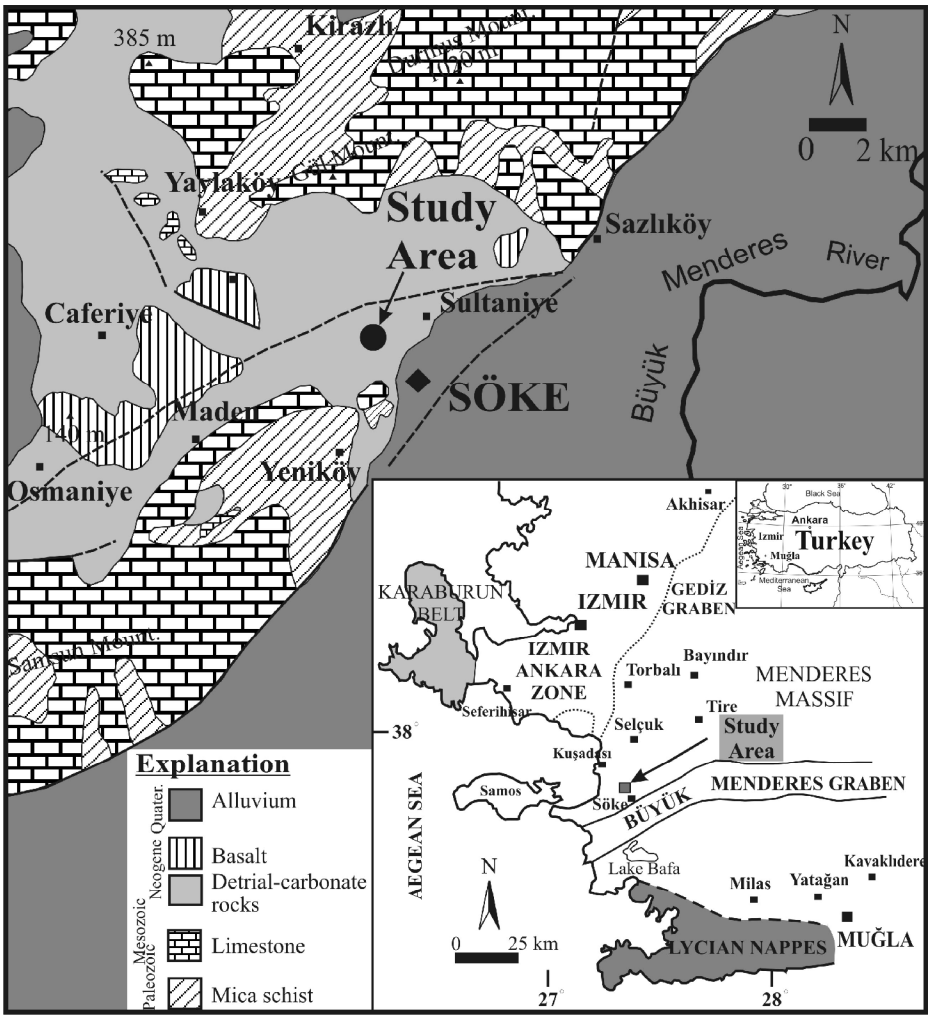

Figure 8.1 General geology and location map of the study area (Kıncal and Koca, 2009).

Having already been defined as a high landslide risk area in official geological maps, the steep slopes with an overall angle of 36° from the North East to the East of Söke failed catastrophically during a highly intensive rainy season. In order to find out the causative mechanism of the landslide and to decide the slope maintenance requirements, geotechnical site and laboratory investigations were performed. In addition to the engineering boreholes and standard penetration tests, geophysical studies (i.e. seismic refraction and electrical resistivity) were also conducted alongside the boring locations. The slide area is mapped in Figure 8.2 with geotechnical and geophysical investigation locations.

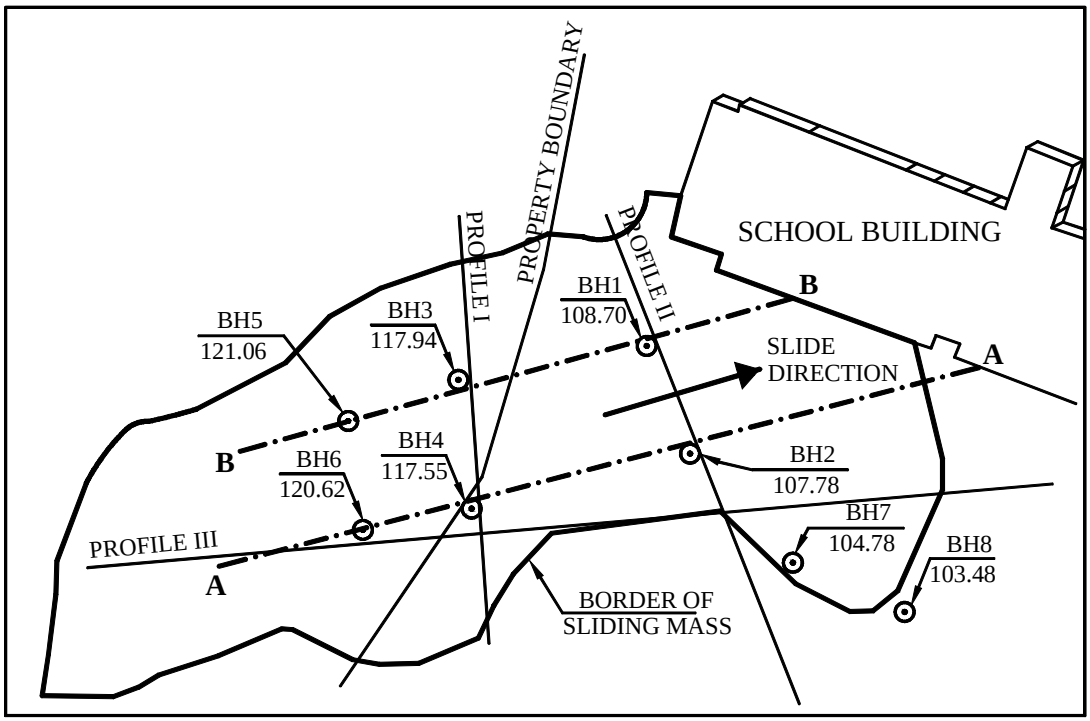

Figure 8.2 Borehole and geophysical profile locations.

The sliding material of the slope, the thickness of which varied between 4.5 to 10.0 m., was generally composed of clayey and silty sand. The base rock was identified as sand stone. Borehole logs are plotted on the section of the electrical resistivity tomography (Figure 8.3).

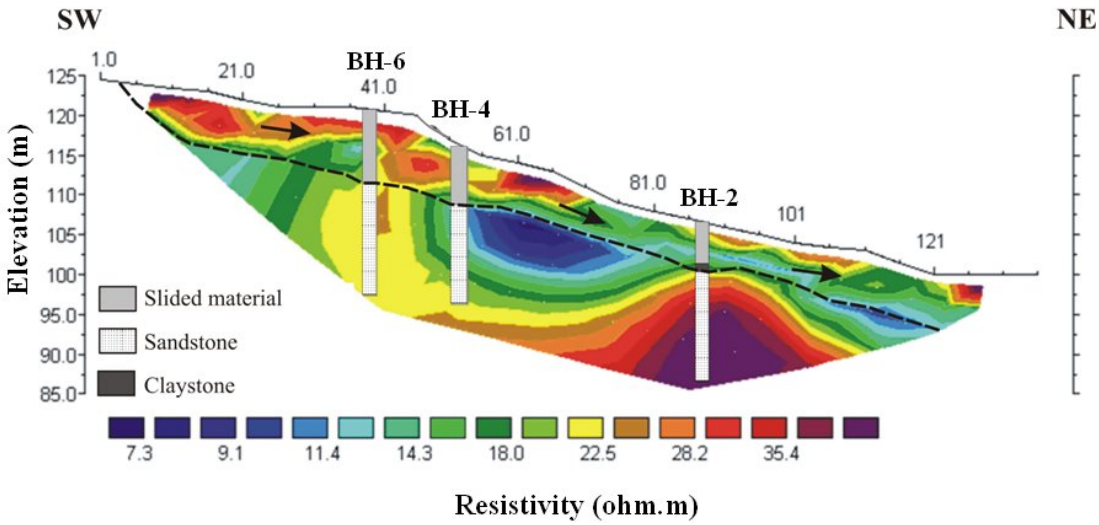

Figure 8.3 Electric resistivity tomography for Profile-III.

Although free ground water table was not encountered during site investigations, heavy rainfall may have led to a large amount of infiltration and high pore pressures may also have developed in certain zones. The excavation pursued during landscape works, nevertheless, disturbed the delicate balance of the former residual shear planes and triggered the landslide.

The fact that the school area was constrained by a private property avoided lowering the site slopes by means of excavation since such an action required soil removal in the privately owned fields as well. Therefore, a piled retaining system appeared to be the best choice that could be realized by local contractors.

8.2 Design of the Piled Retaining System

The most appropriate position and elevation of the bedrock considering the necessity to stay within the school parcel borders was sought in order to provide satisfactory socket length and consequent passive resistance to the piles while minimizing project costs as much as possible. Subsequent to examining the alternatives, the section through Profile II was selected as the optimum location. A remediation project consisting of double-row piles connected with a single continuous rigid pile cap was performed.

Numerical analyses for the design of the piled retaining system were made using finite element method with assigned effective stress parameters in the Mohr-Coulomb plasticity model. The idealized plain strain soil profile consisted of three zones: sandstone at the bottom, the sliding mass at the top and a thin band of soil layer in between to simulate the residual shear zone. The effective residual shear strength parameters of the shear zone were obtained as $c'=5$ kN/m^2, $\phi'= 13^0$ based on residual shear test data and back analyses. The respective soil model is given in Figure 8.4.

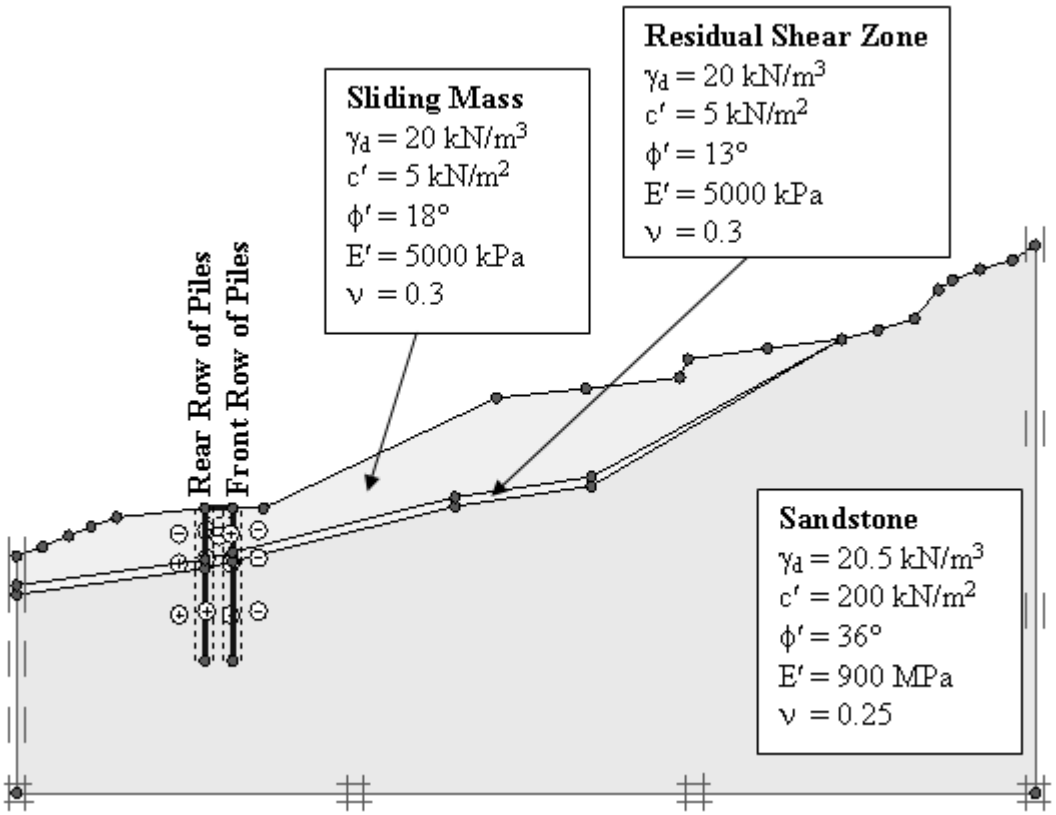

Figure 8.4 Finite element soil model.

The piled retaining system was designed as double-row 49 cast-in-place reinforced concrete piles. The total pile length is 15 m with a diameter of 120 cm. Pile rows were connected with an 80 cm thick rigid pile cap. Center to center pile spacing in a row was arranged as 2.4m (S = 2B). The distance between the pile rows, on the other hand, was 3.15 m. Computed bending moments for each pile rows in plain strain FE analyses were adjusted to account for the pile spacing and structural design of the piles to carry the maximum bending moment (~1900 kNm) were finalized as 32Φ26 bending reinforcements with 10Φ10 spirals. The maximum pile head deflection of the system was calculated as 3.5 mm. The embedment length necessary to provide the passive resistance in the base rock was computed as 8.0 m. A ground water drainage system consisting of 12 drilled drains each 20 m long and parallel to the base rock in two rows was also designed to prevent pore water pressure accumulation during rainy seasons. The center to center spacing between individual drains was set as 4.8 m. Cross section view of the designed piled retaining system is given in Figure 8.5.

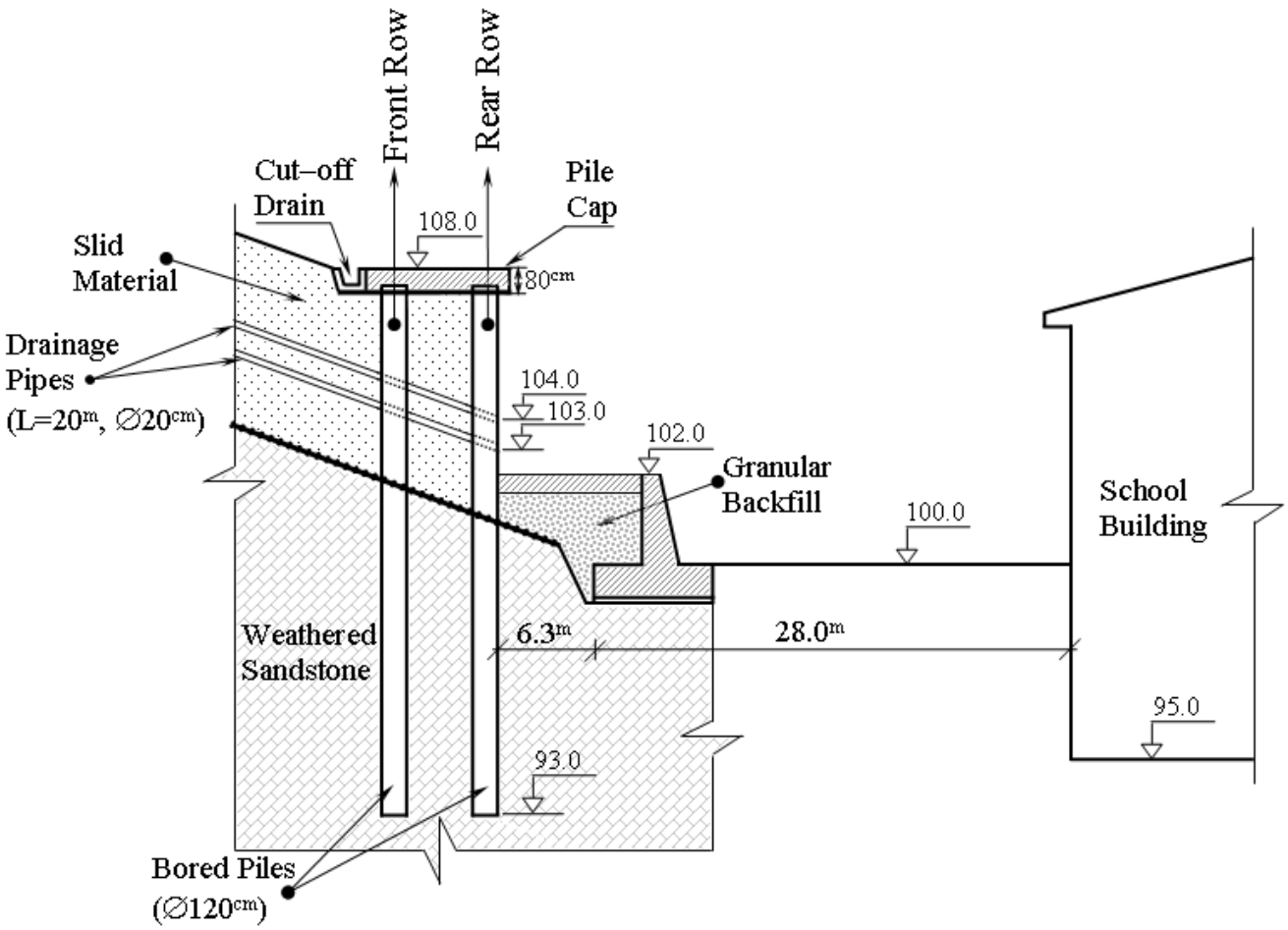

Figure 8.5 Cross section view of the piled retaining system.

8.2.1 Inclinometer Monitoring

In order to assess the performance of the system under service loads, four piles were instrumented by means of inclinometer casings. The inclinometer data were then utilized in back analyses of the piled retaining system. It happened that some of the piles were constructed shorter than their projected length due to insufficient drilling capacity of the piling equipment.

Pile deformations that would take place following removal of the debris material in front of the retaining system were measured by means of the above mentioned inclinometers installed at the center of the pile shafts (Pile#9, Pile#19, Pile#27 and Pile#38 in Figure 8.6). The inclinometer casings, each 100mm in diameter, were socketed 5m into the bedrock.

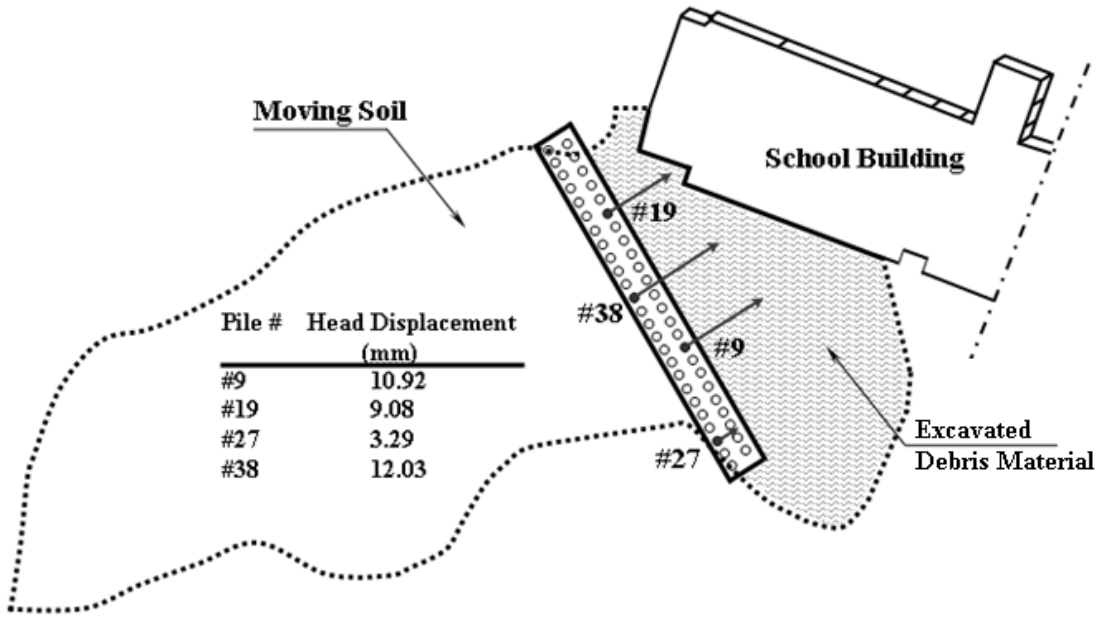

Figure 8.6 Pile head deformations following the removal of debris material.

Initial inclinometer readings were recorded immediately following completion of the retaining system. Subsequent readings upon the removal of the debris in front of the piles were taken during a 5 months long rainy season. The cumulative inclinometer data are plotted in Figure 8.7.

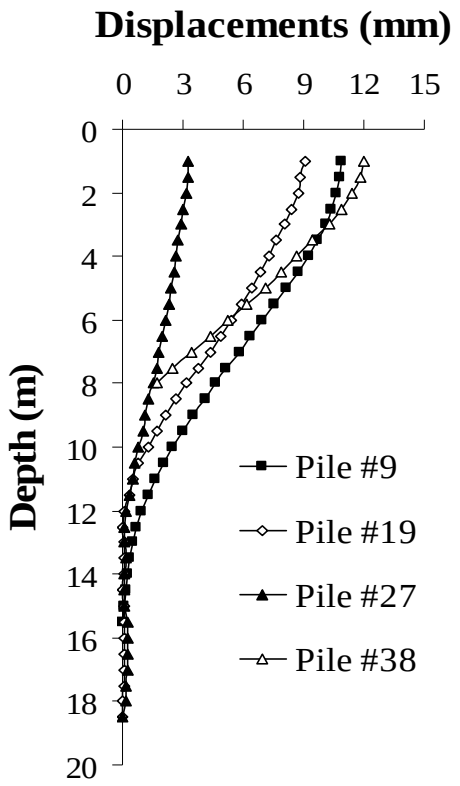

Figure 8.7 Cumulative displacement graphics.

The maximum pile head deflection of the system was measured as 12 mm which was larger than the predicted maximum from the design analysis (3.5 mm). One can notice that the measured head displacements of each pile were different in spite of rigid pile cap effect. The inclinometer readings demonstrated the displacement of pile tips inferring insufficient constructed pile socket length. These results revealed a necessity of back analyses of the constructed system.

8.3 Three Dimensional Back Analysis of the System Performance

Constructed piled retaining system was back analyzed by means of three dimensional finite element models. In this respect, two different models were established. One of the models targeted structural analysis of the double row system where soil pressure due to the sliding soil was applied to the piles at finite element nodes. The subgrade to the piles was modeled by means of equivalent soil-pile

springs. The second FEM model, on the other hand, included three dimensional finite elements in order to account for the surrounding soil. The results of 3D analyses were utilized in order to explain discrepancies between the inclinometer data and pile displacements obtained in structural finite element analyses.

8.3.1 Structural Finite Element Analyses

Three dimensional structural FE analysis utilizing SAP2000® was performed to determine the constructed system performance. Soil pressures that would act on the piles of the structural model were defined using Ito-Matsui (1975) and DeBeer-Carpentier (1977) approaches after they were adjusted by multipliers obtained from plain strain finite element analyses in order to account for the double row piled system. One should note that Ito-Matsui and DeBeer-Carpentier formulations were originally developed for single pile rows. The plain strain finite element analyses established to determine the multipliers are explained in the proceeding paragraphs. The soil-pile springs in pile sockets were determined by making use of inclinometer data in order to obtain the field pile displacements so that corresponding equivalent subgrade moduli could be assigned based on p-y curves for weak rock available in the literature (Reese, 1985) (Appendix F). The three dimensional structural FE model of the constructed system is given in Figure 8.8.

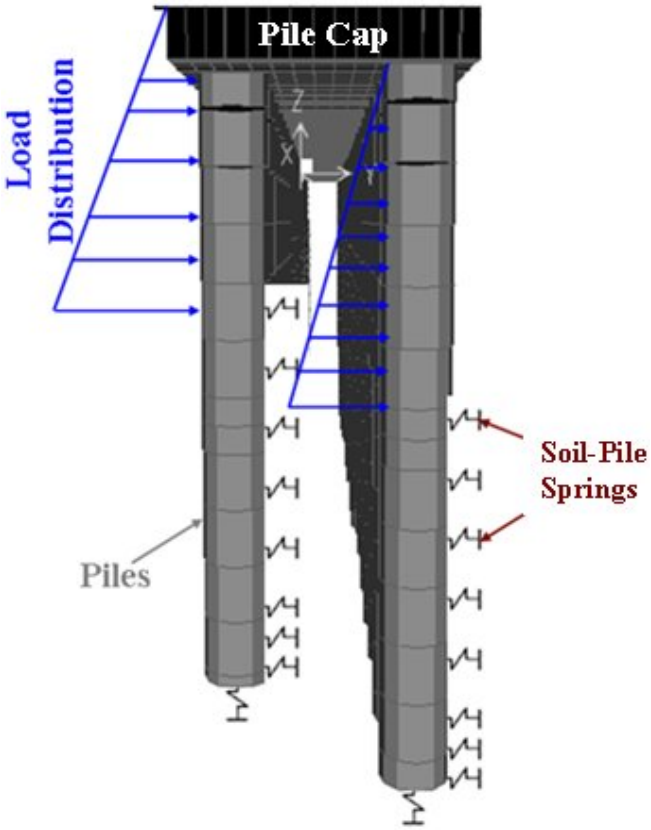

Figure 8.8 Three dimensional structural FE model of the constructed system.

8.3.1.1 Estimation of Lateral Load Distribution

The magnitude and distribution of the load transferred from the moving soil to the resisting piles should depend on the relative movement between the soil and the pile as well as the pile geometry and disposition. Existing theories regarding the soil pressure acting on the passive piles focus on the influence of limit state soil strength characteristics, arching as a function of the pile disposition (i.e. center-to-center pile spacing), and principal stresses acting on the moving soil wedge through the piles (Ito and Matsui, 1975; DeBeer and Carpentier, 1977).

Previous studies that were based on field observations and measurements targeted influence of several factors such as pile spacing, fixity condition of the pile head, pile length above the sliding surface, and pile diameter on the factor of safety against

sliding (Ito and Matsui, 1979; Ito et al., 1981). Soil pressures measured during laboratory tests on small scale pile models agreed with the theory to some extent. It was stated that the ultimate lateral pressure from the theory of Matsui should be factored by 1.6 in order to match the test data (Matsui et al., 1982). Field evidence based on full scale passive piles, however, are rare in the literature.

DeBeer and Carpentier proposed some modifications to the theory of Ito and Matsui by taking into consideration variations in the principal stress directions as a function of soil characteristics and pile spacing. According to DeBeer and Carpentier, loads imposed by sliding cohesionless soils are considerably smaller than those estimated by the Ito-Matsui theory. The difference between the two methods is not significant for cohesive soils.

Current theories assume that piles are rigid and the soil above the sliding surface reaches a plastic state only just around the piles. In such a case these assumptions do not hold, that is, the effect of pile deformation is considerable; the measured lateral force differs from the theoretical value due to arching effect. Existing methods, however, were originally developed for single pile rows without taking into consideration influence of relative soil-pile movement on arching mechanism.

Inclinometer readings revealed that pile deformations at four different locations of the double row piled retaining system varied considerably. Although pile heads were connected by means of a rigid pile cap, deformations decreased towards the sides of the piled retaining system, reminding that thickness and plan geometry of the sliding mass could be effective on the measured deformations. A rather comprehensive plain strain finite element analysis program was pursued in order to investigate influence of relative movements of the piles with respect to each other and to the sliding soil mass. The finite element model established in this study was similar to those of Liang and Zeng (2002) with the exception that limited pile movements of the double row piled retaining system in the direction of soil movement could be accounted for

by means of fixed-end anchors of which axial rigidity could be adjusted to yield measured pile head displacements.

The typical FEM model representing pile rows is shown in Figure 8.9 with the assigned boundary conditions (i.e. constrained in the lateral axis and free to deform along the vertical axis). Fixed-end anchors served as deformation constraints. Applied stress at the top of the model forced the soil to displace through the pile rows. The elastic soil with a low deformation modulus provided the displacement constraint along the direction of the soil movement. The dimension of the model parallel to the direction of the soil displacement was decided upon several trials until boundary effects became negligible on the obtained results.

The soil behavior was simulated by an elastic perfectly-plastic model with Mohr-Coulomb yield criterion while the piles were modeled using non-porous linear elastic material. The piles and the surrounding soil were discretized using a fine mesh near the piles. The mesh consisted of 1380 triangular elements with fifteen nodes. The soil-pile interface strength parameter is set to two-thirds of the corresponding soil strength parameter by means of the interface parameter (R_{inter}) so that strength reduction due to slippage of the soil around the pile is taken into consideration.

The loads acting on the front and the rear rows were determined as 56% and 44% of the applied load (P), respectively. Anchor rigidity values representing equivalent stiffness of the front and rear pile rows were set to 150P for both rows as a result of several FEM trials until displacements of the piles matched measured pile head displacements. It appears that lateral soil pressure estimated using Ito-Matsui and DeBeer-Carpentier approaches, may be adjusted by 0.56 for the front piles and 0.44 for rear piles.

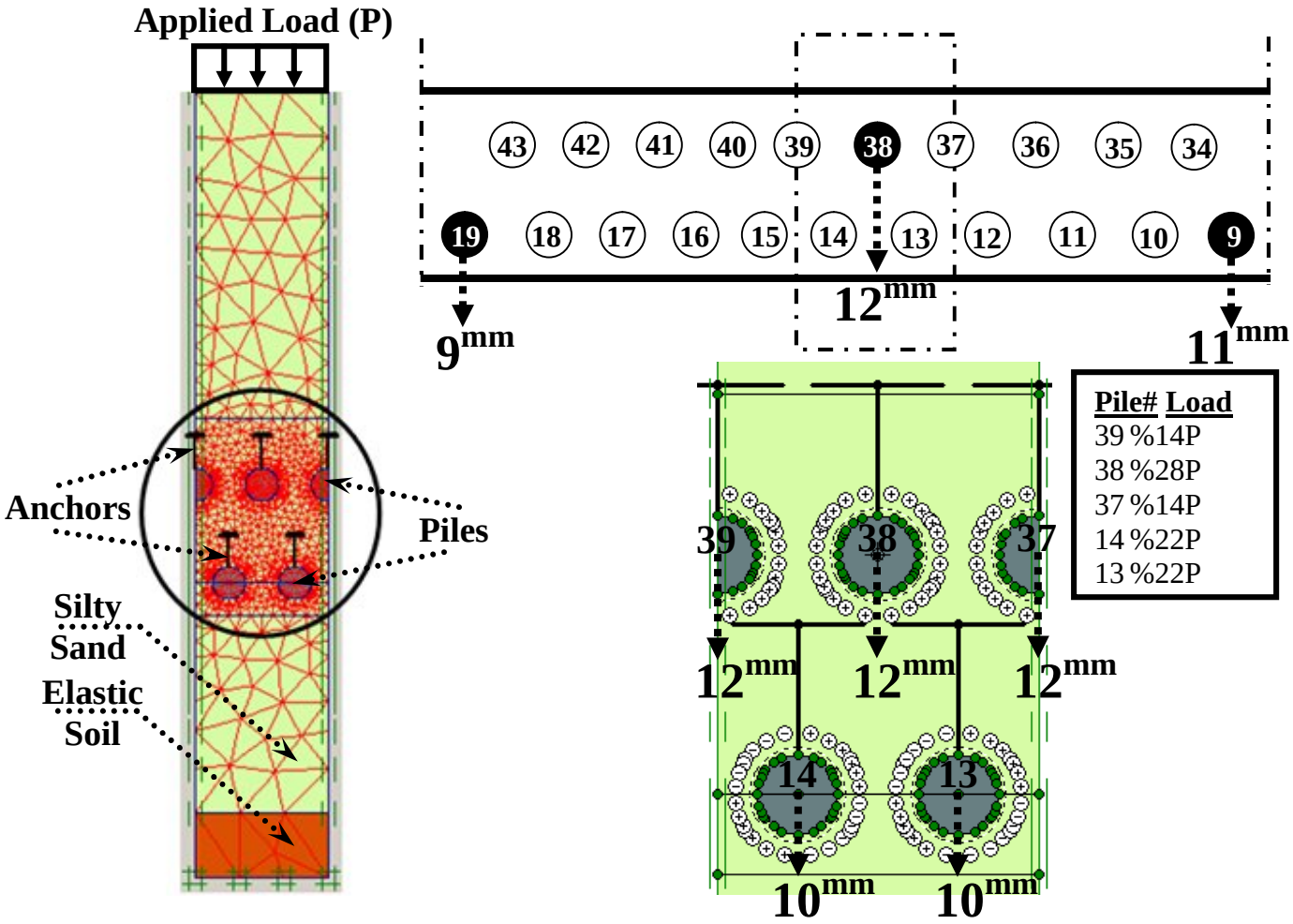

Figure 8.9 Finite element model representing moving soil and pile rows.

8.3.1.2 Structural Analysis Results

Computed displacements in structural FE analyses and measured displacements by inclinometer for Piles #9, #19, #27 and #38 are plotted in Figure 8.10. It is interesting to note that computed displacements of piles #19 and #38 according to soil pressure distribution by Ito-Matsui are in relatively good agreement with inclinometer readings. The displacement of pile #27 is better predicted according to De Beer. However, the displacement of pile #9 from both theories is much smaller than the inclinometer readings along the pile length.

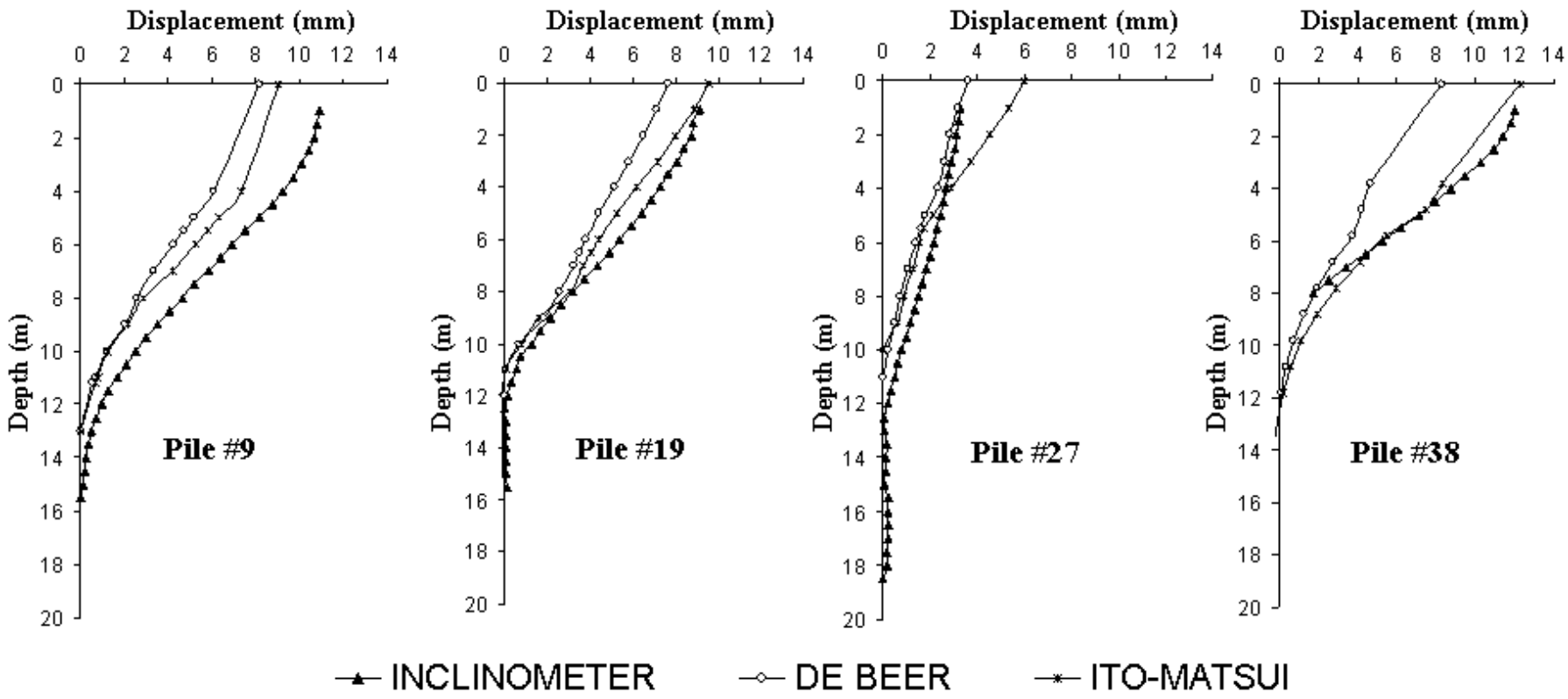

Figure 8.10 Measured and calculated displacements of piles #9, #19, #27, #38.

8.3.2 Full 3D Finite Element Analyses (Plaxis 3D)

It is quite possible, depending on the border conditions of the problem that larger pressures exist, and therefore, depending on these conditions the action on a rigid single pile can be larger than the values deduced from the theories. In order to investigate the reason of the difference between the theoretical and real loads acting on the piles, 3D numerical analyses for the constructed piled retaining system were examined using Plaxis program. The parameters used in FEM analysis were taken directly from the real case. In order to simulate a landslide mechanism, a soil boundary (horizontal line fixities), which enables displacements in the horizontal direction were used in the soil surface. A typical model with the assigned boundary conditions (i.e. constrained in the lateral axis and frees to deform along the vertical axis) of the FE simulation is shown in Figure 8.11.

Due to the bowl shaped landslide geometry, shear force (Q_{13}) is generated perpendicular to the direction of sliding. This shear force restricted the pile deformation and the pile with less displacement is subjected to more shear force in the direction of sliding (Q_{12}). The third dimension effect on the load acting on pile is shown in Figure 8.12. Due to the high shear force perpendicular to the sliding direction, pile is subjected to more load than the expected load.

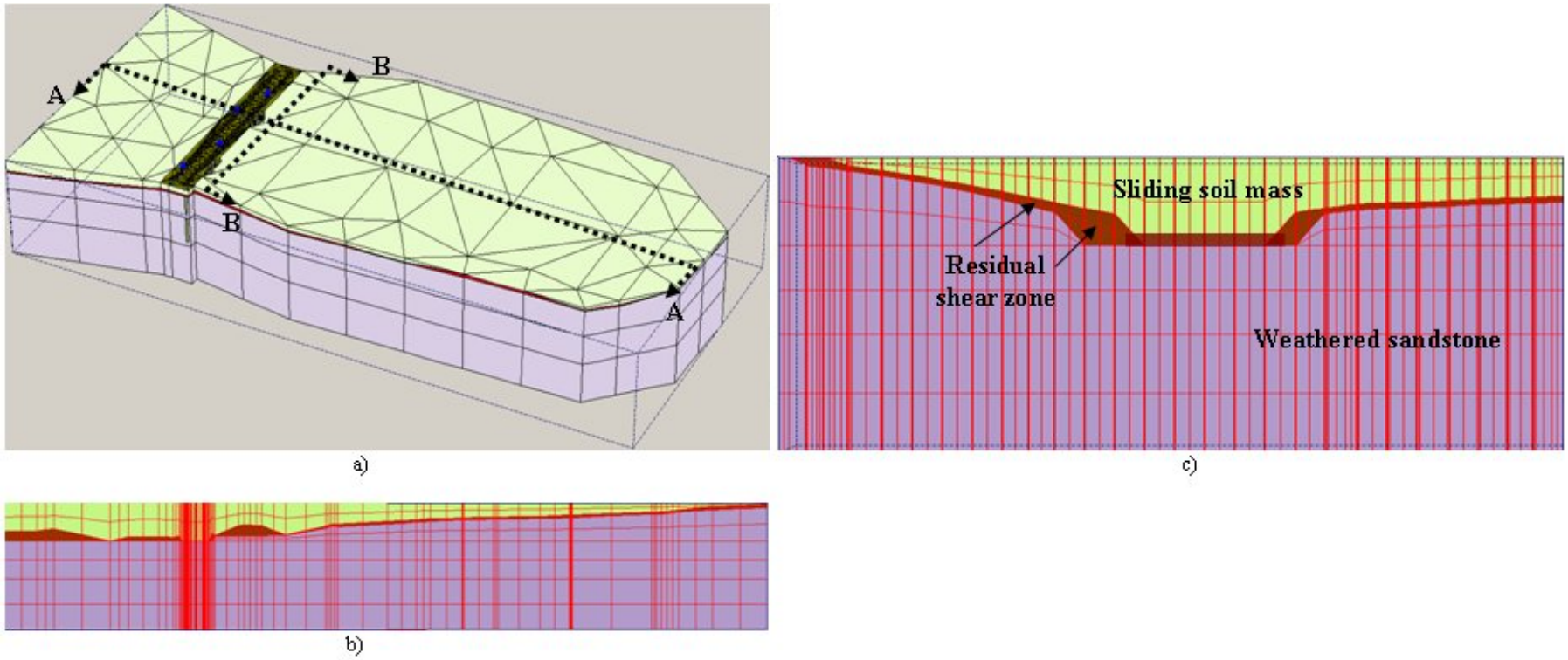

Figure 8.11 3D Model of the FE simulation: a) 3D Model with boundary conditions b) A-A section of the model c) B-B section of the model

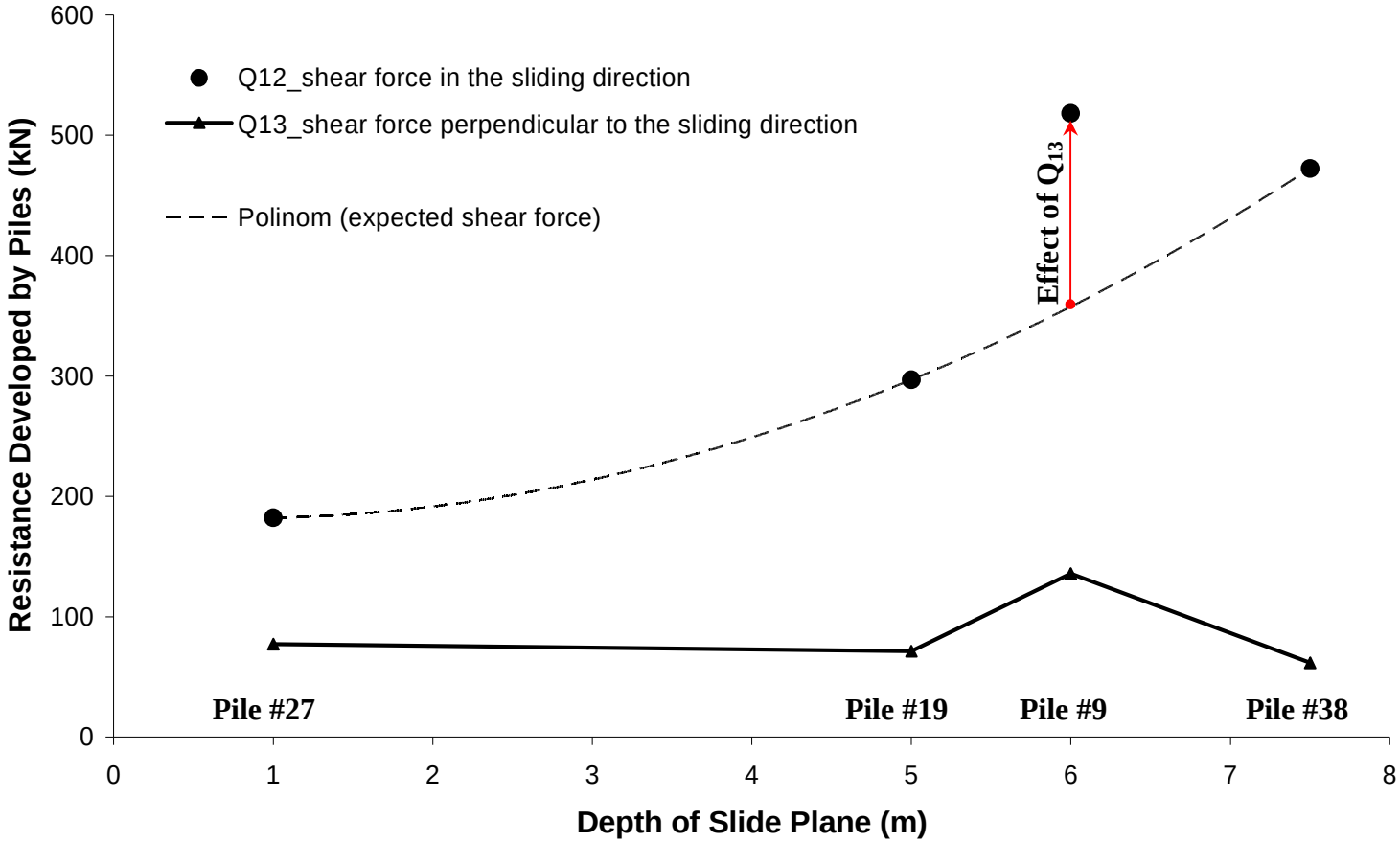

Figure 8.12 Predicted shear forces of piles #9, #19, #27, #38.

Deep sliding mass in the middle on account of bowl shaped landslide compels the middle pile to act as flexible pile, while the pile on the corner behaves as rigid due to shallow sliding mass. Middle flexible piles displaced more than the corner rigid piles and they transferred their loads to the corner piles owing to arching mechanism. So, corner rigid piles were subjected to more soil pressure, therefore more moment and shear force. According to the results of 3D Plaxis analyses, the influence of depth of the sliding plane becomes more marked as the pile length increases and there appears to be an optimum depth at which the pile resistance developed is a maximum. For shallow depths of sliding, pile resistance is independent of pile length since the dominant mechanism is flow of soil past the piles. However, for large sliding depths the resistance developed by pile increases significantly as the length of the pile increases.

The inclinometer readings demonstrated the displacement of pile tips. These pile tip displacement values could not be estimated by the design analysis due to the prediction of high deformation modulus of weathered sandstone (E=900 MPa). In the full 3D Plaxis analyses, the deformation modulus of weathered sandstone was varied between 600 and 1000 MPa. The deformation modulus of weathered sandstone was adjusted as 770 MPa in order to achieve the measured pile displacements. Calculated displacements by full 3D FE analyses with different deformation modulus of weathered sandstone and measured displacements by inclinometer for Piles #9, #19, #27 and #38 are plotted in Figure 8.13.

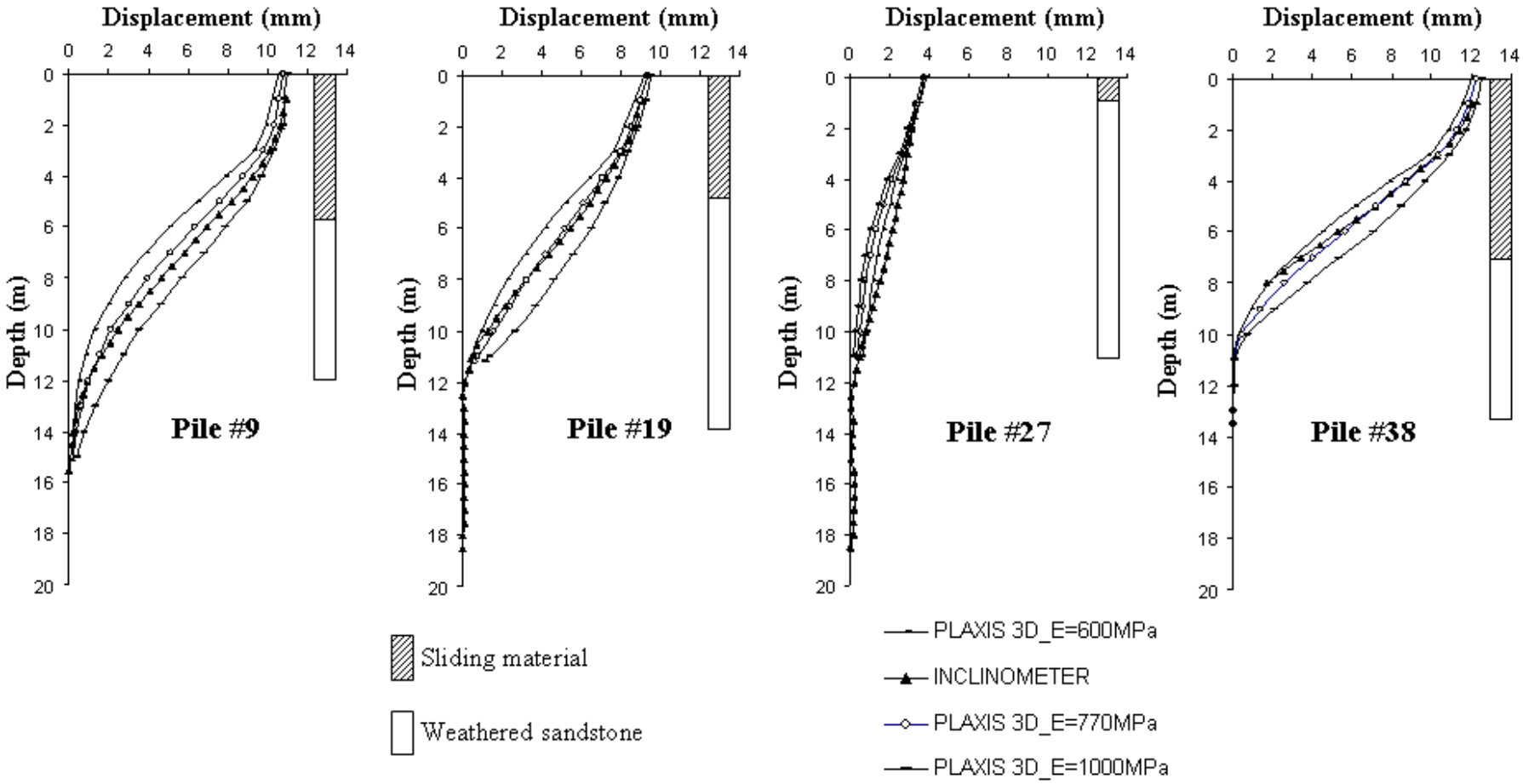

Figure 8.13 Measured and calculated displacements of piles #9, #19, #27, #38.

8.4 Determinations from Back Analyses

This study involves the investigation of the landslide mechanism, preparation of remediation project with stabilizing piles, three dimensional back analyses of the constructed piled retaining system including inclinometer data evaluations and determination of load distribution.

Soil pressures that would act on the piles of the structural model were defined using Ito-Matsui (1975) and DeBeer-Carpentier (1977) approaches after they are adjusted by multipliers obtained from plain strain finite element analyses considering arching effect and relative movement of the front and rear pile rows in order to account for the double row piled system. The results showed that load transfer mechanism is not only the function of soil properties and pile spacing, but also the function of relative pile/soil displacement and the rigidity of the pile. It is revealed that relative movement of the front and rear pile rows has a significant influence on load share.

It is interesting to note that the head displacements of piles #19 and #38 are approximately predicted with Ito-Matsui theory and the head displacement of pile #27 is predicted with De Beer theory. However, the head displacement of pile #9 from theories is much smaller in magnitude than measured from the inclinometer due to the bowl shaped landslide geometry; shear force (Q_{13}) is generated perpendicular to the direction of sliding. This shear force restricted the pile deformation and the pile with less displacement is subjected to more shear force in the direction of sliding (Q_{12}). Pile is subjected to more load than the expected load owing to the high shear force perpendicular to the sliding direction (the third dimension effect).

The inclinometer readings demonstrated the displacement of pile tips inferring insufficient constructed pile socket length. These pile tip displacement values could not be estimated by the design analysis due to the prediction of high deformation modulus of weathered sandstone (E=900 MPa). In the full 3D Plaxis analyses, the deformation modulus of weathered sandstone was determined as 770 MPa.

CHAPTER NINE
SUMMARY AND CONCLUSIONS

The objective of this research is to evaluate the load transfer from the sliding soil to the slope stabilizing piles as a function of soil type, pile spacing, pile bending stiffness, and the pile head fixity condition. The work described in this dissertation was divided into three tasks.

In the first task of the research, the complex interaction between piles and surrounding soil in piled-slope problems using 3D finite element method (FEM) models has been investigated. The effects of pile spacing, pile-soil interface roughness, pile arrangement and relative displacement between the pile and soil on the lateral loads acting on piles in a row were studied. At first, the problems associated with the displacement effects of embankments sliding on a weak soil on passive piles were examined with a finite number of piles. Then, the slope stabilizing pile case was simulated with a slice from infinitely long row of piles. The load acting on the piles and group behavior of the piles in two different passive pile cases were determined by making use of the numerical results. In using pile loads or moments for evaluating the group effect on the lateral pile response, a group factor is introduced which compares the load or moment acting on a pile from a pile group test with those of the single pile test at the same amount of soil displacement. The load acting on pile and group factors are given in Figure 9.1 and Table 9.1, respectively.

With an increase of the pile spacing, s, the loads acting on the piles increase for the case of piles adjacent to embankments, whereas for the case of piles used to stabilize slopes, the load acting on the piles decreases. However, for s>8d, each pile behaves like a single pile without arching effect for both two passive pile cases. The group factor is also influenced by the pile spacing. Parallel to a decrease in pile spacing, group factor values decrease for piles adjacent to embankments and increase for piles used for slope stabilization.

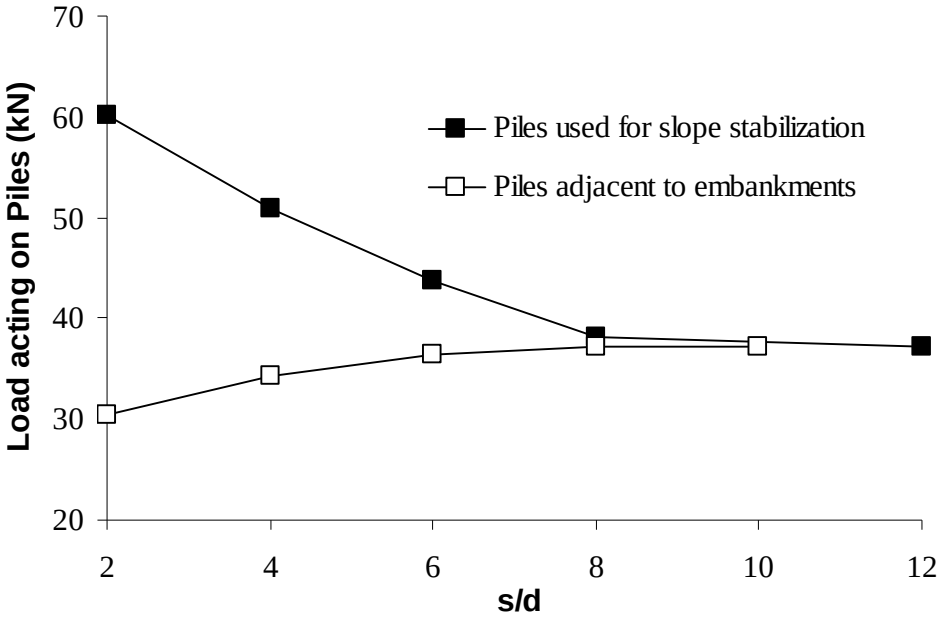

Figure 9.1 Load acting on piles from FEM analyses for two different passive pile cases.

Table 9.1 The effect of pile spacing variation on group factors as obtained from FEM analyses

s / d	**Finite Number of Piles**		**A slice from infinitely long row of piles**	
	F_L	**F_M**	**F_L**	**F_M**
12	-	-	1.00	1.00
10	1.00	1.00	-	-
8	1.00	1.00	1.02	1.01
6	0.98	0.98	1.08	1.07
4	0.93	0.91	1.17	1.15
2	0.82	0.83	1.72	1.70

In the second task of the research, an experimental testing apparatus was specially designed and manufactured for investigating the pile spacing and pile rigidity effect on soil arching, the lateral soil pressure and moment acting on piles, and behavior of soil around piles. In this experiment, a slice of infinitely long row of piles installed in an inclined sand bed, which were subjected to sliding soil mass, was simulated. The experimental apparatus consisted of a box in which model tests are performed, a pluviation system to prepare homogeneous and uniform loose sand bed, aluminum model piles, load measurement, deformation measurement and data acquisition

systems. The apparatus enables both flexible and rigid pile tests with fixed pile tip for various pile spacings. The movement of soil due to the box displacement was controlled by an automatically operated support to facilitate the soil slid under its own weight. Pile spacing, slope angle, pile rigidity and pile head fixity condition were chosen as variables in one and two rows of pile tests to provide experimental data for a better understanding of the load transfer process. The soil surface displacements were also monitored and evaluated via digital image analysis techniques in order to observe the trace of the soil arching mechanism on the soil surface. Relative displacements between the soil particles were determined by recording time-lapse images throughout the test. The load transfer process between the moving soil and piles and the behavior of soil around piles were observed and evaluated throughout the tests.

It has been observed that the response of a passive pile is significantly influenced by the magnitude of the soil movement. The pile deflection, shear force and bending moment values increase with the increase of soil movement. When the soil movement reaches a certain value, the acting loads reach an ultimate value and remain constant as the soil movement continues to increase. The results indicate that this ultimate value is reached at $\Delta/d=1.05$ in 10° slope angle series, and $\Delta/d=1.15$ in 20° slope angle series. The ultimate group factor values (F_L and F_M) of flexible and rigid piles are summarized in Table 9.2.

Table 9.2 Group factors of all test series of rigid and flexible piles

s / d	**Flexible Piles**				**Rigid Piles**	
	10° slope angle		**20° slope angle**		**20° slope angle**	
	F_L	**F_M**	**F_L**	**F_M**	**F_L**	**F_M**
24	1.00	1.00	1.00	1.00	1.00	1.00
12	1.04	1.03	1.04	1.04	1.03	1.04
8	1.11	1.11	1.15	1.11	1.12	1.13
6	1.22	1.21	1.26	1.20	1.22	1.21
4	-	-	1.50	1.42	1.44	1.42
3	-	-	-	-	-	-
2	-	-	-	-	-	-

It can also be concluded that the load and the bending moment acting on a pile increases with a decrease of pile spacing. This behavior can only be explained by soil arching between the piles along the box depth. The group factor values tend to increase up to 6 mm soil displacement for all s/d ratios considered, then decrease up to a 21~23 mm displacement and become constant thereafter. It is interesting to note that the slope angle and pile rigidity have very little effects on group factors.

Soil pressure distribution along the length of free head piles has been obtained from measured bending moments for the ultimate state. Pile head movement exceeds the soil movement, resulting in negative pressure on free head flexible piles over a certain depth approximately 20% of the sliding soil thickness. Below this depth, positive pressure occurs up to approximately 80% of the sliding soil thickness, and below this depth negative pressure starts to develop. The determined maximum negative pressure is nearly three fold maximum positive pressure. The soil pressure is increased with a decrease of pile spacing. The soil pressure profiles are very similar in shape in both 10° and 20° slope angle series. However, for s>12d, each pile behaves like a single pile.

For the case of free head pile, the response of the passive pile is significantly influenced by the pile stiffness. For a pile with free head and fixed tip conditions, the load carried by piles, bending moment and soil pressure on pile are increased with the increase of pile stiffness. Rigid piles carry nearly 1.8 times the load carried by the flexible piles. The moment acting on rigid piles is ~1.8 times higher than that on flexible piles. It is interesting to note that in the case, where no head restraint is provided, the movement of the top of a rigid pile is substantially greater than the surficial soil movement, so that negative pressure occurs over a certain depth like in flexible piles. The magnitude of negative pressure is larger than flexible piles. Decrease in pile spacing causes negative pressure to increase. Surficial displacements of soil particles surrounding the piles also increase with a decrease in pile spacing

The behavior of the passive piles is significantly influenced by the pile head boundary conditions. The provision of the head restraint reduces the pile movements

near the surface. The fixed head condition results in the smallest bending moment in the piles. The maximum bending moment in free head piles is about two times that in fixed head piles. The determined pressures on the piles show that the reaction force is almost the same for flexible and rigid piles when the pile head is fixed. The bending moment profile of both rigid and flexible piles with s/d=4 in 20° slope angle are shown in Figures 9.2.

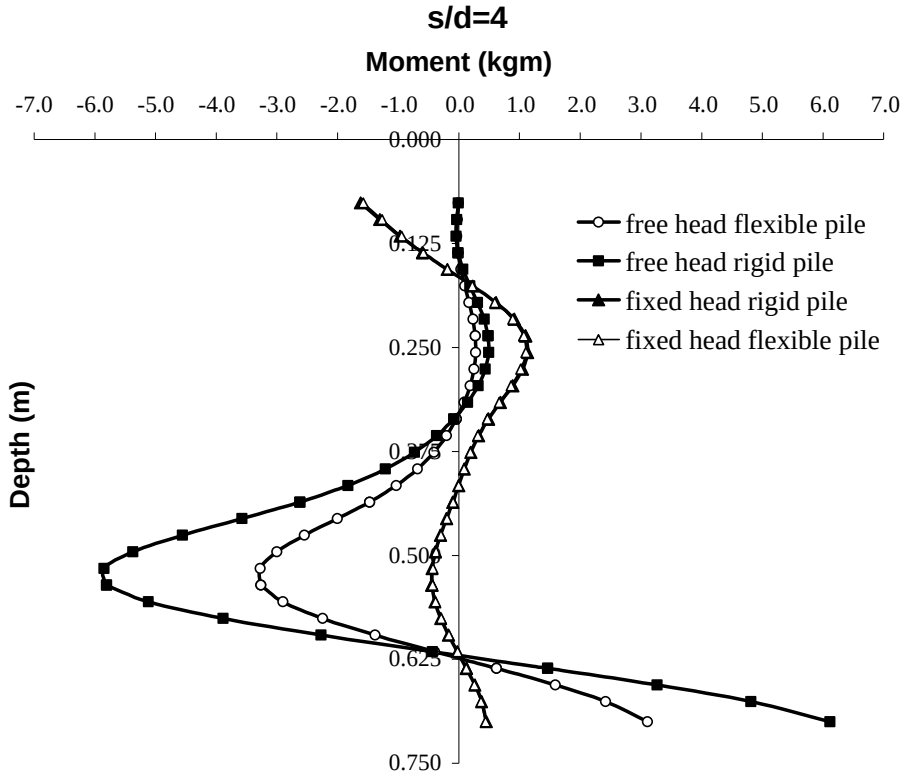

Figure 9.2 Moment profiles of rigid and flexible piles in 20° slope angle

For the case of fixed head pile, piles resist against sliding and reduce the surficial soil displacements in contrast to the case of free head piles. Therefore, soil particles in the pile affected zone have less surficial displacements than the box displacement. Paths resembling arches can be established by connecting the soil particles having the same minimum surficial displacements. The surficial displacement of soil particles located over the developed arches increased towards the upslope direction, similarly that below the arches increased towards the downslope direction. This displacement behavior of soil particles are the evidence of the existence of soil arching mechanism on the soil surface.

For the case of two rows of flexible piles in parallel arrangement, the moments acting on the front row of piles and the moments acting on the rear row of piles were found to be approximately the same, while for rigid piles in parallel arrangement, the moments on front piles were 3 times the moments on rear piles. Pile moments determined in the zigzag arrangement are approximately 5% higher than in parallel arrangement. Therefore, multi soil arching effects for a zigzag arrangement of piles provide more restraint to soil movement. The experimental results also show that load transfer mechanism is not only the function of spacing and rigidity of the pile, but also the function of relative movement of the front and rear pile rows. It is shown that relative movement of pile rows has a significant influence on the load share.

Finally, a case study has been carried out where double-rows of passive piles were used to stabilize sliding soil mass was back analyzed by means of three dimensional finite element models with an emphasis on the influence of arching mechanism on the transfer and distribution of the soil load between the front and rear pile rows. In this respect, two different models were established. One of the models targeted structural analysis of the double row system whereas the second one was a full three dimensional model including piles and the surrounding soil. Measured displacements of the piled retaining system were also compared with the back calculated displacements. In the light of back analyses, the loads acting on pile rows, considering the loads calculated by theories based on plastic deformation have been determined and the importance of pile socket length and third dimension effects have been decided.

The records of four inclinometer readings have shown that the measured head displacements of each pile were different in spite of rigid pile cap effect. Due to the bowl shaped landslide geometry; inner piles displace more than the outer piles and the inner piles transfer their loads to the outer piles owing to arching mechanism. Soil pressures that would act on the piles can be defined using Ito-Matsui (1975) and DeBeer-Carpentier (1977) approaches after they are adjusted by multipliers obtained from plain strain finite element analyses considering arching effect and relative

movement of the front and rear pile rows. Soil pressures measured during laboratory tests agreed with the multipliers to some extent (Table 9.3).

Table 9.2 Determined load sharing values for piles in zigzag arrangement

Zigzag Arrangement	**Load sharing value**		
	Laboratory tests		**2D FEM Analyses**
	Flexible Piles	**Rigid Piles**	
Front row	0.51	0.70	0.56
Rear row	0.49	0.30	0.44

It is interesting to note that computed displacements of three piles according to soil pressure distributions adjusted by multipliers are in relatively good agreement with inclinometer readings. However, the displacement of one pile is much smaller than the inclinometer readings along the pile length.

The results of full three dimensional model revealed the difference between the theoretical and real loads acting on the piles. Pile is subjected to more load than the expected load due to shear force perpendicular to the direction of sliding (the third dimension effect). This shear force restricted the pile deformation and the pile with less displacement is subjected to more soil load in the direction of sliding. For the outer piles subjected to shallow depths of sliding, pile resistance is independent of pile length since the dominant mechanism is flow of soil past the piles. However, for inner piles subjected to large sliding depths, the resistance developed by pile increases significantly as the length of the pile increases.

As a conclusion, a restrained pile head is recommended, and the free head condition should be avoided due to the generation of higher bending moments. A restrained head condition can be obtained by connecting the pile heads with a buried beam, which is fixed by the tie-rods or tension anchors. If the restrained head condition cannot be provided, the bending stiffness should be increased.

RECOMMENDATIONS FOR FUTURE WORK

From the knowledge gained from the study of slope stabilizing piles, the following fields are suggested for future work to investigate further the load transfer mechanism in piled-slope problems:

1. It is postulated that the moving soil due to its own weight in piled-reinforced slopes would have a significant effect on the axial and lateral load response of piles but additional analyses are need to confirm this.
2. Since relative displacements between the pile and soil are important to predict the limit and mobilized load on piles, it is important to consider the different flexibility factors of the piles in future analyses. In addition, soil with varying stiffness with depth should also be considered.
3. An extensive study of the effect of the various boundary conditions (hinged and unrotated) on potential arching mechanism around a pile cap due to moving surrounding soil should help to clarify the stress transfer mechanism.
4. The effects of multiple rows of piles in both vertical and inclined orientations of piles should be considered.
5. A study of pile response analyses can be extended to piles under cyclic loading.

This study has been performed with small-diameter pile elements as a feasible slope stabilization alternative. Immediate recommendations for future research include the construction and monitoring of pilot projects. Implementation of slope reinforcement through pilot studies, which will help us more fully understand and verify the load transfer mechanisms of the stabilization system, is the next most important task for improving the slope remediation alternative. Future research may also include supplementary experimental testing to address the influences of pile orientation and truncation, and advanced numerical studies to address the influences of interactions between adjacent piles.

REFERENCES

Abbot, P. A. (1967). Arching for vertically buried prismatic structures. *JSMFD, ASCE, 93 (5),* 233-255.

Adachi, T., Kimura, M., & Tada, S. (1989). Analysis on the preventive mechanism of landslide stabilizing piles. *Third International Symposium on Numerical Models in Geomechanics*, 691–698.

Adalıer, K. (1992). *Post-Liquefaction behavior of soil systems.* Ms Thesis. Rensselaer Polytechnic Institute. Troy, N.Y.

Adams, J. I., & Radhakrishna, H. S. (1973). The lateral capacity of deep augured footings. *Proc., 8th Int. Conf. Soil Mechanics Foundation Engineering*, Moscow, Russia, 2, 1–8.

Allgood, J. R. (1971). Structures in soil under high loads. *JSMFD, ASCE, 97 (3),* 569-575.

Allison, J. A., Mawditt, J. M., & Williams, G. T. (1991). The use of bored piles and counterfort drains to stabilize a major landslip - a comparison of theoretical and field performance. *International Conf. on Slope Stability*, Isle of Wight, England, Apr. 15-18, 1991, 369-376.

Almeida, V. S., & Paiva, J. B. (2000). Improvements to classical preconditioners in finite element problems. *5th International Conference on Computational Structures Technology/2nd International Conference on Engineering Computational Technology,* Leuven, Belgium, Sep. 06-08, 2000, 43-49.

Analay, B. (1999). *Lateral resistance of a rigid socketed single model pile, fixed at head, in a cohesionless soil.* M.Sc. Thesis in Civil Engineering, Middle East Technical University, Ankara, Turkey.

Anderson, A. H. (1976). Earth retention by drilled reinforced concrete caissons. *Civil Engineering, ASCE, 46 (3),* 54-56.

Andrews, G. H., & Klassell, J. A. (1964). Cylinder pile retaining wall. *HighwayResearch Record,* 56, 83-97.

ASTM Standard A370 (2009) "Standard Test Methods and Definitions for Mechanical Testing of Steel Products," ASTM International, West Conshohocken, PA, 2009, DOI: 10.1520/A0370-09AE01.

Atkinson, J. H., & Potts, D. M. (1977). Stability of a shallow circular tunnel in cohesionless soil. *Geotechnique, 27 (2),* 203-215.

Baguelin, F., Frank, R., & Said, Y. H. (1977). Theoretical study of lateral reaction mechanism of piles. *Geotechnique, 27(3),* 405-434.

Baker, R. F., & Yonder, E. J. (1958). Stability analysis and density control works in landslides and engineering practice. *E.B. Eckel, Ed. Highway Research Board Special Report29,* 189-216.

Banerjee, P. K., & Davies, T. G. (1978). The behavior of axially and laterally loaded single piles embedded in non-homogeneous soil. *Geotechnique, 28 (3),* 309–326.

Barradas, J., & Correia, R. (1995). Numerical and physical modeling of slope soil nailing. *The Interplay between Geotechnical Engineering and Engineering Geology*, Copenhagen, 4, 4.13-4.18.

Başaran, S. (1997). *A model study of laterally loaded piles in sand*. M.Sc.Thesis in Civil Engineering, Middle East Technical University, Ankara, Turkey.

Bierschwale, M., Coyle, H., & Bartowkewitz, R. (1981). Lateral load tests on drilled shafts founded in clay. *Drilled Piers Caissons, ASCE*, 98–113.

Biinagte, J. L., Van Den Berg, P., Zorn, N. F., & Dieterman, H. A. (1991). *Laterally loaded single piles in soft soil-theory and reality*. HERON, 36 (1), Jointly edited by STEVIN Laboratory of the Faculty of Civil Engineering, Delft University of Technology, Delft, and TNO Building and Construction Research, Rijswijk, the Netherlands, 78 pp.

Bishop, A. W. (1955). The use of slip circle in the stability analysis of earth slopes. *Geotechnique, 5 (1),* 7–17.

Bogart, D., & Matlock, H. (1983). Procedures for analysis of laterally loaded pile group in soft clay. *Proc. Conf. on Geotech. Practice in Offshore Engrg.*, ASCE, New York, N.Y.

Borms, B. B. (1969). Stability of natural slopes and embankment foundations. *Proc. 7th ICSMFE,* Mexico, 3, 385-394.

Bosscher, P. J., & Gray, D. H. (1986). Soil arching in sandy slopes. *Journal of Geotechnical Engineering, 112 (6),* 626-645.

Bowles, J. (1996). *Foundation analysis and design.* Fifth edition, the McGraw-Hill Companies, Inc., New York.

Bransby, M. F., & Springman, S. (1999). Selection of load-transfer functions for passive lateral loading of pile groups. *Computers and Geotechnics, 24,* 155-184.

Briaud, J. L., & Smith, T. D. (1983). Using the pressuremeter curve to design laterally loaded piles. *Proc., 15th Offshore Technology Conf.,* Houston, USA, Paper 4501, 495-502.

Brinch Hansen, J. (1961). The ultimate resistance of rigid piles against transversal forces. *Danish Geotechnical Institute Bulletin,* Copenhagen, Denmark, 12, 5-9.

Brinkgreve, R. B. J., Vermeer, P. A. (2001). Finite element code for soil and rock analyses, Version 8.2. Balkema Printers, Rotterdam, Netherlands.

Brinkgreve, R. B. J., & Broere W. (2006). *Plaxis 3D Foundation Manual*, Delft University of Technology & PLAXIS bv, The Netherlands.

Broms, B. B. (1964). Lateral resistance of piles in cohesive soils. *Journal of Soil Mechanics and Foundation Divisi*on, *ASCE, 90 (2)*, 27-63.

Brown, D. A., Morisson, C., & Reese, L. C. (1988). Lateral load behavior of pile group in sand. *Journal of Geotechnical Engineering, ASCE, 114 (11)*, 1261-1276.

Brown, D. A.; Shie, C. F., & Kumar, M. (1989). p-y Curves for laterally loaded piles derived from three-dimensional finite element model. *Proceedings, Third International Symposium, Numerical Models in Geomechanics* (NUMOG III), Niagara Falls, Canada, Elsevier Applied Science, New York, May 1989, 683-690.

Budhu, M. and Davies, T.G. 1987, "Nonlinear analysis of laterally loaded piles in cohesionless soils, *Can. Geotech., 24,* 289-296.

Cai, F., & Ugai, K. 2000. Numerical analysis of the stability of a slope reinforced with piles. *Soils and Foundations, 40 (1),* 73–84.

Cai, F. & Ugai, K. (2003). Response of flexible piles under laterally linear movement of the sliding layer in landslides. *Canadian Geotechnical Journal, 40,* 46-53.

Carruba, P., Maugeri, M., Motta, E. (1989). Esperienze in vera grandezza sul comportamento di pali per la stabilizzazione di un pendio. *XVII Convegno Nazionale di Geotecnica,* Taormina, 81–90.

Carter, D. P. (1984). A non-linear soil model for predicting lateral pile response. *Report No. 359,* Civ. Eng. Dept., University of Auckland, New Zealand.

Carter, J. P., & Kulhawy, F. H. (1992). Analysis of laterally loaded shafts in rock. *Journal of Geotechnical Engineering Division, ASCE, 118 (6),* 839-855.

Cerioni, R., & Mingardi, L. (1996). Nonlinear analysis of reinforced concrete foundation plates. *Computers and Structures, 61 (1),* 87-106.

Chari, T. R., & Meyerhof, G. G. (1983). Ultimate capacity of single piles under inclined loads in sand. *Canadian Geotechnical Journal, 20,* 849–854.

Chelapati, C. V. (1964). Arching in soil due to the deflection of a rigid horizontal strip. *Proceedings, Symposium on Soil-structure Interaction.* University of Arizona, 356-377.

Chen, L. T, & Poulos, H. G. (1997). Piles subjected to lateral soil movements. *Journal of Geotechnical and Geoenvironmental Engineering, ASCE, 123 (9),* 802–811.

Chen, L. T., Poulos, H. G., & Hull, T. S. (1997). Model tests on pile groups subjected to lateral soil movement. *Soils and Foundations, 37 (l),* l-12.

Chen, C. Y. (2001). *Numerical analysis of slope stabilization concepts using piles*. Ph.D. Thesis, The Faculty of the Graduate School University of Southern California, Los Angeles, California.

Chen, C. Y., & Martin, G. R. (2002). Soil-structure interaction for landslide stabilizing piles. *Computers and Geotechnics,* 29 (5), 363-386.

Chow, Y. K. (1996). Analysis of piles used for slope stabilization. *International Journal for Numerical & Analytical Methods in Geomechanics, 20 (9),* 635–646.

Christopher, M., Geiger, G., Liang, R., & Yamin, M. (2007). Design methodology for drilled shafts to stabilize a slope. *First North American Conference*, CD-form.

Clough, G. W., & Duncan, J. M. (1971). Finite element analysis of retaining wall behavior. *ASCE J. Soil Mech.,* 97 (SM12), 1657-1673.

Cox, W. R., Dixon, D. A., & Murphy, B. S. (1983). Lateral load tests of 25.4 mm. diameter piles in very soft clay in side-by-side and in-line groups. *Laterally Loaded Deep Foundations: Analysis and Performance.* ASTM, SPT835.

Cresswell, A., Barton, M. E., & Brown, R. (1999). Determining the maximum density of sands by pluviation. *Geotechnical Testing Journal, 22 (4),* 324-328.

Dagistani, I. (1992). *Model study of lateral earth pressure distribution developed on a rigid passive pile*. M.Sc.Thesis in Civil Engineering, Middle East Technical University, Ankara, Turkey.

Davie, J. R., & Sutherland, H. B. (1978). Modeling of clay uplift resistance. *Journal of the Geotechnical Engineering Division, ASCE, 104 (6),* 755–760.

Davies, T., & Budhu, M. (1986). Nonlinear analysis of laterally loaded piles in heavily overconsolidated clay. *Geotechnique, 36,* 527–538.

Davisson, M. T. (1970). *Lateral load capacity of piles.* High. Res. Rec., 333, 104-112.

De Beer, E., & Wallays, M. (1970). Stabilization of a slope in schist by means of bored piles reinforced with steel beams. *Proc. 2th International Congress on Rock Mechanics,* 1970, Belgrade, 3, 361-369.

De Beer, E. E., & Wallays, M. (1972). Forces induced in piles by unsymmetrical surcharges on the soil round the piles. *Conf. Soil Mech. Found. Eng.,* 1, 325–332.

De Beer, E. (1977). Piles subjected to static lateral loads. *Proc. 9th International Conference on Soil Mechanics and Foundation Engineering,* Tokyo, 1977, 1-14.

De Beer E., and Carpentier, R. (1977). Discussions: Methods to estimate lateral force acting on stabilizing piles, *Soils and Foundions*, 17(1): 68-82.

Desai, C. S., & Appel, G. C. (1976). 3-D analysis of laterally loaded structures. *Proc. 2nd Int. Conf. on Numerical Methods in Geomechanics,* Blacksburg, ASCE, 1, 405-418.

Desai, C. S., & Kuppusamy, T. (1980). Application of a numerical procedure for laterally loaded structures. *Numerical Methods in Offshore Piling*, ICE, London, 93-99.

Dobry, R., Vicente, E., O'Rourke, M. J., & Roesset, J. M. (1982). Horizontal stiffness and damping of single piles. *J. Geotech. Eng. Div., ASCE, 108,* 439–459.

Doherty, J. P., Houlsby, G. T., & Deeks, A. J. (2005). Stiffness of flexible caisson foundations embedded in nonhomogeneous elastic soil. *J. Geotech. and Geoenvir. Engrg., 131 (12),* 1498-1508.

Douglas, D. J., & Davies, E. H. (1964). The movement of buried footings due to moment and horizontal load and the movement of anchor plates. *Geotechnique,* London, England, 14, 115–132.

Dunnavant, T. W., & O'Neill, M. W. (1985). *Performance, Analysis, and Interpretation of a Lateral Load Test of a 72-Inch-Diameter Bored Pile in Over-Consolidated Clay*, Department of Civil Engineering, University of Huston-University Park, Houston, Texas, Report No. UHCE 85-4, September 1985, 57 pages.

Evans, C. H. (1983). *An examination of arching in granular soils*. M.Sc. Thesis. Department of Civil Engineering, MIT.

Ellis, E. A., & Springman, S. M. (2001). Modeling of soil-structure interaction for a piled bridge abutment in plane strain FEM analyses. *Computers and Geotechnics, 28 (1),* 79−98.

Esqueda, H. (2004). *Numerical Models of the Interaction Soil-Structure by the Finite Element Method*. Professional Thesis "Cum-Laude", University of Guanajuato.

Esqueda, H., & Botello, S. (2005). Simulation of retaining walls by the finite element method and the Mohr-Coulomb model. *VIII International Conference on Computational Plasticity COMPLAS VIII*, CIMNE, Barcelona, Spain, Oñate, E. and. Owen D. R. J (Eds).

Estorff, O.von, & Firuziaan, M. (2000). Coupled BEM/FEM approach for nonlinear soil/structure interaction. *Engineering Analysis with Boundary Elements, 24 (10),* 715-725.

Esu, F., & D'Elia, B. (1974). Interazione terreno-struttura in un palo sollecitato da una frana tipo colata. *Rivista Italiana di Geotecnica*, 8 (1), 27–38.

Faruque, M. O., & Desai, C. S. (1982). 3-D material and geometric non-linear analysis of piles. *Proceedings of the Second International Conference on Numerical Methods for Offshore Piling*, Austin, Texas.

Fellenius, W. (1936). Calculation of the stability of earth dams. *Proceedings of the Second Congress on Large Dams*, 4, 445-463.

Finn, W. D. L. (1967). Applications of limit plasticity in soil mechanics. *JSMFD, ASCE, 93 (5)*, 101-120.

Fleming, W. G. K., Weltman, A. J., Randolph, M. F., & Elson, W. K. (1994). *Piling Engineering*, 2nd Edition Routledge, New York: Blanckie and Son Ltd.

Fukumoto, Y. (1972). Study on the behavior of stabilization piles for landslides. *Journal of JSSMFE, 12 (2),* 61-73.

Fukumoto, Y. (1973). Failure condition and reaction distribution of stabilization piles for landslides. *Proc., 8th annual meeting of JSSM,* 549-562.

Fukumoto, Y. (1975). Experiment study on the behavior of lateral resistance of piles against a land-sliding. *Journal of Landslides, 12 (1),* 20-24.

Fukumoto, Y. (1976). The behavior of piles for preventing landslide. *Soils and Foundations, 16 (2),* 91-103.

Fukuoka, M. (1977). The effects of horizontal loads on piles due to landslides. *Proceedings, 9th International Conference on Soil Mechanics and Foundation Engineering,* Tokyo, Japan, 27-42.

Gabr, M. A., & Borden, R. H. (1990). Lateral analysis of piers constructed on slopes. *Journal of Geotechnical Engineering, 116 (12),* 1831-1850.

Georgiadis, M., & Butterfield, R. (1982). Laterally loaded pile behavior. *ASCE, 108 (1),* 155-165.

Getzler, Z., Gellert, M., & Eitan, R. (1970). Analysis of arching pressures in ideal elastic soil. *JSMFD, ASCE, 96 (4),* 1357-1372.

Goh, A. T. C., Teh, C. I., & Wong, K. S. (1997). Analysis of piles subjected to embankment induced lateral soil movements. *Journal Geotechnical and Geoenvironmental Engineering, 123 (9),* 792-801.

Gould, J. P. (1970). *A summary of some performance records.* New developments in earth support – case histories, Metropolitan Section ASCE, Foundations and Soil Mechanics Group Seminar, December.

Gray, D. H. (1977). Creep movement and soil moisture stress in forested vs. cutover slopes: Results of field studies. *Final report submitted to the National Science Foundation*, ENG 74-02427, 141.

Greimann, L. F., Abendroth, R. E., Johnson, D. E., & Ebner, P.B. (1987). *Pile design and tests for integral abutment bridges*. Iowa State University, December 1987, pp. 302.

Gudehus, G., & Schwarz, W. (1985). Stabilization of creeping slopes by dowels. *Proc. 11th International Conference on Soil Mechanics and Foundation Engineering*, San Francisco, 1697–700.

Guo, W. D. (2003). Response of laterally loaded rigid piles. *Proceedings of 12th Panamerican Conference on Soil Mechanics and Geotechnical Engineering*, Cambridge, Massachusettes, USA, Verlag Gluckauf GMBH. Essen (Germany), 2, 1957-1962.

Guo, W. D. (2006). On limiting force profile, slip depth and lateral pile response. *Computers and Geotechnics, 33 (1),* 47-67.

Gültekin, S. (2001). *Yatay yüklü düşey kaziklarin laboratuvar koşullarinda modellenmesi*. M.Sc. Thesis, Yıldız Teknik Üniversitesi, İstanbul, Türkiye.

Hannigan, P. J., Goble, G. G., Thendean, G., Likins, G. E., & Rausche, F. (1997). Design and Construction of Driven Pile Foundations – Volume I, *Federal Highway Administration Report No. FHWA-HI-97-013*, Sections 9.10-9.10.3.

Hartmann, F., & Jahn, P. (2001). Boundary element analysis of raft foundations on piles. *Meccanica, 36 (4),* 351-366.

Hassiotis, S., & Chameau, J. L. (1984). Stabilization of slopes using piles. In slope

stabilization. *Report FHWA/IN/JHRP-84-8* (pp. 181). Purdue University, West Lafayette, Indiana.

Hassiotis, S., Chameau, J. L., & Gunaratne, M. (1997). Design method for stabilization of slopes with piles. *J. Geotech. Geoenviron. Eng., ASCE, 123 (4),* 314–323.

Heteny, M. (1946). *Beams on elastic foundations*. University of Michigan Pres, Ann Arbor, Mich.

Hewlett, W. J., & Randolph, M. F. (1988). Analysis of piled embankments. *Ground Engineering, 21 (3),* 12–18.

Heyman, L., & Boersma, L. (1961). Bending moments in piles due to lateral earth pressure. *Proc. 5th Int. Conf. on Soil Mech. and Found. Eng.*, 2, 422-429.

Hong, W. P., & Han, J. G. (1996). The behavior of stabilizing piles installed in slopes. *Proc. 7th International Symposium on Landslides,* Rotterdam, 1709–1714.

Hsiung, Y., & Chen, Y. (1997). Simplified method for analyzing laterally loaded single pile in clays. *Journal of Geotechnical and Geoenvironmetal Engineering, 123 (11),* 1018-1029.

Hsuing, Y. (2003). Theoretical elastic-plastic solution for laterally loaded piles. *Journal of Geotechnical and Geoenvironmental Engineering, ASCE, 129,* 475-480.

Iai, S. (1989). Similitude for shaking table tests on soil-structure-fluid model in 1g gravitational field. *Soils and Foundations, 29 (1),* 105-118.

Iglesia, G. (1991). *Trapdoor experiments on the centrifuge: A study of arching in geomaterials and similitude in geotechnical models.* Ph.D. Thesis. Department of Civil Engineering, Massachusetts Institute of Technology.

Ishihara K. (1996). *Soil behavior in earthquake geotechniques.* Oxford:Clarendon Press.

Ito, T., & Matsui, T. (1975). Methods to estimate lateral force acting on stabilizing piles. *Soils and Foundations, 15 (4),* 43-59.

Ito, T. &Matsui, T. (1977). The effects of piles in a row on the slope stability. *Proceedings, 9th I.C.S.M.F.E., Specialty Session. 10,* Tokyo.

Ito, T., Matsui, T., & Hong, W. P. (1979). Design method for the stability analysis of the slope with landing pier. *Soils and Foundations, 19 (4),* 43–57.

Ito, T., Matsui, T., & Hong, W. P. (1981). Design method for stabilizing piles against landslide-one row of piles. *Soils and Foundations, 21 (1),* 21-37.

Ito, T., Matsui, T., & Hong, W. P. (1982). Extended design method for multi-row stabilizing piles against landslide. *Soils and Foundations, 22 (1),* 1–13.

Jaky, J. (1944). The coefficient of earth pressure at rest. *Journal of the Society o Hungarian Architects and Engineers*, 355-358.

Jamiolkowski, M., Ladd, C. C., Germaine, J. T., Lancelotta, R. (1985). New developments in field and laboratory testing of soils. *Proceedings of the 11th International Conference on Soil Mechanics and Foundation Engineering.* San Fransisco, CA: A.A. Balkema, 57–153.

Janbu, N. (1954). Stability analysis of slopes with dimensionless parameters. *Harvard Soil Mechanics Series no. 46,* 1954.

Janssen, H. A. (1895).Versuche über getreidedruck in silozellen. Zeitschrift des Vereins Deutscher Ingenieure 39, 1045-1049 (partial English translation in Proceedings of Institution of Civil Engineers, 1986, pp. 553).

Jeong, S., Kim, B., Won, J., & Lee, J. (2003). Uncoupled analysis of stabilizing piles in weathered slopes. *Computers and Geotechnics, 30*, 671–682.

Joo, J. S. (1985). *Behavior of large scale rigid model piles under inclined loads in sand*. M.Sc. Engineering Thesis, Memorial Univ. of Newfoundland, St. John's, Newfoundland, Canada.

Kahyaoglu, M. R., Imancli, G., Ozturk, A. U., Kayalar, A. S. (2009). Computational 3D finite element analyses of model passive piles. *Computational Materials Science*, 46 (1), 193-202.

Kın, Y. (1993). *Effect of penetration depth and soil stiffness on the behavior of a rigid pile*. M.Sc.Thesis in Civil Engineering, Middle East Technical University, Ankara, Turkey.

Kıncal, C., & Koca, M. Y. (2009). A proposed method for drawing the great circle representing dip angle and strike changes. *Environmental and Engineering Geoscience*; *15 (3),* 145-165.

Klar, A., & Frydman, S. (2002). Three-Dimensional analysis of lateral pile response using two-dimensional explicit numerical scheme. *J. Geotech. and Geoenvir. Engrg. 128 (9)*, 775-784.

Kooijman, A. P. (1989). Comparison of an elastoplastic quasi three-dimensional model for laterally loaded piles with filed tests. *Proceedings, Third International Symposium, Numerical Models in Geomechanics* (NUMOG III), Niagara Falls, Canada, Elsevier Applied Science, New York, May 1989, 675-682.

Krawinkler, H. (1979). Possibilities and limitations of scale-model testing in earthquake engineering. *Proc. 2nd US National Conf. on Earthquake Engineering*, Stanford University, 283-292.

Kristoff, S. (2008). Strain gauge installation methods-How strain measurement sensors are applied to test specimens. *mechanical-engineering.suite101.com,* April.

Kuhlemeyerr, L. (1979). Static and dynamic laterally loaded floating piles. *Journal of the Geotechnical Engineering Division, ASCE, 105 (2),* 289-304.

Kumar, B. S. (1992). *Three dimensional non-linear finite element analysis of laterally loaded piles in clay*. Ph.D. Thisis, University of Illinois at Urbana-Champaign.

Ladanyi, B., & Hoyaux, B. (1969). A study of the trapdoor problem in a granular mass. *Canadian Geotechnical Journal, 6 (1),* 1-15.

Ladd, C. C., Foott, R., Ishihara, K., Schlosser, F., & Poulos, H. G., (1977). Stress deformation and strength characteristics. *Proceedings of the Ninth International Conference on Soil Mechanics and Foundation Engineering,* 394–421.

Lambe, T. W., & Whitman, R. V. (1969). *Soil mechanics*. Wiley, New York.

Lee, C.Y., Hull, T.S., & Poulos, H. G. (1995). Simplified pile-slope stability analysis. *Computers and Geotechnics, 17*, 1–16.

Leussink, H., & Wenz, K. P. (1969). Storage yard foundations on soft cohesive soils. *Proc. 7th Int. Conf. on Soil Mech. and Found. Eng.*, 2, 149-155.

Liang, R., Yamin, M. (2009). Three-dimensional finite element study of arching behavior in slope/drilled shafts system. International Journal for Numerical and Analytical Methods in Geomechanics, DOI: 10.1002/nag.851

Liang, R. & Zeng S. (2002). Numerical study of soil arching mechanism in drilled shafts for slope stabilization. *Soils and Foundations, 42 (2),* 83-92.

Lieng, J. T. (1988). *Behavior of laterally loaded piles in sand-large scale model tests*. Ph.D. Thesis, Dept. of Civil Engr., Norwegian Institute of Technology.

Lo Presti, D. C. F., Pedroni, S., & Crippa, V. (1992). 'Maximum dry density of cohesionless soil by pluviation and by ASTM D 4253-83: a comparative study. *Geotech. Testing J., 15 (2),* 180–189.

Maheshwari, B. K., Truman, K. Z., El Naggar, M. H, & Gould, P. L. (2004). Three dimensional nonlinear analysis for seismic soil–pile-structure interaction. *Soil Dynamics and Earthquake Engineering, 24 (4),* 343-356.

Matlock, H., & Reese, L. C. (1960). Generalized solutions for laterally loaded piles. *Journal of Soil Mechanics and Foundation Division, ASCE, 86 (5),* 63-91.

Matlock, H., & Reese, L. C. (1961). Foundation analysis of offshore pile supported Structures. *Proceeding Fifth International Conference on Soil Mechanics and Foundation Engineering*, Paris, France, 2, 91-97.

Matlock, H., & Reese, L. C. (1962). Generalized solutions for laterally loaded piles. *Transactions of the American Society of Civil Engineering*, 127 (1), 1220-1247.

Matlock, H. (1970). Correlations for design of laterally loaded piles in soft clay. *Proceedings of the 2nd Annual Offshore Technology Conference,* Houston, TX, Paper ITC 1204, 1, 577–594.

Matsui, T., Hong, W. P., & Ito, T. (1982). Earth pressures on piles in a row due to lateral soil movements. *Soils and Foundations, 22 (2),* 71-81.

McClelland, B., & Focht, J. A. Jr. (1958). Soil modulus for laterally loaded piles. *Trans., ASCE, 123,* 1049-1063.

McVay, M., Zhang, L., Molnit, T., & Lai, P. (1998). Centrifuge testing of large laterally loaded pile groups in sands,. *J. of Geotech. and Geoenviron. Engrg., ASCE, 124 (10),* 1016-1026.

Merriam, R. (1960). Portuguese Bend landslide, Palos Verdes Hills, California. *Journal of Geology, 68,* 140-153.

Mesri, G., & Choi, Y. K. (1985). The uniqueness of the end-of-primary (EOP) void ratio effective stress relationships. *Proceedings of International Conference of Soil Mechanics and Foundation Engineering* (ICSMFE), 587–590.

Meyerhof, G. G., Mathur, S. K., & Valsangkar, A. J. (1981). Lateral resistance and deflection of rigid wall and piles in layered soils. *Canadian Geotechnical Journal, 18,* 159-170.

Meyerhof, G. G., & Sastry, V. V. R. N. (1985). Bearing capacity of rigid piles under eccentric and inclined loads. *Canadian Geotechnical Journal, 22,* 267–276.

Meyersohn, W. D., Rourke, T. D., & Miura, F. (1992). Lateral spread effects on reinforced concrete pile foundations. *Fifth US–Japan workshop on earthquake disaster prevention for lifeline system,* Tsukuba, Japan, October, 26–30.

Mindlin, R. D. (1936). Force at appoint in the interior of a semi-infinite solid. *Physics, 7,* 195-202.

Moayed, R. Z., Judi A., & Rabe, B. K. (2008). Lateral bearing capacity of piles in cohesive soils based on soils' failure strength control. *EJGE*, 13, 1-11.

Morgenstern, N. R., & Price, V. E. (1965). The analysis of the stability of general slip surface. *Geotechnique, 15*, 77-93.

Morgenstern, N. R. (1982). The analysis of wall supports to stabilize slopes. *In application of walls to landslide control problems*, Edited by Reeves, R. B., ASCE, 19-29.

Murchison, J. M., & O'Neill, M.W. (1984). Evaluation of *p-y* relationships in cohesionless soils, in analysis and design of pile foundations. *ASCE*, New York, 174-191.

Murthy, V. N. S., & Subba Rao, K. S. (1995). Prediction of nonlinear behavior of laterally loaded long piles. *Foundation Engineer*, New Delhi, 1 (2).

Nakamura, H. (1984). Design of rigid dowel piles for landslide control. *4th International Symposium on Landslides*, 2, 149-154.

Nalçakan, M. S. (1999). *Stabilization of landslides by piles in cohesive soils with special reference to group action reduction.* Ph.D. Thesis in Civil Engineering, Middle East Technical University, Ankara, Turkey.

Navy Design Manual, Foundations and earth Structures, DM 7.02, Department of the Navy Naval Facilities Engineering Command, September, 1986.

Nethero, M. F. (1982). Slide control by drilled pier walls. *In application to landslide control problems*, Edited by Reeves, R. B., ASCE, 61-76.

Nicoletti, J. P., & Keith, J. M. (1969). External shell stops soil movement and saves tunnel. *Civil Engineering, ASCE, 39 (4)*, 72-75.

Nunez, I. L. (1988). Driving and tension loading of piles in sand on a centrifuge. *Proceedings International Conference Centrifuge 88,* Paris, Corté, J.F. (ed.), Balkema, Rotterdam, 353–362.

Oakland, M. W., & Chameau J. L. A. (1984). Finite-element analysis of drilled piers used for slope stabilization. *Laterally Loaded Foundation-American Society for Testing and Materials*, 182–193

O'Neill, M. W., & Gazioglu, S. M. (1984). An evaluation of p-y relationships in clays. *A Report to the American Petroleum Institute, PRAC 82-41-2,* The University of Houston-University Park, Houston, Texas, April 1984.

Oteo, C. S. (1972). Dsplacement of a vertical pile group subjected to lateral loads. *Proc. 5th, EC.S.M.F.E.,* Madrid, 1, 397-405.

Otsu, N. (1979). A Threshold Selection Method from Gray-Level Histograms. *IEEE Transactions on Systems, Man, and Cybernetics. 9 (1),* 62-66.

Ovesen, N. K. (1979). The use of physical models in design: The scaling law relationship. *Proc., 7th European Conf. on Soil Mechanics and Foundation Engineering*, Brighton, 4, 318–323.

Önal, O & Özden, G. (2006). Sayısal görüntü işleme tekniklerinin geoteknikte uygulama örnekleri. *Zemin Mekaniği ve Temel Mühendisliği Onbirinci Ulusal Kongresi, 7-8 Eylül*, Karadeniz Teknik Üniversitesi, Trabzon, Turkiye.

Özçelik, Ç. (2007). *Şevlerde yanal yüklü kazıkların laboratuar koşullarında modellenmesi.* M. Sc. Thesis, Yıldız Teknik Üniversitesi, İstanbul, Türkiye.

Palmer, L. A., & Thompson, J. B. (1948). The earth pressure and deflection along the embedded lengths of piles subjected to lateral thrusts. *Proc. 2nd Int. Conf. S. M. and F. E.*, Rotterdam, 5, 156-161.

Pan, J. L., Goh, A. T. C., Wong, K. S., & TEH, C. I. (2000). Model tests on single piles in soft clay. *Canadian Geotechnical Journal, 37,* 890-897.

Pan, J. L., Goh, A. T. C., Wong, K. S., & Teh, C. I. (2002). Ultimate soil pressures for piles subjected to lateral soil movements, *Journal of Geotechnical and Geoenvironmental Engineering, ASCE, 128 (6),* 530–535.

Parakash, S. (1962). *Behavior of pile groups subjected to lateral loads*. Unpublished Dissertation, University of Illinois, Illinois, USA.

Perry, C. C., & Lissner, H. R., (1962). *The Strain Gage Primer.*, Second Edition, Mc Graw-Hill Book Company, New Y

Petrasovits, G., & Award, A. (1972). Ultimate lateral resistance of a rigid pile in cohesionless soil. Proceedings of the 5th European Conference on Soil Mechanics and Foundation Engineering, Madrid, Spain, 3, 407–412.

Popescu, M. E. (1991). Landslide control by means of a row of piles. *Slope stability Engineering*, London, Thomas Telford, 389-394.

Poulos, H. G. (1971). Behavior of laterally loaded piles-single piles. *Journal of Soil Mechanics and Foundation Division, ASCE, 97 (5),* 711–731.

Poulos, H. G. (1971a). Behavior of laterally loaded piles: I—Single piles. *J. Soil Mech. Found. Div., 97 (5),* 711–731.

Poulos, H. G. (1971b). Behavior of laterally loaded piles: I—Pile groups. *J. Soil Mech. Found. Div., 97 (5),* 733–751.

Poulos, H. G. (1973). Analysis of piles in soil undergoing lateral movement. *Journal of Soil Mechanics and Foundation Engineering Division, ASCE, 99,* 391-406.

Poulos, H. G. (1979). Settlement of single piles in non-homogeneous soil. *J. Geotech. Eng., ASCE, 105 (5),* 627–641.

Poulos, H. G., & Davis, E. H. (1980). Pile foundation analysis and design. New York: John Wiley & Sons Inc.

Poulos, H. G., & Hull, T. S. (1989). The role of analytical mechanics in foundation engineering. *Foundation Engineering, Current Principals and Practices*, ASCE (2), 1578-1606.

Poulos, H. G. (1995). Design of reinforcing piles to increase slope stability. *Canadian Geotechnical Journal, 32 (5),* 808–818.

Poulos H.G., Chen, L.T., & Hull T.S. (1995). Model tests on single piles subjected to lateral soil movement, Soils and Foundations, 35 (4), 85-92.

Poulos, H. G. (1999). Design of slope stabilizing piles. *Slope Stability Engineering*, Yagi, Yamagami and Jiang.

Rad, N. S., & Tumay, M. T. (1987). Factors affecting sand specimen preparation by raining. *Geotechnical Testing Journal, 10 (1),* 31-37.

Randolph, M. F. (1981). The response of flexible piles to lateral loading. *Geotechnique, 31 (2),* 247-259.

Reese, L. C., Cox, W. R., & Koop, F. D. (1974). Analysis of laterally loaded piles in sand. *Proc. 6th Offshore Technol. Conf.*, Dallas, Tex., 473-483.

Reese, L. C., & Welch, R. C. (1975). Lateral loading of deep foundations in stiff clay, *ASCE, 101 (7),* 633-649.

Reese, L. C., & Desai, C. S. (1977). *Laterally loaded piles, Chapter in Numerical Methods in Geotechnical Engineering,* McGraw-Hill, 783.

Reese, L. C. (1977). Laterally loaded piles: Program documentation. *Journal of Geotechnical Engineering Division, ASCE, 103 (GT4),* 287-305

Reese, L.C. (1985). *Behavior of piles and pile groups under lateral load*. Technical Report No: FHWA/RD-85/106, Federal Highway Administration, Office of Engineering and Highway operations, Research and Development, Washington, D.C.

Reese, L. C., Wang, S. T., & Fouse, J. L. (1992). Use of drilled shafts in stabilizing a slope. *Proc. Specialty Conference on Stability and Performance of Slopes and Embankments,* Berkeley.

Reese, L. C, Wang, S. T, & Fouse, J. L. (1992). Use of shafts in stabilizing a slope, slopes and embankments-II, *A.S.C.E., Specialty Session.*

Robertson, P. K., Hughes, J. M., Campanella, R. G. (1984). Design of laterally loaded displacement piles using a driven pressuremeter. *ASTM Special Technical Publication,* 229-238.

Robertson, P. K., Campanella, R. G., Brown, P. T., Grof, I., & Hughes, J. M. (1985). Design of axially and laterally loaded piles using in situ tests: a case history. *Canadian Geotechnical Journal, 22 (4),* 518-527.

Robertson, P. K., Davies, M. P. and Campanella, R. G. (1987). Design of laterally loaded driven piles using the flat dilatometer. *Geotechnical Testing Journal,* 14 (8), 30-38.

Rollins, K. M., & Rollins, R. L. (1992). Landslide stabilization using drilled shaft walls. *In ground movements and structures,* Vol. 4, Edited by Geddes, J.

Rowe, R. K., & Poulos, H. G. (1979). A method for predicting the effect of piles on slope behavior. *Proceedings of the 3rd ICONMIG*, Aachen, 3, 1073–1085.

Ruesta, P. F., & Townsend, F. C. (1997). Evaluation of laterally loaded pile group at Roosevelt Bridge,. *J. of Geotech. and Geoenviron. Engrg., ASCE, 123 (12),* 1153-1161.

Sabnis, G. M., Harris, H. G., White, R. N., & Mirza, M. S. (1983). *Structural modeling and experimental techniques.* Englewood Cliffs:Prentice-Hall.

Sarma, S. K. (1973). Stability analysis of embankments and slopes. *Geotechnique, 23 (3),* 423-433.

Sastry V.V.R.N., & Meyerhof, G.G. (1994). Rigid piles under inclined and eccentric loads. *Indian Geotechnical* Journal, 17, 209-232.

Shibata, T., Yashima, A., & Kimura, M. (1989). Model tests and analyses of laterally loaded pile groups. *Soils and Foundations, 29 (1),* 29-42.

Smith, T. D. (1987). Pile horizontal modulus values. *Journal of Geotechnical and Geoenvironmental Engineering, ASCE, 113 (9),* 1040-1044.

Soletanche Design Criteria, *Permanent Ground Anchors,* Final Report No. FHWA/RD-81/150, U.S. Department of Transportation, Federal Highway Administration, September, 1982, 18-22.

Sommer, H. (1977). Creeping slope in a stiff clay. *Proc. 9th International Conference on Soil Mechanics Foundation Engineering,* Tokyo, 113–8.

Spencer, E. (1967). A method of analysis of the stability of embankments assuming parallel interslice forces. *Geotechnique, 17 (1),* 11-26.

Spillers, W. R., & Stoll, R. D. (1964). Lateral response of piles. *ASCE*, 90 (6), 1-9.

Springman, S. M. (1989). *Lateral loading on piles due to simulated embankment construction*. PhD thesis, University of Cambridge.

Springman, S. M., & Bolton, M. D., (1989). The effect of surcharge loading adjacent to piles. *Final Contractor's Report to Transport and Road Research Laboratory, TRR/842/447*. University of Cambridge.

Sirawardane, H. J., Moulton, L. K., & Ched, T. J. (1984). Prediction of lateral movement of bridge abutments on piles. *Transportation Research Record*, 998, TRB, Washington, 14-24.

Stevens, J. B., & Audibert, J. M. E. (1979). Re-examination of p-y Curve Formulation. *Proceedings, Offshore Technology Conference*, Houston, Texas, Vol. I, Paper No. 3402, 397-403.

Stewart, D. P. (1992). *Lateral loading of piled bridge abutments due to embankment construction*. Ph.D. Thesis, University of Western Australia.

Stewart, D. P., Jewell, R. J., Randolph, M. F. (1993). Numerical modeling of piled bridge abutments on soft ground. *Computers and Geotechnics, 15 (1),* 21−46.

Stewart, D. P., Jewell, R. J., & Randolph, M. F. (1994). Design of piled bridge abutments on soft clay for loading from lateral soil movements. *Geotechnique, 44 (2),* 277−296.

Sun, K (1994). Laterally loaded piles in elastic media. *Journal of Geotechnical Engineering Division, ASCE, 120 (8),* 1324-1344.

Terzaghi, K. (1936). Stress distribution in dry and saturated sand above a yielding trap door. *Proceeding, 1st I.C.S.M.F.E.*, 307-311.

Terzaghi, K. (1955). Evaluation of coefficients on subgrade modulus. *Geotechnique*, 297-326.

Thompson, G. (1977). *Application of finite element method to the development of p-y curves for saturated clays*. Ph.D. Thesis, University of Texas, Austin.

Thompson, M. J., David, J. W., & Muhannad, T. S. (2005). Lateral load tests on small-diameter piles for slope remediation. *Proceedings of the 2005 Mid-Continent Transportation Research Symposium*, Ames, Iowa, August 2005, 1-13

Tschebotarioff, G. P. (1973). Lateral pressure of clayey soils on structures. *Proceedings of the 8th ICSMFE Specialty Session 5*, Moscow, 4 (3), 227–240.

Vaid, Y. P., & Negussey, D. (1984). Relative density of pluviated sand samples, *Soils and Foundations, 24 (2),* 101-105.

Vallabhan, C. V., & Alikhanlou, F. (1982). Short rigid piers in clays. *Journal of Geotechnical Engineering, ASCE, 108 (10),* 1255-1272.

Verruijt, A., & Kooijman, A. P. (1989). Laterally loaded piles in a layered elastic medium. *Géotechnique, 39 (1),* 39-46.

Viggiani, C. (1981). Ultimate lateral load on piles used to stabilize landslides. *Proceedings. 10th I.C.S.M.F.E.,* Stockholm, Sweden, 3, 555-560.

Vitharana, N. (1997). Rational prediction of lateral behavior of concrete piles incorporating pile (concrete) non-linearity. *14th International Conference on Soil Mechanics and Foundation Engineering*, Hamburg, Germany, September 06-12, 1997, 915-920.

Wang, X. D. (1997). Finite element analysis of air-sheet interactions and flutter suppression devices. 11th ADINA Conference on Nonlinear Finite Element Analysis, Cambridge, MA, Jun. 18-20, 1997, 983-994.

Winkler, E. (1867). Die lehre von elasticzitat and festigkeit (on elasticity and fixity). *Prague*, 182 p.

Winter, H., Schwarz, W., & Gudehus, G. (1983). Stabilization of clay slopes by piles. *Proc., 8th Eur. Conf. On Soil Mech. and Found. Eng.*, 2, 545.

Wang, W. L., & Yen, B. C. (1974). Soil arching in slopes. *JGED*, ASCE, 100, 61-78.

Wang, S. T., & Reese, L. C. (1986). Study of design method for vertical drilled shaft retaining walls. *Research Report 415-2F*, Center of Transportation Research, Bureau of Engineering Research, The University of Texas at Austin.

Wood, D. M. (2004). *Geotechnical modeling*. Spon Press, Abingdon, Oxfordshire.

Yoshida, N., & Hamada, M. (1991). Damage to foundation piles and deformation pattern of ground due to liquefaction-induced permanent ground deformations. *Proc. Third Japan-US Workshop on Earthquake Resistant Design of Lifeline Facilities and Countermeasures for Soil Liquefaction*, Report NCEER-91-0001, 141-161.

Zeng, S., & Liang, R. (2002). Stability analysis of drilled shafts reinforced slope. *Soils and Foundations*, *42 (2),* 93-102.

Zhao, M. H., Liu, D. P., Zhang, L., Jiang, C. (2008). 3D finite element analysis on pile-soil interaction of passive pile group. *Journal of Central South University of Technology*, 15 (1), 75-80.

APPENDICES

APPENDIX A – Engineering Drawing of Experimental Setup

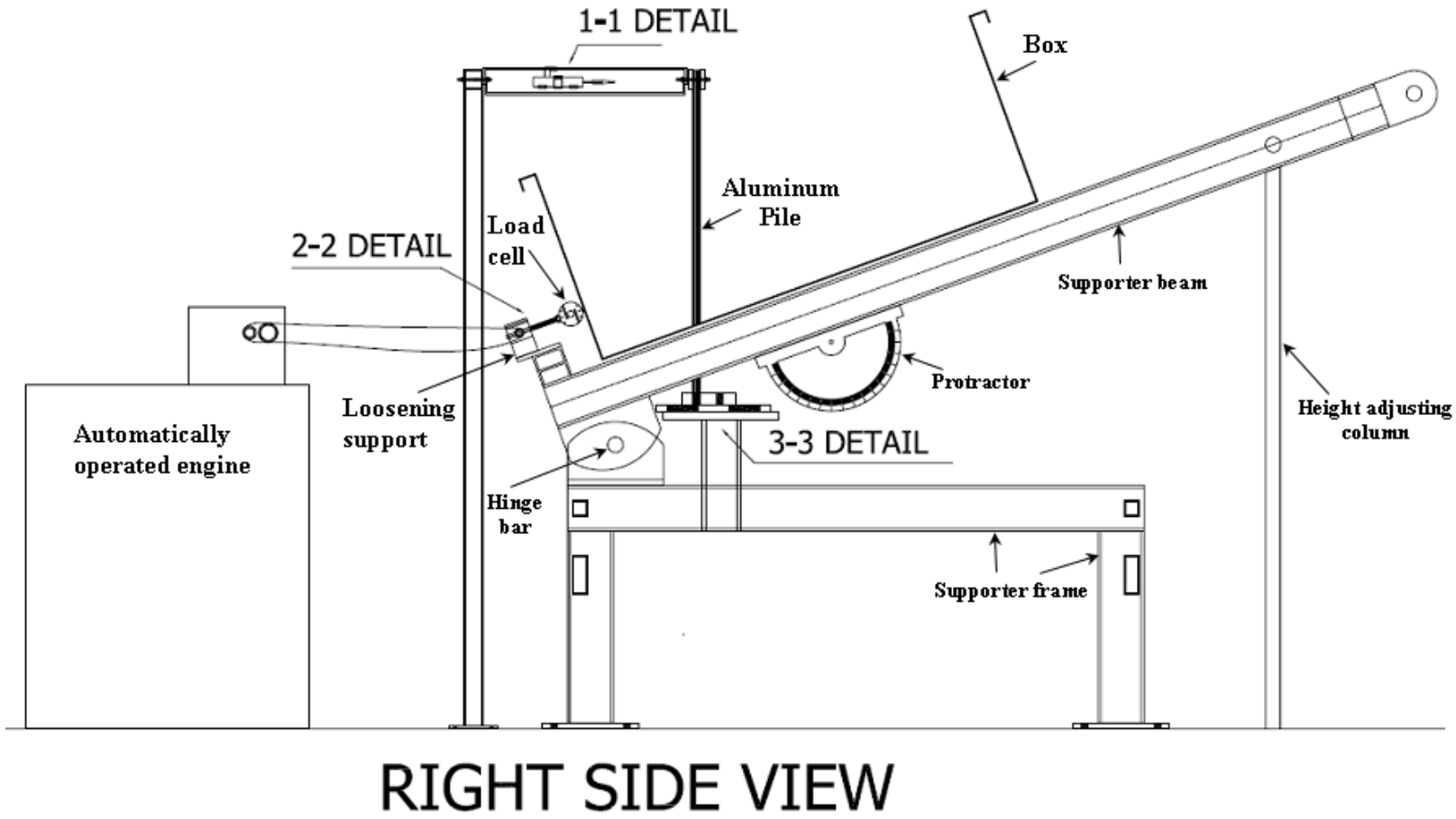

Figure A.1 Right Side View of the Test Setup

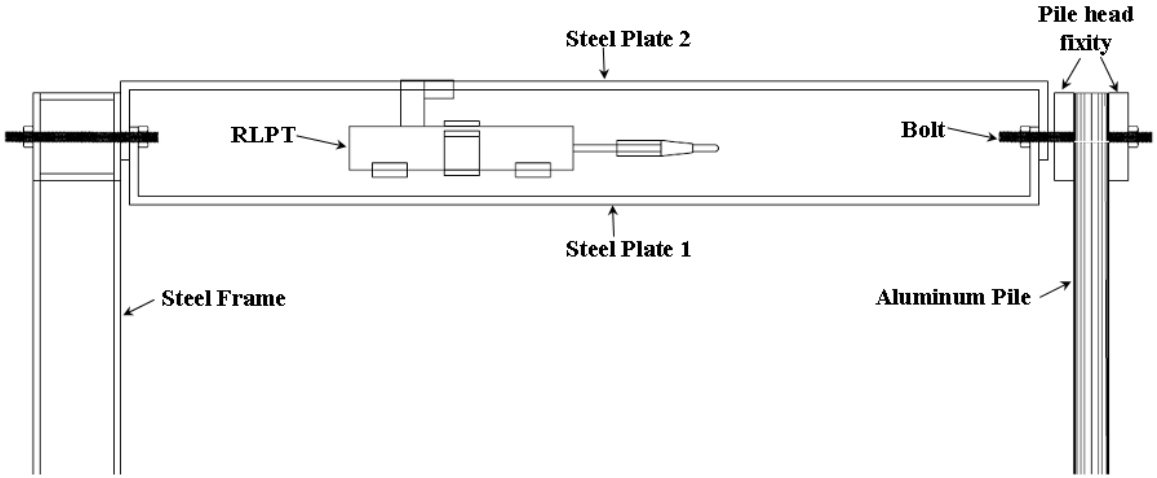

Figure A.2 Detail 1-1 of Right Side View

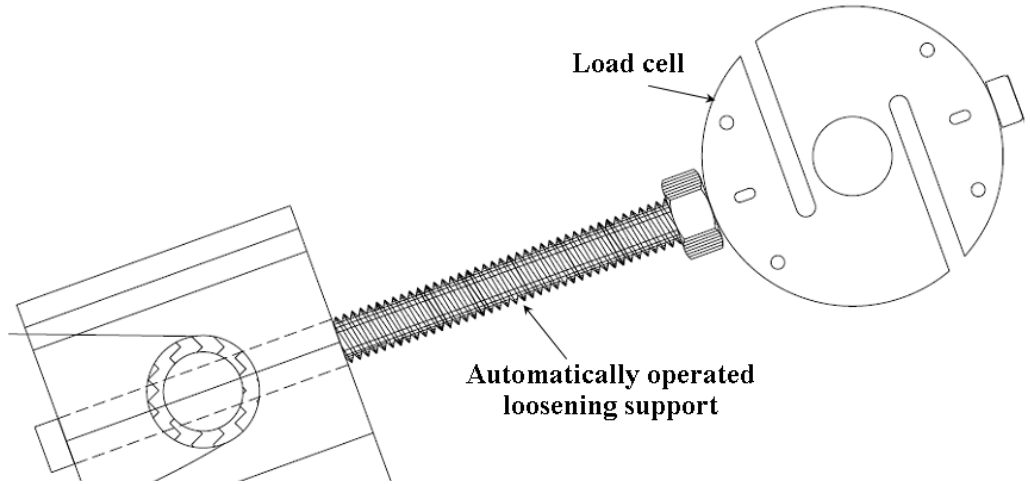

Figure A.3 Detail 2-2 of Right Side View

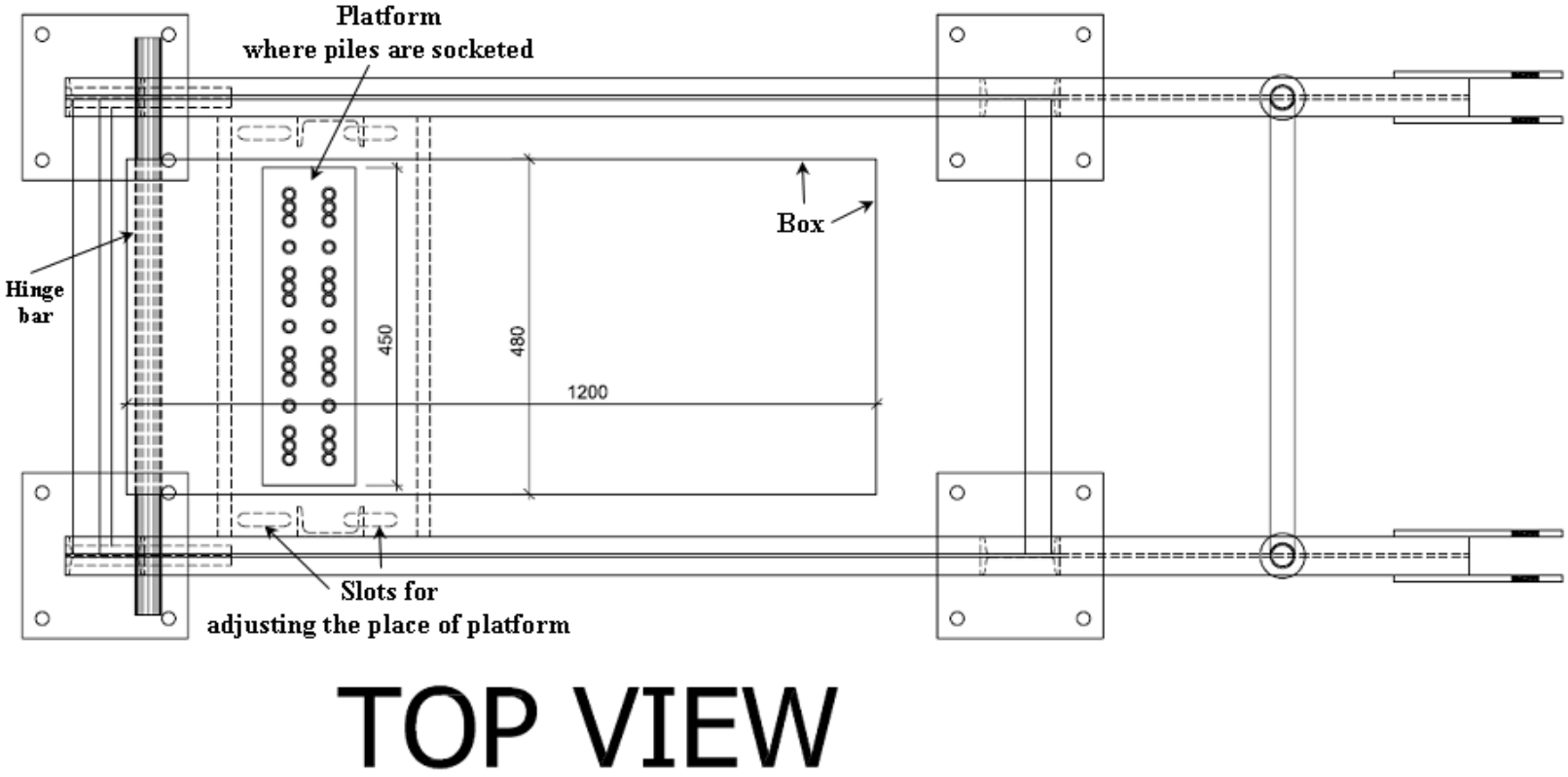

Figure A.4 Top View of the Test Setup

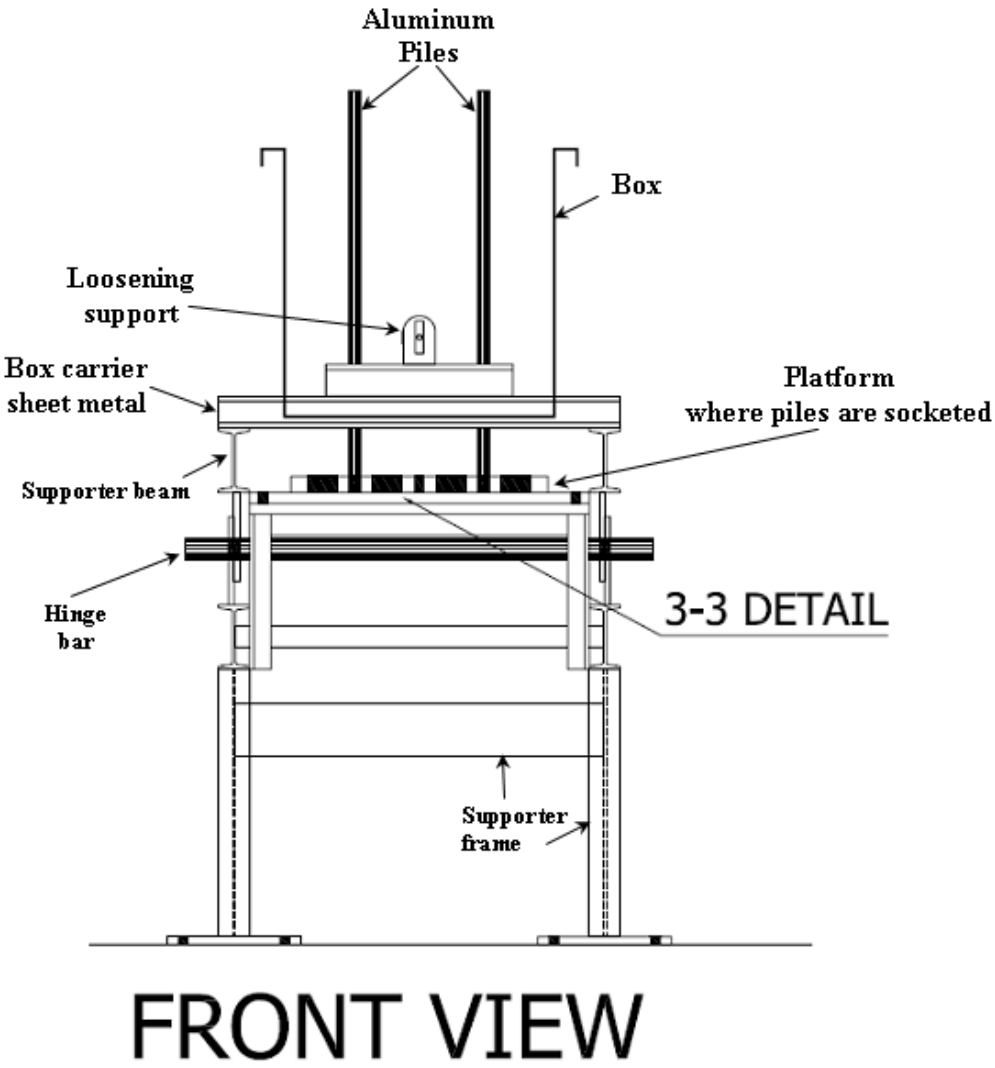

Figure A.5 Front View of the Test Setup

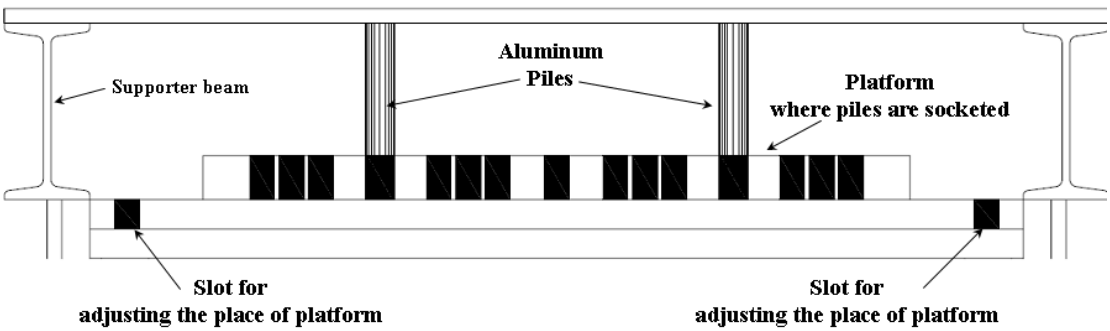

Figure A.6 Detail 3-3 of Front View

APPENDIX B – Load Cell

Load cell is an electronic device (transducer) used to convert a force into an electrical signal. This conversion is indirect and happens in two stages. Through a mechanical arrangement, the force being sensed deforms a strain gage. A load cell usually consists of four strain gages in a Wheatstone bridge configuration. The output of the transducer is plugged into an algorithm to calculate the force applied to the transducer.

The TB S-type load cell which was capable of measuring both tension and compression loads was used to measure the lateral load transferred to the pile in this study. With its steel alloy construction coated with corrosion-returdant paint as well as its strain gage area which is fully welded with a stainless steel cover, the TB load cells are protected to IP68 standards meaning that they are fully immersable. The technical features and the technical drawing of the load cell are given in Table B.1 and Figure B.1, respectively. Calibrations were checked before using the load cell.

Table B.1 Technical Features of TB type Load Cell

Maximum Capacity (kg) (E_{max})	1000
Accuracy Class (OIML R60)	C3
Max. Number of Verification Intervals (nLC)	3000
Min. Verification Interval (V_{min})	E_{max}/5000
Combined Error (%)	$\leq \pm 0.02$
Zero Return Error (DR)	0.01
Stretching (for E_{max}) (mm)	≤ 0.4
Maximum excitation Voltage (Umax) (V)	15
Rated Output (Cn) (mV/V)	$2 \pm 0.1\%$
Zero Balance (%Cn)	$\leq \pm 1.0$

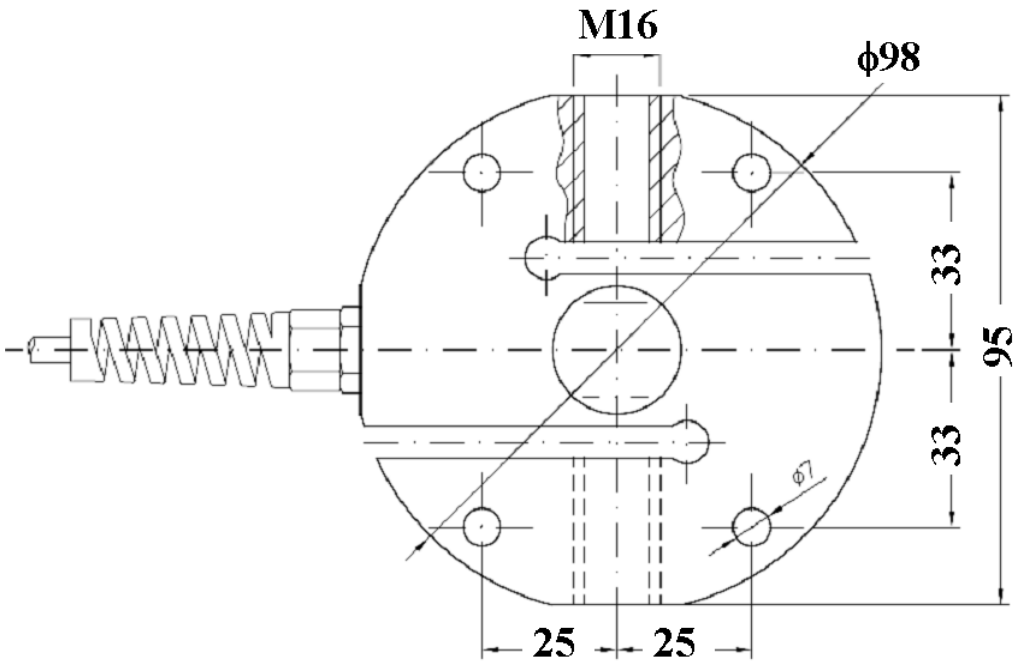

Figure B.1 Technical Drawing of Load Cell

APPENDIX C1 – Strain Gages

While there are several methods of measuring strain, the most common method is performed with a strain gage, a device whose electrical resistance varies in proportion to the amount of strain in the device (Kristoff, 2008).

The metallic strain gage consists of a very fine wire or, more commonly, metallic foil arranged in a grid pattern. The grid pattern maximizes the amount of metallic wire or foil subject to strain in the parallel direction (Figure C1.1). The cross sectional area of the grid is minimized to reduce the effect of shear strain and Poisson Strain. The grid is bonded to a thin backing, called the carrier, which is attached directly to the test specimen. Therefore, the strain experienced by the test specimen is transferred directly to the strain gage, which responds with a linear change in electrical resistance.

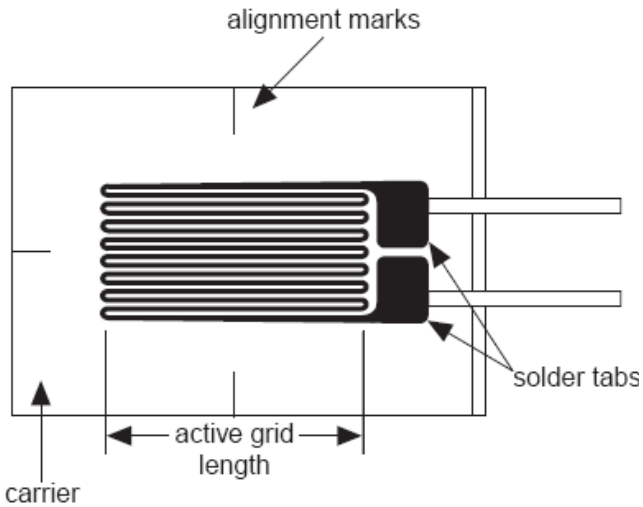

Figure C1.1 Bonded Metallic Strain Gage

A fundamental parameter of the strain gage is its sensitivity to strain, expressed quantitatively as the gage factor (GF). Gage factor is defined as the ratio of fractional change in electrical resistance to the fractional change in length (strain):

$$GF = \frac{\Delta R / R}{\Delta L / L} = \frac{\Delta R / R}{e} \qquad \text{(C1.1)}$$

The Gage Factor for metallic strain gages is typically around 2.

It is very important that the strain gage be properly mounted onto the test specimen so that the strain is accurately transferred from the test specimen, though the adhesive and strain gage backing, to the foil itself.

The strain gages used in this study were TML FLA-10 model by Tokyo Sokki Kenkyujo Co., with dimensions of 10mm x 2.5mm having 8 mm active grid length. Cu-Ni alloy foil strain gages backing with epoxy had a minimum limit as %3 strain. The manufacturers reported specification gives 5% accuracy of measured strains up to 3% elongation. The resistance of the gages is 120 Ohms ±0.3%, and the gage factor at 24 ^{o}C is 2.090 ± 0.5%.

Strain Gage Splicer made from Cyanoacrylate metarial has a shape of tube with a mass of 2 grams with 6 months shelf life beginning from production date. Prossesing temperature interval is -30 up to 120°C. Epoksy glass based TML Connecting Terminals provide convenient junction points to connect strain gages to instrumentation leads. They were manifactured from Cyanoacrylate material and its operation temperature interval was between -30 and +200°C. Strain Gage Connection Cable consisted of two flat fiber cables which are 0.11 mm^2, 10/∅0.12 copper wires having 0.16 ohm/m interior resistance at max.

A photograph of instrumented piles with the strain gages, connecting terminals, and strain gage connection cable are given in Figure C1.2.

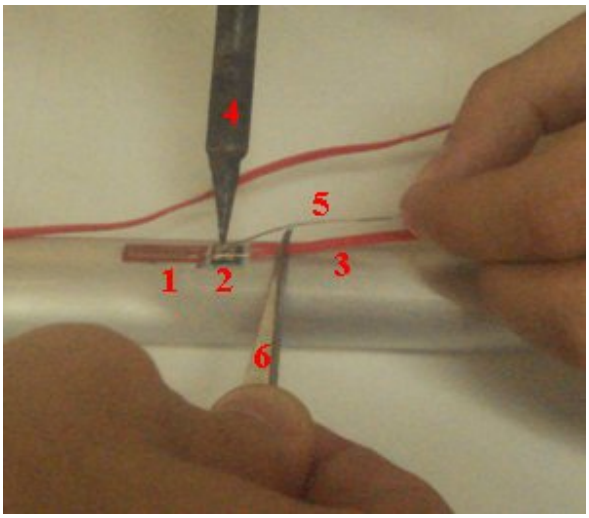

1. Strain gage
2. Connecting terminals
3. Connection cable
4. Soldering iron
5. Wicking tape
6. Tweezers

Figure C1.2 Instrumented Piles with the Strain Gages, Connecting Terminals, Connection Cable

APPENDIX C2 – Measurement Processes

To measure such small changes in resistance, strain gages are almost always used in a bridge configuration with a voltage or current excitation source. The general Wheatstone bridge, which transforms strain to voltage at specified measurement locations, is illustrated in Figure C2.1.

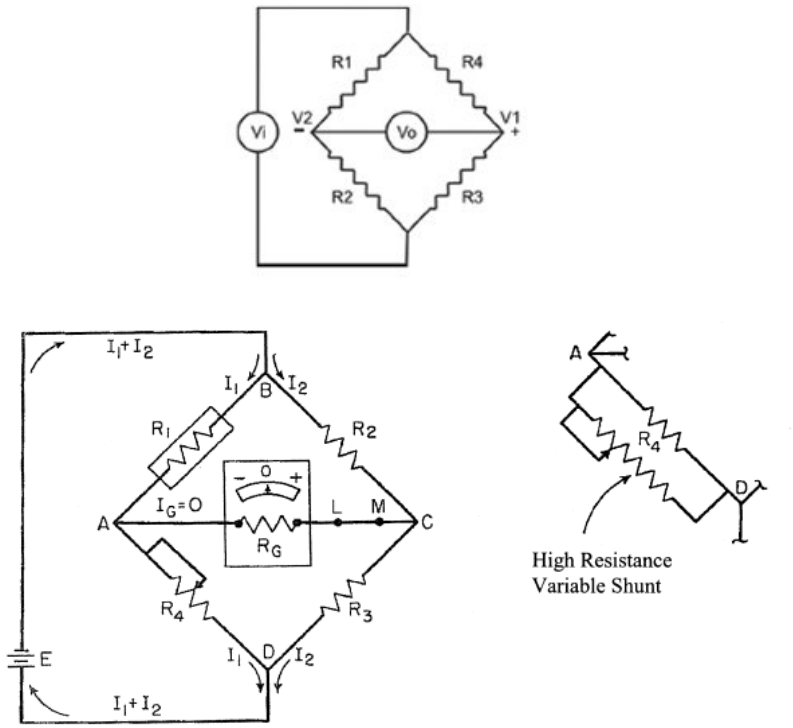

Figure C2.1 Wheatstone bridge circuit (after Perry and Lissner, 1962)

The Wheatstone bridge consists of four resistive arms with an excitation voltage (V_i). The basic idea of constructing a Wheatstone-bridge is to adjust the resistances R_1, R_2, R_3, and R_4 such that no current flows in the galvanometer branch (I_G=0). In such condition, E_G, the voltage across the galvanometer is also zero.

The galvanometer resistance R_G, can be considered as the load impedance sensed by the bridge circuit. The unbalance in the bridge can be reserved, by changing one or more

of the other resistances in the Wheatstone-bridge circuit. Kirochhoff's laws and the method of determinants are used to derive the formula output voltage (E_0) across the load resistance, in the case of allowing resistance changes in all four legs of the Wheatstone bridge as follows (Eq.C2.1):

$$E_0 = \frac{ER_G}{4(R+R_G)}\left[\frac{\Delta R_1}{R_1} - \frac{\Delta R_2}{R_2} + \frac{\Delta R_3}{R_3} - \frac{\Delta R_4}{R_4}\right] \quad \text{(C2.1)}$$

where R_1, R_2, R_3, and R_4 are the resistances composing the Wheatstone-bridge circuit; ΔR_1, ΔR_2, ΔR_3, and ΔR_4 are the changes in the resistances composing the bridge; E is the voltage across the circuit and R is the nominal resistance of all four gages.

Equation C2.2 can be acquired, when voltage division practice for each legs of Wheatstone Bridge is performed.

$$V_{out} = \left[\frac{R_3}{R_3+R_4} - \frac{R_2}{R_1+R_2}\right] x V_i \Rightarrow V_{out} = [V_1 - V_2] x V_i \quad \text{(C2.2)}$$

From Equation C2.2, it is apparent that when $R_1/R_2 = R_{G1}/R_{G2}$, the voltage output V_0 will be zero. Under these conditions, the bridge is said to be balanced. Any change in resistance in any arm of the bridge will result in a nonzero output voltage.

In case of replacing one of the resistances composing the bridge with a strain gage (Figure C2.2), any changes in the strain gage resistance will unbalance the bridge and produce a nonzero output voltage. If the nominal resistance of the strain gage is designated as R_G, then the strain-induced change in resistance, ΔR, can be expressed as $\Delta R = R_G \times GF \times \varepsilon$. Assuming that $R_1 = R_2$ and $R_3 = R_G$, the bridge equation above can be rewritten to express V_O/V_i as a function of strain. Note the presence of the

1 / (1+GF x ε/2) term that indicates the nonlinearity of the quarter-bridge output with respect to strain.

$$\frac{V_{out}}{V_i} = \frac{-GF \times e}{4} \bullet \left(\frac{1}{1 + GF \times \frac{e}{2}} \right) \tag{C2.3}$$

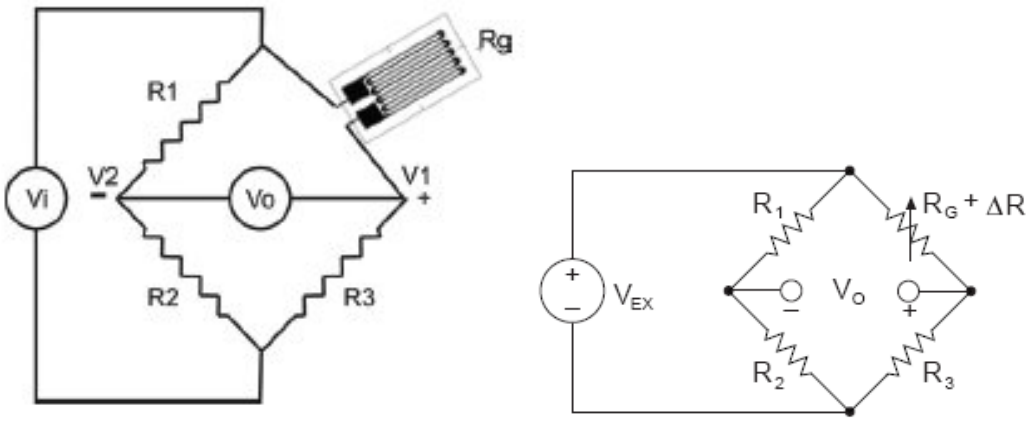

Figure C2.2 Quarter-bridge circuit

Alternatively, the sensitivity of the bridge to strain by making both gages active can be doubled, although in different directions. For example, Figure C2.3 illustrates a bending beam application with one bridge mounted in tension ($R_G + \Delta R$) and the other mounted in compression ($R_G - \Delta R$). This half-bridge configuration, whose circuit diagram is also illustrated in Figure C2.3, yields an output voltage that is linear and approximately doubles the output of the quarter-bridge circuit.

$$\frac{V_{out}}{V_i} = \frac{-GF \times e}{2} \tag{C2.4}$$

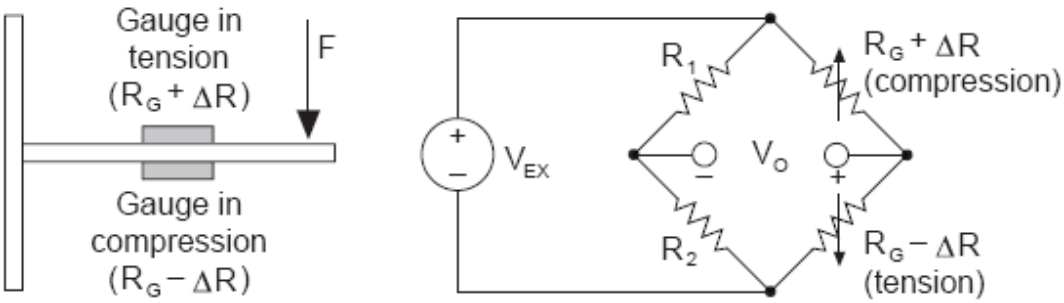

Figure C2.3 Half-bridge circuits

Quarter/Half Bridge Completion Cable of 120 ohm Strain Gage

Q-cable120 is a cable that is improved for connecting and balancing the strain gage to TDG-CODA Ai8b data collecting system. Q-cable120 is designed for connecting quarter/half bridge shaped strain gages to more than one canalized data collecting system. There is a zero calibrating potentiometer (zero trimpot having a function of strain reduction to zero) at the head of connector of cable, and utilizing this potentiometer, bridge balancing processing can be made. Cable, which was manufactured as a standard length of 3.3 m, connects to CODA AI8b data acquisition system with Standard MIC type 4 tipped plug. Q-cable's electrical scheme and plan view are given in Figure C2.4.

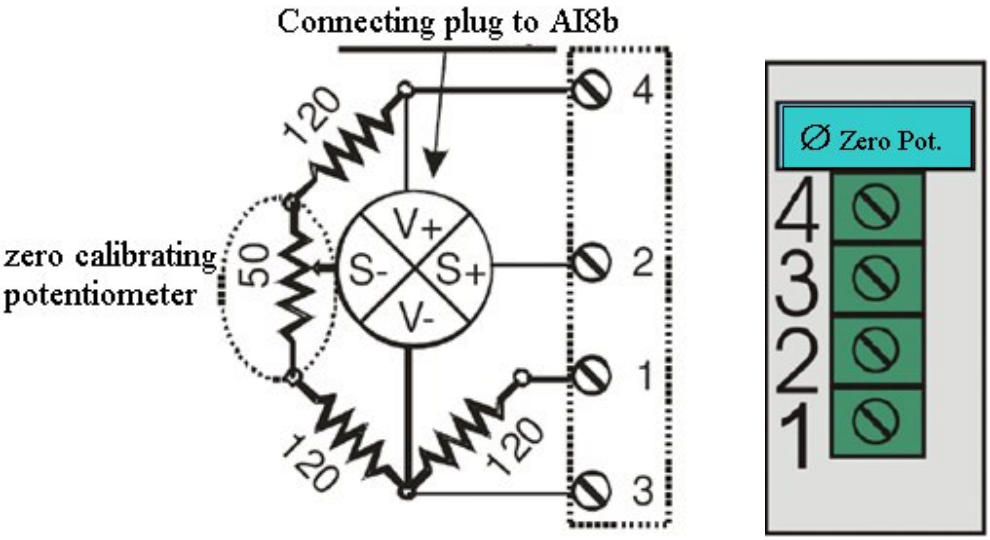

a) Electrical scheme b) Plan view

Figure C2.4 Electrical scheme and plan view of Q-cable

Q-cable reduces electrical noise and cable strain effect occurred by the cables between strain gage and data acquisition system, so less noisy measurements are to be measured. Measurement sensibility of quarter bridge depends on signal voltage and channel gain. On the other hand, measurement sensibility is affected negatively by electrical noise. For the best results, screwed connection terminal taking place at the tip of the cable should be connected to strain gage as close as possible.

The connection terminals standing on cable are suitable for quarter or half bridge connections. Measurements of quarter and half bridge using Q-cable are represented in Figure C2.5.

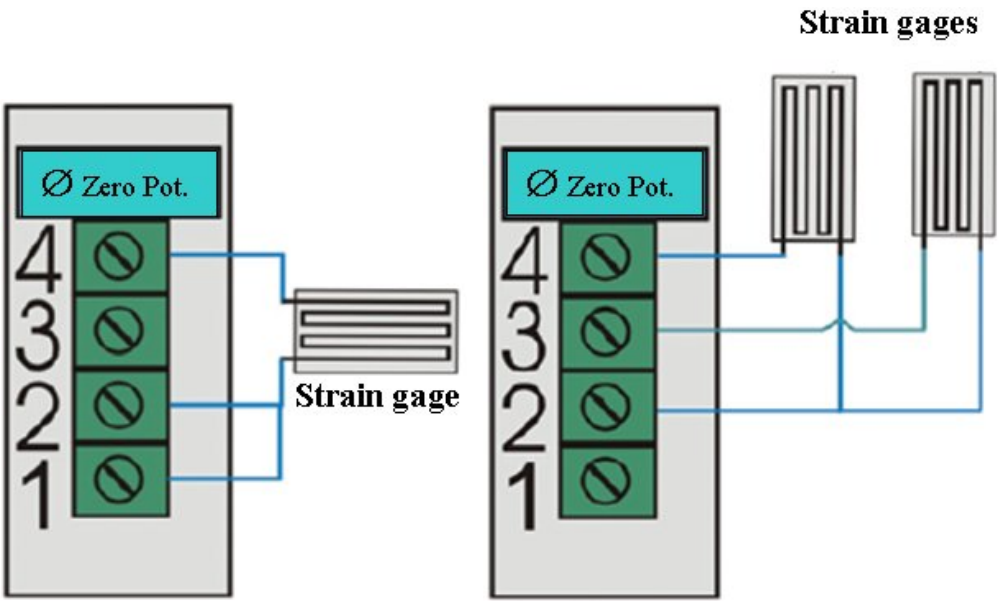

a) Quarter Bridge using Q-cable120 b) Half Bridge using Q-cable120

Figure C2.5 Measurement of quarter and half bridge using Q-cable120

If the Equation C2.3 is consubstantiate for quarter bridge;

$$V_{out} = \frac{-GFxe}{4} x \left(\frac{1}{1+\left(\frac{GFxe}{4} \right)} \right) xV_i xV_{gain} \qquad \text{(C2.5)}$$

strain value (ε) is found, when voltage value obtained from the measurement is placed in the Formula. For finding unit strain (ε) from measured voltage values with the quarter bridge system is given in Equation C2.6.

$$e = \frac{4\, v_{out}}{GFxV_i xGain} \qquad \text{(C2.6)}$$

Strain is proportional to bending moment within the elastic stress range of pile material. If it is accepted that loading is in the elastic region, the stress value can be found by Equation C2.7.

$$s = Exe \text{ (Hooke) and } s = \frac{M}{I} y \qquad \text{(C2.7)}$$

The relationship between output voltage and moment for the circuitry involved is as follows:

$$M = \frac{4xV_{out}xEI}{GFxV_i xGain x \frac{d}{2}} \qquad \text{(C2.8)}$$

APPENDIX C3 – Linear Position Transducers

Lateral pile head displacement measurements were made utilizing a resistive linear position transducer (RLPT) with 50 mm electrical measuring stroke for sensing the position of an attached pile. The RLPT uses a strain gage to detect the position of the pile. The sensor includes housing and a ramp shaped actuator located in the housing. A strain gage is positioned in contact with the actuator. The actuator is attachable to the pile. The actuator applies a strain to the strain gage as the actuator is moved. The strain gage generates an electrical signal that is proportional to the position of the pile. The technical drawing of the RLPT is given in Figure C3.1.

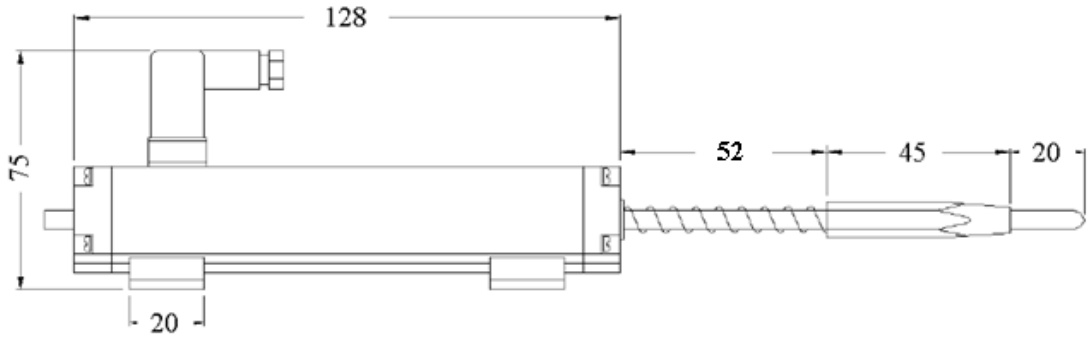

Figure C3.1 Technical Drawing of RLPT

Each RLPT was calibrated immediately before used. The data from these transducers was used to obtain load deflection curves during the tests.

APPENDIX D1 – Data Acquisition System

The acquisition of data was accomplished using Ai8b Measurement and Control System manufactured by TDG. Ai8b consists of data logger, which is arranged in different four chassises each of which having eight channels, and communication unit, which transfers the data from data logger to the computer. Analog signal circuits are assembled into each data chassises where sensor connection connectors are mounted on. The data logger supplies a predetermined excitation (supply) voltage to a sensor (i.e., strain gage or RLPT) through internal bridge configurations. The excitation and output voltages, V_i and V_{out} are precisely measured and processed by the data logger. Excitation voltage can be chosen as +5V or + 10V by selective switch on each channel of the Ai8b. The analog data can be increased 1, 150,248,397,494,673,741 and 890 times via these switches (gain switches). Reading sensibility is 0.000305 volt at the +/- 10 volt reading interval with the help of high quality digital converter. On the other hand, all channels can read the data 8 times in a second and reading speed does not depend on channel number. Connection units communicate with computer by using USB and with data logger by using RS485. Channel readings can be transformed to 16 bits resolution digital data. Front and back views of data logger are given Figure D1.1 below.

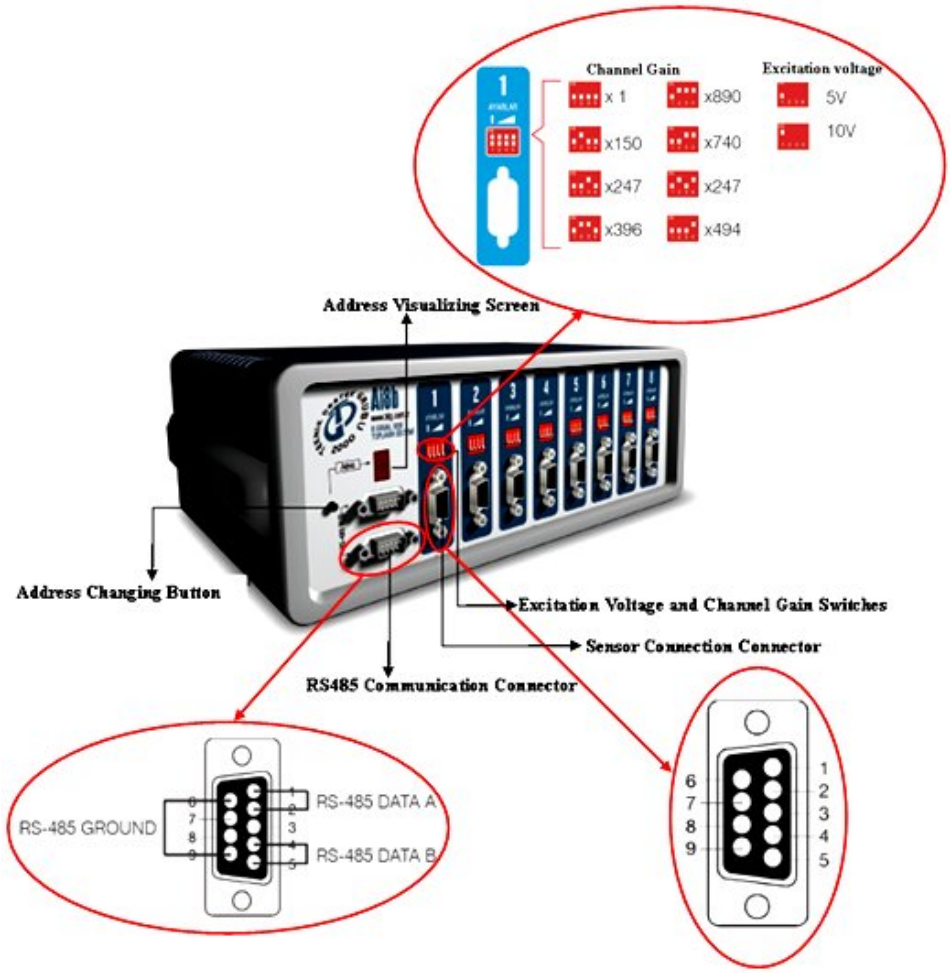

a) Front View

b) Back View

Figure D1.1 Front and Back Views of Data Logger

APPENDIX D2 – Conversion from Analog Signal to Digital Signal

AI8b is a 16 bit data logger having 2^{16} = 65536 step measuring sensibility. Step value is a digital code executed between 0 and 65535 corresponding to the voltage value. Transfer function for changing voltage value taken from sensor to the step value is given in Figure D2.1. This code is used for calibration of sensors.

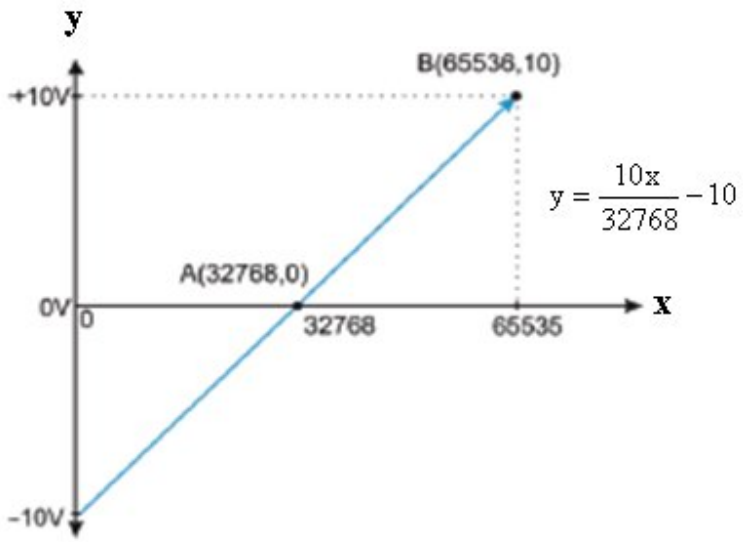

Figure D2.1 Data Logger Resolution and Voltage Interval

Data collecting resolution : 2^{16} = 65536 step
Measured total voltage interval : +/-10V=20V
Data logger voltage/step resolution : 20/65536, 0.000305 Volt / step

If 10 volt is applied to the entrances of AI8b's sensor, step value must be 65635
If 0 volt is applied to the entrances of AI8b's sensor, step value must be 32768
If -10 volt is applied to the entrances of AI8b's sensor, step value must be 0

By increasing the gain, voltage value and the step number are increased so that the more sensible measurement is achieved.

Appendix E – Bending Moment Distributions of Flexible Piles for Different Box Displacements

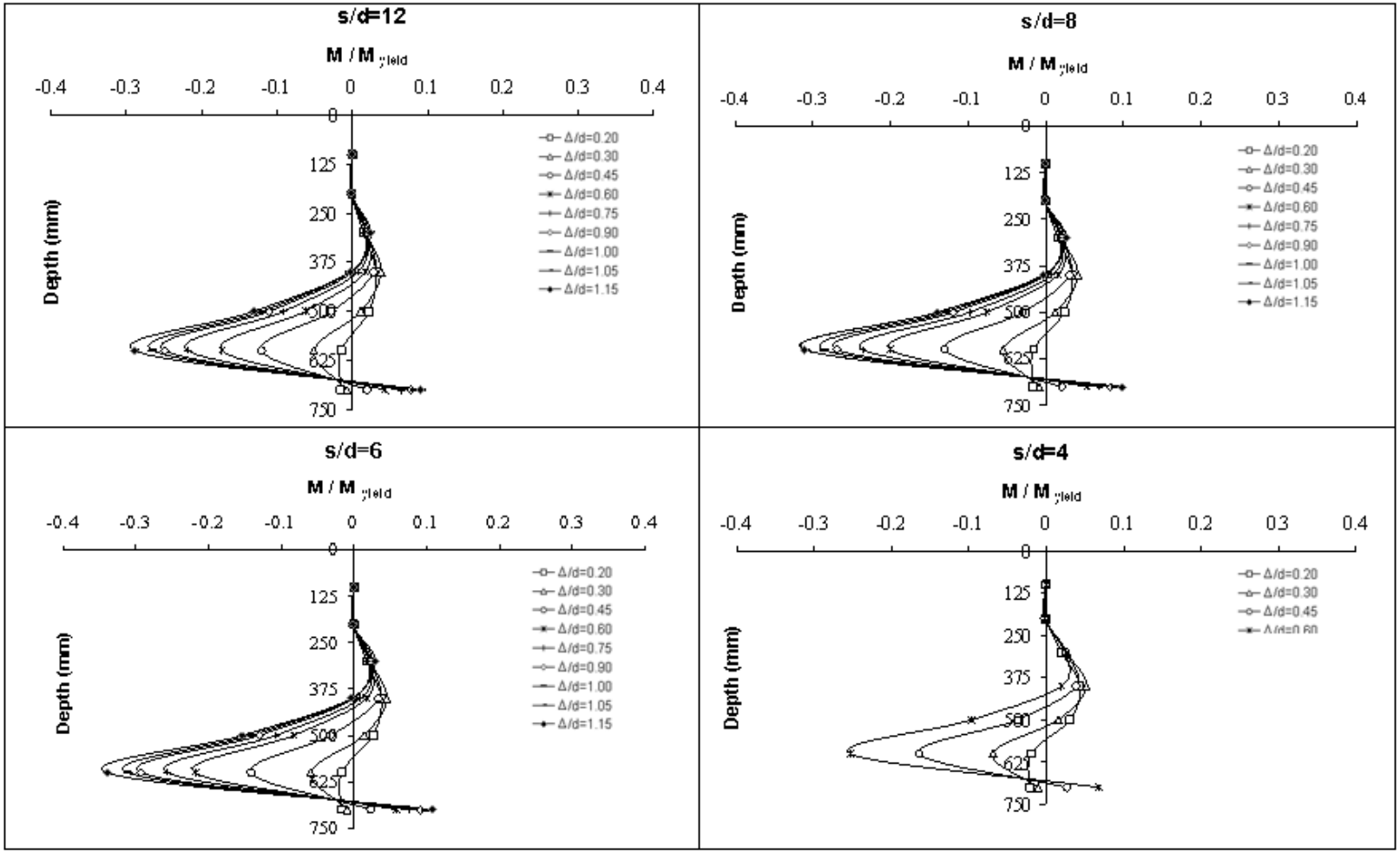

Figure E. 1 Normalized Moment (M / M_{yield}) Profiles for Flexible Piles in 10° Slope Angle

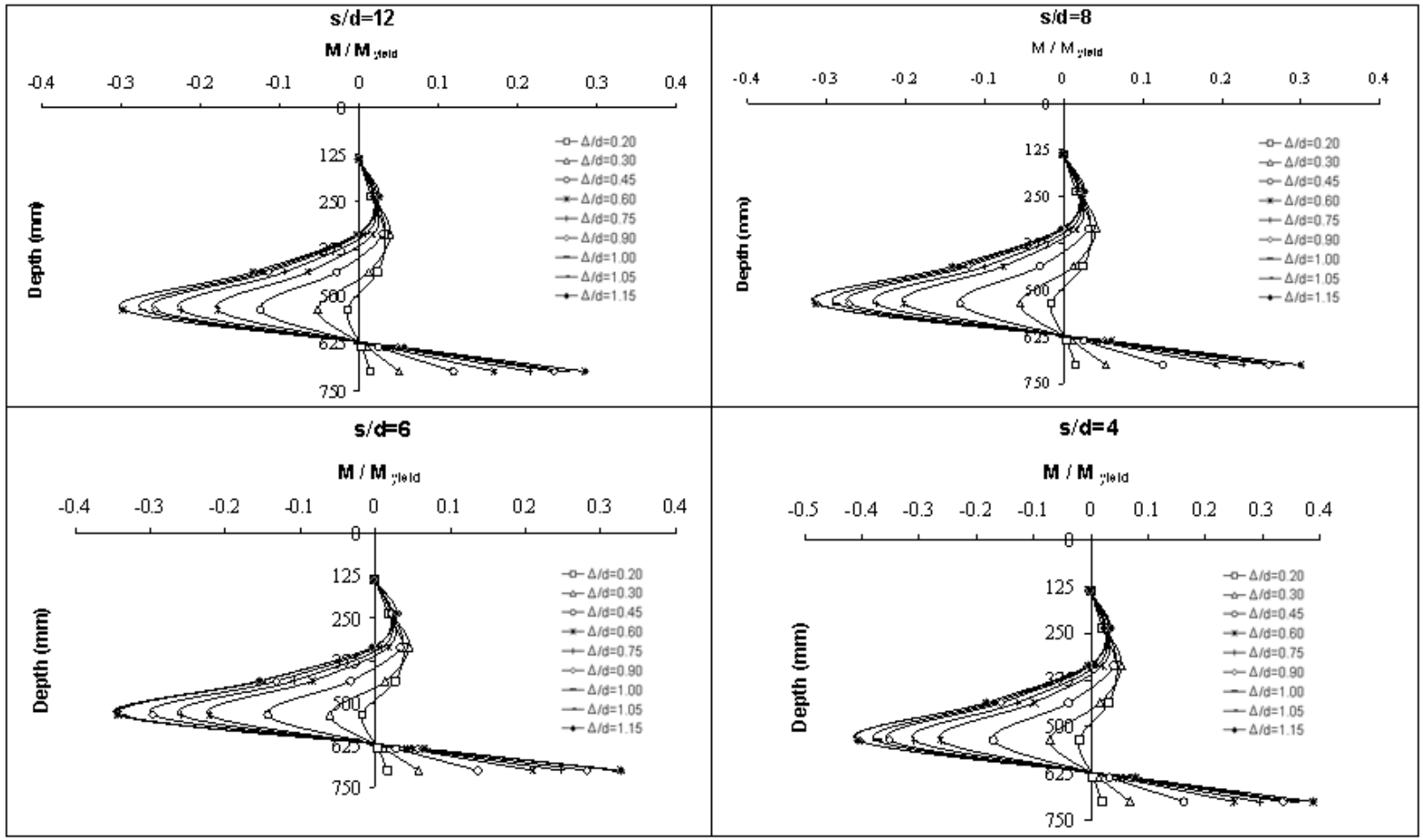

Figure E. 2 Normalized Moment (M / M_{yield}) Profiles for Flexible Piles in 20° Slope Angle

Appendix F – Equivalent Subgrade Modulus Assignment Based on p-y Curves for Weak Rock

The soil-pile deformation moduli (E_s) along the embedded portions of the piles (i.e. in the weak rock) were estimated by making use of the inclinometer data and the p-y curves (Reese et al., 1992) Figure F). The governing parameters of the p-y curves were determined using the RQD values (40%) and unconfined compression test results (q_u=20 MPa).

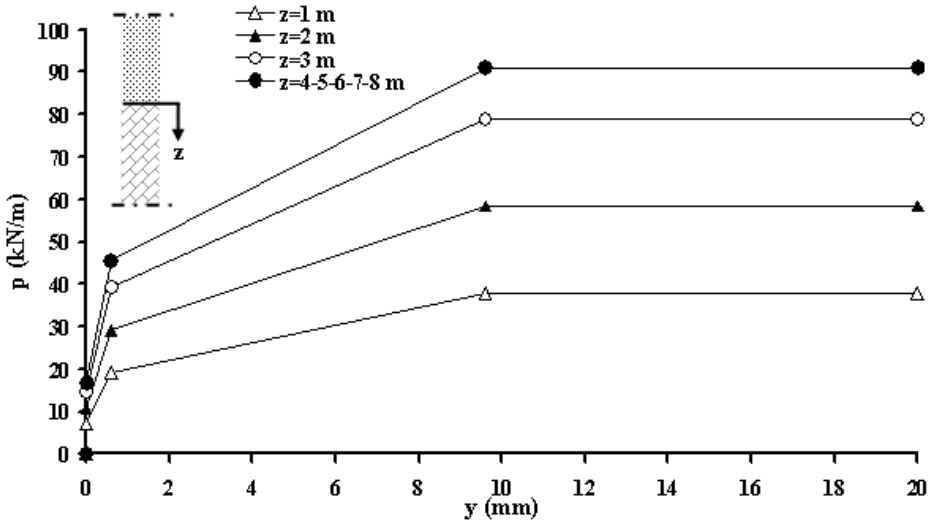

Figure F p-y curves of weathered sandstone

The lateral displacements (y) at four inclinometer stations (Pile#9, Pile#19, Pile#27 and Pile#38) were used to estimate soil-pile springs of the model that were calculated by first establishing p-y curves of the weathered sandstone and then reading soil-pile deformation moduli (E_s) corresponding to field pile deformations. The spring coefficients to be employed for structural analyses were calculated using the following relations. One should note that the sandstone was assumed isotropic throughout the back calculation process.

$$k_x = k_y = \frac{E_s}{B} \quad \text{and} \quad k_z = \frac{E_s}{4B\left(1-u^2\right)} \tag{F.1}$$

The k_x, k_y, k_z are the spring coefficients in the global coordinate system of the FEM model; B is the pile diameter; E_s and υ are the soil-pile deformation modulus and the Poisson's ratio of the weathered sandstone, respectively in the above equations.